Role of the S100A7 Gene in Breast Cancer Progression

by

Ethan David Emberley

A thesis submitted to the Faculty of Graduate Studies

in partial fulfillment of the requirements for the degree of

Doctor of Philosophy

Department of Biochemistry and Medical Genetics

University of Manitoba

Winnipeg, Manitoba

THE UNIVERSITY OF MANITOBA

FACULTY OF GRADUATE STUDIES

*****

COPYRIGHT PERMISSION PAGE

Role of the S100A7 Gene in Breast Cancer Progression

BY

Ethan David Emberley

A Thesis/Practicum submitted to the Faculty of Graduate Studies of The University of Manitoba in partial fulfillment of the requirements of the degree of

DOCTOR OF PHILOSOPHY

Abstract

For breast cancer to occur, the breast cells must go through a spectrum of changes. Between the earliest beginnings of cancer to the final stage of the disease, there are many known and unknown changes that must occur to enable the disease of breast cancer, that occurs in a non-vital organ, to develop and then spread beyond the breast. Once the cancer cells have left the breast and spread throughout the body, they are able to influence the function of vital organs, and so lead to the death of the individual. Of the many changes that must occur for breast cancer to result in death, the transition from a localized tumor in the breast duct, to a tumor that has started to spread from the primary site, is the best defined clinical transition and probably the single most important aspect of early breast tumor progression. If we were able to confine breast cancer to the breast duct and prevent it from spreading, we would have effectively cured this disease since it is only after breast cancer cells have developed and demonstrated the capability to spread through out the body that there can be any significant threat to the patient. To better understand how and why breast cancer cells leave the confined space of the breast duct, we have used molecular tools applied to human breast tissues. It is our belief that one of the differences between a localized primary tumor and a tumor that has just started to spread is a difference in their molecular composition. We have identified a gene named S100A7 (also named psoriasin) that is abundantly expressed in the primary tumor, but is much less abundant in spreading cancer cells. There is almost no S100A7 in normal cells. In tumors that have S100A7, we have found it to be associated with poor patient outcome. This suggests that this gene could be functionally involved in early tumor progression.

We have manipulated S100A7 expression in breast cancer cells in the lab and have found that S100A7 enhances the ability of cells to leave the breast duct in both artificial assays and more importantly in animal experimental models. Cells that have S100A7 also have a higher rate of growth, which is another hallmark of cancer. To better understand the pathway(s) which S100A7 potentially regulates to influence the invasiveness of breast cancer, we have searched for factors that form a physical interaction with S100A7. We have identified the factor Jab1 as one that interacts with S100A7. Jab1 has been described as having several different functions in other cell types, some that may be important in the process of promoting cancer development. We have found several changes in Jab1 associated functions in the presence of S100A7. It is our belief that S100A7 alters Jab1 and it is this alteration in Jab1 function that leads to the promotion of breast cancer. By better understanding S100A7's effect on Jab1 and the net effect of S100A7's alteration of Jab1 functions in breast cells, we would have a better understanding about the key steps that lead to the early stages of tumor cells spreading in breast cancer. This might illuminate other S100A7-Jab1 pathway components that could become used as markers in the clinic to predict how breast tumors will behave in the future and possibly make S100A7-Jab1 pathway a potential target for therapy.

Acknowledgements

I wish to express my deepest gratitude to my supervisor and mentor Dr. Peter Watson who provided me with an excellent training environment and stellar guiding support. Peter has taught me so much about science, problem solving, research, and academia while nurturing me to discover on my own. Peter's passion and enthusiasm for good science are contagious. He created an exciting environment where it felt like anything could be done, while still maintaining a sense of reality by balancing my ideas and imagination with his own. Peter gave me the freedom to do as much as I could and any successes I have had are directly resulting from Peter's superior mentorship and vast knowledge. I could not have chosen a better advisor.

My lab mates have been a wealth of resources during this project and without them I would not have accomplished everything detailed in this report. I am indebted to them for all their efforts and support. Kate Hole showed me at the very beginning of the project the basics to success and instilled confidence in a very green graduate student. Andrea Fristensky has an amazing attention to detail and willingness to take on less desirable tasks, and this is the reason why she was able to generate the stable S100A7 expressing clones in sometimes (often) difficult cell lines. Linda Curtis, Sandy Troup, and Yulian Niu performed all of the expert tissue processing and immunohistochemical work. Yulian and Sandy were also crucial to the success of the mouse xenograft experiments. Molly Pind is always the "go to" person when expert technical advice is needed and taught me to ask questions to obtain knowledge. It was a pleasure to collaborate with all of these stellar people and I was truly thankful to work along side such gifted individuals.

I was very lucky in that I was able to interact with brilliant individuals outside of the laboratory as well. Drs. Leigh Murphy, Etienne Leygue, Dan Gietz, Bob Shiu and Yvonne Myal are among the top faculty members at the University of Manitoba. They were always willing to share their insight and knowledge as well as ask the really hard

questions to stimulate my thinking. I was always treated like a peer and always benefited from interaction with these individuals. Because of the critical assessment and advice offered by this group, my work became better. I thank them for their key contribution to my training and development as a scientist.

A very special thank you to Zarene, Paul and my family. They always gave me their full support throughout my University schooling, and because of this, I'm extremely grateful. Even though they may not have always understood what I was studying or what all the scientific abbreviations stood for, they were always interested and encouraging. Paul is a true friend and ally. Even though he was published first, I like to think my Westerns look better. Thank you Zarene for always being there and sharing in all my adventures. With you, anything is possible.

I am very grateful for the financial support I have received from various groups. I was fortunate enough to obtain salary support from a United States Army Medical Research and Materiel Command Pre-Doctoral Traineeship Award and National Cancer Institute of Canada/Terry Fox Foundation Research Studentship. Thank you Cancer Care Manitoba and the University of Manitoba Research Day symposium for poster and presentation awards as well as the Faculty of Graduate Studies and the Department of Biochemistry and Medical Genetics for travel awards. I also wish to thank the Health Sciences Centre for the DeWiele-Topshee Award for Research Excellence in the field of Oncology.

Table of Contents

Material and Methods

List of Figures

List of Tables

Abbreviations

A	Adenine
Å	Angstrom
AD	Activation domain
ADH	Atypical ductal hyperplasia
Amp	Ampicillin
AP-1	Activator protein 1
Asp	Aspartic acid
BD	Binding domain
BRCA1	Breast cancer 1
BSA	Bovine serum albumin
C	Cytosine
Ca	Calcium
CA9	Carbonic anhydrase 9
cDNA	Complementary deoxyribonucleic acid
cm^2	Centimetre square
CMV	Cytomegalovirus promoter
CTP	Cytosine triphosphate
DCIS	Ductal carcinoma in-situ
DMBA	7,12-dimethylbenzanthracene
DMEM	Dulbecco's Modified Eagle's Medium
DNA	Deoxyribonucleic acid
dNTP	Nucleotides
DTT	Dithiol threitol
ECM	Extracellular matrix
EDTA	Ethylenediaminetetraacetic acid
EGF	Epidermal growth factor
EGFR	Epidermal growth factor receptor
ER	Estrogen receptor

ER +ve	Estrogen receptor positive
ER -ve	Estrogen receptor negative
ER-α	Estrogen receptor alpha
ER-β	Estrogen receptor beta
EtBr	Ethidium bromide
FBS	Fetal bovine serum
fmol	Fento mole
g	Gram
G	Guanine
GAPDH	Glyceraldehyde 3-phosphate dehydrogenase
Gln	Glutamine
Gly	Glycine
h	Hour
HCl	Hydrochloric acid
HER2	Human epidermal growth factor receptor 2
HIF-1	Hypoxia inducible factor 1
His	Histidine
HRP	Horseradish peroxidase
IHC	Immunohistochemistry
Jab1	Jun activation domain binding protein 1
JNK	Jun N-terminal kinase
kb	Kilo base
KCl	Potassium chloride
kDa	Kilo dalton
KH_2PO_4	Potassium phosphate monobasic
L	Litre
LCIS	Lobular carcinoma in-situ
Leu	Leucine
Lys	Lysine

M	Moles/litre (Molar)
MAPK	Mitogen activated protein kinase
Met	Methionine
$MgCL_2$	Magnesium chloride
ml	Milli litre
mm	Millimeter
mM	Milli molar
MMLV	Moloney Murine Leukemia Virus
MMP	Matrix metalloproteinase
MMTV	Mouse mammary tumor virus
Mr	Relative molecular mass
mRNA	Messenger RNA
mths	Months
mut	Mutant
NaAc	Sodium acetate
NaCl	Sodium Chloride
ng	Nanogram
nm	nanometer
^{o}C	Degrees celcius
p	phosphate
PAGE	Polyacrylamide gel electrophoresis
PBS	Phosphate buffered saline
PCR	Polymerase chain reaction
PDWA	Proliferative disease without atypia
PI3K	Phosphatidylinositol 3-kinase
PR	Progesterone Receptor
PTM	Psoriasin triple mutant
rATP	Ribo adenosine triphosphate
RMS	Root mean square
RNA	Ribonucleic acid

rpm	Revolutions per minute
RT	Room temperature
RT-PCR	Reverse transcription PCR
SCR1	Steroid receptor co-activator 1
SDS	Sodium dodecyl sulfate
SIB	sample isolation buffer
T	Thymine
TBS	Tris buffered saline
TBS-T	Tris buffered saline - tween
TE	Tris EDTA
TEMED	N,N,N',N-tetramethylethylenediamine
TGF	Transforming growth factor
TPA	Phorbol 12-tetradecanoate 13-acetate
Tris	Tris(hydroxymethyl)aminomethane
Triton X-100	Octyl phenoxyl polyethoxy
Trp	Tryptophan
Tween 20	Polyxyethylene-sorbitan monolaurate
µg	Microgram
µl	Micro litre
µM	Micro molar
UV	Ultra violet
V	Volt
VEGF	Vascular endothelial growth factor
Zn	Zinc

1.1.0- Introduction: Basic Background on Breast Cancer

Breast cancer is an ancient disease and was described by the Egyptians over 5000 years ago. Numerous articles about breast cancer and its treatment were written by Greek and Roman physicians. Surgery is the oldest method of treating breast cancer with different operations reflecting the beliefs at the time about breast cancer's causes and natural history. A variety of 'medical' therapies have also been described during these times, especially in the Middle Ages, which to the modern observer were more similar to witchcraft than the application of scientific knowledge to the treatment of the disease. Changing fashions in the treatment of breast cancer over the centuries have reflected not only changes in beliefs regarding its pathogenesis, but also growth in the knowledge about the disease as well as advances in science and technology.

Almost all breast cancers start in the glandular tissue of the breast and are classified pathologically as adenocarcinomas. Breast cancer is predominantly a female disease but can also be found in men, but this is very rare, at least in western countries (less than 1% of all cases). The transformation of normal cells to cancer cells most often occurs within the ducts, with ductal carcinoma being the most common type of breast cancer. When breast cancer is diagnosed early, it may be very small and still confined to the few ducts or lobules where it has started, in which case the lesions are called in-situ cancers. At this early stage, before the cancer cells have invaded into the surrounding tissue, there is no risk of the cancer cells spreading to other organs (metastasis) and removal of the cancer by surgery is curative. However, most in-situ cancers can only be diagnosed with some effort and cost by individuals and heath systems respectively, as they typically do not

form a lump that can be detected by the patient or by clinical examination. Nevertheless, both patients and health care systems have come to learn and appreciate the personal and economic benefits of early breast cancer detection. Breast cancer is the most frequently diagnosed cancer in western societies and therefore exerts enormous individual and collective costs. This is the reason for the investment in mammography screening programs by societies that can afford it.

1.1.1- Breast Cancer Statistics in Canada

Breast cancer is the most frequently diagnosed cancer in Canadian women, comprising 30% of total cancer cases. In 2004, it is estimated that in Canada 21,000 women will be diagnosed with this disease, which effectively translates into approximately 400 Canadian women being diagnosed with breast cancer every week. More importantly, an estimated 5200 women will loose the fight against the disease this year, which represents 16.3% of cancer related deaths in women, second only to lung cancer at 25.5% (FIG 1). On average, 100 Canadian women die of breast cancer every week. Contemporary statistics which reflect current detection and treatment technologies estimate that one in 9 women is expected to develop breast cancer during her lifetime and one in 27 will die of the disease. There may be some positive aspects to current figures that show progress in the fight against breast cancer, but these should be viewed with caution. Although the Age-Standardized Incidence Rate (ASIR) for breast cancer has been steadily rising for the past 30 years, this can be argued to be mostly due to an increase in awareness and improvements in detection methods such as mammography (1, 2).

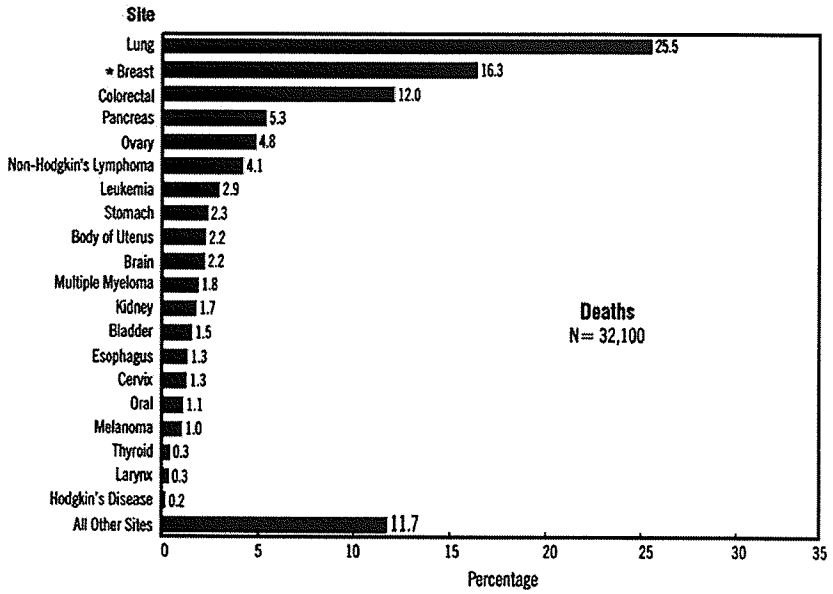

FIG 1 - Deaths Caused by Cancers in Canadian Women. Percentage distribution of estimated new cases and deaths for selected cancer sites in Canadian females for 2004. Source: Canadian Cancer Society

On the other hand, this leads to the inclusion of earlier stages of the disease as "cancer" in statistical analyses, so the death rates caused by the disease have apparently declined steadily since 1986 (FIG 2). In fact, the most recent data show the breast cancer death rate to be at its lowest since 1950. But these gains should be considered carefully. Due to discussion of breast cancer in the press, a change in social inhibitions about discussing breast cancer and most importantly due to the deployment of mammography screening programs earlier and earlier stages of breast cancer are being detected. Largely because of this, the current 5-year survival rates are better than those of the pre-mammography era. The detection of earlier stages of breast cancer will translate into the patient enduring a longer time with the disease, which skews the comparison of 5-year survival rates. Also, an unknown proportion of the lesions currently detected will never develop into

metastatic cancer and would never have been detected in the pre-mammography era. These cases may be inaccurately categorized as 'cures', when they would probably never have presented a threat to the patient if left untreated.

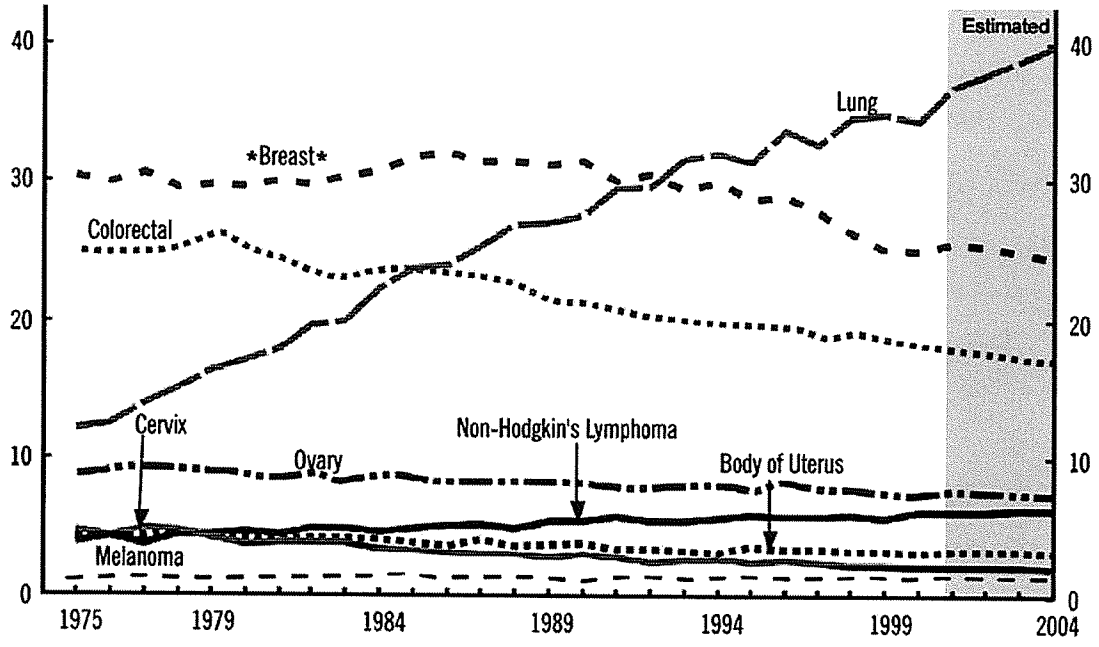

FIG 2 - Incidence Rates for Cancers in Canadian Women. Age-standardized mortality rates for selected cancer sites in Canadian females for the period of 1975 to 2004. Source: Canadian Cancer Society

1.1.2- Anatomy of the Breast

The breast is mainly composed of adipose (fat) and glandular breast tissue, along with connective tissue, nerves, veins, and arteries. Breast tissue is a complex network, with each breast comprising an independent unit, or mammary gland. Within that gland, there

are 15-20 lobes separated by adipose tissue. Within each lobe are several smaller compartments called lobules. Lobules are composed of clusters of milk-secreting glands termed alveoli, which are embedded in a specialized connective tissue. Myoepithelial cells surround the alveoli and in a lactating breast these cells contract to help propel milk toward the nipple. There are about one million lobules contained within each breast. The lobules are connected by tiny ducts that are joined together into increasingly larger ducts. Within each breast, there are between 5 and 10 ductal systems and each has its own opening at the nipple. Most epithelial breast cancers arise from luminal cells within the distal duct-lobular component of the system as opposed to the larger proximal ducts close to the nipple. Morphological appearances of epithelial breast cancers have also suggested that most of these (~90%) have origins within the terminal ductal system while a smaller proportion (<10%) arise from within the lobular component. Tumor classification and terminology is also partly based on this principle.

1.1.3- Benign Lesions of the Breast

The wide spectrum of complex benign changes occurring within breast tissues can be usefully categorized as 'nonproliferative' and 'proliferative' lesions. Nonproliferative lesions include cysts, apocrine metaplasia and duct ectasia. Proliferative lesions include two subcategories: a) 'usual type' lesions without atypia and b) atypical lesions. Proliferative lesions without atypia encompass intralobular and intraductal hyperplasias which have more than two layers of cells within the epithelium but are cytologically benign. Intraductal papillomas and sclerosing adenosis that also involve complex

intraluminal and stromal changes are also grouped into this category. The second subcategory of lesions is less defined by positive diagnostic criteria but rather by failure to exhibit clear dominant features of either a recognizable benign proliferative lesion or those of a malignant lesion. These so called atypical hyperplasias therefore encompass a hodgepodge of lesions that include those with either cellular or architectural atypia or a combination of both aspects, resembling the changes that are used to define DCIS (ductal carcinoma in-situ). Atypical hyperplasia is therefore a hyperplastic lesion that often has some but not all of the characteristics of in-situ carcinoma or comprises a very small in-situ carcinoma that defies definitive classification. Atypical hyperplasias are subdivided into lobular and ductal types on the basis of the predominant cellular phenotype. These two lesion types share other similarities with in-situ carcinoma, including occurrence within similar anatomical locations within the breast and association with microcalcifications, but all three lesions (typical hyperplasia, atypical hyperplasia, and in-situ carcinoma) can currently only be distinguished by microscopy.

1.1.4- Carcinoma In-Situ

Pathological and morphological classification recognizes two types of in-situ carcinoma, Lobular carcinoma in-situ (LCIS) and ductal carcinoma in-situ (DCIS). These two lesions are usually clearly distinguishable on morphological grounds as well as their typical clinical presentation and natural history in terms of risk of progressing directly to invasive breast cancer (cancer cells that have broken free from the constraints of the primary site and have begun to spread away from the primary tumor). Classically, lobular

carcinoma in-situ presents as an incidental finding and is thought to indicate a generalized increased risk of subsequent invasive disease throughout the breast. In contrast, ductal carcinoma in-situ presents as a palpable mass or mammographic lesion and indicates a localized threat to subsequent invasive disease in the same ductal tree/region of the breast. A diagnosis of lobular carcinoma in-situ is therefore regarded as a risk factor rather than the basis for the development of an invasive carcinoma. A diagnosis of lobular carcinoma in-situ warrants increased effort to survey and monitor the breast tissue over time and no specific attempt is made to secure complete local removal of the lesion in terms of clear surgical margins. In contrast, a diagnosis of ductal carcinoma in-situ is an indicator of risk mostly at the location of the lesion and therefore serves as a red flag or risk factor and also the basis of the possible development of invasive carcinoma at that site. Therefore a diagnosis of ductal carcinoma in-situ necessitates complete local resection to reduce local risk. However the distinction between these lesions may not be as clear as once was thought. The following sections (1.1.5 and 1.1.6) will discuss aspects dealing with the specific lesions of lobular carcinoma in-situ and ductal carcinoma in-situ, with later sections focusing exclusively on ductal carcinoma in-situ, as relating to the research question of this project. Topics discussed include molecular and phenotypic properties that are important in the management and treatment of the disease.

1.1.5- Lobular Carcinoma In-situ (LCIS)

This lesion arises from and is found within the lobules of the breast and is considered to be pre-cancerous. Recent molecular studies indicate that at various genetic loci, DCIS and LCIS can be indistinguishable (3-6). This is of particular interest, as it has emerged that some categories of LCIS seem to be equally liable as DCIS to go on to invasive carcinoma.

LCIS is typically identified as an incidental finding, as there are no clinical or mammographic or ultrasound features other than an association with microcalcifications. It is usually only discovered when benign (non-cancerous) breast lumps which have been removed, are examined under the microscope. These lesions have low proliferation rates and are often multifocal and bilateral. A central problem for preventing invasive cancer in this respect is the character and location of the subsequent carcinomas: about half of the cases occur in the opposite breast and many of the tumors are invasive ductal. Under these conditions LCIS is considered from a practical management standpoint to be a marker of increased breast cancer risk rather than a true precursor lesion for invasive disease.

LCIS perhaps should not be classifed as a 'cancer' but when it is present there are abnormal cells in the lobules, or glands of the breast which increase the risk of a breast cancer developing. The risk of breast cancer is five to ten times greater in women who have LCIS than those who do not (7, 8), which effectively translates into 1 in 3 women with LCIS will develop a breast cancer at some time during their life. In the past LCIS

was often treated by mastectomy, but this is no longer considered necessary. Instead, careful check-ups are recommended with breast examinations every 6-12 months and mammograms every one or two years so that any cancerous change is detected.

1.1.6- Ductal Carcinoma In-situ (DCIS)

Proliferating malignant lesions of the ductal epithelium that populate the ductal lumen and expand the duct, but do not manifest cellular infiltration beyond the epithelial basement membrane, can be identified by microscopic analysis and are termed ductal carcinoma in-situ (DCIS). DCIS is alternatively described as pre-cancerous, pre-invasive, non-invasive or intraductal cancer.

The frequency of DCIS being diagnosed has increased markedly in the United States and Canada since the widespread adoption of breast screening programs using breast X-rays or mammograms (9, 10). Women who have been screened with mammography are therefore much more likely to be diagnosed with DCIS than unscreened women. Cancer cells inside the ducts can not be detected on the mammogram, but may often coexist with tiny specks or calcifications that are detected by this method. Micro-calcifications arise from the buildup of calcified material that is probably derived from altered pH in the microenvironment or dead cancer cells. DCIS is now generally detected by a mammogram, as small lesions are clinically undetectable and DCIS does not usually have any symptoms. Nearly 90% of DCIS lesions that are clinically undetectable are diagnosed by mammographic detection of either microcalcifications (in 76% of cases),

soft tissue densities (11%) or both (13%) (11). DCIS accounts for almost 20% of the total number of all breast cancers detected by screening (1 case of DCIS is detected per 1300 screening mammograms) in North America (10, 12). Confirmation of the diagnosis is needed for mammographically suspicious, non-palpable lesions of the breast. This requires guided fine needle aspiration cytology (FNAC) (13), stereotactic core biopsy (SCB) (14), or wire-guided open biopsy (15). The material removed from the patient is analyzed by a pathologist for the diagnosis of the lesion. The standardization of these biopsy procedures has been an important clinical issue, as many factors influence their sensitivity, such as the number of samples acquired, needle placement accuracy, diameter of the area of micro-calcification and histological density of DCIS. Patients with DCIS that is diagnosed on core needle biopsy require surgical removal of the lesion to both remove a lesion that may progress to invasive disease in the future, and to rule out the presence of coexisting invasive carcinoma at the time of detection, which is found in approximately 10-15% of cases. The likelihood of finding associated invasive carcinoma increases with the grade of DCIS (16, 17).

1.1.7- Types of DCIS

The term ductal carcinoma in-situ (DCIS) refers to a category of several forms of cancers that occur within the breast ducts. Various subtypes of DCIS have been described based on their morphology: comedo, cribriform, micropapillary, papillary, solid, and several less common patterns such as clinging, signet-ring, and apocrine. These subtypes can be grouped into two overall categories of DCIS: non-comedo and comedo. The term comedo

describes a specific pattern or appearance of the cancer. Comedo type DCIS tends to be more aggressive than the non-comedo types of DCIS in terms of association with coexisting invasive disease and likelihood of progression. Pathologists distinguish between comedo type DCIS and other non-comedo types when examining the lesions under a microscope on the basis of several parameters, but principally on the basis of the presence of marked necrosis (dead cells) in the central lumen of the breast ducts. Necrosis is often seen with microcalcifications. The most common non-comedo types of DCIS are: Solid DCIS, where the cancer cells completely fill the affected breast ducts; Cribiform DCIS is described as having cancer cells that do not completely fill the affected breast ducts; there are gaps between the cells. Papillary and micropapillary DCIS have cancer cells that arrange themselves in a fern-like pattern within the affected breast ducts. Classification and diagnosis of DCIS is a challenge due to differing pathological criteria, interobserver variability (18) and the heterogeneous nature of cancer growth.

1.1.8- Grading of DCIS

Recently, several DCIS classification schemes have been developed which attempt to predict clinical outcome (19, 20). Because the major issue in the management of DCIS is the risk of progression to invasive carcinoma (cancer cells that have broken free from the constraints of the primary site and have begun to spread away from the primary tumor), several classification systems have been suggested according to cellular differentiation, cytonuclear features, and degree of necrosis. Ideally, pathological assessment should involve both nuclear grade and necrosis as some studies have demonstrated a correlation

between architectural features and clinical behavior (21, 22). Well-differentiated DCIS probably gives rise to low-grade invasive breast carcinoma, which have a better long term clinical outcome than high-grade invasive breast carcinoma (23). A correlation was found between recurrence and differentiation as defined by nuclear features and cell polarization, but this failed to reach statistical significance at the 5% level. A stronger and statistically significant correlation was found between nuclear grade and recurrence when cell polarization was disregarded (22). A significant correlation between histology and recurrence was also observed using the Van Nuys classification (see below), which is based on nuclear grade and necrosis. Whether the tumor recurred as in-situ or invasive carcinoma was unrelated to histological classification, as was the time course over which it occurred. These findings strongly support the use of nuclear grade to identify cases of DCIS at high risk of recurrence after local excision, but further work is necessary to determine whether nuclear grade or necrosis is more appropriate to subdivide the non-high-grade cases (22).

The Van Nuys Grading System for DCIS is a fairly new prognostic classification that deserves specific mention since it has now become relatively widely accepted in North America. This classification combines high nuclear grade and comedo-type necrosis to predict clinical recurrence (24). In this system the following DCIS grades are recognized: low grade (Grade 1) lesions are those with small nuclei and no necrosis. Intermediate grade (Grade 2) lesions are those with intermediate size nuclei and with zonal necrosis.
High grade (Grade 3) lesions are those with large abnormal nuclei and typically manifest associated necrosis, although this is not required.

The Van Nuys classification defines three distinct and relatively easily recognizable groups, each of which has a different likelihood of local recurrence if treated with breast conservation. The original report (24) found 31 local recurrences in 238 patients after breast-conservation surgery: 3.8% (3/80) for Low grade DCIS, 11.1% (10/90) for Intermediate grade DCIS, and 26.5% (18/68) in high grade DCIS. The 8-year actuarial disease-free survivals were 93%, 84%, and 61%, respectively (all $p \leq 0.05$). The specific importance of the recognition of necrosis within the morphologic assessment is further underscored by the observation within the context of a large clinical trial, that comedo type DCIS (necrosis present) is more aggressive with a higher probability of associated invasive ductal carcinoma than non-comedo type DCIS (necrosis negative) (25).

1.1.9- Treatment of DCIS

The significance of the several different types of DCIS is that treatment varies according to the risk that they are associated with. Often a small operation to remove the affected area is all that is needed. In many cases radiotherapy to the region is also offered. More recently tamoxifen (an antagonist for estrogen that is used in the treatment of breast cancer (26-28)) is sometimes recommended as well. Factors such as the size of the DCIS, size of the breast, extent of surgery, and the method of pathological examination all affect the surgical margin status following initial surgery. The status of the surgical margins combined with histological assessment and classification of the DCIS lesion are the principal factors that influence the decision of whether to undertake further treatment. If

the area of DCIS is very large or if there are several patches of DCIS within the same breast, then it is still possible that a mastectomy might be advised.

Until recently, the standard treatment for DCIS was mastectomy (29). Mastectomy was the preferred treatment because without it, the patient had a 30% incidence of multicentric disease. For a palpable tumor, the incidence of recurrence is between 25% to 50% following limited surgery, with half of those recurrences being invasive carcinoma (29, 30). For patients with DCIS, the total recurrence rate for local and distant sites following mastectomy is 1% to 2% (31).

Due to the success of breast conserving surgery for invasive carcinoma in place of mastectomy (32), this approach was extended to noninvasive carcinoma. To determine whether breast conserving surgery was a viable approach for the management of DCIS, the National Surgical Adjuvant Breast and Bowel Project (NSABP) study B-17 randomly assigned 818 women with localized DCIS, and negative surgical margins following excisional biopsy to breast irradiation (50 Gy) or to no further therapy (33). In this study, 80% of the women were diagnosed by mammography and 70% had small lesions ($\leq$1 cm). Events were defined as the presence of new ipsilateral disease, contralateral disease, metastases, a second primary tumor, or death from any cause. The study found that after 8 years, the patients who were treated with both lumpectomy and radiation had an event free survival of 75%, compared to 62% for patients treated with lumpectomy alone ($p=0.00003$) (33). The cumulative incidence of recurrent ipsilateral breast cancer was reduced from 26% to 12% ($p<0.000005$) by the combination of radiation and surgery.

The occurrence of invasive cancer also decreased from 13.4% to 3.9% with the addition of radiation ($p<0.001$) and recurrence of DCIS was reduced from 13.4% to 8.2% ($p=0.007$). The study also reports that only 1% of patients in this trial have died from breast cancer, which is similar to the historical data after mastectomy (31). In summary, this trial found the combination of excision and breast irradiation is an acceptable therapy for localized DCIS. These results have been confirmed in a trial of the same design conducted by the European Organization for Research and Treatment of Cancer (EORTC) (34). Meta-analysis of another cohort of patients revealed a summary recurrence rate of 22.5% for local surgery only, 8.9% for local surgery with radiotherapy and 1.4% for mastectomy (25, 35).

To determine if the anti-estrogen compound tamoxifen enhances the efficacy of local therapy for the management of DCIS, the NSABP performed a double-blind prospective trial of 1,804 women (36). Patients were randomly assigned into two groups: the control group was treated with lumpectomy, radiation therapy (50 Gy) and placebo, the second group was treated with lumpectomy, radiation therapy, and tamoxifen (20 mg/day for 5 years) (36). Approximately 80% of the lesions measured 1 cm or less and more than 80% of the tumors were first detected mammographically. Breast cancer events were defined as the presence of new ipsilateral disease, contralateral disease, or metastases. Women in the tamoxifen group had fewer breast cancer events at 5 years than did those on placebo (8.2% versus 13.4%, $p=0.0009$). With the addition of tamoxifen, there was a drop in ipsilateral invasive breast cancer decreased from 4.2% to 2.1% at 5 years ($p=0.03$). The incidence of contralateral breast neoplasms (invasive and noninvasive) decreased from 0.8% per year to 0.4% per year ($p=0.01$) for the tamoxifen treated group. Because of

these studies, tamoxifen is now under consideration for routine use in the treatment of DCIS and is referred to as hormonal therapy.

Based on the success of tamoxifen, several next generation hormonal therapeutics have been developed and are currently being tested. Anti-aromatase agents inhibit the cytochrome P-450 component of the aromatase enzyme complex responsible for the final step of estrogen biosynthesis in peripheral tissues which is the main source of estrogen in postmenopausal women (37-40). Anastrozole (41) is a third-generation non-steroidal aromatase inhibitor that has been shown to be superior to megestrol acetate (a synthetic compound that is similar to the hormone progesterone which is used during hormonal therapy of breast cancer (42)), in terms of survival and adverse effects, as a second-line therapy in postmenopausal women with estrogen receptor (ER) and/or progesterone receptor (PR) positive advanced breast cancer. In a large randomized trial composed of 9,366 patients, the use of anastrozole and the combination of anastrozole and tamoxifen with tamoxifen alone as adjuvant therapy was compared for postmenopausal patients with node-negative and node-positive invasive disease (43). The large majority (84%) of the patients in the study were hormone-receptor positive and slightly more than 20% had received chemotherapy. At the time of the planned initial analysis of the trial, when the median follow-up was 33.3 months, there was no benefit observed for the combination arm relative to tamoxifen. However, patients on anastrozole alone had a significantly longer disease-free survival than those patients only given tamoxifen (hazard ratio (HR) 0.83,95% CI 0.71-0.96, p=0.013). This trial demonstrated that anastrozole significantly

prolongs the time to tumor progression compared with tamoxifen as a first-line therapy for ER and/or PR positive advanced invasive breast cancer in postmenopausal women.

Furthermore, the preliminary results of the Arimidex, Tamoxifen, Alone and in Combination (ATAC) study have shown that adjuvant anastrozole is superior to tamoxifen in terms of disease-free survival (DFS), non-musculoskeletal adverse effects and prevention of contralateral breast cancer in postmenopausal women with early, ER positive invasive breast cancer (44). The drug has been recently approved for adjuvant use in postmenopausal women with early, ER positive breast cancer who are unable to tolerate tamoxifen or for women who have an increased risk of developing thromboembolism or endometrial cancer. The potential role of anastrozole and similar agents such as exemestane in the neoadjuvant setting for premenopausal invasive breast cancer, and the management of earlier stages of disease (DCIS), and breast cancer prevention in women with other indicators of high risk, is currently being investigated.

We have learned much about the treatment of DCIS over the past 20 years. Treatment of DCIS with small conserving surgery when combined with adjuvant therapy has become the preferred treatment, where radical mastectomy was once the standard treatment. A very promising area of investigation that may guide treatment in the future is the identification of molecular and biological features of DCIS that can be used as targets for treatment. The "estrogen receptor story" has taught us the value in identifying cases that will and will not respond to therapies as well as the identification of cases that will and

will not recur. The development and application of new therapies for the treatment of DCIS will need to be based on specific targets within DCIS if they are going to have a dramatic benefit on patient survival.

1.2.0- Introduction: Specific Background on Breast Cancer Relating to Research Question

With the development of molecular tools to detect and quantify changes in gene expression, comprehensive epidemiological data, and the availability of well characterized human cancer specimens within archives, it has become possible to advance our understanding of breast cancer by combining three fields of study that have historically stood alone. The result of this fusion of disciplines has been the emergence of hypothetical cancer progression models that attempt to relate the transition of a normal cell through various stages of transformation resulting in the formation of a cancer cell. One aim of these hypothetical models is to identify key stages or features during cancer development that may be used for prediction of clinical behavior.

1.2.1- Lesions of the Breast and Progression Model

The precise cues and signals that cause invasive breast cancer (cancer cells that have broken free from the constraints of the primary site and have begun to spread away from the primary tumor) remain for the large part unknown. But invasive breast cancer is

thought to develop over long periods of time from specific types of pre-existing non-invasive lesions. Some of the more common breast lesions, atypical ductal hyperplasia (ADH), atypical lobular hyperplasia (ALH), ductal carcinoma in-situ (DCIS) and lobular carcinoma in-situ (LCIS) have been recognized by pathologists for many years as being part of a histological continuum between normal breast epithelium and invasive breast cancer (45, 46). These specific lesions are much less common in non-cancerous breasts than those with invasive cancer (45-47). Women with a history of hyperplasias and in-situ carcinomas have approximately a 5 to 10 fold increase, respectively, in their relative risk of eventually developing invasive breast cancer (48-52).

The current morphological breast cancer progression model has been assembled from animal models of breast cancer, molecular, epidemiological and histological observations (53, 54), and attempts to relate morphological changes with molecular changes and the development of increased malignancy. This model is unproven and debated, but is widely accepted as it attempts to order the spectrum of previously identified lesions into a stepwise transition of epithelial hyperplasia (PDWA) through atypical hyperplasia (ADH) and ductal carcinoma in-situ (DCIS), to invasive carcinoma and eventually metastatic disease (FIG 3). In this model, the transition of pre-invasive DCIS to invasive disease is the best defined and single most important event in breast tumor progression. The histology of microinvasive carcinomas (invasive cancer cells measuring less than 1 mm, usually associated with and originating from DCIS), is consistent with DCIS being a precursor of invasive cancer (55). Molecular analysis of DCIS and adjacent invasive tumors further supports the hypothesis that most invasive tumors arise through evolution

of pre-existing in-situ disease (4, 56, 57). The acquisition of the invasive phenotype by ductal epithelial cells probably marks the biggest change in breast cancer biology and certainly marks the biggest threat to the patient, as it enables the development of metastatic disease.

Traditionally, breast cancer progression was thought to occur through a multi-step process that heavily resembled the model for colon carcinogenesis (58). In recent years, the multi-step model of breast cancer progression has become considered by some to be oversimplified with conceptual flaws (59). While most of the concepts regarding the morphologically defined breast cancer precursor lesions remain valid (e.g. atypical ductal hyperplasia), phenotypic and genotypic analysis using techniques such as immunohistochemistry and comparative genomic hybridization have changed the way that the breast cancer multi-step model is seen (60-63). Some no longer view the development of breast cancer as being a single pathway, but rather as a complex series of stochastic genetic events that led to distinct and divergent pathways culminating in invasive breast cancer (59).

It has only been in the last few years that there has been a focus on early stages of breast cancer as the standards and practices of clinical practice have changed. Thus the long term epidemiological and pathological history for lesions like atypical ductal hyperplasia (ADH) and atypical lobular hyperplasia (ALH) are relatively poorly understood.

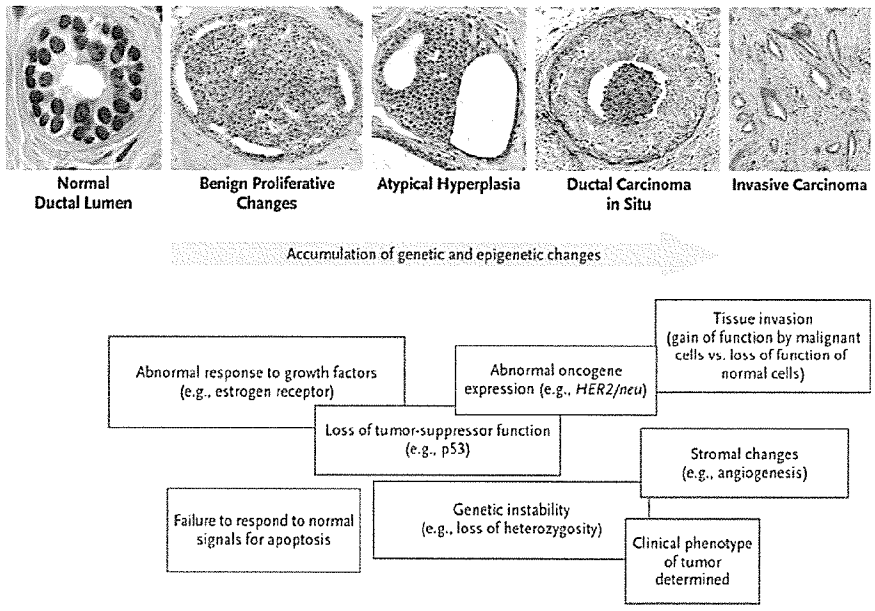

FIG 3 - Breast Cancer Progression Model. The molecular, cellular, and pathological processes that are known to occur in the transformation from healthy tissue to preinvasive lesions, such as ductal carcinoma in-situ, and leading to invasive breast cancer are shown. The majority of the changes that give rise to cancer, including the accumulation of genetic changes, oncogene expression, and the loss of normal cell-cycle regulation, appear to have occurred by the time ductal carcinoma in-situ is present. Most of the clinical features of a subsequent invasive breast cancer are already determined at this stage, although additional events, including tissue invasion and changes in the surrounding stroma, characterize the invasive tumor. Image taken from (64).

1.2.2- Is DCIS a Precursor Lesion for Invasive Breast Carcinoma?

DCIS is believed by many to be the true precursor of invasive ductal carcinoma (IDC) based on the evidence discussed above and the fact that it is frequently associated with invasive lesions and demonstrates a high but unpredictable tendency to recur as an invasive tumor if left untreated or inadequately resected (65, 66). The similarities in the histology of co-existing microinvasive carcinomas is also consistent with DCIS being a precursor of invasive cancer (55, 67). Recent comparative molecular analysis of DCIS

and invasive tumors further supports this hypothesis and confirms that most invasive tumors arise through clonal evolution from pre-existing in-situ disease (56).

1.2.3- Chances of DCIS Becoming Invasive

Ductal carcinoma in-situ (DCIS) is a noninvasive lesion that is classified as being 'high risk' because DCIS can progress to become invasive cancer by breaking free of the physical constraints that keep the cancer cells in the primary site. Estimates for the probability of this occurring vary widely. An analysis of SEER data (Surveillance Epidemiology End Data) found that 1.9% of women with newly diagnosed DCIS treated between 1984 and 1989 died of breast cancer within 10 years of diagnosis (68). However estimates such as this must be considered in the context of the prevailing therapies, which would predominantly involve mastectomy over this period. The natural history of untreated DCIS is not well understood because past and current practice for almost all women diagnosed with DCIS was and remains to be treatment with surgery as a minimum. Estimates of breast cancer recurrence in women with treated in-situ disease vary as well. In one large clinical trial, the incidence of ipsilateral invasive breast cancer among women with DCIS who had been treated by lumpectomy alone was 13.4% after 90 months of follow-up and 3.9% among those treated by both lumpectomy and radiation (33). In a retrospective review (48, 49) of 11,760 biopsies performed between 1952 and 1968, 28 cases of untreated DCIS (noncomedo type) were discovered. All were diagnosed by clinical examination, underwent biopsy treatment only, and were followed for 30 years. Of the 28 cases, 9 (32%) developed invasive breast cancer in the area of

prior DCIS. Of these, 7 cancers were diagnosed within 10 years of DCIS biopsy, and 2 within 10 and 30 years. Four of the 9 breast cancer patients eventually died of the disease. These findings have been used as an argument both for and against aggressive diagnosis and treatment of DCIS. In any case, this series came from the pre-mammography screening era and it is unknown if DCIS lesions discovered by mammography have a natural history different from those described in this series. There are no large cohorts of untreated women with mammographically detected DCIS on whom estimates of the likelihood of disease progression in the absence of treatment can be based. Also currently absent are good data based on prospective randomized trials to identify any differences in breast cancer mortality among women with DCIS who undergo different types of treatment. Based on a few studies involving cohorts of small number of patients, it is estimated that if left untreated, between 25% to 50% of all areas of DCIS will progress to form an invasive breast cancer (48, 49).

Because a significant but unknown fraction of mammographically detected DCIS cases will progress to invasive cancer, one view is that mammographic detection and treatment are beneficial. However, some DCIS cases may not progress to invasive cancer within a woman's natural lifespan, and some recurrent DCIS cases may be managed successfully if and when that progression occurs. Therefore, there exists a potential for overdiagnosis and overtreatment, since nearly all DCIS cases that were detected by screening are treated with combined modality surgery, radiation, and/or tamoxifen. The Canadian National Breast Screening Study-2 of women aged 50 to 59 found no difference in breast cancer mortality between women screened by clinical breast examination plus mammography

and those screened by clinical breast examination alone. However, 4 times as many in-situ cases were found among women in the group that included mammography relative to the group that was assessed by clinical examination (69). The fact remains that most forms of treatment for DCIS are usually very successful with a high cure rate.

1.3.0- Experimental Laboratory Models of Pre-Invasive Lesions

Several *in-vitro*, xenograft and animal models of early stages of breast tumor progression have been developed. These model systems have played an important role in demonstrating that mammary tumorigenesis progresses through defined stages and more importantly that DCIS is a precursor lesion of invasive carcinomas.

1.3.1- *In-Vitro* and Xenograft Models of Breast Cancer

As well as increasing our understanding of homeostasis, cellular differentiation and tissue organization, *in-vitro* models provide a well defined environment for breast cancer research, in contrast to the complex environment of an *in-vitro* model. A large number of extracellular matrix components are commercially available, allowing *in-vivo* like microenvironments to be recreated in a culture dish. These tissue like structures more realistically model the structural architecture and differentiated function of breast cancer than a cellular monolayer because they provide *in-vivo* like responses to stress and growth stimuli. Three-dimensional *in-vitro* models allow the study of cell-cell and cell-extracellular matrix interactions, as well as the influence of the microenvironment on

cellular differentiation, proliferation, apoptosis and gene expression (70). *In-vitro* models have the advantage that all components of the culture can be defined and human cells can be used (71). But it is becoming more evident however that it is nearly impossible to reconstitute the complex three-dimensional tissue environment with its mixture of different cell types.

Currently, only a handful of xenograft models of premalignancy for breast disease have been developed. A good model of human premalignant breast disease would lead to the formation of lesions which resemble high risk human breast disease in xenografts and sporadically progress to invasive cancer with time. Xenograft models are somewhat more physiological than 3D culture systems and they can still utilize human cells if experiments are performed in nude mice. Although several human breast cell lines will form tumors in nude mice such as MDA-MB-231, BT-20 and MCF-7 (72, 73) many more do not and none of these cell lines was established from a preinvasive lesion. Invasive cell lines established from established metastases and effusions are not necessarily representative of the biology of a preinvasive cell and even these models are not always metastatic in immune deficient mice. Conversely, cells derived from normal or benign tissue may behave malignantly when implanted into mice. This was demonstrated by the isolation of a cell line from non-neoplastic tissue that was next to a breast cancer, which was subsequently found to be highly tumorigenic and metastatic in nude mice (73). Thus, there is considerable variability in the behavior of cell lines in the context of xenograft models. Never the less, the current consensus is that the ability to form xenograft tumors is the best available indication that a cell line is malignant, and a

good model of human premalignant breast disease would lead to recognizable high risk lesions in xenografts which would sometimes progress to invasive lesions and then to generate metastases.

The well characterized MCF10 xenograft model is attractive because it encompasses all stages of mammary tumorigenesis including benign and atypical hyperproliferations, low and high grade DCIS, and invasive ductal carcinomas (74, 75). MCF10M cells were derived from a woman with fibrocystic disease (76). These cells had a normal diploid karyotype but senesced with passage. However, the cells could be maintained in medium with low calcium and eventually spontaneously immortalized variants arose which do not senesce. Each time the immortalization occurred, both an adherent and a free-floating variant were derived. The first immortalization resulted in MCF10A and MCF10F (76). MCF10A and MCF10F have been used extensively as normal immortalized breast epithelium controls for studies of human breast cancer cell lines. Both were near diploid 46,XX and shared a reciprocal translocation t(3;9) but with time additional differences became apparent (76, 77). Cytogenetic analysis reveals that the T-24 mutant (val-12) c-Ha-ras transfected MCF10AneoT cells have an additional normal chromosome 9 but no other alterations compared to MCF10A (78). A xenograft model of premalignant human breast disease which meets the criteria of forming recognizable high risk lesions in xenografts which sometimes progress to malignancy has been derived from the ras transfected MCF10AneoT cells that form unique lesions in immune deficient mice. Initially MCF10AneoT cells were thought to be tumorigenic because small lesions removed 4 weeks after injection consisted of unorganized epithelial cells (79). However,

studies in which mice carrying MCF10AneoT xenografts were observed for a longer period time revealed that the MCF10AneoT xenografts persisted, but became organized and formed simple ducts within 7–8 weeks, and only occasionally produced invasive carcinomas (78, 80). Cells established from a 100 day old MCF10AneoT lesion that had formed a squamous carcinoma did not produce carcinomas when injected back into mice (78). Rather, these cells (MCF10AT1) initially formed simple ducts which became proliferative with time. Surprisingly, these lesions now included a wider spectrum of premalignant breast lesions including atypical hyperplasia and carcinoma in-situ. Attempts to select for more aggressive variants by serial passage of cells over multiple *in-vitro/in-vivo* cycles failed, as was done to select the more highly metastatic mouse B16 melanoma variant F10. Multiple derivatives, e.g. MCF10AT3 (from third passage xenografts), and so on through 6 passages failed to produce a more aggressive form of MCF10AT. All variants produced similar lesions with a similar propensity to progress to invasive cancers. The MCF10AT model system develop into a spectrum of lesions which recapitulates those seen in human patients: benign hyperplastic lesions without atypia, atypical hyperplastic lesions, and carcinoma in-situ develop with time and approximately 25% progressing to invasive cancer within the lifespan of the xenografted mouse (78, 80). These data further support the notion that DCIS is a precursor lesion of invasive ductal carcinoma.

Another xenograft model that was specifically developed for experimentation on human DCIS involves the implantation of 2mm x 2mm x 1mm pieces of breast cancer tissue from therapeutic surgical procedures onto the back of athymic BALB/c nu/nu mice (81).

Xenografts from the majority of specimens are able to survive up to 56 days in the mice and maintain good architectural and cellular preservation. This xenograft model has been useful in studying the growth of DCIS in response to ligands and inhibitors of receptor mediated cell signaling as well as growth differences between different DCIS subtypes. ER-alpha negative DCIS cells were found to proliferate at rates 10-fold higher than ER negative comedo DCIS. Estrogen treatment of the xenografts bearing mice had no effect on the high level of cell proliferation observed in ER negative comedo DCIS xenografts. In contrast, increased levels of cell proliferation in response to estrogen supplementation were observed in ER positive DCIS xenografts. However, even with estrogen treatment, cell proliferation levels in ER positive DCIS xenografts did not reach those seen in ER negative DCIS specimens. Treatment of xenograft bearing mice with the pure anti-estrogen faslodex were compared to those treated with estrogen and untreated controls. Two weeks after implantation into mice, both the apoptotic index and proliferation index within ER negative DCIS did not differ between xenografts exposed to 17beta-estradiol or anti-estrogen treatment when compared with the controls or pretreatment values (82). In contrast, treatment of mice bearing ER positive DCIS xenografts with 17beta-estradiol raised both the apoptotic index and proliferative index. These results suggest that hormonal therapy of ER positive DCIS xenografts did not affect proliferation rates but resulted in higher apoptosis than in controls. Treating these types of xenografts with EGFR inhibitors resulted in a reduction in epithelial proliferation in tumors that were EGFR positive, regardless of ER status (83).

The mouse mammary gland is not fully developed at 3 weeks of age and it is possible to remove the pre-developed mouse mammary epithelium from the fat pad at this time. This procedure yields a ''cleared'' fat pad devoid of any epithelium. Subsequent engraftment of mouse mammary epithelial cells before puberty yields an anatomically normal functional mammary gland that lacks only connections with the nipple. The successful outgrowth of the engrafted mouse mammary epithelial cells indicates that the systemic hormones present during puberty work together with the stroma of the cleared fat pad to provide all of the signals that are required for normal epithelial morphogenesis. Transplantation of human mammary epithelial cells in to the cleared fat pad of immuno-compromised mice requires co-transplantation of irradiated human fibroblast cells to produce the correct microenvironment (84). Normal breast architecture could be recreated in the mouse mammary gland using normal human breast tissue from reduction mammmoplasty. In one xenograft experiment using presumed normal tissue from a woman in her 20's, DCIS as well as invasive carcinoma was found to develop in the mouse (84). This observation supports the notion that occult preneoplastic or neoplastic cells exist in breast tissues from young and middle-aged women who have not been diagnosed for breast cancer or in tissues obtained from reduction mammoplasties (47, 85-87).

1.3.2- Transgenic Mouse Models of Breast Cancer

Of the currently established animal models, mice have the advantage of easy genetic manipulation and a well characterized genome. Unfortunately, mouse mammary glands

do not closely resemble the architecture and histology of the human mammary gland. Mice lack the physiological concentration and fluctuation of hormone levels that are known to be important in human breast cancers. This hormonal difference between mice and humans is also reflected by the absence of ER-alpha positive tumors in mice, a phenotype characteristic of two thirds of human breast cancers (88). Also, the mouse mammary gland appears to be particularly susceptible to tumorigenesis as indicated by the high frequency of mammary hyperplasias in transgenic and knockout mouse models (89, 90).

Mice with targeted expression of the SV40 T antigen in the mammary epithelial cells develop mammary in-situ carcinoma with some tumors progressing to develop into invasive carcinomas after a period of latency (91). The C3(1)/Tag transgenic mouse model shares many important characteristics with human breast cancer. The progression of mammary tumor development follows a predictable time course where low grade mammary intraepithelial neoplasia arises at about 8 weeks of age, progresses through DCIS and advances to palpable invasive adenocarcinomas after about 20 weeks of age in 100% of female mice (92). This model is based on the ability of the 5' flanking region of the C3(1) component of the rat prostate steroid binding protein (PSBP) to target expression of the SV 40 large T antigen (Tag) to the mammary epithelial cells. The WAP (whey acidic protein) and MMTV (mouse mammary tumor virus) promoters are other 'mammary specific' promoters that have been used to target gene expression to mouse mammary epithelial cells. Transcriptional activity of the MMTV and WAP promoters is often dependent on and highly responsive to pregnancy or administration of

hormones (93, 94). Pregnancy dependent transgenic models of mammary cancer are not similar to human breast cancer where pregnancy has been identified most often as a protective factor. This suggests that transcriptional activity of MMTV or WAP tend to be higher in mammary epithelial cells that are hormone stimulated and differentiated. These promoters are not well suited to study the influence of hormones on mammary oncogenesis since hormones will modulate the levels of transgene expression. In addition, expression driven from the MMTV promoter is often sporadic through out the mammary gland (95). Many other oncogenes such as myc (96), ras (97), HER2/neu (98), Polyoma middle T (99), and Wnt-1 (100) have been expressed in the mouse mammary gland to study cancer development and progression. Tumor suppressor genes such as p53, BRCA1, Rb have all had their expression knocked out in the mouse mammary epithelial cells in an attempt to form lesions which are then studied to infer information regarding human breast cancer. However these models mostly lack a stage where tumor development passes through a true pre-invasive phase.

Chemically induced mammary tumors in rats more closely resemble human disease regarding both pathologic stages and phenotypic features (101). Development of mammary tumors in rats is similar to humans regarding ovarian hormone dependence (102). Copenhagen rats (a particular strain of rats) are resistant to mammary carcinogenesis, which suggests that invasive carcinomas develop from in-situ lesions, because these rats do not develop in-situ lesions and no invasive tumors are ever detected (103). The disadvantage of using rat models is that they are much less amenable to genetic manipulation than mice and chemical carcinogens are likely to introduce multiple

genetic alterations that are not easily identifiable and may not be relevant to human disease.

2.1.0- Specific Background on Project

The goal of mammographic screening programs is to detect breast cancer at an earlier and more treatable stage. Many of the lesions detected now represent either very small invasive tumors or DCIS. This makes prediction of the tumor's future behavior more difficult because many of the established old parameters used for prediction (tumor grade, size, nodal status, hormone receptor status and S-phase fraction (104)), have become much less meaningful as indicators of biological potential. A decision on how to treat the tumor must now rely on tissue-based markers. For patients with lesions that have not yet acquired invasive properties and very small lesions that have not yet spread to the lymph nodes, the discovery of tissue based biomarkers to predict the risk of progression and recurrence is needed to define those who would benefit from further treatment and those who would not.

This laboratory has previously taken a direct approach to identify genetic alterations relevant to these small and early lesions, and specifically those that might be relevant to the invasive phenotype in human breast cancer, using microdissection and molecular techniques. This has led to the identification of the S100A7 gene (also named Psoriasin) as being one of the most highly expressed genes in pre-invasive ductal carcinoma in-situ (DCIS) (105, 106). Several other groups have independently confirmed this observation

at both RNA and protein levels using newer RNA and proteomic screening techniques (107, 108). The expression profile of S100A7 also appeared to change with the transition to invasive disease, suggesting that it could have a functional role in early breast tumor progression.

Our approach to identify genes important in pre-invasive cancer differed from that which had previously been employed by other groups. Several genes were already described as having altered expression in cancer, but these genes (e.g. overexpression of EGFR and HER2, mutated p53) were identified from invasive carcinoma and not DCIS. As well, their importance in DCIS was only inferred. Our belief was that unique aspects about DCIS would not be uncovered by studying invasive cancer.

Our over-riding hypothesis is that "S100A7 influences progression of breast cancer through a direct impact on the breast epithelial cell." My initial goal was to test this hypothesis by attempting to identify interacting proteins in breast cells that might shed light on a mechanism of action. In the initial phase of my work we found the ubiquitously expressed Jab1 protein to specifically interact with S100A7. This stimulated a series of experiments in the second phase to understand the consequence of this interaction and to begin to understand the importance and relationship of S100A7 and Jab1 expression in breast cancer. Several specific issues emerged from the initial studies and formed the basis of several avenues of exploration. A systematic survey of S100A7 expression in breast cancer would need to be conducted, as we did not know if S100A7 was differentially expressed during progression in occasional, many, or most tumors. We also

did not know if altered expression of this gene was a primary or secondary consequence of the malignancy process, so experimental models and assays would need to be constructed. Finally the ability of S100A7 to influence some or all of the many potential activities of Jab1 and to modify breast cancer cell biology became the central theme for the experimentation on S100A7.

The following sub-sections provide some of the specific background to the current status of knowledge of molecular alterations in DCIS, the S100A7 gene in the context of the S100 gene family, and the Jab1 gene to help the reader to understand the rationale behind the experiments in the subsequent Results section.

2.1.1-Molecular Alterations of DCIS

A handful of molecular markers have been identified whose expression is associated with breast tumorigenesis. The ER alpha (ERα) is normally expressed at very low levels by normal luminal breast epithelial cells, but its expression is dramatically elevated in over 70% of ductal carcinoma in-situ lesions (109, 110). The HER2/neu proto-oncogene is overexpressed in roughly half of all ductal carcinoma in-situ lesions but not in atypical hyperplasia (111). The p53 tumor-suppressor gene is mutated in approximately 25% of all ductal carcinoma in-situ lesions, but is rarely mutated in normal or benign proliferative breast tissue (112). The frequency these molecular markers are expressed in ductal carcinoma in-situ in general mirrors their expression in invasive breast cancers.

Investigation into the molecular composition of DCIS has been dependant on the development of methodological approaches. Loss of heterozygosity (LOH) studies have identified numerous chromosomal regions where recessive oncogenes relevant to breast cancer may be located (113). The vast majority of these studies however, were not reproducible between observers and did not result in the identification of a specific important gene in breast cancer whose expression was lost due to chromosomal changes. Studies on the loci that eventually revealed the PTEN gene may be a rare exception to this statement. The development of numerous antibodies to measure gene expression by immunohistochemistry is another important ancillary technology. But until recently it was only possible to study limited numbers of tumors by immunohistochemistry. This has changed with the development of tissue microarrays (114, 115) which has enabled comparable scales of analysis to those of high throughput DNA microarrays (116) and the examination of hundreds of individual tumors in one small experiment. Our knowledge about the molecular composition of DCIS will continue to evolve as new techniques are developed.

The expression of prognostic molecular markers has been found to be associated with pathological assessment of DCIS. The gene expression profile of High grade DCIS is different from that of Low grade DCIS and exhibits a greater overall genetic change from normal breast tissue. More than 90% of Low grade DCIS lesions are positive for ERα, and less than 20% exhibit overexpression of HER2/neu or p53 mutations. In contrast, overexpression of HER2/neu or p53 mutations arise in two thirds of High grade ductal carcinoma in-situ lesions, whereas only one quarter express estrogen receptors. Most of

the clinically relevant features of breast cancer, such as hormone receptor status, level of oncogene expression and histological grade are most likely determined by the time DCIS has evolved to invasive disease (23, 117-119). This implies that invasive breast cancer may be explained or caused by the heterogeneous features of the precursor DCIS lesion.

Although the initiating steps and specific pathways of breast tumorigenesis remain poorly described, it appears that nearly all invasive breast cancers arise from in-situ carcinomas. The presence of shared chromosomal changes that are present in both DCIS and adjacent invasive cancers demonstrates their clonal and presumably evolutionary relationship (120, 121). Loss of heterozygosity is noted in more than 70% of high-grade ductal carcinomas in-situ, as compared with 35 to 40% of cases of atypical hyperplasia and 0% in specimens of normal breast tissue (61, 122, 123). Low and intermediate grade DCIS and IDC show frequent LOH of 16q, while LOH of 17p, 17q and gains of 8q and 17q22 are often found in high grade lesions (56, 124-126). The target genes of all these chromosomal changes remains to be identified.

The most dramatic changes in patterns of gene expression during breast tumorigenesis appear during the transition from normal tissue to ductal carcinoma in-situ. Several studies have identified changes in gene expression in DCIS in the hope that they may be used as molecular markers. When compared to different groups of DCIS, normal mammary epithelial cells showed the most distinct and least variable gene expression profiles (127). In addition, very few genes were universally upregulated in all tumors regardless of their stage and histological grade, indicating a high degree of diversity at

the molecular level that likely reflects the clinical heterogeneity characteristic of breast carcinomas. Tumors of different histology type had very distinct gene expression patterns and no genes seemed to be specific for metastatic or for in-situ carcinomas (127-129).

Several studies have found the gene expression profile of DCIS to be very similar to that of adjacent invasive cancer (127-131). Genes that are uniquely associated with invasive cancer have not been identified. This suggests that many of the cellular events that are specific for cellular transformation of breast cells must occur during or before the formation of DCIS (129). Different tumor grades are associated with distinct transcriptional signatures and tumor grade is linked across the DCIS to IDC stage transition. This has also been demonstrated by the detection of measurable changes in the expression of genes related to adhesion, cell motility and extracellular matrix composition that occur as DCIS evolves into invasive carcinoma. In general, High grade DCIS lesions and High grade invasive carcinomas are more frequently estrogen and progesterone receptor negative, have HER2 amplification or overexpression of the receptor and decreased Bcl-2 protein levels. Individually and cumulatively, these changes in gene expression in High grade DCIS may contribute to higher proliferation and/or lower apoptosis rates compared to Low grade DCIS (132-134). The pathologically discrete stages of DCIS and IDC of breast cancer are highly similar to each other at the level of RNA expression (127) and the transcriptome (129). Therefore, it would appear that relatively few genes have alterations in their level of expression at the transition to invasive disease and no single gene or group of genes has been implicated as being the central controlling factor for the invasive mechanism. This finding supports the idea that

the distinct stages of progression are evolutionary products of the same clonal origin, and that genes conferring invasive growth are mostly active in the preinvasive stages.

However, given the very limited study of DCIS that has been conducted to date, it is still an open question that some unique alterations may exist within DCIS. For example, one physiologic factor that may contribute to unique differences between DCIS and both normal tissue and invasive cancer and that is also emerging as being important in the direct regulation of gene expression in cancer, is the presence of hypoxia. Hypoxia is generically assessed by the presence of necrosis, and while this can occur within invasive tumors, it is very common in DCIS and as described above, and is the hallmark of high grade DCIS. Therefore it is relevant that DCIS lesions having necrosis were found to have a different genetic expression profile when compared to DCIS without necrosis (130). A popular hypothesis is that hypoxic upregulation of genes is important in promoting an enhanced biological behavior, and this notion is therefore consistent with these observations and the known fact that DCIS lesions with necrosis (hypoxia) are more likely to progress to invasive disease (25) and be more clinically aggressive.
The classical approach to identify genes thought to be important in breast cancer was to compare invasive carcinoma with normal tissue. This yielded some genes (ER, HER2, EGFR) that are slowly emerging as useful therapeutic targets by virtue that they are over-expressed in the cancer state. Several therapies have been developed for each of these proteins and there has been encouraging results based on their use in the treatment of invasive carcinoma. Currently, there are several clinical trials testing the utility of these agents in the treatment of DCIS. The problem with this classical approach is that it has

not given us any new unique tools to treat the distinct stage of disease that is DCIS with the ultimate aim of preventing the development of invasive disease.

2.2.0- The S100 Family of Proteins

The S100 gene family is composed of at least 20 members that share a common structure defined in part by the Ca^{2+} binding EF-hand motif (Table 1, FIG 4). These genes which are expressed in a discriminate fashion in specific cells and tissues, have been described to have either an intracellular or extracellular function, or in some cases both. There is a relatively short but increasing list of reports describing regulatory roles for the S100 protein family in both the intracellular and extracellular compartments (135-138). S100 proteins are implicated generally in the immune response, differentiation, cytoskeleton dynamics, enzyme activity, Ca^{2+} homeostasis and growth. A potential role for S100 proteins in neoplasia stems from these activities and from the observation that several S100 proteins have altered levels of expression in different stages and types of cancer. While the precise role and importance of S100 proteins in the development and promotion of cancer is poorly understood, it appears that the binding of Ca^{2+} is essential for exposing amino acid residues that are important in forming protein-protein interactions with effector molecules. The identity of some of these effector molecules has also now begun to emerge, and with this the elucidation of the signaling pathways that are modulated by these proteins. Some of these interactions are consistent with their diverse functions. Others suggest that many S100's may also promote cancer progression through specific roles in cell survival and apoptosis pathways as significant findings have

been made to suggest that S100 proteins can enhance cancer progression by stimulating signaling pathways known to be important in cell survival (136, 139, 140).

Table 1. S100 Family Members

Gene Name	GenBank #	Gene Map Locus	Function in Cancer
S100A1	BC014392	1q21	activation of RAGE
S100A2 (S100L)	BC002829	1q21	inhibition of tumor cell motility
S100A3 (S100E)	BC012893	1q21	
S100A4	BC016300	1q21	tumor promoting activity by inhibiting p53
S100A5 (S100D)	Z18954	1q21	
S100A6 (calcyclin)	BT006965	1q21	modulation of calcium signaling that regulates the cell cycle
S100A7 (psoriasin)	BC034687	1q21	stimulates activity of Jab1, chemoattractant for CD4+ cells
S100A8 (calgranulin A)	BC005928	1q21	
S100A9 (calgranulin B)	BC047681	1q21	
S100A10	BC015973	1q21	
S100A11 (S100C)	BC001410	1q21	inhibition of tumor cell motility
S100A12	D49549	1q21	activation of RAGE
S100A13	BC000632	1q21	release of fibroblast growth factor-1
S100A14	BC005019	1q21	
S100A15	NM_176823	1q21	
S100B	BC001766	21q22.2-q22.3	inhibition of microtubule assembly, activation of RAGE
S100P	BC006819	4p16	
S100Z	AF437876	5q14.1	

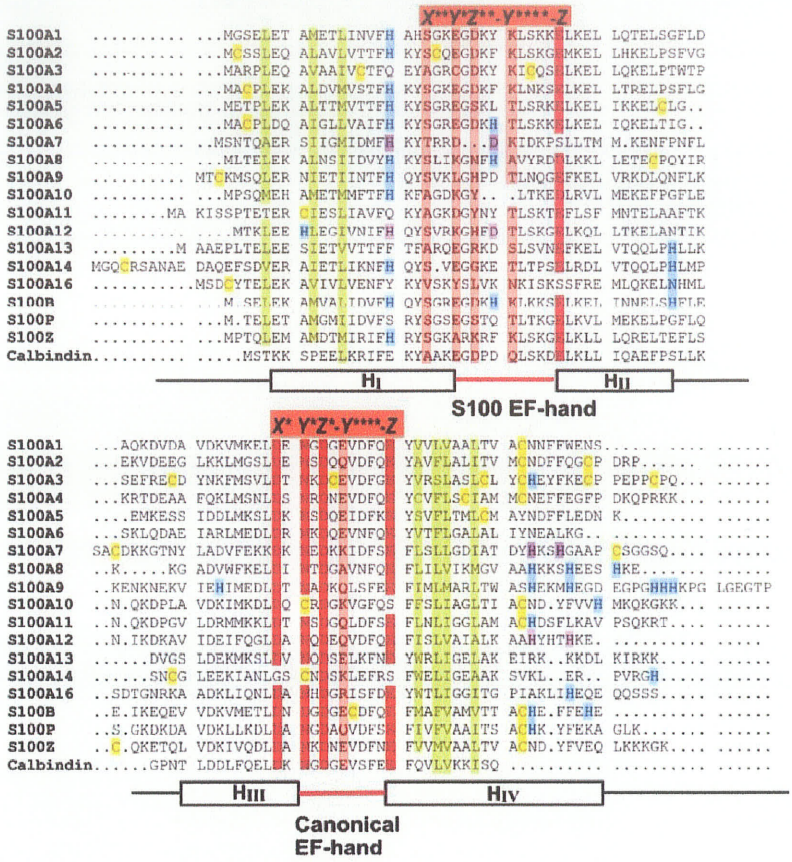

FIG 4- Multiple Sequence Alignment of Human S100 Proteins. The Ca^{2+}-coordinating residues are highlighted in dark red (side chain coordination) and light red (backbone oxygen coordination). The Zn^{2+}-coordinating residues in S100A7 and the Cu^{2+}-binding site in S100A12 are highlighted in magenta. Hydrophobic residues that are essential for dimerization are highlighted in green. Residues that are putative Zn^{2+} ligands in other S100 proteins are highlighted in yellow (cysteine) and blue (histidine). Image taken from (141).

The S100 family of proteins are low molecular weight proteins, ranging in individual size between 9 and 13 kDa. However most S100 proteins can form hetero- and homodimers which are thought to be important for generating their active form (136). The 20 plus members of the S100 protein family are only expressed in vertebrates but not all S100's are expressed in all cell types (142). This implies that different S100's have different

functions and that these roles are not redundant for a common S100. In apparent contrast to this assumption, there are examples of different S100's interacting with the same target protein, but this mostly occurs in different cell types (136). When considering their function, a central feature is the calcium binding capacity of all S100 proteins. The N-terminal portion of these proteins typically possess imperfect Ca^{2+} binding EF-hand motifs (helix-loop-helix domains), sometimes referred to as a half EF-hand. Not surprisingly, if Ca^{2+} binds to this portion it is only with a relatively weak affinity. On the other hand, the C-terminal portion has a more complete EF-hand domain which is better conserved across different proteins and confers 100 times greater binding affinity to Ca^{2+} as compared to the N-terminal portion (135). Ca^{2+} binding by S100 proteins is thought to be important for their functional activity. For review see (135). Separating the EF-hand domains is an intermediate region known as the hinge region and following the C-terminal EF-hand region is a stretch of amino acids referred to as the C-terminal extension. Together, the hinge and C-terminal extension are the most variable regions between the different S100 members and consequently may confer the unique biological activities manifested by different S100's. For a more detailed review of S100 protein structure see reference (135).

2.2.1- S100 Expression in Cancer

Several S100 proteins have been implicated in the process of cancer by virtue of the observation that they have altered levels of expression in cancer cells compared to normal cells. The current list of S100's over-expressed in cancer includes S100A4, S100A6,

S100A7 and S100B. S100A2 has also been found to be differentially expressed between transformed and normal cells, but its alteration is manifested in a decrease rather than increase in expression in cancer cells as compared to normal cells. Elucidation of the mechanisms of action of these S100's and the functional implications of their altered expression remains to be resolved. However, several studies have demonstrated that over expression of S100 proteins may have clinical implications for diagnosis and staging of human tumors, and for prediction of prognosis.

2.2.2- S100B

This is the most widely studied member of the S100 gene family. It is particularly important in neurodermally derived tissues and pathologies, where it has been found to be overexpressed in malignant melanoma (143), anaplastic astrocytomas (144) and glioblastomas (145). While the function of S100B expression remains unknown, the presence of the protein in serum of melanoma patients has been proposed as a marker of the response to chemotherapy (146). S100B forms interactions with Annexin II (147) and p53 (148). Also, in common with S100A4, S100B is thought to have a functional role in modifying the activity of p53 and so contributing to cancer progression by inhibiting apoptosis (149). But a role for S100B in apoptosis is still up for debate as other groups have found S100B contributes to the induction of apoptosis (150, 151). In melanoma, S100B is also thought to increase the activity of the Ndr kinase, on the basis of the observation that S100B and Ndr kinase activity have been positively correlated (152). An alternative pathway of action that has been proposed for several S100 proteins is via

interaction with the cell surface receptor RAGE (Receptor of Advanced Glycation of End Products) (153). Since many S100 proteins are secreted, RAGE may offer a common pathway for extracellular S100 action. While functional evidence to support this concept remains to be gathered for many S100's, in neuronal cells S100B causes nuclear translocation of NF-κB via RAGE dependant activation of Ras/MAPK and cdc42/Rac pathways (153). This is thought to promote cell survival by increasing the expression of the anti-apoptotic protein Bcl-2.

2.2.3- S100A2

This gene is typically down regulated in carcinomas compared to normal tissues and this has been shown to occur in breast (154), prostate (155) and lung tumors (156). Primary cutaneous melanomas were found to be positive for S100A2, whereas metastases or benign naevi appeared negative (143). Nevertheless, S100A2 has been hypothesized to be a potential tumor suppressor and down regulation of the gene is thought to occur primarily via hypermethylation of the promoter at CpG sites (157). S100A2 may exert a similar but opposing function to S100A4. In human head and neck squamous cell carcinoma lines, forced 're-expression' was found to exert an inhibitory influence on cell motility which was attributed to effects on polymerization/depolymerization dynamics of the actin microfilamentary cytoskeleton (158). S100A2 was also found to negatively regulate the motility of certain RAGE-expressing cell lines (158), although a direct interaction with RAGE has yet to be proved.

2.2.4- S100A4

Also known as Mts1 and p9Ka, S100A4 is the best characterized in terms of having a role in cancer. It was first described to be an mRNA up regulated in a rodent model of mammary metastasis (159). It was then shown that S100A4 expression in a murine model could encourage the development of lung metastasis from the mammary gland tumors (160, 160, 161). S100A4 expression has been reported in several diverse cancer types such as breast (162), colorectal (163), gastric (164), medulloblastoma (165), prostate (155) and bladder (166). A transgenic mouse model for S100A4 has also been generated where protein production was targeted to the mammary gland under control of the Mouse Mammary Tumor Virus (MMTV) promoter. Protein expression did not result in the spontaneous formation of mammary tumors. When the S100A4 transgenic mouse was crossed with a neu transgenic mouse, harboring a neu oncogene also targeted by MMTV to the mammary gland, it was found that S100A4 enhanced the development of metastasis from mammary tumors in the offspring (167).

The implication is that this S100 may not play a role in the instigation of tumor development but can synergize with altered growth factor pathways to promote tumor progression. Consistent with this conclusion is additional data that suggests a specific role in invasion. For example, inhibition of S100A4 by antisense RNA in a highly metastatic cell line can result in a decrease in cell motility and invasiveness *in-vitro* (168). The mechanism of action for S100A4 is largely unknown although there have been several interacting proteins identified that may give clues to its metastasis promoting properties. For example, several proteins involved in cellular architecture and the

cytoskeleton have been shown to interact with S100A4, including F-actin (169), myosin (170) and non-muscle tropomyosin (171). S100A4 has also been described to have a role in the polymerization of tubulin in melanoma cells (172).

In addition to interactions that may impact on the cytoskeleton, the tumor suppressor protein p53 has also been found to interact with S100A4. One consequence of this interaction is that phosphorylation of p53 by protein kinase C is inhibited. But similar *in-vitro* inhibition by another phosphorylating kinase, casein kinase II does not occur (173). S100A4 binding to p53 may also interfere with the DNA binding activity of p53 *in-vitro*. A down regulation of transcription for some p53 target genes such as p21/WAF, thrombospondin-1, and mdm-2 has been observed upon S100A4 induction in cells expressing wild type p53. However, in other experimental systems, expression of the pro-apoptotic and p53 regulated gene Bax, was found to be induced upon S100A4 expression. This latter observation underlies the view that S100A4 may exert part of its effect on tumor progression by cooperation with wild type p53, enhancing p53-dependent apoptosis which might accelerate the loss of wild type p53 function in tumors (173). However an alternative view is that S100A4 may in fact bind to and sequester p53 in the cell cytoplasm, inhibiting p53 nuclear functions (174).

2.2.5- S100A6

Also known as calcyclin, S100A6 has been extensively studied in systems other than cancer. It is thought to play several different roles depending on the cell type it is

expressed in. The majority of work has been centered on expression in normal neuronal cells. S100A6 is normally expressed in the G1 phase of the cell cycle in neuronal cells. Upon retinoic acid-induced neuroblastoma cell differentiation, S100A6 mRNA was found to be induced, suggesting another facet of transcriptional regulation. S100A6 was also found to regulate cell-cycle progression in these cells (175). However other functions attributed to S100A6 range from regulating pulmonary fibroblast proliferation (176) to the Ca^{2+}-dependent release of insulin from pancreatic beta cells (177).

Increased expression has been reported in several types of cancer such as colorectal (178), hepatocellular carcinoma (179) and malignant melanoma (180). S100A6 has been found to interact with a spectrum of proteins tropomyosin (181), Annexins II (182) and XI (183), glyceraldehyde-3-phosphate dehydrogenase (182) and caldesmon (184). The consequence of these interactions and their impact on S100A6's functional importance in cancer remains for the most part unknown.

2.2.6- S100A7

This was the first S100 protein to have its crystal structure solved (185) and based on amino acid sequence, S100A7 is the most unique (FIG 5) protein amongst the S100 protein family (141, 186). S100A7, also known as Psoriasin, was first described to be an mRNA highly expressed in keratinocytes derived from psoriatic skin (187). The protein was found to be intracellular as well as secreted. In skin, expression of S100A7 mRNA detected by in-situ hybridization is restricted to epithelial cells and is not detected in

stromal cells such as fibroblasts, lymphocytes, or endothelial cells. However the protein can be found in granulocyte extracts which has suggested that its overexpression and secretion by psoriatic keratinocytes might be linked to the inflammatory component of psoriasis. The link between inflammation and S100A7 was further strengthened when it was found to be chemotactic for CD4+ T-cells and granulocytes *in-vitro* (188).

The S100A12 protein, like S100A7, has also been found to act as a chemotactic protein for T-cells. The receptor mediating this activity of S100A12 has been identified as RAGE (Receptor for Advanced Glycation of Endproducts) (189). Inhibiting the activity of RAGE in neural cancer cells was found to suppress metastases in both implanted tumors and tumors developing spontaneously in susceptible mice (190). However, molecular profiling of several tumor types, including breast, found S100A12 was not significantly expressed (191), suggesting that if RAGE acts to promote breast tumor progression, its activation is probably through binding of ligands other than S100A12.

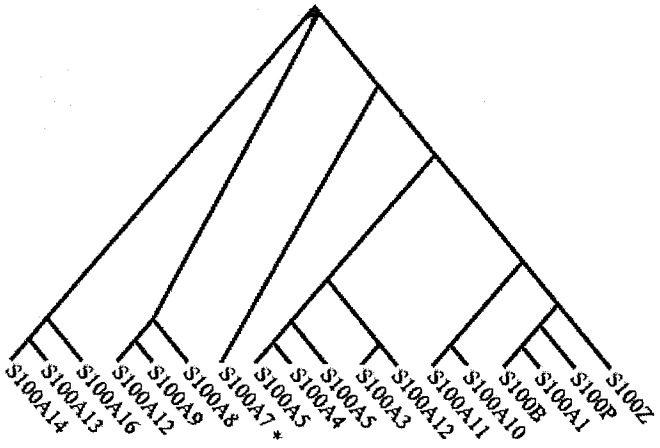

FIG 5- Phylogenetic Tree of Human S100 Proteins. The construction of the phylogenetic tree was based on multiple sequence alignments obtained with ClustalW. For clarity no relative distances between the different S100 proteins are shown. The tree divides into four major branches which comprise evolutionary related S100 proteins. Image taken from (141).

S100A7 expression is predominantly associated with highly specialized or abnormal forms of squamous epithelial cell differentiation in both non-neoplastic and neoplastic pathologies in diverse organs including skin, lung, head and neck, and cervix (192) and bladder (193). For example, in normal skin, S100A7 is rarely detected in epidermis but can found to be expressed in underlying adnexae. In skin pathologies, S100A7 was frequently expressed in abnormal keratinocytes in actinic keratosis, in-situ and invasive squamous cell carcinoma, but was rarely observed in superficial or invasive basal cell carcinoma subtypes (194). However additional factors to differentiation are clearly involved in determining S100A7 expression since even across the continuum of development of squamous carcinoma, the highest levels of expression were seen within the in-situ stage compared to the preceding and subsequent stages of actinic keratosis and invasive disease.

Despite this prominent linkage to squamous differentiation within tumors, S100A7 has also been found to be expressed in some non-squamous tumors including gastric cancer (195), and in breast cancer, where expression may relate to distant 'embryological connections'. In breast, S100A7 was first found to be differentially expressed at higher levels in primary breast cancer compared to nodal metastasis or normal tissue (107). However subsequent studies suggest that it is predominantly expressed in the pre-invasive in-situ component of primary breast cancer, and that it is in fact one of the most abundantly expressed genes in ductal carcinoma in-situ (105, 196).

Subsequent molecular analysis has shown S100A7 expression in breast tumorigenesis mirrors the expression profile seen in skin. Expression is absent or almost undetectable in normal breast epithelial cells. The frequency of expression then increases in lesions associated with increasing risk of progression to invasive cancer, with its highest level of expression seen in high grade ductal carcinoma in-situ (DCIS) (105). The frequency and level of expression then drops in invasive carcinoma. The reason for the typical pattern with a peak in expression within preinvasive lesions and subsequent decrease in expression in invasive disease for both skin and breast remains unknown. However, the work described below may offer some clues to this peculiar profile and its role in this critical stage in tumor progression.

The S100A7 protein product is found to be nuclear and cytoplasmic, as well as secreted in breast tumors (106). The relative significance and contribution *in-vivo* of the several regulatory factors that are now emerging remains to be deciphered. but it has been shown in breast cancer cell lines that loss of attachment to extracellular matrix, growth factor deprivation, and confluent conditions can up-regulate S100A7 expression (196). Retinoic acid was found to induce expression in human skin cells *in-vitro* and *in-vivo* (197). In the MCF7 breast cell line, expression was also induced by estradiol treatment (107). This finding may identify a relationship with steroid hormone action, however the net effect is unclear as *in-vivo* S100A7 expression is highly correlated with the ER negative phenotype (106). Subsequent studies suggest that S100A7 may be expressed to some degree in up to 50% of ER negative tumors. Furthermore, in this subset of invasive ductal

carcinomas expression can also be associated with a shorter time to recurrence and poorer patient survival (198).

It is possible that S100A7 has several functions depending on the cellular context and predominant localization of expression. For example, in cultured skin cells, S100A7 has been found to associate with and serve as a substrate for transglutamases (199) and epidermal fatty acid binding protein (200). Observations on the context of induction of S100A7 expression, both *in-vitro* in cell lines and *in-vivo* within breast tumors where S100A7 is related to loss of substrate adhesion, also suggest a possible role in response to cellular stress leading to anoikis (196, 201).

2.2.7- S100 Proteins and Activation of Pro-Survival Pathways in Cancer

Although the S100's share a high degree of sequence homology, they are very distinct in terms of their tissue distribution and the biochemical pathways that they modulate. A significant finding relevant to the possible mechanism of action of extracellular and secreted S100's is the identification of an interaction with RAGE and activation of the relevant signaling pathways. Expression of RAGE was found in breast and lung tumor tissues where abundant S100A4 and S100A6 expression was also observed (191) although a direct effect of S100 proteins on RAGE activity and downstream pathways has yet to be shown, inhibition of RAGE signaling is able to inhibit tumor growth (190). Confirmation of the notion that all S100's can activate RAGE needs further experimentation. Nevertheless, the idea opens the door for targeted therapeutic

intervention to interfere with S100 action at the cell surface by blocking RAGE directly. It also raises the concept that some of the downstream effects of extracellular S100 action may occur through altered RAGE signaling that is known to influence NF-κB and pro-survival pathways.

However, many S100's are also found in intracellular compartments and probably also exert a different action at these sites. Since these proteins appear to have no catalytic activities of their own, it is likely that they modify the activity of other proteins.

Amongst the several intracellular interactions attributed to S100's, one of the more intriguing is the interaction with the tumor suppressor protein p53. In some cases the result of the interaction is that p53 can no longer bind to target sites in the promoter regions of genes and activate gene transcription. Several of these p53 responsive genes can be classified as pro-survival in their effects. In other cases the interaction is thought to result in sequestration of p53 in the cytoplasm which will not allow the cell to initiate apoptosis. This effect on p53 is hypothesized to lead to selection of p53 mutant containing tumor cells by virtue of their ability to evade signals that initiate apoptosis. These particular cancer cells are then presumed to thrive within heterogeneous tumor cell populations due to their growth advantage, ultimately resulting in a more aggressive tumor. To advance this hypothesis further, it will be necessary to account for several unresolved discrepancies such as the observation that the p53 responsive gene Bax is induced upon addition of S100A4. This could be due to other regulatory factors acquiring a dominant function or to the variations between cell types and model systems used in

different studies. Regardless of S100A4's interaction with p53, S100A4 seems to also demonstrate a consistent cellular role in the acquisition or promotion of invasive properties. This is most likely due to an interaction with proteins other than p53. The demonstration of interactions with cytoskeletal proteins and an alteration in cytoskeletal dynamics emphasizes the point that S100's can interact with several different proteins in different locations of the cell.

2.2.8- S100A7 Expression in Breast Cancer and Potential Biological Importance

In comparison with the other members of the S100 gene family, S100A7 is less studied but perhaps the most unique both in terms of structure (186) and in terms of a prominent association with preinvasive carcinoma. This gene was originally named Psoriasin because it was first identified as a highly expressed secreted protein in abnormally differentiated keratinocytes from psoriatic lesions (187). It was later found to be located within the S100 family gene cluster of chromosome 1q21, and has since been shown to be a true S100 family member (135). It has since been found to be expressed in association with neoplasia in several tissues including squamous carcinomas of the head and neck, cervix, lung, (192) skin (194), bladder (193), as well as adencarcinomas of the stomach (195) and breast (105-107, 196). Some of these expression data are consistent with a role as a chemotactic factor in mediating the inflammatory response, similar to that initially postulated in psoriasis (188). But other data point to an additional intracellular action within epithelial cells that express the protein, namely that the protein can be

localized to the cytoplasm and nucleus. From study of S100A7 expression at different stages of progression in both skin and breast, it is clear that while the protein is not generally expressed in normal epithelia, increasing frequency of expression is seen beginning with early stages of progression (105, 194). S100A7 is expressed in lesions such as hyperplasia and atypical hyperplasia, but is particularly prominent in preinvasive carcinoma in-situ. In some pre-invasive ductal carcinoma in-situ samples, S100A7 has even emerged as amongst the most highly expressed genes using relatively unbiased SAGE assays to determine relative global expression levels (127). Intriguingly, expression of S100A7 is then often down-regulated with progression to invasive carcinoma (105, 194). This is a dominant feature of individual lesions where both preinvasive in-situ (DCIS) and invasive components can be directly compared, but is also reflected in a lower frequency of expression in invasive carcinomas (194, 202).

This pattern could indicate a primary role in mediating this stage of progression or a bystander event associated with a change in the requirement for this protein. S100A7 expression may contribute to the onset of the invasive phenotype within the context of the breast duct but selection pressures might change in the foreign microenvironment of the stroma, such that S100A7 function may become redundant or less important for success or survival. S100A7 may be due to genomic or gene regulation changes within individual cells or cell selection. Although the 1q21 chromosomal locus has been fingered by early cytogenetic and loss of heterozygosity studies as commonly altered in breast tumor progression (203), S100 genes and S100A7 have yet to be linked to specific amplification, mutation or other genomic events in tumors (196). As noted above

relatively little is known about the regulation of S100A7, but diverse stress stimuli are implicated in both breast and skin systems, including UV stimulation, serum depletion, and loss of substrate attachment (196), that may be mediated in part through estrogen and/or retinoic acid receptors or AP-1 (107, 197, 204). Certainly these are factors that are prominent within the neoplastic breast duct, where there is increasing hypoxic stress and disruption of cellular polarization and basal attachment, but these factors are less evident in the stroma.

To resolve the possible role of S100A7 as a primary factor or as a bystander in early tumor progression, several additional factors can be considered. These include the relationship between S100A7 expression and specific tumor pathologies, parameters and cellular factors, the relationship with clinical outcome, and the biological effects of S100A7 when expressed in breast cells in the laboratory. It is clear that one of the most intriguing facets of S100A7 expression is its strong association with the absence of estrogen receptor (ER) expression. Earlier studies documented a very strong association with ER negative carcinomas (106). Subsequent studies confirmed this association but also showed expression at lower frequencies in ER positive tumors (196).

In cell lines S100A7 has been shown to be constitutively expressed at high levels in some ER negative breast carcinoma lines (127) or induced by stress (196), but is induced by estradiol in ER positive MCF7 cells (107). ER positive status is both the hallmark of a distinct differentiation pathway phenotypic subgroup and also an indicator of a tumor that can respond to estrogen with the accompanying induction or repression of a subset of

specific estrogen responsive genes. But the basis for recognition of ER positive status is in need of reassessment with the recognition of a second ER, Estrogen Receptor Beta. While estrogen can induce expression of S100A7 *in-vitro* and *in-vivo* in ER positive cell lines and tumors, other differentiation related factors might dominate and lead to highest levels of expression and functional importance in both preinvasive and invasive ER negative tumors.

2.2.9- Summary of S100 Expression in Breast Cancer

Members of the S100 gene family are highly homologous but, despite this, they appear to have different expression profiles during breast cancer development. Based on these expression profiles, S100 proteins are emerging as potentially useful diagnostic and prognostic tools. S100A2, S100A4 and S100A7 appear to be the important players and, in recent years, a potential biological mechanism of action for two of these, S100A4 and S100A7 has begun to emerge. Further study of the S100 gene family in breast cancer has the potential to discover new aspects to the biochemical pathways that promote cancer, and through understanding the interactions of S100's, may identify new targets for therapeutic intervention.

2.3.0- Jab1

We have become interested in the Jab1 protein because we have found it to interact with the S100A7 protein in human breast cells (as will be described in the Results section 4

below). The majority of work described in this thesis details the ability of S100A7 to interact with Jab1 and cause an enhancement in Jab1 activity (for a detailed description, see Results section 4). Jab1 was originally identified in mammalian cells as a factor that interacts with c-Jun and influences c-Jun transcription of AP-1 regulated genes (205), Jab1 has subsequently been described to be a component of the large multimeric COP9 signalosome protein complex (206). The CSN/COP9 signalosome (207-209), had been studied previously in systems other than mammalian and has been shown to have a role in protein degradation via the Ub-26S proteasome (208-210). Jab1 has recently been shown to form interactions with many diverse proteins and enhance components of cell signaling pathways *in-vitro*, in yeast and human cell line model systems. These interactions result in either translocation of Jab1 between the cytoplasm and nucleus by an unidentified mechanism in the case of LFA-1 integrin (211), HER2 signaling (212), enhanced activity of transcription factors such as c-Jun/AP-1 (205, 213, 214), HIF-1 (215), steroid receptors and cofactors (216) or promoting the degradation of an interacting protein, as is the case for the interaction with p27 (217, 218), SMAD4 (219), p53 (220) and HIF-1 (220). See FIG 12 for an overview of Jab1 and its interacting partners. A possibly interesting scenario exists where a competition between different Jab1-binding proteins could determine which signaling pathways are modulated by Jab1. This may explain why activated Jab1 does not result in all Jab1 pathways being stimulated in the presence of "activated" Jab1. For example, unmutated p53 can downregulate Jab1 activation of c-Jun (220) and inhibition of Jab1 causes reciprocal upregulation of p53 (220). The physiological relevance of some of these interactions (221), specifically in the context of breast epithelial cells, are mostly unknown.

2.3.1- Jab1 and Cancer

Jab1 has the potential to directly alter several important aspects of early breast tumor progression. See FIG 12 for an overview of Jab1 relating to cancer progression. Jab1 can do this by altering several important cellular properties. Increased proliferation may occur through increased ER and PR activation (216), increased AP-1 activity and upregulation of cyclin D1 (222), degradation of the cell cycle inhibitor $p27^{kip1}$ (217) and the TGF-β signaling component SMAD4 (219). Increased ability to survive hypoxic stress may occur through augmented HIF-1 activity and hypoxic response (128). Increased invasiveness may result from activation of AP-1 (223-225) and HIF-1 dependent genes such as matrix metalloproteinases and VEGF, that are implicated as critical factors in tumor progression (226-229). Also of note, is that the natural plant pigment curcumin, is a promising chemopreventive agent (230), as it may act by inhibiting Jab1 (231, 232). Curcumin may also inhibit other pathways (233), but many demonstrate inhibitory effects on HER2 (234) and ER signaling (235), cell proliferation (236), and invasion (235, 237) in breast cells which could in theory be attributable to the effects of activated Jab1.

Alteration of Jab1 activity in tumors could be caused by changes in a) cytoplasmic-nuclear distribution (211, 212, 238, 239), b) free Jab1 to COP9 associated Jab1 ratio (206), competition between different interacting proteins (220), or direct elevation of Jab1 expression and activation. A single study of Jab1 in ovarian cancer found increased nuclear Jab1 associated with progression, reduced expression of p27, and poor outcome (240), and Jab1 has also been implicated in renal cancer (241) and pituitary cancer (242). In node negative invasive breast cancer, an increase in Jab1 expression has been

correlated with a decrease in the cytoplasmic amount of p27 (243). Tumors with high p27 expression were rarely positive for Jab1 and tumors that were negative for Jab1 had no evidence of relapse (244). There are several common events in early breast tumor progression that can be associated with an alteration in Jab1 activity and the transition from low grade to high DCIS. These changes are mutation of p53 (113, 245, 246) and amplification of HER2 (247), induction of HIF-1 with hypoxia associated necrosis (248), altered cell adhesion and probably integrin signaling (249-251). S100A7 can be added to this list (239) of factors that impact on Jab1 activity. Jab1 appears to be able to influence several critical pathways that might have a role in early tumor development i.e. transition of a pre-invasive tumor to invasive disease. Jab1 may be an important player in the modulation of these individual pathways, which would have a major role in promoting the shift towards increased malignancy in the breast cancer cell.

2.4.0- Objective and Hypothesis of Study

Our objective was to understand the significance and the biological mechanism of action of S100A7, one of the most highly expressed genes in pre-invasive breast cancer. We tested the hypothesis that "S100A7 influences progression in breast cancer and that this effect may be due to a direct impact on the epithelial cell, mediated through modulation of the central cell signaling regulator, Jab1".

2.4.1- Specific Aims of Study

1. Determine the biological importance of S100A7 with respect to breast cancer progression and invasion. This will be through study of the effect of S100A7 expression within breast cancer cell models by both *in-vitro* and *in-vivo* analysis of parameters of invasion and malignancy.

2. Explore the nature and biological significance of the interaction between S100A7 and Jab1. The S100A7-Jab1 interaction will be studied by site directed mutagenesis to define the structural regions of interaction. We will then determine if the interaction is conserved and compare the effect of mutant-S100A7 on invasion and growth to unmutated S100A7. We will also look for alterations in signal transduction pathways that increase AP-1 activity in an attempt to understand if S100A7 can influence Jab1 activity directly.

3. Examine the relationship between S100A7 and Jab1 in early tumor progression and invasiveness *in-vivo* to confirm the relevance of observations made in cell and animal models. We will dissect the importance of S100A7 in tumor progression and the relationship between expression of S100A7, Jab1, and downstream markers of Jab1 activity, in human breast cancer. This will be studied by analysis of expression in ductal carcinoma in-situ and invasive carcinoma.

3.0- Material and Methods

3.1-Growth Media

YPAD see ref (252)

600 ml distilled water

6 g yeast extract (Difco)

12 g peptone (Difco)

12 g glucose (Fisher)

24 mg Adenine Sulfate (Sigma)

For solid media: add 10 g agar (Difco)

To sterilize: autoclave at 121^0C for 20 minutes at 103 kPa

Synthetic Complete drop out (SC) (252)

600 ml distilled water

3 g $(NH_4)_2SO_4$ (Sigma)

1 g yeast nitrogen with out amino acids, with out $(NH_4)_2SO_4$ (Difco)

12 g glucose (Fisher)

0.4 g Synthetic Complete dropout mix*

Final pH 5.6

For solid media: add 10 g agar (Difco)

To sterilize: autoclave at 121^0C for 15 minutes at 103 kPa

***Synthetic Complete dropout mix** (all components from Sigma)

Omit the appropriate component(s), indicated in bold and italics, to prepare SC -his, SC -leu, SC -trp, SC – trp –leu and SC – trp –leu -his

Adenine hemisulfate	1.8 g	30 mg/L
Arginine HCl	1.2 g	20 mg/L
Glutamic Acid	6.0 g	100 mg/L
Histidine HCl	***1.2 g***	***20 mg/L***
Inositol	2.0 g	33 mg/L
Isoleucine	1.8 g	30 mg/L
Leucine	***1.8 g***	***30 mg/L***
Lysine HCl	1.8 g	30 mg/L
Methionine	1.2 g	20 mg/L
p-aminobenzaic acid	0.2 g	3 mg/L
Phenylalanine	3.0 g	50 mg/L
Homoserine	6.0 g	100 mg/L
Tryptophan	***2.4 g***	***40 mg/L***
Tyrosine	1.8 g	30 mg/L
Uracil	1.2 g	20 mg/L
Valine	9.0 g	150 mg/L

M9 –leu (252)

60 ml 10X M9 Salts

540 ml distilled water

10 g agar (Difco)

autoclave at 121^0C for 30 minutes at 103 kPa

Then add:

0.6 ml 1M $MgSO_4$

0.6 ml 0.1M $CaCl_2$

0.5 ml of 4 mg/ml thymine

6 ml 20% glucose (w/v, filter sterilized)

0.15 ml 0.01 M $FeCl_3$

0.6 ml 2 mg/ml vitamin B1

10X Salts Solution:

60 g Na_2HPO_4 (Fisher)

30 g KH_2PO_4 (Fisher)

5 g NaCl (Fisher)

10 g NH_4Cl (Fisher)

total volume of 1 L with distilled water

To sterilize: autoclave at 121^0C for 30 minutes at 103 kPa

store at 4^0C

Luria-Bertani (LB)

6 g Bacto-tryptone (Difco)

3 g Bacto-yeast extract (Difco)

6 g NaCl (Fisher)

600 ml distilled water (final volume)

pH 7.5

For solid media: add 10 g agar (Difco)

To sterilize: autoclave at 121^0C for 30 minutes at 103 kPa

For LB+carb plates: after autoclaving, add 600 ml carbenicillin (40 mg/ml) when flask has cooled to about 45^0C

SOB

4 g Bacto-tryptone (Difco)

1 g Bacto-yeast extract (Difco)

0.12 g NaCl (Fisher)

0.036 g KCl (Fisher)

Make up to a volume of 200 ml with distilled water.

To sterilize: autoclave at 121^0C for 30 minutes at 103 kPa

SOC

To 10 ml SOB add

100 µl 2 M Mg^{2+} (Filter sterilized and stored at 4^0C)

100 µl 2 M glucose (filter sterilized)

Dulbecco's Modified Eagle Medium (D-MEM)

1X minimal media powder (InVitrogen) reconstituted in distilled water according to manufactures directions

Filter sterilize

Aliquot 460 ml into 500 ml sterilized glass bottles

Store at 4^0C

To 460 ml DMEM add:

5 ml Penicillin-Streptomycin- 10000 units penicillin, 10000 µg streptomycin (Gibco)

5 ml filter sterilized 35% glucose (w/v)(Fisher)

5 ml 200 mM L-glutamine (Gibco)

25 ml heat inactivated fetal bovine serum (Gibco)

MCF10 Growth Media

To DMEM add:

25 ml heat inactivated horse serum (Gibco)

20 ng/ml hEGF (Upstate)

500 ng/ml Hydrocortisone (Sigma)

100 ng/ml Cholera Toxin (Sigma)

10 μg/ml Insulin (Upstate)

5 ml Penicillin-Streptomycin- 10000 units penicillin, 10000 μg streptomycin (Gibco)

3.2- Solutions

Cell Culture Freezing Medium

5 ml DMSO (Fisher)

10 ml Fetal Bovine Serum (Sigma)

35 ml DMEM with 5% serum (v/v) and supplements

Stored at -20^0C

Bacteria and Yeast Freezing Solution

20 ml glycerol (Fisher)

80 ml distilled water

mix thoroughly

To sterilize: autoclave at 121^0C for 30 minutes at 103 kPa

Carbenicillin (40 mg/ml)

40 mg carbenicillin (Sigma) added to 500 µl sterile distilled water and 500 µl 100% Ethanol (Fisher). Store at -20^0C.

Use 1 µl per ml for LB plates or 0.5 µl per ml for liquid cultures.

0.5 M EDTA pH 8

Disodium ethylene diamine tetraacetate $2H_2O$ FW=372.2

Add 186.1 g in 800 ml distilled water

Stir vigorously

Adjust pH to 8.0 –will need ~ 20 g NaOH pellets (Fisher)

Adjust volume to 1 L with distilled water

To sterilize: autoclave at 121^0C for 30 minutes at 103 kPa

50X TAE (Tris Acetate buffer)

96.8 g Tris base (Fisher)

22.8 g glacial acetic acid (Fisher)

16 ml 0.5 M EDTA

Make up to a final volume of 400 ml with distilled water.

Dilute to 1X solution for agarose gel buffer

To make 1X solution, dilute with distilled water.

5X TBE (Tris Borate buffer)

108 g Tris base (Fisher)

55 g Boric acid (Fisher)

40 ml 0.5 M EDTA

Make up to a final volume of 2 L with distilled water.

Final pH will be approximately 8.2-8.3

To make 1X solution, dilute with distilled water.

Agarose DNA Elution Buffer

400 µl 5 M NaCl

500 µl 1 M Tris-HCl pH 7.5

20 µl 0.5 M EDTA pH 8.0

100 µl 10% SDS (w/v)

Make up to a final volume of 10 ml with sterile distilled water

3 M Sodium Acetate pH 5.2

Sodium Acetate $3H_2O$ (Fisher) FW=136.08

Dissolve 40.824 g in 60 ml distilled water.

Adjust pH to 5.2 with glacial acetic acid (Fisher)

Adjust volume to 100 ml with distilled water

To sterilize: autoclave at 121^0C for 30 minutes at 103 kPa

PBS (Phosphate Buffered Saline) pH 7.3-7.5

1 PBS tablet (Amresco) is completely dissolved in 100 ml distilled water to yield:

137 mM Sodium Chloride

10 mM Phosphate Buffer

2.7 mM Potassium Chloride

To sterilize: autoclave at 121^{0}C for 30 minutes at 103 kPa

Crystal Violet

0.125 g crystal violet (Fisher)

1 ml 1 M Tris-HCl pH 7

0.45 g NaCl (Fisher)

10 ml methanol (Fisher)

Bring up to a total volume of 50 ml with distilled water

1 M Tris

Tris base FW=121.1

Dissolve 60.55 g Tris base (Fisher) in 400 ml distilled water

Adjust pH to desired value with concentrated HCl (Fisher)

Allow solution to cool before making final adjustments to pH

Make up to a final volume of 500 ml with distilled water

To sterilize: autoclave at 121^{0}C for 30 minutes at 103 kPa

TE Buffer

1 ml 1M Tris pH 8 final concentration = 10 mM

200 µl 0.5 M EDTA final concentration = 0.1 mM

Make up to a final volume of 100 ml with distilled water

To sterilize: autoclave at 121^0C for 30 minutes at 103 kPa

Ethidium Bromide (10 mg/ml)

Add 0.1 g Ethidium Bromide (Sigma) to 10 ml distilled sterile water.

Stir/shake for several hours to ensure dye has dissolved.

Store in dark bottles, preferably at 4^0C.

10X Loading Dye (for DNA agarose gels)

0.025 g Bromophenol Blue (Fisher)

0.025 g Xylene Cyanol FF (Fisher)

10 ml glycerol (Fisher)

Store at 4^0C

DNA Ladder (1 Kb or 100 bp)

3 0 µl ladder [1 µg/ul] (InVitrogen)

100 µl 10X restriction enzyme of PCR buffer (InVitrogen)

770 µl sterile distilled water

100 µl 10X Loading Dye

Store at 4^0C

1 M DTT (Dithiolthreitol)

Dithiolthreitol (Fisher) FW=154.5

Dissolve 3.09 g in 20 ml 0.01 M Sodium Acetate pH 5.2

Filter sterilize, do not autoclave

Store in aliquots at -20^0C

Sodium Hydroxide (NaOH) Solutions

For 10 M Dissolve 200 g NaOH pellets (Fisher) in a final volume of 500 ml

For 5 M Dissolve 100 g NaOH pellets (Fisher) in a final volume of 500 ml

For 1 M Dissolve 20 g NaOH pellets (Fisher) in a final volume of 500 ml

Store in polypropylene containers

SDS-Isolation Buffer (SIB)

500 µl 1M Tris pH 6.8

400 µl 0.5 MM EDTA pH 8

5 ml 10% SDS (Fisher) (w/v)

100 µl 0.5 M β-glucerophosphate (Fisher)

4 ml sterile distilled water

1 tablet Mini-Complete Protease Inhibitor Cocktail (Roche)

Store in aliquots at -20^0C

4X Separating Gel Buffer - 1.5 M Tris pH 8.8; 0.4% SDS (w/v)

27.26 g Tris base (Fisher)

0.6 g SDS (Fisher)

Dissolve in a final volume of 150 ml with distilled water

Adjust pH to 8.8

4X Stacking Gel buffer – 0.5 M Tris pH 6.8; 0.4% SDS (w/v)

6.07 g Tris base (Fisher)

0.4 g SDS (Fisher)

Dissolve in a final volume of 100 ml with distilled water

Adjust pH to 6.8

3X Gel Buffer - 3.0 M Tris pH 8.45, 0.3% SDS (w/v)

90.86 g Tris base (Fisher)

0.75 g SDS (Fisher)

Dissolve in a final volume of 250 ml with distilled water

Adjust pH to 8.45

5X SDS-PAGE Running Buffer – 125 mM Tris, 960 mM Glycine, 0.5% SDS pH ~8.3

15 g Tris base (Fisher)

72 g Glycine (Fisher)

5 g SDS (Fisher)

Dissolve in a final volume of 1L with distilled water

Do not adjust pH

5X Tricine-SDS-PAGE Cathode Running Buffer – 500 mM Tris, 500 mM Tricine, 0.5% SDS (w/v)

60.57 g Tris base (Fisher)

89.59 g Tricine (Fisher)

5 g SDS (Fisher)

Dissolve in a final volume of 1 L with distilled water

Do not adjust pH

5X Tricine-SDS-PAGE Anode Running Buffer – 1 M Tris pH 8.9

121.12 g Tris base (Fisher)

Dissolve in a final volume of 1 L with distilled water

Adjust pH to 8.9

10X Tris Glycine Transfer Buffer – 250 mM Tris, 1.92 M Glycine

60.6 g Tris base (Fisher)

288 g Glycine (Fisher)

Dissolve in a final volume of 2 L with distilled water

Do not adjust pH

1X Tris Glycine Transfer Buffer – 25 mM Tris, 192 mM Glycine, 20% Methanol (v/v)

100 ml 10X Tris-Glycine Transfer Buffer

200 ml ACS Methanol (Fisher)

700 ml distilled water

10X Tris Buffered Saline (TBS) – 200 mM Tris, 1.37 mM NaCl, pH 7.6

48.4 g Tris base (Fisher)

160 g NaCl (Fisher)

Make up to a final volume of 2 L with distilled water

1X TBS-T – 20 mM Tris, 137 mM NaCl, 0.5% Tween 20 (v/v), pH 7.6

200 ml 10X TBS-T

1 ml Tween 20 (Fisher)

Make up to a final volume of 2 L

Stir vigorously

Western Blocking Solution

10 ml 1X TBS-T

0.5 g Dried Skim Milk Powder (Carnation)

5X SDS-PAGE Sample Buffer (non-reduced)

3.125 ml 1M Tris pH 6.8

6.25 g (5 ml) Glycerol (Fisher)

1 g SDS (Fisher)

5 mg Bromophenol Blue (Fisher)

1 ml distilled water

Heat to dissolve

4X SDS-PAGE Sample Buffer

400 µl 5X SDS-PAGE Sample Buffer (non-reduced)

20 µl 5M DTT

280 µl distilled water

Store at -20^0C

Z-Buffer

16.1 g Na_2HPO_4 $7H_2O$ (Fisher)

5.5 g NaH_2PO_4 H_2O (Fisher)

750 mg KCl (Fisher)

246 mg $MgSO_4$ $7H_2O$ (Fisher)

Bring to a final volume of 1 L

X-Gal (5-bromo-4-chloro-3-indolyl-β-D-galactopyranoside) 20 mg/ml

Dissolve 1.0 gm of X-Gal (Promega) in 50 ml of N,N-dimethylformamide (Sigma)

Store at -20^0C.

Z-buffer + X-Gal

This should be made fresh by adding 270 µl of β-mercaptoethanol (Fisher) and 1.67 ml of X-Gal solution to 100 ml of Z buffer.

2 M Glucose (Dextrose)

Glucose FW=180.16 (Fisher)

Dissolve 18 g glucose (Fisher) in 40 ml distilled water.

Make up to a final volume of 50 ml

Filter sterilize

2 M Mg^{2+}

$MgCl_2$ $6H_2O$ FW=203.31 (Fisher)

$MgSO_4$ $7H_2O$ FW=246.5 (Fisher)

To 80 ml distilled water, add 20.33 g $MgCl_2$ $6H_2O$ and 24.65 g $MgSO_4$ $7H_2O$

After dissolved, make up to a final volume of 100 ml with distilled water

Filter sterilize and store at 4^0C

Mouse Tail PCR Buffer

1.86 g KCl (Fisher)

40.5 ml distilled water

5 ml 1M Tris-HCl

Stir and pH to 8.3 with 1 M NaOH

Then add:

5 mg gelatin (Sigma)

2.25 ml 10% Tween 20 (Sigma) (final=0.45% Tween 20)

2.25 ml 10% NP-40 (Sigma) (final=0.45% NP-40)

Stir and heat to ~37^{0}C for 20 minutes to dissolve gelatin

Bring up to a final volume of 50 ml with distilled water

Store at room temperature

Southern Gel Denaturation Buffer

150 ml 5 M NaCl

50 ml 5 M NaOH

300 ml distilled water

Southern Neurtalizing Buffer

200 ml 5 M NH_4Ac (Fisher)

4 ml 5 M NaOH

796 ml distilled water

20X SCP

233.76 g NaCl (Fisher)	2 M NaCl
170.35 g Na_2HPO_4 (Fisher)	0.6 M Na_2HPO_4 FW=141.96
11.69 g EDTA	0.02 M EDTA FW=292.25

Dissolve in 1.8 L distilled water and heat to 65^0C

pH to 6.2 with 30-40 ml concentrated HCl (Fisher)

Bring up to a final total volume of 2 L with distilled water

Pre-hybridization Solution

33.3 ml 20X SCP

2 ml 20% N-lauryl sarcosine (Sigma)

2.5 ml 10 mg/ml sheared salmon sperm DNA (Sigma)

8 ml 50X Denhardt's Solution (Sigma)

50 ml 98% formamide (Fisher)

4.2 ml distilled water

Stored at -20^0C

Genomic Southern Blot Wash Solution 1

150 ml 20X SCP

25 ml 20% N-lauryl sarcosine (Sigma)

325 ml distilled water

Genomic Southern Blot Wash Solution 2

25 ml 20X SCP

25 ml 20% N-lauryl sarcosine (Sigma)

450 ml distilled water

3.3.0- Standardized Procedures

3.3.1- Growth of Cell lines in Culture

All cell manipulations were conducted in a Labgard laminar flow biological safety cabinet (NuAire Inc.).

Cells were routinely cultured in Dulbecos modified Eagles medium (DMEM) supplemented with 5% Fetal Bovine Serum (Sigma), unless otherwise noted. For detailed description of all media and components, see Growth Media section.

Cell cultures were maintained in a T25 culture flask (Nunc) with 8 ml of appropriate media. When cell confluency reached 90%, media was removed and cells washed with 5 ml PBS, which was then removed. Cells were detached from the surface of the flask by covering the culture surface with 0.5 ml trypsin-EDTA (InVitrogen). After 5 minutes, flask was checked to see if cells were detaching from surface and incubated longer if needed. Once cells were detached from surface, 4.5 ml of culturing media was added to

the flask to inhibit trypsin activity. Cells were vigorously pipetted up and down to disrupt cell clumps. Cells were then used for experimentation or to maintain culture.

For cell line maintenance, when a confluency of 90% was reached, cultures were split back to a dilution of 1:6 to 1:40, depending on the individual cell line. A new T25 was used after every other splitting procedure.

All cell lines were grown in a water-jacketed incubator at 37^0C with a humidified atmosphere containing 5% CO_2 (Forma Scientific).

Culture plates are purchased from Costar, dishes from Corning (60 mm, 100 mm) and Nunc (150 mm), flasks from Nunc.

For protein and RNA extraction or freezing of cells, seeding conditions are as follows:

Type	Surface Area	Seeding Density	Cells at Confluency	Growth Medium
6-well plate	903 mm^2	$0.3x10^6$	$1.1x10^6$	4 ml
12-well plate	366 mm^2	$0.1x10^6$	$0.41x10^6$	1 ml
24-well plate	191 mm^2	$0.05x10^6$	$0.22x10^6$	0.5 ml
60mm dish	2210 mm^2	$0.6x10^6$	$2.5x10^6$	5 ml
100 mm dish	6010 mm^2	$1.7x10^6$	$6.8x10^6$	10 ml
150 mm dish	14780 mm^2	$4.2x10^6$	$16.7x10^6$	20 ml
25 cm^2 flask	2500 mm^2	$0.7x10^6$	$2.8x10^6$	8 ml
75 cm^2 flask	7500 mm^2	$2.1x10^6$	$8.5x\ 0^6$	10 ml
150 cm^2 flask	15000 mm^2	$4.2x10^6$	$16.9\ x10^6$	20 ml

3.3.2- Extraction of Protein from Culture Cells

-Cells are cultured under standard conditions in their appropriate media as described above.

-For protein extraction, cells are seeded at the above densities for either a 60 mm or 100 mm dish, and grown under standard conditions until the surface confluency reaches 80%.

-Growth media is aspirated off and cells are washed with 8 ml ice cold PBS.

-PBS is aspirated off (as much as possible) and cells are lysed with 100 µl SIB for a 60 mm dish and 250 µl for a 100 mm dish.

-Cells are scraped of surface of dish with a plastic cell scraper (Costar) and transferred to a 1.5 ml Eppendorf tube.

-Tube is vortexed vigorously for 30 seconds then placed at -20^0C.

-Once lysate is completely frozen, tubes are thawed at room temperature, vortexed vigorously for 30 seconds, and then kept on ice.

-Protein lysate is sonicated with a Sonic Dismembranator (Fisher Scientific) for 30 seconds at setting of 4 to sheer genomic DNA.

-Lysate are stored at -20^0C.

3.3.3- Protein Assay

Protein assayed using the Micro BCA Protein Assay Kit (Pierce) according to the manufactures instructions.

-1 µl of protein lysate is added to 499 µl of sterile distilled water in a 1.5 ml Eppendorf tube.

-Protein assay reagents A, B and C mixed in a ratio of 50:48:2, respectively and 500 µl added to tube already containing 1 µl of protein lysate and 499 µl water.

-Tube vortexed vigorously for 15 seconds and then centrifuged at maximum speed for 15 seconds.

-Tube placed in a 60^0C water bath for 60 minutes.

A Standard Curve of protein concentration vs. absorbance (562 nm) is used to determine the protein concentration of an unknown sample. 1 mg/ml stock solution of dissolved BSA (Pierce) is diluted with distilled sterile water to produce a working concentration of 2 µg/ml. The standard curve is set up in the following way in 1.5 ml Eppendorf tubes:

Std. Curve µg/ml	Stock Solution BSA (2 µg/ml)	1 µl BSA + water
0	0 µl	499 µl
2	50 µl	449 µl
5	125 µl	374 µl
10	250 µl	249 µl
15	375 µl	124 µl
20	500 µl	0 µl

-Protein assay reagents A, B and C mixed in a ratio of 50:48:2, respectively and 500 µl added to tube already containing 500 µl for Standard Curve.

-Tube vortexed vigorously for 15 seconds and then centrifuged at maximum speed for 15 seconds.

-Tube placed in a 60^0C water bath for 60 minutes.

-200 µl of protein assay reaction loaded into a clear bottom 96-well pate (Costar) and absorbance is read at 562 nm using a Spectra Max 190 spectrophotometer (Molecular

Devices) and SoftMax Software. The tube from the standard curve containing 0 μg/ml BSA is used as the Blank.

Equation for Standard Curve generated by plotting values for protein concentration (X-axis) vs. absorbance at 562 nm (Y-axis) in Graph Pad Prism statistical software (Graph Pad). Linear regression statistics is performed to calculate the equation for the best fit line (not forced through the origin 0,0). The Y-intercept and the slope of the line are used to calculate the protein concentration of the unknown samples using Excel (Microsoft) and the equation:

μg/ml protein in a 1:500 dilution = (absorbance at 562 nm – Y-intercept)/slope

(μg/ml protein in a 1:500 dilution)/2 = concentration in μg/μl

For Western blotting, 50 μg or 100 μg of total protein are typically run per lane.

3.3.4- Preparation of Protein Samples for Western Blot

-Stock protein lysates removed from -20^0C and thawed at room temperature. Tubes vortexed and centrifuged quickly, then placed on ice.

-Amount of protein lysate needed for 50 μg or 100 μg of total protein is placed in a 500 μl Eppendorf tube.

-Appropriate volume of 4X Sample Buffer is added to yield a final concentration of 1X.

-20 µl of Pre-Stained Broad Range Protein Marker (New England BioLabs) pipetted into its own tube and processed with the protein sample tubes.

-Tubes placed in a PTC 100 PCR machine (MJ Research) and tubes "boiled" at 100^0C for 5 minutes.

-Samples are now ready for electrophoresis or can be stored at -20^0C until needed.

3.3.5- Western Blot for proteins <20 kDa, Tricine-SDS-PAGE

Adapted from (253). Apparatus used is the BioRad mini gel system.

Glass plates washed with 70% ethanol, then distilled water and set up according to manufactures instructions.

Separating Gel (16.5% acrylamide (v/v)):

3x Gel Buffer	3.0 ml
30% Polyacrylamide*	4.95 ml
distilled water	1.0 ml
10% APS (BioRad)	45 µl
TEMED (Sigma)	5 µl

*30% Polyacrylamide (36.5:1, 2.67%C) purchased from BioRad.

10% (w/v) APS (Ammonium Persulphate) is made fresh each time.

Separating gel vortexed quickly, then poured to the separating gel fill line. 0.1% SDS (dissolved in distilled water) is layered over separating gel. Separating gel allowed to polymerize for 30 minutes.

0.1% SDS is removed and the Stacking gel is poured.

Stacking Gel (4%):

3X gel Buffer	1000 µl
30% Polyacrylamide*	400 µl
distilled water	1582 µl
10% APS	15 µl
TEMED	3 µl

*30% Polyacrylamide (36.5:1, 2.67%C) purchased from BioRad.

10% APS (Ammonium Persulfate) is made fresh each time.

Stacking gel vortexed quickly, then poured on top of separating gel. Combs inserted (75 mm) and gel allowed to polymerize for 30 minutes.

Gels are then placed into the gel-running apparatus. Inner chamber is filled with 1X Tricine-SDS-PAGE Cathode Running Buffer while the outer chamber is filled with 1X Tricine-SDS-PAGE Anode Running Buffer.

Combs are removed and wells are washed with inner chamber buffer 2 times using a syringe.

Wells are loaded with pre-boiled samples using 200 µl small-bore pipette tips (BioRad).

Electrophoresis conditions were performed at constant current using a BioRad Powerpack to supply 35 mAmps. Electrophoresis stopped when the 6.5 kDa band in the Marker lane has traveled through 80% of the separating gel.

3.3.6- Western Blot for proteins >20 kDa

Gel system setup is exactly as described above. Percentage of acrylamide used in separating gel is dependant on the size of the protein of interest.

8% acrylamide for proteins between 80-130 kDa

10% acrylamide for proteins between 40-80 kDa

12% acrylamide for proteins between 20-40 kDa

Separating Gel:

	8%	10%	12%
4X Separating Gel Buffer	2.25 ml	2.25 ml	2.25 ml
30% polyacrylamide	2.4 ml	3.0 ml	3.6 ml
distilled water	4.3 ml	3.7 ml	3.1 ml
10% APS	45 µl	45 µl	45 µl
TEMED	5 µl	5 µl	5 µl

30% Polyacrylamide (36.5:1, 2.67%C) purchased from BioRad.

10% APS (Ammonium Persulphate, BioRad) is made fresh each time.

Stacking Gel: (4%)

4X Stacking Gel Buffer	750 µl
30% polyacrylamide	400 µl
distilled water	1832 µl
10% APS	15 µl
TEMED (Sigma)	3 µl

Electrophoresis conditions were performed at constant current using a BioRad Powerpack to supply 30 mAmps. Electrophoresis stopped when the 16.5 kDa band in the Marker lane has traveled through 90% of the separating gel.

3.3.7- Transfer of Proteins from Acrylamide gel to Nitrocellulose

For transfer, use the BioRad Mini-Gel Transfer Apparatus.

-Nitrocellulose (BioRad), filter paper and scrub pads soaked for 15 minutes in 1X Transfer Buffer at room temperature.

-For Tricine gel system (proteins <20 kDa), use 0.2 µm pore size nitrocellulose, otherwise use 0.65 µm pore size nitrocellulose.

-Gel removed from glass plates and stacking gel removed.

-Transfer "sandwich" assembled according to BioRad's Transfer Apparatus Instruction Manual and placed in Transfer Apparatus with an ice block and magnetic stir bar.

-Apparatus filled to the top with cold 1X Transfer Buffer and placed on top of a magnetic stir pad.

-Stir pad turned on to ensure stir bar mixes Transfer Buffer.

-PowerPack set at 100 mVolts for 1 hour.

-After Transfer is complete, nitrocellulose is placed in Blocking Buffer for 30 minutes with gentle agitation.

-Nitrocellulose blot can now be probed with primary antibody or stored at -20^0C in a sealed bag with all the air removed.

3.3.8- Probing of Nitrocellulose Blot with Antibody and Detection of Signal

-Antibodies are diluted to according to manufacturer or optimal dilution determined by probing identical blots with a range of antibody concentrations.

-For probing of blots, all primary antibodies were diluted in 10 ml TBS-T containing 5% non-fat milk powder (w/v). Phospho-specific antibodies were diluted in 10 ml TBS-T containing 5% (w/v) BSA (Fisher). Antibodies were diluted in a range between 1:100 and 1:5000.

-Blots with primary antibody were incubated overnight at 4^0C with gentle shaking.

-Primary antibody mixture was removed and blots were washed 3 times with 15 ml TBS-T for 5 minutes with gentle shaking at room temperature. After each was step, TBS-T was discarded.

-Secondary antibody (GoatαRabbit-HRP or GoatαMouse-HRP, BioRad) were diluted 1:5000 in 10 ml TBS-T containing 5% non-fat milk powder and incubated on blots for 1 hour at room temperature with gentle shaking.

-Secondary antibody mixture was removed and blots were washed 3 times with 15 ml TBS-T for 5 minutes with gentle shaking at room temperature. After each was step, TBS-T was discarded.

-For secondary antibody detection, surface of the blot was completely covered (~2 ml) with the HRP substrate Super Signal (Pierce) for 10 minutes at room temperature.

-Blot then sealed in a clear plastic bag after excess Super Signal and air bubbles were removed.

-Blot exposed to photographic film (Kodak MR) in a darkroom for various times. Exposure times depend on intensity of signal but generally range from 30 seconds to 2 minutes.

-Blot then stored at -20^0C.

Antibodies Used for Western Blot

Target Protein	Molecular Mass (kDa)	Source of Antibody	Dilution used	Species
S100A7	11	Custom Made	1:2500	rabbit
CA9	50	Dr. Jaromir Pastorik	1:1000	mouse
HIF-1α	120	Novus Biologicals	1:500	mouse
phospho c-Jun	48	Cell Signaling	1:1000	rabbit
phospho Akt	60	Cell Signaling	1:1000	rabbit
Actin	42	Sigma	1:10000	mouse
Jab1	38	Santa Cruz	1:1000	rabbit
$p27^{Kip1}$	27	Becton	1:1000	mouse
phospho JNK	46&54	Cell Signaling	1:1000	rabbit
EGFR	175	Cell Signaling	1:500	rabbit
$p21^{Cip1}$	21	Santa Cruz	1:1000	rabbit
IκBα	41	Cell Signaling	1:1000	rabbit
PTEN	54	Dr. Charis Eng	1:1000	mouse
p53	53	Dako	1:1000	rabbit

3.3.9- Extraction of Total RNA

For extraction of total RNA from culture cells:

-A 10 cm diameter dish of cells was cultured under standard conditions until reaching a confluency of 80%.

-Growth media was removed and 1 ml of Tri Reagent (Sigma) was added.

-Plate was then rotated to cover entire surface of plate with Tri Reagent.

-A cell scraper was used to scrape cells from plate.

-Cell/Tri Reagent slurry was transferred to a sterile 1.5 ml Eppendorf tube and either processed for RNA extraction immediately or stored at -70^0C for 1 month.

-RNA extraction performed according to manufacturers instructions:

To 1 ml Tri Reagent/cell slurry add 0.2 ml chloroform (Fisher), mix, incubate at room temperature for 3-5 minutes.

-Centrifuge at 12000g for 15 minutes at 4^0C.

-Aqueous phase transferred to a fresh 1.5 ml Eppendorf tube. Add 0.5 ml isopropanol (Fisher), mix, and incubate 5-10 minutes at room temperature.

-Centrifuge 12000g 15 minutes 4^0C.

-Remove supernant and wash pellet with 1 ml 75% ethanol.

-Centrifuge 7500g for 5 minutes at 4^0C.

-Remove supernatant and air dry pellet for 10 minutes at room temperature.

-Pellet resuspended in 100 µl DEPC water and stored at -70^0C.

Extraction of total RNA from frozen tissue:

-100 mg of sectioned frozen material was placed in a sterile 1.5 ml Eppendorf tube.

-1 ml Tri Reagent added to tissue and vortexed vigorously for 1 minute.

-Total RNA extracted identically as described above according to manufacturers instructions.

3.3.10- Quantitation of RNA Concentration

-Sample removed from -70^0C storage.

-Tubes placed in 65^0C water bath for 5 minutes, mixed gently, then centrifuged for 5 seconds at maximum speed and put on ice.

-2 µl total RNA added to 198 µl DEPC treated water (1:100 dilution) in a 500 µl DNase and RNase free tube (Eppendorf). Sample gently mixed and centrifuged at maximum speed for 5 seconds.

-Tube kept on ice.

-All 200 µl placed into the well of a non-UV absorbing clear bottom 96-well plate (Falcon). 200 µl DEPC water used as a blank.

-Optical Density measurement performed at 260 nm using a Spectra Max 190 spectrophotometer (Molecular Devices) and SoftMax Software.

µg/µl = (O.D. x dilution x 40)/1000

3.3.11- Dilution of Total RNA for Reverse Transcription

-Stock sample that has had its concentration of RNA previously determined were removed from -70^0C storage.

-Tubes placed in 65^0C water bath for 5 minutes, mixed gently, then centrifuged for 5 seconds at maximum speed and put on ice.

-Volume required to contain 400 ng total RNA was transferred from stock RNA tube to a DNase and RNase free 500 µl tube and placed on ice. Volume in tube brought up to a total of 4 µl (100 ng/µl).

3.3.12- Reverse Transcription Reaction

-Total reaction volume is 20 µl. Reaction reagents added to a DNase and RNase free 1.5 ml tube (Eppendorf).

4 µl 5X Reverse Transcription Buffer (InVitrogen)

2 µl x4 dNTPs, 2.5 mM (Pharmacia)

2 µl 0.1% (w/v) BSA (Sigma)

2 µl 100 mM DTT (Sigma)

2 µl DMSO (Sigma)

2 µl 50 µM random hexamer primer (InVitrogen)

2 µl MMLV RNA reverse transcriptase (InVitrogen)

2 µl RNA at 100 ng/µl

-Tube gently mixed and then centrifuged at maximum speed for 5 seconds.

-Tubes placed at 37^0C for 2 hours after which time total volume in tube was brought up to 40 µl by adding 20 µl sterile double distilled water.

-Tubes stored at -20^0C until needed for PCR.

3.3.13- Design of PCR Primers

-cDNA sequence of genes downloaded from NCBI website (http://www.ncbi.nlm.nih.gov/entrez/query.fcgi?db=Nucleotide&itool=toolbar) and imported into Oligo (Version 5.0, National Biosciences, Inc.).

-Search parameters were set so primer pairs would be "compatible pairs" and would be duplex free, have 3'-end stability, hairpin free, homooligo free, and false priming oligonucleotides were not selected.

-All primers were check for specificity with their desired target cDNA by subjecting the primer sequence to a BLAST search (http://www.ncbi.nlm.nih.gov/BLAST/).

3.3.14- Dilution of DNA Primers for PCR

All DNA primers ordered from Invitrogen Custom Primer Service.

50 nmoles ordered for each primer.

Each primer resuspended in 50 µl sterile distilled water.

Want a final concentration of 50 µM for PCR.

nmoles in tube/50 µl = X nmoles/µl

50/(X nmoles/µl*1000)*100 = Y µl of primer needed for a final concentration of 50 µM in a final volume of 100 µl.

All primers are stored at -20^0C once resuspended in water.

3.3.15- Polymerase Chain Reaction (PCR)- reaction components

50 µl total volume

35.78 µl double distilled sterile water

5.0 µl 10X PCR Buffer pH 9.0 (InVitrogen)

2.0 µl 50 mM $MgCl_2$ (InVitrogen)

4.0 µl x4 dNTPs. 2.5M (Amersham)

1.0 µl DMSO (Fisher)

0.5 µl Primer 1 (50 µM)

0.5 µl Primer 2 (50 µM)

0.22 µl Taq polymerase, 5 U/µl (Invitrogen)*

1.0 µl DNA or cDNA template

**Pfu* Turbo polymerase used for high fidelity PCR i.e. gene cloning (Stratagene). In which case, 2.0 µl of 50 mM $MgCl_2$ is omitted and replaced with 2.0 µl sterile water. *Pfu* Turbo polymerase comes with its own 10X PCR Buffer, in which case it is substituted for the 10X PCR Buffer pH 9.0 from InVitrogen.

3.3.16- Primer Pairs Used for Semi-Quantitative RT-PCR

Target Gene	Sequence 5'-3'	Primer Name
VEGF	CGC AGA CGT GT AAA TGT TCC AAG AAA AAT AAA ATG GCG AAT CC	VEGF-UPPER (sense) VEGF-LOWER (antisense)
MMP13	ATG CGG GGT TCC TGA T CGC AGC AAC AAG AAA CAA	MMP13-UPPER (sense) MMP13-LOWER (antisense)
EGF	CAC AAC CCA AGG CAG AAG AT ACA TTG CGT GGA CAG GAA	EGF-UPPER (sense) EGF-LOWER (antisense)
GAPDH	ACC CAC TCC TCC ACC TTT G CYC TTG TGC TCT TGC TTG TTG G	GAPDH-UPPER (sense) GAPDH-LOWER (antisense)
S100A7	TCT ACT CGT GAC GCT TCC CAT TTT ATT GTT CCT GGG TCT	PSOR-Full-U (sense) PSOR-Full-L (antisense)
Cyclin D1	GCT GGA GCC CGT GAA AAA GAG GGA GGG CGG ATT GGA AAT GA	Cyclin D1-U (sense) Cyclin D1-L (antisense)

3.3.17- PCR Reaction Conditions

Performed in a PTC 100 PCR machine (MJ Research).

Denaturation: 95^0C for 5 minutes

Amplification: 95^0C denaturation for 45 seconds

X^0C primer annealing (primer pair specific) for 30 seconds

72^0C polymerase extension*

Extension: 72^0C for 7 minutes

End: 4^0C

*time dependent on length of product, 30 seconds/500 bp

3.3.18- Plasmid DNA Preparation

2 ml overnight cultures of LB+carb are processed with the High Pure Plasmid Isolation Kit (Roche) according to the manufacturers directions. The DNA is eluted in a final volume of 100 µl TE buffer. One 2 ml bacterial culture typically yields >10 µg of plasmid DNA.

3.3.19- Plasmid DNA Precipitation

-The product of 5 plasmid preps (500 µl) are pooled into a 1.5 ml Eppendorf tube.

-1/10 the volume (50 µl) 3 M NaAc pH 5.2 added to tube.

-2X the volume of ice cold 100% Ethanol added (1 ml)

-Tube quickly vortexed and then centrifuged for 5 seconds at maximum speed.

-Tube then placed at -70^0C for 1 hour, or at -20^0C for longer than an hour.

-Tube centrifuged at 4^0C for 15 minutes at 10000g.

-Supernatant removed and pellet washed with 200 µl 70% Ethanol.

-70% Ethanol removed and pellet air dried for 20 minutes.

-Pellet resuspended in 20 µl TE, or sterile distilled water for DNA sequencing.

-Concentration of DNA determined by measuring absorbance at 260 nm, as described in section 3.3.10, but using a correction factor of 50.

3.3.20- DNA Sequencing

DNA was sequenced at the University of Calgary Core DNA Facility, Calgary Alberta (http://dnaservices.myweb.med.ucalgary.ca/UCDNAServicesHome.html). Automated sequencing performed with an ABI Prims 377 DNA Sequencer (Applied Biosystems). For sequencing reaction, 5 µg of template double stranded plasmid DNA was diluted in a total volume of 10 µl and submitted in a DNase and RNase free 500 µl Eppendorf test tube. The specific sequencing primer was submitted at a concentration of 3.2 pmol/µL, 5 µl total in a separate DNase and RNase free 500 µl Eppendorf test tube. Sequencing results were downloaded from the Core DNA Facility's FTP server. Sequencing results were submitted to BLAST (http://www.ncbi.nlm.nih.gov/BLAST/) for either DNA identification (Yeast 2-Hybrid screen) or for identification of mutations.

Primer Name	Sequence (5'-3')	Plasmid Template
T7	TAATACGACTCACTATAGGG	pcDNA3.1 Zeo
GAL4-Activation Domain	TACCACTACAATGGATG	pACT2
GAL4-Binding Domain	TCATCGGAAGAGAGTAG	pGBT9
CMV Forward	CGCAAATGGGCGGTAGGCGTG	pShooter-CMV
pTRE2-Hygro Forward Primer	AGCGGACCTCTGCGGT	pTRE2-Hygro

3.3.21- Restriction Enzyme Cutting

In a 500 µl Eppendorf test tube the following components are added:

5 µl DNA from a plasmid prep

2.5 µl 10X Reaction Enzyme Buffer

1 µl restriction enzyme

16.5 µl sterile distilled water

25 µl total volume

In the case of a double digest, decrease water to 15.5 µl and add 1 µl of the second enzyme.

Tube contents are gently mixed then centrifuged for 5 seconds. Tubes are then placed in a 37^0C water bath for at least 1 hour.

Restriction enzymes were purchased from either Invitrogen or New England Biolabs and stored at -20^0C.

3.3.22- Electrophoresis of PCR Products or Restriction Enzyme Digests

-DNA bands were resolved by electrophoresis through a 0.5-1% agarose (Fisher) 1X TBE gel.

-A comb with a length of 6 mm and a width of 1 mm was used to create the wells.

-5 µl of Ethidium Bromide was added to the molten gel for analysis of products other than those from RT-PCR. Gels used for the analysis of RT-PCR reactions were post-stained following electrophoresis for 45 minutes with 100 ml 1X TBE + 10 µl EtBr with gentle shaking.

-Once the gel had solidified, it was submerged in 1X TBE running buffer.

-2.5 µl of 10X Loading Dye (Recipe) was added to 25 µl of an unpurified PCR reaction or a 25 µl restriction enzyme digest and mixed by gentle pipetting. All 27.5 µl for each sample were loaded into one lane.

-A 100 base pair or 1 kb base pair ladder (Invitrogen) was loaded in one well for determination of DNA band size.

-Wells of the gel were placed near the negative electrode (cathode), as the DNA will migrate to the positive electrode.

-Electrophoresis was carried out at 100 mV until the Bromophenol Blue tracking dye had migrated ¾ of the way through the gel.

Post electrophoresis, DNA bands were visualized under long wave ultra violet light and images of the gels captured with MCID software (Imaging Research Inc.).

3.3.23- DNA Fragment Isolation from Agarose Gel

Described in (254),

-Method can be used for 500 bp fragments and larger

-Make a 0.7% or 1% agarose gel depending on the size of fragment to be isolated with EtBr.

-Use TAE for making the gel and for running buffer.

-Load into well as much DNA as possible: a full 25 µl restriction enzyme digest or 25 µl from a PCR reaction. Add 2.5 µl 10X DNA Loading Dye.

-Separate DNA at 100 V until band to be isolated is well resolved and separated from other bands.

-Cut a piece of 3MM Whatman paper and dialysis tubing (Fisher) to the same size, 2.5 well widths.

-Cut a slit in the gel all the way through with a scalpel just below the DNA fragment to be isolated.

-Put the paper and tubing together and insert it into the slit. The paper is closest to the fragment.

-Run the gel for 15 minutes at 110 V.

-Remove the paper and tubing from the gel and put into a 500 µl tube (cap removed) that has had a hole poked in the bottom with an 18.5 g needle. Do not pack paper/tubing into bottom of tube.

-Insert the 500 µl tube into a 1.5 ml tube that has had its cap removed.

-Add 100 µl Elution Buffer. Pipette up and down 5 times making sure the filter paper is well washed with Elution Buffer.

-Centrifuge tubes together for 10 seconds at 500g in a bench top centrifuge.

-Transfer the Elution Buffer from the 1.5 ml tube to a new 1.5 ml tube.

-Repeat washing and centrifugation step 2 more times, collecting the Elution Buffer from the bottom of the 1.5 ml tube each time.

-Centrifuge at maximum speed for 30 seconds. Save the Elution Buffer as before.

-Add 400 µl phenol:chloroform (1:1) to the collected Elution Buffer.

-Vortex for 20 seconds 2 times with 20 seconds incubation in between.

-Transfer the aqueous layer to a new 1.5 ml Eppendorf tube.

-Precipitate the DNA with 1/10 the volume of 3 M NaAc pH 5.2 and 2X the volume with ice cold 100% Ethanol.

-Put tube at -70^0C for 10 minutes.

-Tube centrifuged at 4^0C for 15 minutes at 10000g.

-Supernatant removed and pellet washed with 200 µl 70% Ethanol.

-70% Ethanol removed and pellet air dried for 20 minutes.

-Pellet resuspended in 20 µl sterile distilled water.

3.3.24- Ligation of DNA Insert into a Plasmid

-Plasmid that were to receive the DNA insert was linearized and purified via agarose gel electrophoresis, as described above.

-If DNA insert was a PCR product, it is first purified with a Wizard PCR Preps DNA Purification System (Promega), otherwise the DNA insert is purified by agarose gel electrophoresis. DNA insert must be cut with same restriction enzymes used to linearize

plasmid DNA to generate cohesive ends and allow for directional orientation of the DNA insert.

-If only one restriction enzyme is used, orientation of the DNA insert must be confirmed by DNA sequencing or a diagnostic restriction enzyme cut.

-In a 500 µl DNase and RNase free tube, 0.025 µg of plasmid DNA is added, followed by 2-10X the amount of DNA insert.

-2 µl of 10X Ligation Buffer that includes rATP (Roche) and 0.5 µl T4 DNA ligase (100 U/ml, Roche) are added to the tube.

-The final reaction volume was brought up to a total of 20 µl with sterile distilled water.

-Reaction was allowed to take place overnight at 12^0C.

-The next day, 1 µl ligation reaction was electroporated into *E. coli* DH5α (see below for procedure).

-50 µl, 100 µl and 200 µl of transformed bacteria were grown on LB+carb plates overnight.

-Isolated colonies are picked and used to inoculate an overnight liquid culture of 2 ml LB+carb.

-Plasmid preps on 2 ml overnight cultures were performed with the High Pure Plasmid DNA Isolation Kit (Roche).

-5 µl of plasmid prep DNA was used for a restriction enzyme digest to identify clones that contain the insert (for detailed description see Standardized Procedures section).

-Clones that were identified to contain the DNA insert were further analyzed by DNA sequencing (see Standardized Procedures section) to: detect unwanted mutations from the

PCR reaction, confirm orientation of DNA insert, establishment of correct reading frame for generation of fusion protein.

3.3.25- Cloning of S100A7 into Various Expression Vectors

Vector	Company	EE's Name	Bacterial Selection	Mammalian Selection	Amino Acids Encoded
pcDNA3.1 Zeo	InVitrogen	pcDNA3.1-psor Zeo	Amp	Zeocin	1-101
pShooter-Cyto	InVitrogen	pShooter psor cyto	Amp	Neomycin	1-101
pGBT9	Clontech	pGBT9-psor	Amp	NA	1-101
pGBT9	Clontech	pGBT9-Cterm-psor	Amp	NA	43-101
pGBT9	Clontech	pGBT9-Nterm-psor	Amp	NA	1-52
pJ5	ATCC	pJ5-psor	Amp	NA	1-101
pTRE2-Hygro	Clontech	pTRE2-Hygro-psor	Amp	Hygromycin	1-101

3.3.26- Electrocompetant *E. coli* DH5α

Described in (255)

-DH5α was grown overnight in 50 ml LB without antibiotics at 37^0C with shaking at 200 rpm.

-5 mls of overnight culture used to inoculate 4 flasks containing 500 ml LB.

-Flasks grown until an OD 600 nm = 0.7 is reached. 1 ml LB used as a blank.

-Culture transferred to four sterile 500 ml centrifuge bottles and centrifuged for 10 minutes at 8000g and 4^0C.

-Supernant removed and pellet resuspended in 100 ml sterile cold water. Volume brought up to 500 ml.

-Centrifuged again for 10 minutes at 8000g and 4^0C.

-Supernant removed and pellet resuspended in 100 ml sterile cold water. Two pellets combined and brought up to 500 ml with sterile cold water.

-Centrifuged again for 10 minutes at 8000g and 4^0C.

-Supernant removed and pellet resuspended in 20 ml sterile cold water. Transfer to sterile 30 ml centrifuge tubes.

-Centrifuge for 10 minutes at 6000g and 4^0C.

-Supernant removed and pellet resuspended in 20 ml of cold sterile 20% glycerol.

-Centrifuge for 10 minutes at 6000g and 4^0C.

-Remove supernant and resuspend pellet in 1 ml sterile and cold 10% glycerol.

-30 µl aliquoted into sterile 500 µl Eppendorf tubes on ice.

-Tubes were flash frozen in liquid nitrogen and stored at -70^0C until needed.

3.3.27- Electroporation of Plasmid DNA into Electrocompetant *E. coli* DH5α

-An electroporation chamber with a channel gap of 0.1 cm (BioRad) is placed on ice for 15 minutes.

-Tube containing 30 µl of electrocompetent bacteria is placed on ice and allowed to thaw.

-1 µl of DNA sample is added to bacteria and mixed.

-Bacteria DNA mixture was pipetted between electrode surface of the electroporation chamber.

-Using a Gene Pulser (BioRad) conditions are: 400 ohms, 25 µFD and 1.25 V

-Bacteria collected in 1 ml SOC and incubated at 37^0C with shaking at 200 rpm for 30 minutes.

-10, 100 and 200 µl bacteria plated onto LB+carb plates.

-Plates grown overnight at 37^0C.

-Colonies are picked and used to inoculate 2 ml LB+carb cultures that are then grown overnight at 37^0C with shaking at 200 rpm.

-2 ml cultures used for plasmid preps using the High Pure Plasmid DNA Isolation Kit (Roche).

-5 µl plasmid DNA is then used for a diagnostic restriction enzyme digestion to confirm the presence of a DNA insert or the identity of the plasmid.

3.3.28- Freezing of Bacterial and Yeast

-Actively growing bacteria or yeast, in the presence of selective agent were scraped from an agar plate with sterile toothpicks.

-Bacteria or Yeast were transferred to a cryovial (Nalgene) containing 500 µl of sterile 20% glycerol.

-Tubes were vortexed for 10 seconds to dissolve clumps and stored at -70^0C.

3.3.29- Site Directed Mutagenesis

-The complete open reading frame sequence for S100A7 was previously cloned into the pcDNA3.1 Zeo (InVitrogen) expression vector.

-The three amino acids comprising the putative Jab1-binding domain were altered from Asp58/Gly58, Leu80/Met80 and Gln90/Lys90 using mutagenic oligos to produce the plasmids pGBT9-psor, pGBT9-Cterm-psor and pcDNA3.1mut-psor using the Transformer Mutagesesis Kit (Clontech) according to the manufacturers instructions.

-The presence of all desired mutations were confirmed by DNA sequencing.

-Mutagenic oligonucleotides used to generate mutant pcDNA3.1-psor mut and pGBT9-Cterm-psor-mut are:

For Asp58/Gly58: 5'-TAC CTC GCC GGC GTC TTT GAG-3'

For Leu80/Met80: 5'-TCT GTC CTT GAT GGG AGA CAT-3'

For Gln90/Lys90: 5'-CTA CCA CAA GAA GAG CCA TGG-3'

3.3.30- Transfection of Mammalian Cell Lines

-Used Effectene (Qiagen) according to the manufactures instructions.

-Plasmid DNA was prepared in TE buffer at a concentration of at least 1 μg/μl.

-Transfection was performed in 60 mm or 100 mm culture dishes.

-Transient transfection efficiency was determined for each expression construct and each cell line by setting up multiple dishes containing the same number of cells, but transfecting with varying amounts of DNA and Effectene transfection reagent. Optimal

transfection conditions were determined by luciferase reporter assay or by Western Blot for the protein of interest.

-For transient transfection studies, protein was typically harvested 24 hours post transfection, but in some situations 48 or 72 hours were required.

3.3.31- Generation of Stablely Transfected Clones

-The concentration of selective agent required is first tested for each cell line and expression construct. 100 mm dishes were plated with enough cells such that after 24 hour incubation at 37^0C, the surface of the plate will be approximately 25% confluent with cells.

-Selective agent was added to 250 ml of DMEM with appropriate supplements (depending on the specific cell line) to yield a final concentration of 500 mM.

-The stock media containing 500 mM selective agent was diluted with DMEM (plus appropriate supplements) in separate culture dishes to produce working concentrations of selective agent: 50 mM, 100 mM, 200 mM, 250 mM, 300 mM, 400 mM and 500 mM.

-The plates were incubated at 37^0C and had their media replaced every 2 days.

-The concentration of selective agent used to generate stable clones is the lowest concentration that killed all the cells in the dish after 1 week.

To generate stable clones:

-Four 100 mm culture dishes were plated with cells such that the surface of the plate would be approximately 25% confluent with cells after 24 hours of incubation at 37^0C.

-2 μg of DNA (linearized or uncut plasmid) was transfected with Effectene (Qiagen) according to the manufactures instructions. Plates were incubated at 37^0C for 24 hours.

-24 hours post-transfection, media was removed and replaced with media containing the appropriate concentration of selective agent.

-Plates were incubated at 37^0C and have their media changed every 2 days.

-Once isolated colonies have appeared that are large enough to see by eye, they were ready to be transferred to their own well in a 96-well plate. This is accomplished by removing the media from the dish followed by a wash with PBS which was then removed. Sterile Cloning Rings (Fisher) were coated on one edge with silicon vacuum grease and placed firmly on the plate such that the colony is in the middle of the ring. The ring was flooded with Trypsin-EDTA (InVitrogen) and incubated at 37^0C for 5 minutes.

-Contents of the ring were gently pipetted up and down to break apart the colony and then transferred to a well in a 96-well plate. Growth media containing selective agent was added to the well.

-Transfection plate was discarded once it has been picked clean of large clones that were physically separated from other clones.

-Clones were grown in 96-well plate until they have grown to cover the surface of the well, at which time they are trypsinized and transferred to a 24-well plate.

-Once clones had covered the surface of the 24-well plate, they were transferred to a 6-well plate and then eventually their own T25 flask.

-From an almost confluent T25, cells were split to seed a 60 mm dish for protein or RNA extraction to check for expression of the transfected gene, and a T75 was used to freeze cells once it had reached 80% confluency.

Parental Line	Transfection Plasmid	Expression Regulation	Clone Name	Expression level
MDA-MB-231	pcDNA3.1 neo	-	231-neo	none
MDA-MB-231	pcDNA3.1 neo psor	CMV	231-LP1	low
MDA-MB-231	pcDNA3.1 neo psor	CMV	231-HP1	high
MDA-MB-231	pcDNA3.1 neo psor	CMV	231-HP2	high
MDA-MB-231	pcDNA3.1 zeo psor mut	-	231-PTM.1	none
MDA-MB-231	pcDNA3.1 zeo psor mut	CMV	231-PTM.2	high
MDA-MB-231	pcDNA3.1 zeo psor mut	CMV	231-PTM.14	high
HeLa	pcDNA3.1 zeo psor	-	HeLa psor.12	none
HeLa	pcDNA3.1 zeo psor	CMV	HeLa psor.16	high
MCF10AT3B	pcDNA3.1 zeo psor	CMV	ZP1B3	high
MCF10AT3B	pcDNA3.1 zeo psor	CMV	ZP5E12	high
MCF-7 clone 89	pTRE2-Hygro-psor	-	Mag01	none
MCF-7 clone 89	pTRE2-Hygro-psor	-	Mag02	none
MCF-7 clone 89	pTRE2-Hygro-psor	tetracycline inducible	Mag06	high
MCF-7 clone 89	pTRE2-Hygro-psor	tetracycline inducible	Mag07	high

3.3.32- Freezing of Tissue Culture Cells

-A T75 culture flask was grown under standard culture conditions to a confluency of 80%.

-Growth media was removed and cells washed with 10 ml sterile PBS.

-PBS was removed and cells detached from flask surface by addition of 1 ml Trypsin-EDTA (InVitrogen) for 6 minutes.

-Cell clumps were broken up by pipetting up and down with 10 ml of complete medium.

-Cells resuspended in 10 ml of growth medium were transferred to a sterile 15 ml conical tube.

-Cells were pelleted by centrifugation for 10 minutes at 500g.

-Supernant was removed and cells resuspended in 6 ml of Cell Culture Freezing Medium.

-1 ml of cells was resuspended in Cell Culture Freezing Medium and transferred to a sterile 2 ml cryovial (Nalgene).

-Cryovials were placed at -70^0C for a week before being transferred to liquid nitrogen storage tank or -150^0C freezer.

3.3.33- Treatment of Culture Cells with Inhibitors

-Cells were grown under standard culture conditions in 100mm dishes for at least 24 hours after being trypsinized.

-Inhibitors were added to culture dishes when the cell confluency reached 60-70%.

-Inhibition of Akt phosphorylation was accomplished by addition of the PI3 kinase inhibitor LY2942002 (Calbiochem) at a concentration of 15 μM in DMED supplemented with 5% fetal calf serum.

-EGFR inhibition was accomplished by addition of the specific inhibitor BPIQ (Alexis) at 0.29 nM in DMED supplemented with 5% fetal calf serum.

-Total protein was isolated after cells were exposed to inhibitors for 24 hours using SIB according to the procedure described above.

3.3.34-Yeast 2-Hybrid screen for proteins interacting with S100A7

Adapted from reference (252).

Cloning of S100A7 into the Bait Yeast expression plasmid

-Human S100A7 (GenBank accession Number NM_002963) was amplified by PCR using the plasmid pcDNA3.1psor-zeo as a template. The PCR reaction was performed using 0.01 μg of template in TE buffer under conditions described in the Standardized Procedures section. A temperature of 60°C was used for primer annealing followed by a total of 35 cycles. The resulting PCR product was purified using a Wizard PCR Preps DNA Purification System (Promega) according to the manufacturers instructions. Both the pGBT9 Bait plasmid (Clontech) and the purified PCR product were cut with restriction enzymes EcoRI and BamHI as described in the Standardized Procedures section. After restriction enzyme cutting, the linearized pGBT9 plasmid was purified by electrophoresis through a 0.5% TAE agarose gel and extracted as described in the Standardized Procedures section. The restriction enzyme cut S100A7 PCR product again was purified via the Wizard PCR Preps DNA purification System (Promega). Ligation of S100A7 into pGBT9 was performed as described in Standardized Procedures using 0.05 μg of plasmid and 0.2μg S100A7 purified and cut PCR product. 1 μl of ligation mix was added to 35 μl of electrocompetent *E. coli* DH5α, mixed and added to a 0.1 cm

electroporation chamber (BioRad). Generation of electrocompetent DH5α and electroporation conditions are described in the Standardized Procedures section. Bacterial colonies that grew in the presence of carbenicillin selection were picked and subcultured overnight in 2 ml LB+carb. Following incubation, plasmid preps were generated using the High Pure Plasmid Isolation Kit (Roche) according to the manufacturers directions. 5 μl of purified plasmid from each separate clone was used for diagnostic restriction enzyme cuts (using enzymes EcoRI and BamHI, as described in Standardized Procedures) to check for the presence of the S100A7 insert. Clones positive for the ~300 base pair S100A7 insert were sent for automated DNA sequencing (University of Calgary, Core DNA Facility). Results from sequencing reactions were entered into BLAST to confirm the fidelity of the sequence (http://www.ncbi.nlm.nih.gov/BLAST/) and only those clones having a sequence identical to that of the GenBank sequence were kept for further study. The DNA sequencing also confirmed the GAL4-DNA binding domain and S100A7 insert were in the same reading frame in order to generate a fusion protein. The resulting bait plasmid (pGBT9-psor) was used for subsequent 2-hybrid studies.

Transformation of pGBT9-psor into Yeast and detection of S100A7-Bait fusion protein

-*Saccharomyces cerevisiae* strain KGY37 (gift from R.D. Gietz, University of Manitoba) was used for all yeast studies. Transformation of plasmids into yeast were performed as previously described (256) using the lithium acetate/single-stranded carrier

DNA/polyethylene glycol method. Briefly, ~40 µl of competent yeast that had been actively growing on YPAD agar medium (see description in Growth Medium Table) were added to 1.5 ml Eppendorf test tubes with 200 µl sterile distilled water. The yeast were washed quickly by vortexing briefly and then centrifuged at maximum speed for 30 seconds in a bench top centrifuge. The supernatant was removed and replaced with transformation components:

-240 µl polyethyleneglycol (PEG 50% w/v 3350, Sigma)

-36 µl 1M Lithium Acetate (Sigma)

-50 µl carrier DNA (boiled single stranded salmon sperm DNA, Sigma)

-29 µl sterile distilled water

-5 µl of plasmid DNA in TE buffer from a plasmid prep (~1 µg of pGBT9-psor)

Tubes were then vortexed vigorously until all the yeast pellet was fully resuspended in solution. Tubes were placed at 30^0C for 30 minutes followed with heat shock treatment in a 42^0C water bath for 20 minutes. Following heat shock, tubes were centrifuged at maximum speed in a bench top centrifuge for 1 minute. Supernatant was removed and yeast resuspended in 1 ml sterile distilled water by gentile pipetting. 10 µl of transformation sample was plated on SC –trp (Synthetic Complete drop out –tryptophan, for description see Growth Media Table) and grown at 30^0C for 3 days.

Detection of GAL4 DNA-Binding Domain-S100A7 fusion protein in Yeast

-*S. cerevisiae* strain KGY37 that had been transformed with pGBT9-psor and grown on SC-trp medium were analyzed for the production of the GAL4 DNA Binding Domain-

S100A7 fusion protein. To isolate protein from Yeast: 10 ml starter cultures of SC –trp that had been inoculated with KGY37-pGBT9-psor and 10 ml YPAD inoculated with KGY37 were grown overnight at 30^0C with shaking at 200 rpm. The next day, 40 ml of YPAD was added to each flask that were then returned to the incubator. Yeast were counted with a hemocytometer and allowed to grow until reaching a density of between $1.0\text{-}2.0\text{x}10^7$ cells/ml (log phase of growth). Contents of flask was then added to a sterile 50 ml conical flask (Fisher) and centrifuged in a bench top centrifuge at 5000 rpm for 5 minutes. Supernatant was removed and pellet resuspended in 1 ml sterile distilled water. Resuspended yeast was transferred to a sterile 1 ml Eppendorf tube followed by centrifugation at 13000 rpm for 1 minute. Supernatant was removed and pellet was resuspended in approximately an equal volume of Yeast Cracking Buffer (see description in Solutions Table). Glass beads (0.5 mm) were added to tubes to a level of 5 mm below the meniscus. Tubes were vigorously vortexed for 30 seconds then placed on ice for 1 minute (repeated 3 more times). Tubes were then centrifuged at 13000 rpm for 15 minutes at 4^0C after which time the supernatant was removed and stored at -20^0C until needed. Protein concentration of Yeast protein lysate was determined by the Micro BCA Protein Assay Kit (Pierce) according to the manufacturers instructions. 50 μg of total protein for each sample was used for Western Blot (described in Standard Protocol section) to detect GAL4 DNA Binding Domain-S100A7 fusion protein.

Amplification of Yeast 2-hybrid Prey cDNA library

-The Human Mammary Gland MATCHMAKER cDNA Library (Clontech catalog number HL4036AH) was selected to screen for interacting proteins with the GAL4 DNA

Binding Domain-S100A7 fusion protein. The mRNA source used to generate the library was normal whole mammary glands pooled from 8 Caucasians, ages 23-47. The library was cloned in to the pACT2 Prey vector and grown in *E. coli* BNN132 where 82% of colonies were estimated to contain an insert with insert size ranging from 0.5-5.0 kbp and the average size being 1.6 kbp. The library was estimated to contain $3.5x10^6$ independent clones at a titer of $\geq 10^8$ colony forming units per ml.

10 µl of cDNA library stock was added to 40 ml LB broth and mixed. 400 µl of diluted bacteria was spread on the surface of one hundred 15 cm diameter bacterial plates containing LB+carbinicilin agar and grown overnight at 37^0C. The next day, plates had heavy growth but still single isolated colonies. All plates were scraped to harvest bacteria: 10 ml of sterile saline was added to the surface of one plate. A glass spreader was used to remove bacteria from the surface of the plate. Saline and bacteria mixture was poured onto the surface of a new plate and scraping repeated. After the fifth plate was scraped, the saline bacterial mixture was poured into a 50 ml conical tube. After all plates were scraped, 10 ml of saline was used to wash 4 plates. The wash slurry was added to the 50 ml tubes to give them an approximate volume of 40 ml. 50 ml tubes were centrifuged at 6500 rpm for 10 minutes and supernatant was poured off and the pellet was then resuspended in 10 ml 1X TGE. Resuspended pellets were combined and transferred to sterile 250 ml centrifuge bottles. Bacteria were lysed in order to collect plasmid by alkali treatment:

-20 ml of Solution 1 was added to each tube and left at room temperature for 5 minutes.

-40 ml of Solution 2 was added followed by vigorous mixing.

-30 ml of Solution 3 was added followed by gentle mixing and 10 minute incubation of tubes on ice.

-Tubes were centrifuged at 4^0C for 5 minutes at 5000 rpm and supernatant poured into a fresh tube and centrifuged again at 4^0C for 5 minutes at 5000 rpm.

-12.5 ml of supernatant added to new sterile 50 ml conical tube then 12.5 ml phenol-chloroform (1:1) added to each tube followed by gentle mixing.

-Tubes then centrifuged at 5000 rpm for 5 minutes.

-7.5 ml of aqueous layer transferred to a new sterile 50 ml centrifuge tube.

-DNA precipitated by adding 2X the volume of 100% Ethanol (15 ml) and 0.1X the volume of 3 M Sodium Acetate pH 5.2 (0.75 ml). The tubes were placed at -20^0C overnight.

-Tubes centrifuged at 10000 rpm for 20 minutes at 4^0C.

-Supernant was discarded and pellet washed with 1 ml of 70% Ethanol.

-Pellet air-dried, then resuspended in 10 ml TE buffer.

-5 ml of cDNA library was equally divided into two 15 ml conical tubes and treated with RNaseA (Invitrogen) by addition of 30 µl to tube, followed by incubation at 37^0C for 1 hour.

DNA precipitated via PEG precipitation method:

-6.6 ml 2.5 M NaCl, 20% PEG added to each tube, mixed gently and put on ice for 1 hour.

-Tubes centrifuged at 12500 rpm for 15 minutes at 4^0C.

-Supernatant removed and pellet washed with 1 ml of 70% Ethanol.

-Pellet was allowed to air dry, and then resuspended in 10 ml TE.

-Both tubes combined to give library DNA in 20 ml total volume and stored to -20^0C until needed.

Quantitation of cDNA library

-Samples of 1 µl, 10 µl and 50 µl of cDNA library were added to 3 separate sterile 500 µl Eppendorf tubes. Total volume in tubes was brought up to 10 µl with TE. Absorbance was measured with a Spectra Max 190 spectrophotometer (molecular Devices) using a wavelength of 260 nm and a blank of 100 µl TE. Absorbance was measured for the three samples was measured and used to calculate the concentration of the stock sample (µg/µl). For double stranded DNA (plasmid) an Absorbance of 1 = 50 µg/µl, therefore µg/µl = (OD x 50 x dilution)/1000. The concentration for the three samples were averaged to determine the concentration of the stock cDNA library = 0.500 µg/µl.

Determination of Transformation Efficiency of cDNA Library

-Into 10 ml of SC –trp media the yeast strain KGY37-pGBT9-psor was inoculated with and allowed to grow overnight at 30^0C with shaking at 200 rpm.

-The ells were counted with a hemocytometer to determine titer. The volume of media that contains $2.5x10^8$ cells was calculated and transferred to a sterile 15 ml conical tube and centrifuged at 5000 rpm for 5 minutes.

-The supernatant was removed and pellet was resuspended in 5 ml YPAD, followed by the addition of an addition al 5 ml YPAD.

-The mixture of 10 mls YPAD and cells was transferred to a sterile 250 ml flask and brought up to a total volume of 50 mls with YPAD.

-The cells were incubated at 30^0C with shaking and allowed to grow until density reached at least $2.0x10^7$ cells/ml.

-The culture transferred to a sterile 50 ml conical tube and centrifuged at 5000 rpm for 5 minutes.

-The cell pellet was resuspended in 25 ml sterile water and centrifuged again at 5000 rpm for 5 minutes.

-Supernatant discarded and pellet resuspended in 1 ml 100 mM LiAc, then transferred to a 1.5 ml Eppendorf tube and incubated at 30^0C for 10 minutes.

-Cells were pelleted by centrifugation at maximum speed for 15 seconds. Supernatant was removed and pellet resuspended with ~350 µl 100 mM LiAc to give a final volume of 500 µl. 50 µl of this suspension was transferred to new 1.5 ml Eppendorf tubes for each transformation reaction.

-The transformation Mix added to tubes containing 50 µl prepared yeast.

Transformation Mix:

240 µl PEG (50% w/v)

36 µl 1.0 M LiAc

25 µl single stranded salmon sperm DNA (2.0 mg/ml)

One of the following- 1 μg plasmid (2 μl) + 48 μl ssDNA, 2.5 μg plasmid + 45 μl ssDNA, 5 μg plasmid + 40 μl ssDNA, 10 μg plasmid + 30 μl ssDNA, 20 μg plasmid + 10 μl ssDNA.

-Contents of tubes were gently mixed by vortexing and incubated at 30^0C for 30 minutes.

-Heat shocked in 42^0C water bath for 20 minutes followed by centrifuged at 6000 rpm for 15 seconds.

-The transformation reagents removed and 1 ml sterile water added to each tube.

-Pellet resuspended by gentle pippeting and 10 μl of transformed Yeast were plated on duplicate SC –trp plates for each transformation and allowed to grow at 30^0C for 3 days.

-The colony count was used to generate the Transformation Yield (Average # of colonies per plate divided by the dilution factor plated from the of transformation reaction), which was the total number of transformants generated in the reaction tube. Transformation Efficiency (Transformation Yield/μg plasmid DNA in transformation reaction) was also calculated which represents the number of transformants per μg plasmid DNA in transformation reaction.

μg cDNA Library	Avg. # of colonies/plate	Transformation Yield	Transformation Efficiency
1.25	21.5	2150	1720
2.5	36.5	3650	1460
5	95	9500	1900
10	126.5	12650	1265
25	197	19700	788

Precipitation of cDNA Library for Screen

-50 µl cDNA library yields ~ 20,000 transformants and want a 120X screen = 2,400,000 clones screened. Have enough library to do two 120X screens, therefore 100 µl cDNA library should screen 4,800,00 clones. 100 µl x 120X=12 mls of cDNA library needed for screen, have 20 mls.

6 mls of cDNA library put in to two 30 ml centrifuge tubes. 18 mls 100% Ethanol and 60 0µl 3M NaAc added to each tube. DNA precipitated at -20^0C for 6 hours then centrifuged at 4^0C at 10,000 rpm for 15 minutes. Supernatant removed and pellet washed with 2 mls 70% Ethanol. Pellet air dried and resuspended in 2 ml TE.

120X cDNA Library Screen

-KGY37-pGBT9-psor was picked from an actively growing SC –trp plate and used to inoculate two 1 L flasks containing 100 ml SC –trp media. Flasks incubated at 30^0C for 20 hours with shaking at 200 rpm.

-Contents of flasks were combined and volume of culture needed for $3.0x10^9$ cells was calculated (76.2 ml) by calculating the number of cells/ml with a hemocytometer.

-1/2 the volume of culture needed for $3.0x10^9$ cells (38.1 ml) was transferred to two sterile 50 ml clonical tubes.

-Culture was centrifuged at 3000g for 5 minutes.

-Supernatant was removed and pellet washed with 25 ml sterile water.

-Cells centrifuged again at 3000g for 5 minutes.

-Supernatants removed and both pellets resuspended in 10 ml of 30^0C YPAD and then combined into one tube.

-5 ml of cells transferred to a sterile 500 ml flask containing 145 ml 30^0C YPAD, 4 flasks total. Flasks put in 30^0C incubator with shaking at 200 rpm until cell concentration reached at least $2.0x10^7$ cells/ml.

-Culture aliquoted into 12 sterile 50 ml conical tubes and centrifuged at 3000g for 5 minutes.

-Supernatant removed and pellet resuspended in 20 ml sterile water and centrifuged at 3000g for 5 minutes.

-Each pellet was resuspended in 1 ml of 100 mM LiAc. Pellets were pooled into one tube and mixed well and then divided equally into two sterile 50 ml conical tubes labeled "A" and "B".

-Tubes were incubated at 30^0C with gentle agitation for 15 minutes.

-Tubes were then centrifuged at 3000g for 5 minutes and supernatant discarded.

Transformation Mix added in order indicated:

A (60X)	B (60X)
14.4 ml 50% PEG (w/v)	14.4 ml 50% PEG (w/v)
2.16 ml 1 M LiAc	2.16 ml 1 M LiAc
2.5 ml carrier ssDNA (2.0 ml/ml)	2.5 ml carrier ssDNA (2.0 ml/ml)
2 ml cDNA Library	2 ml cDNA Library
Total=21.06 ml	Total=21.06 ml

-Tubes vortexed to resuspend pellet followed by gently pipetting up and down with a P1000.

-Tubes were incubated at 30^0C for 30 minutes. At 10 minute intervals the tubes were inverted 4 times to mix contents.

-Tubes then placed in 42^0C water bath for 40 minutes to heat shock cells. Tubes gently inverted four times every 5 minutes.

-Tubes centrifuged at 1000g for 6 minutes, supernatant removed and pellet resuspended in 40 ml sterile water.

-400 µl of cells plated on a 15 cm petri dish (Fisher) containing SC- trp –leu –his +5 mM 3-AT. 100 plates total.

-Plates put into plastic bags, inverted and incubated for 6 days at 30^0C.

-From day of transformation a total of 242 clones were picked for analysis.

Determination of Number of Clones Screened

-15 µl of "A" and "B" were added separately to 135 µl of sterile water (1/10 dilution). 1 µl, 10 µl and 100 µl of 1/10 dilution were plated on SC- trp –leu and allowed to grow for 3 days at 30^0C.

Dilution	"A" Average Colonies	"B" Average Colonies
0.1 µl	52	43
1.0 µl	410	367
100 µl	too many to count	too many to count

For "A": 52 x 10 x 20,000= $10.4x10^6$

410 x 20,000= $8.2x10^6$ Avg.= $18.6x10^6/2= 9.3x10^6$

For "B": 43 x 10 x 20,000= $8.6x10^6$

410 x 20,000= $7.34x10^6$ Avg.= $15.94x10^6/2= 7.97x10^6$

$7.97x10^6 + 9.3x10^6 = 17.27x10^6$ clones screened in total

β-Galactosidase Activity of 2-Hybrid Clones

-2-Hybrid clones that grew from the screen were patch streaked on a plate containing SC -trp -leu -his +5 mM 3-AT.

-A round, sterilized Whatman filter paper the size of a petri plate, was layered over top of and gently pressed down on the actively growing clones on the patch plate. Filter paper and plate were marked for easy identification of individual clones.

-Filter paper removed from plate quickly and frozen in liquid nitrogen to disrupt yeast cell wall.

-Filter paper then thawed completely and 3 more freeze/thaw cycles performed.

-1.5 ml Z-buffer/X-gal solution was used to soak a fresh piece of circular Whatman filter paper which was then layered underneath the freeze/thawed clones.

-Layered filter papers were placed in a sealed bag and incubated at 37^0C. They were checked every hour for the appearance of a bright blue color.

Isolation of GAL4-Activation Domain cDNA Plasmid from 2-Hybrid Clones

-For each clone to be tested, approximately 50 µl of cells were picked from and actively growing plate and transferred to a 1.5 ml Eppendorf tube.

-200 µl Yeast Cracking Buffer added

-200 µl of glass beads added (0.5 mm diameter).

-200 µl buffer saturated phenol:chloroform (1:1).

-Tube vortexed vigorously for 30 seconds then left to sit for 30 seconds. Vortexing repeated 3 more times.

-Tube centrifuged in a bench top centrifuge at 13,000g for 3 minutes.

-Aqueous phase removed and transferred to a fresh 1.5 ml tube.

-DNA precipitated by adding 20 µl 3 M NaAC (pH 6) and 500 µl 100% Ethanol.

-Tube put at -20^0C for 1 hour then centrifuged at 13,000g for 5 minutes at 4^0C.

-Supernatant removed and pellet washed with 100 µl 70% Ethanol.

-Pellet air dried at room temperature, then resuspended in 25 µl TE.

-Stored at -20^0C until needed.

-2 µl of purified glass bead preparation electroporated into *E. coli* KC8. For electroporation procedure, see Standardized Procedures section.

-Post-electroporation, bacteria collected in 1 ml SOC media by pipetting up and down twice very gently.

-Bacteria incubated at 37^0C for 30 minutes with gentle shaking at 100 rpm.

-50 µl and 100 µl bacteria plated on separate M9 –leu agar plates (for description see Growth Media section) and incubated overnight at 37^0C.

-For each 2-hybrid clone, 4 colonies were picked from M9 –leu plates and were used to inoculate 4 separate 2 ml LB+carb cultures that were frown overnight at 37^0C with shaking at 200 rpm.

-The 2 ml LB+carb cultures were used with the High Pure Plasmid DNA Isolation Kit (Roche) to produce purified plasmid.

-To confirm that only one Prey plasmid from the cDNA library was transformed into each positive 2-hybrid clone, restriction enzyme digests were performed. All 4 clones picked from the M9 -leu plates should give the same fragment profile if digested with the same restriction enzymes.

-For the Prey plasmid used in the screen (pACT2), the restriction enzymes XhoI and EcoRI will cut out the cDNA insert.

-Plasmids were digested and products were separated by electrophoresis through a 1% agarose TBE gel. DNA bands were visualized by post staining the gel with ethidium bromide (see Standardized Procedures section for description).

-If a 2-hybrid clone did not yielded an identical restriction profile for all 4 clones picked from M9 –leu plates, it was not kept for further analysis and was considered a false positive.

-1 µl from plasmid prep of KC8 clones was electroporated into *E. coli* DH5α, as described in the Standardized Procedures section.

-As before, 4 colonies were picked per 2-hybrid clone and restriction enzyme digested as described above. This confirms the presence of the cDNA insert and should yield the identical restriction profile obtained with plasmid DNA obtained from KC8.

Reconstruction of 2-Hybrid Positives

-Used Standard High Efficiency Transformation (1X) (256) of 2-hybrid prey plasmid (pACT2-cDNA, isolated as described above) into KGY37-pGBT9-psor.

-10 ml of SC –trp inoculated with KGY37-pGBT9-psor and grown overnight at 30^0C with shaking at 200 rpm.

-The cells were counted with a hemoctyometer to determine volume of culture needed for $2.5x10^8$ cells, which were used to inoculate 50 ml of 30^0C YPAD.

-Culture was grown at 30^0C with shaking at 200 rpm until concentration was at least $2.0x10^7$ cells/ml.

-In a sterile 50 ml conical tube, the cells were harvested by centrifugation at 5000g for 5 minutes. The supernatant was discarded and pellet resuspended in 25 ml sterile water and centrifuged again at 5000g for 5 minutes.

-The supernatant was removed and pellet resuspended in 900 µl water and transferred to a sterile 1.5 ml Eppendorf tube.

-The cells were pelleted by centrifugation at 13000 rpm for 1 minute, supernatant removed and pellet resuspended in a final volume of 1 ml 100 mM LiAc.

-Tube were then placed in 30^0C incubator for 10 minutes and.

-For each transformation, 100 µl of 100 mM LiAc and cell suspension transferred to a new 1.5 ml tube for each transformation.

Transformation Mix for each transformation (tube):

240 µl 50% PEG (w/v)

36 µl 1 M LiAc

74 µl single stranded carrier DNA (salmon sperm, 2.0 mg/ml, Sigma)

10 µl plasmid DNA (from plasmid preps of KC8 clones grown in 2 ml LB+carb)

-Mixture vortexed to fully resuspend pellet.

-Transformation incubated at 30^0C for 30 minutes.

-The cells were heat shocked in a 42^0C water bath for 30 minutes.

-The cells were centrifuged at top speed for 1 minute, transformation mix removed and pellet resuspended in 1 ml sterile water with gentle pipetting.

-100 µl and 200 µl plated onto SC –trp –leu –his +5 mM 3-AT. 100 µl plated on SC –trp –leu as a control to determine if transformation was successful.

-Plates placed in 30^0C incubator for 4 days to allow colony formation.

Segregation Analysis of 2-Hybrid Positives

-Performed on 13 clones from 2-hybrid screen that had strong activation of LacZ and passed reconstruction step. Cultures used were from reconstruction experiment.

-colony picked from actively growing SC –trp –leu –his +5 mM 3-AT and used to inoculate 2 ml of SC –leu.

-Culture incubated overnight at 30^0C with shaking at 200 rpm.

-Next day, optical density of cultures is measured to determine cell density.

$OD_{600} = 1 = 1.0x10^7$ cells/ml

-Volume calculated required for 1000 and 500 cells and plated on separate SC – leu plates that were incubated at 30^0C for 5 days.

-Colonies were replica plated onto plates containing SC media in the order of and deficient in: -leu, -trp, -trp –leu, -his +5 mM 3-AT. Plates incubated at 30^0C overnight.

-The next day, colonies were assessed for their ability to grow on the different selective medium. Colonies should have lost the Bait plasmid, therefore expect no growth on SC -trp and SC –trp –leu.

-Colonies should not be able to grow on SC -his +5 mM 3-AT. If growth is seen, the Prey plasmid is able to autoactivate Histidine reporter gene and clone should be dropped from analysis.

Elimination of False Positives from Yeast 2-Hybrid Screen - Check interaction of Prey plasmid for specificity with Bait by transforming with either empty pGBT9 (will make GAL 4 DNA-binding domain protein) or with a different Bait such as pRA4 (from R. D. Gietz, University of Manitoba) makes a fusion protein containing the GAL 4 DNA-binding domain protein fused with the RAD18 protein).

-pGBT9 and pRA4 transformed separately into pKGY37 containing a clone isolated from 2-Hybrid screen using the "Quick and Dirty" method (256). 100 µl of transformation mix plated onto duplicate SC –trp –leu, SC –trp –leu –his +5 mM 3-AT and SC –his +5 mM 3-AT.

-Plates incubated at 30^0C for 5 days to allow colony formation.

-Plates containing SC –trp –leu should have growth (positive result for success of transformation), but there should be no growth on SC –trp –leu –his +5 mM 3-AT and SC –his + 5 mM 3-AT plates as this would indicate that the Prey clone is able to interact with multiple Bait clones and is not specific for pGBT9-psor.

-Any clone showing the ability to activate the Histidine reporter gene in the absence of pGBT9-psor would be discarded.

Plasmids present	HIS Reporter gene activated?	Result
pGBT9-psor	no	Bait suitable for 2-Hybrid screen
pGBT9-psor + Prey (screen)	yes	Potential interaction
Prey	yes	False positive
Prey	no	Potential interaction
pGBT9-psor + Prey (reconstruction)	yes	Potential interaction
pGBT9 + Prey	yes	False positive
pGBT9 + Prey	no	Potential interaction
pRA4 + Prey	yes	False positive
pRA4 + Prey	no	Potential interaction

Identification of cDNA Insert in Prey Clones Specifically Interacting with pGBT9-psor in Yeast- Plasmid DNA for each Prey clone was electroporated (for procedure see Standardized Procedures section) into and propagated in *E. coli* DH5α.

-Five 2 ml cultures of LB+carb for each clone of interest was inoculated from a colony growing on LB+carb agar.

-Liquid cultures were incubated at 37^0C overnight with shaking at 200 rpm.

-Plasmid DNA was extracted from bacteria using the High Pure Plasmid Isolation Kit (Roche) according to the manufacturers directions.

-Plasmid DNA for each clone was pooled (500 µl total) and precipitated using the NaAc/Ethanol Method (see Standardized Procedures section).

-Once DNA pellet is air dried, it is resuspended in 20 µl sterile distilled water.

-Concentration determined by measuring absorbance at 260 nm (see Standardized Procedures section) using sterile distilled water as a blank.

-Plasmid DNA and Activation Domain sequencing primer diluted as requested by University of Calgary Core DNA Facility.

-Results of sequencing reactions downloaded from U of C FTP server and submitted to BLAST for identification.

-Using results from BLAST, region of gene present in Prey vector is determined as well as conservation of reading frame of insert, as determined by the upstream Activation Domain. CDNA inserts having a reading frame other than the one described in GenBank are discarded as they will not make the predicted protein product.

-Using Oligo software (Version 50. National Biosciences, Inc.) software, restriction enzyme sites within the cDNA insert are identified and a diagnostic restriction enzyme cut is performed to confirm the identity of the cDNA insert, if possible.

3.3.35- PCR to Identify Transgenic Founders

-Cut ~1.5 cm of tail from 4-5 week old mouse. Placed into a 1.5 ml Eppendorf tube and kept on ice. Samples kept at -70^0C until needed.

-A ~1.5 cm mouse tail from potential founders is removed from -70^0C storage and cut into 2 pieces: one piece is about 0.5 cm which is used for the following PCR method. The other mouse tail piece which is about 1 cm is immediately returned to -70^0C. It can have its DNA extracted and analyzed by Southern blot.

-0.5 cm mouse tail piece placed in a 1.5 ml Eppendorf tube and then 80 µl of Mouse Tail PCR Buffer is added, along with 4 µl of 10 mg/ml Proteinase K (Roche).

-Tubes incubated overnight at 55^0C in a waterbath with shaking at 100 rpm.

-The next day, all the solution in the tube is transferred to a 500 µl PCR tube and boiled for 5 minutes at 100^0C.

-Tubes centrifuged at maximum speed for 1 minute.

-1 µl of homogenate is used in a 50 µl PCR reaction using pJ5 cloning primers and 35 cycles.

-PCR reactions using MDA-MB-231 cDNA (negative control) and MDA-MB-468 cDNA (positive control) are processed at the same time.

-25 µl of PCR reaction are added to 2.5 µl 10X loading Dye and electrophoresed through a 1% agarose TBE gel with EtBr as described in the Standardized Procedures section.

-Mice that are PCR positive for the S100A7 transgene are then analyzed by Southern blot for confirmation. Some mice that were PCR negative are also included in Southern analysis as a negative control.

3.3.36- Southern Analysis of MMTV-S100A7 CD1 Transgenic Mice

-Cut ~1.5 cm of tail from 4-5 week old mouse. Placed into a 1.5 ml Eppendorf tube and keep on ice. Samples stored at -70^0C until needed.

-700 µl Mouse Tail Solution added to each tube:

Mouse Tail Solution

1 ml 2 M Tris-HCl pH 8

8 ml 0.5 M EDTA

0. 8 ml 5 M NaCl

4 ml 10% SDS

26.2 ml sterile distilled water

Stored at room temperature

-35 µl of 10 mg/ml Proteinase K (Roche) dissolved in sterile distilled water is added to each tube.

-Tubes incubated overnight at 55^0C in a shaker at 100 rpm.

-700 µl Buffer Saturated Phenol (Invitrogen) is added to each tube. Tubes mixed by inverting 10 times.

-Tubes centrifuged for 5 minutes at 10,000g.

-Aqueous phase transferred to a new 1.5 ml Eppendorf tube along with as much of the interphase as possible, but avoiding hair.

-700 µl phenol/chloroform (1:1) is added to aqueous phase and mixed by inverting tubes 10 times.

-Tubes centrifuged for 5 minutes at 10,000g.

-Aqueous phase transferred to a new 1.5 ml Eppendorf tube along with as much of the interphase as possible, but avoiding hair.

-700 µl chloroform (Fisher) added to each tube and mixed by inverting tubes 10 times.

-Tubes centrifuged for 5 minutes at 10,000g.

-Aqueous phase transferred to a new 1.5 ml Eppendorf tube. Avoid transferring any of the interphase.

-An equal volume of isopropanol (Fisher) is added to the tube to precipitate the DNA. Tube mixed by inverting 20 times.

-Tubes centrifuged for 5 minutes at 10,000g. Isopropanol is removed, being careful not to disturb the DNA pellet.

-1 ml 70% Ethanol added to tube followed by gently inverting the tube 10 times.

-Tube placed at 4^0C for 2 hours.

-Tubes centrifuged for 5 minutes at 10,000g and 70% ethanol carefully removed.

-1 ml 100% ethanol added and tubes gently inverted 10 times.

-Tubes centrifuged for 2 minutes at 10,000g. Ethanol removed and pellet air dried for 3 hours at room temperature.

-Pellet resuspended in 40 µl TE buffer. Tubes placed at 4^0C overnight.

-Concentration of DNA measured by determining absorbance at 260 nm as described in the Standardized Procedures section. Absorbance at 280 nm (protein) is also measured. A good 260/280 ratio is 1.8.

-Mouse tail genomic DNA stored at -20^0C until needed.

Restriction enzyme digestion of Genomic DNA

-The pJ5 vector (257) (ATCC) contains an EcoRI restriction site between the S100A7 cDNA and the MMTV promoter. Therefore cutting with EcoRI will produce a DNA

fragment that contains the S100A7 cDNA transgene flanked by vector sequence and unknown genomic sequence.

-In a DNase and RNase free 500 µl Eppendorf tube, 10 µg of genomic DNA is digested with 1 µl EcoRI (100U/µl, Invitrogen) in a total volume of 40 µl overnight in a 37^0C water bath.

Running of Southern Gel and Transfer of DNA to Nitrocellulose

-4 µl 10X Loading Dye is added to each restriction digest tube and entire digest is electrophoresed overnight through a 25 cm long 0.8% agarose TBE gel containing EtBr at 22 volts using a comb width of 6 mm and depth of 1 mm.

-Electrophoresis is complete when running dye is 2 cm from bottom of gel.

-Gel is photographed under ultra violet light using MCID image capture software.

-Under UV light, any extra areas along the gel edge that do not contain DNA are removed. Bottom right corner of gel is cut as a reference point.

-Gel is submerged in Gel Denaturing Buffer for one hour at room temperature with gentle shaking.

-Gel is then submerged in Gel Neutralizing Buffer for one hour at room temperature with gentle shaking.

-Dimensions of gel are measured and a piece of 45 micron nitrocellulose (Osmonics Inc.) and 2 pieces of Whatmann filter paper are cut to these exact measurements.

-Alkali transfer is set up with components in the following order from bottom to top: wick with ends submerged in Gel Neutralizing Buffer, gel (top side down), nitrocellulose, 2 pieces of Whatmann filterpaper, stack of paper towels.

-A weight is placed on top of the paper towels and checked for level.

-Transfer is allowed to proceed overnight.

-Next day, position of wells from the gel is marked with a pen on the nitrocellulose to show lane position.

-Nitrocellulose is baked at 80^0C for 2 hours after which time it is stored at 4^0C in a sealed bag that has had all the air removed.

Generation of Radioactive Probe for S100A7 Transgene and Probing of Nitrocellulose Blot

-Ten 50 µl PCR reactions were performed using pJ5 S100A7 cloning primers and 1 µl of MDA-MB-468 cDNA from a reverse transcription reaction. PCR product length ~320 nucleotides long.

-Reactions were pooled passed through a Wizard PCR Kit (Promega) to remove unincorporated nucleotides and primers.

-DNA was precipitated using NaAc + ethanol method described in Standardized Procedures section. Final concentration was adjusted to 0.5 µg/µl with sterile distilled water.

-Random Primers DNA Labeling System (InVitrogen) was used according to manufactures instructions to generate a single stranded DNA probe labeled with [α-^{32} P]-dCTP (New England Nuclear).

-Probe purified by removing the unincorporated nucleotides with a NICK Column (Pharmacia).

-Purified probe added to 10ml Prehybridization Solution then boiled at 100^{0}C for 10 minutes followed by incubation on ice for 15 minutes before being added to blot.

-Nitrocellulose prehybridized with 10 ml Prehybridization Solution for at least 1 hour at 42^{0}C with gentle rotation. Prehybridization Solution discarded before addition of probe.

-Probing performed at 42^{0}C with gentle rotation overnight.

-Probe removed and stored at 4^{0}C.

-Nitrocellulose blot washed for 10 minutes at room temperature with gentle shaking in 200 ml Genomic Southern Wash Solution 1.

-Was Solution 1 discarded and blot washed a second time for 10 minutes at room temperature with gentle shaking in 200 ml Genomic Southern Wash Solution 2 that has been heated to ~65^{0}C.

-Wash Solution 2 removed and blot allowed to partially dry at room temperature. Blot then placed in a plastic bag, air removed and then bag sealed.

-Blot placed in a Kodak photographic cassette with amplification screens. A sheet of KodakMS film is placed over top of blot, cassette is then sealed and placed at -70^{0}C for 24 hours. After which time, the film is developed. A new sheet of film is placed over the blot for an exposure longer than 24 hours if signal is week.

Interpretation of Southern Results

-The probe is specific for the transgene as there is no sequence in the mouse genome similar to human S100A7.

-A wild-type mouse will have no strong transgene band. A homozygote transgenic mouse has a band intensity twice that of a heterozygote, as it has the transgene on both alleles. All homozygotes will have the same band intensity if from the same founder mouse.

3.3.37- Extraction of Protein from Mouse Mammary Glands

Extraction procedure performed using TRIzol Reagent (InVitrogen) according to manufactures instructions. Briefly: proteins are isolated from the phenol-ethanol supernant obtained after precipitation of DNA with ethanol.

-Precipitate proteins from phenol-ethanol supernant with isopropanol (~1.5 ml)

-Incubate at room temperature then centrifuge at 12000g for 10 minutes at 4^0C.

-Remove supernatant and wash pellet 3 times using 2 ml of a solution containing 0.3 M guanidine hydrochloride in 95% ethanol. During each wash cycle store the protein pellet in the wash solution for 20 minutes at room temperature then centrifuge at 7500g for 5 minutes.

-After the final wash vortex the protein pellet in 2 ml ethanol. Centrifuge 7500g for 5 minutes.

-Vacuum dry the pellet for 10 minutes then dissolve in 50-100 µl of 1% SDS by pipetting.

3.3.38- Co-Immunoprecipitation of S100A7 with Jab1

-Human breast cancer cell lines expressing S100A7 (231-HP2 and MDA-MB-468) and mutated S100A7 (231-PTM.2 and 231-PTM.14) were grown to 80% confluency in 100mm culture dishes in complete medium. Cells were lysed on ice for 10 minutes with 500 µl Co-immunoprecipitation Buffer [25 mM HEPES pH 7.7, 0.4 M NaCl, 1.5 mM $MgCl_2$, 2 mM EDTA, 1% Triton X-100, 0.5 mM DTT, and protease inhibitor mixture (Roche)].

-Complexes were immunoprecipitated with 0.75 µg Jab1 antibody (Santa Cruz) 150 µl protein G-Sepharose (Pierce) at 4°C for 6 hours with rotational mixing at 100 rpm.

-Washes were performed with rotational mixing at 100 rpm in 500 µl Co-immunoprecipitation Buffer (NaCl concentration was diluted to 0.1 M) for 15 minutes.

-Between each wash, G-Sepharose beads were gently pelleted by centrifugation at 100g for 1 minute at 4^0C. Pellet was gently resuspended by pipetting up and down.

-Protein was extracted from the G-Sepharose beads by adding 100 µl Sample Isolation Buffer, mixing thoroughly, and centrifugation at maximum speed for 5 minutes.

-Protein concentrations were determined using the Micro-BCA protein assay kit (Pierce). Protein lysates were run on a 16.5% SDS-PAGE mini gel using Tricine SDS-PAGE to separate the proteins, and then transferred to 0.2 µm nitrocellulose (BioRad).

-After blocking in 10% skimmed milk powder in Tris-buffered saline-0.05% Tween, blots were incubated with primary antibodies for Jab1 and S100A7, followed by incubation with appropriate secondary antibodies and visualization by incubation with Supersignal (Pierce) as per the manufacturer's instructions and exposure to photographic film as described in the Standardized Procedures section.

3.3.39- Cell Adhesion Assay

-MDA-MB-231 clones were trypsinized from flasks that were 60–70% confluent.

-10,000 cells were plated in triplicate on three different days in 96-well plates having fibronectin, collagen I, or uncoated plastic surfaces (Becton Dickinson).

-After allowing cells to settle and begin to adhere for 1 hour at 37^0C, nonadherent cells were gently washed away with PBS using a multi-channel pipetter.

-Media was removed and 100 µl Crystal Violet was pipetted into each well and incubated for 5 minutes.

-Crystal Violet was removed and wells were washed very carefully 3 times with distilled water.

-Crystal violet was liberated from adherent cells by flooding wells with 200 µl 100% methanol (Fisher).

-Plates were gently rocked back and forth for 15 minutes at room temperature before the spectrophotometric absorbance (590 nm) was determined for each well using a Spectra Max 190 spectrophotometer (Molecular Devices).

3.3.40- Cell Growth Assay

-1000 cells/well were plated in plastic 96-well plates in triplicate on three different days and allowed to grow for 18, 24, 48, and 72 hours.

-Media was removed and wells were flooded with 100 µl crystal violet and incubated for 5 minutes.

-Crystal Violet was removed and wells were washed very carefully 3 times with distilled water.

-Crystal violet was liberated from adherent cells by flooding wells with 200 μl 100% methanol (Fisher).

-Plates were gently rocked back and forth for 15 minutes at room temperature before the spectrophotometric absorbance (590 nm) was determined for each well using a Spectra Max 190 spectrophotometer (Molecular Devices).

3.3.41- Modified Boyden-Invasion Assays

-Preformed in separate triplicate on Matrigel-coated modified Boyden-invasion chambers (24-well plate inserts with 8 μm pores; Becton Dickinson).

-10% FBS DMEM was used as a chemoattractant in the lower chamber, DMEM without L-glutamine or glucose supplementations was used in the upper chamber.

-350,000 cells were added to the upper chamber and allowed 12 hours to degrade the Matrigel and invade through the porous membrane.

-Cells that invaded and were adhering to the bottom of the membrane were stained with crystal violet.

-Invaded cells were visualized by light microscopy and numerated by counting the number of cells per high power field in five random fields.

3.3.42- Hypoxia Treatment of Culture Cells

-Hypoxic stimulation of cells was performed in a Forma Scientific Model 1025 Anaerobic System containing an atmosphere of 0.7% O_2, 5% CO_2, and 5% H_2 at 37°C

-Growth media and sterile distilled were placed in the chamber for 24 hours in 160 mm culture dishes for at least 24 hours to make them hypoxic.

-Cells were trypsinized and plated on 100 mm dishes under normoxic conditions and allowed to grow for at least 24 hours under standard aerobic culture conditions (see Standardized Procedures section).

-Dishes that have reached a cellular confluency of at least 60% are then placed in the aerobic chamber.

-Normoxic media is removed and replaced with 12 ml pre-conditioned hypoxic media and 1 ml hypoxic water. Hypoxic water is produced by placing 40 ml sterile distilled water in a 100 mm culture dish in the hypoxic chamber for 24 hours.

-Dishes are placed into the 37^0C incubator within the hypoxic chamber. Cells allowed to grow for 24 hours.

-To harvest protein, dishes are removed from hypoxic chamber and immediately the media is removed followed by a fast wash with 10 ml PBS, which is then removed.

-Cells are lysed with 200 µl SIB, scraped off the dish's surface with a cell scraper and transferred to a 1.5 ml Eppendorf tube.

-Tubes are vortexed briefly before being stored at -20^0C.

-To determine the protein concentration, samples are processed as described in the Standardized Procedures section.

3.3.43- Generation of Rabbit anti-S100A7 Polyclonal Antibody

-Antibody designed against amino acids 88-101 of human S100A7 corresponding to the amino acid sequence KQSHGAAPCSGGSQ.

-Peptide synthesis, conjugation of peptide to peptide carrier (KLH= keyhole limpet hemocyanin), injection of animals and serum bleeds were all performed by Research Genetics.

Standard protocol for 2 rabbits

Procedure	Time Relative to Placing Order	Time Relative to Injection of Animals	Description
Peptide synthesis	~2 weeks	-	-
Peptide conjugation to KLH carrier	~3 weeks	-	-
Control serum collection	~4 weeks	Day 0	Pre-bleed (~5 ml)
Primary injection	~4 weeks	Day 1	0.25 mg KLH emulsified with Complete Freund's Adjuvant injected subcutaneously
1st boost	~6 weeks	Day 13	0.10 mg KLH emulsified with Incomplete Freund's Adjuvant injected subcutaneously
Serum collection	~8 weeks	Day 26	Bleed 20-25 ml per rabbit
2nd boost	~ 10 weeks	Day 43	0.10 mg KLH emulsified with Incomplete Freund's Adjuvant injected subcutaneously
Serum Collection	~12 weeks	Day 55	Bleed 20-25 ml per rabbit
3rd boost	~12 weeks	Day 56	0.10 mg KLH emulsified with Incomplete Freund's Adjuvant injected subcutaneously
Serum collection	~14 weeks	Day 70	Bleed 40-50 ml sera per rabbit
ELISA and shipping	~16 weeks	Day 84	

-Sera was purified by Research Genetics by first IgG column purification followed by purification by column chromatohraphy using peptide-conjugated beads.

-Final concentration of purified antibody was 1.5 mg/ml and totaling 18.6 ml.

-An equal volume of glycerol was added to purified sera, mixed gently, yet thoroughly.

-200 µl 1:1 (sera:glycerol) was pipetted into sterile 1.5 ml Eppendorf tubes and stored at -20^0C.

3.3.44- Anoikis Assay

-Cells were grown to 40% confluence in 100 mm tissue culture dishes, then trypsinized and resuspended in complete media (for detailed description see Standardized Procedures section).

-Suspended cells were grown in 100 mm sterile bacterial dishes (Fisher) that were continuously rocked back and forth at 40 rpm in a standard tissue culture incubator for 72 hours at 37°C.

-After 72 hour growth period, cells were collected in a 15 ml sterile conical tube and gently pelleted by centrifugation at 100g for 5 minutes.

-Supernant was discarded.

-Cells were gently resuspended in 10 µl PBS with 5 µg/ml acridine orange (Sigma) and 5 µg/ml ethidium bromide (Sigma) and allowed to incubate for 10 minutes on ice.

-A 10µl aliquot was pipetted onto a microscope slide using 200 µl large bore pipette tips.

-A coverslip was placed on top of cells that were then viewed with a fluorescent microscope (Eclipse E1000, Nikon) using a wide band fluorescein filter.

-Apoptosis was defined according to morphological assessment of chromatin condensation using the fluorescent dyes that bind to DNA.

-Early apoptotic cells were defined as having condensed chromatin which lines the nuclear membrane in crescent shapes.

-Late stage or necrotic cells are red and are not counted in the analysis.

-The apoptotic index (%) reflects the proportion of apoptotic cells for 300 cells counted per assay. Triplicate assays were performed on non-consecutive days.

3.3.45- Reporter Gene Assays

-MDA-MB-231 clones expressing S100A7 or mutated S100A7 or no S100A7 were plated onto 60mm culture dishes and grown under standard culture conditions.

-When the plates reached ~70% cellular confluency, they were transfected with either an AP-1-driven Firefly luciferase reporter gene (Stratagene) or an NF-κB driven luciferase (from Dr. S.B. Gibson, University of Manitoba) with a constitutively expressing Renilla luciferase expression vector (Promega) in a 10:1 ratio, in triplicate experiments using Effectene (Qiagen). 2 μg of total DNA was transfected per dish using Effectene (Qiagen) according to the manufactures instructions.

-For each individual cell line, triplicate transfection experiments were performed on non-consecutive days.

-24 hours post transfection, media was removed and cells were washed with cold PBS before being lysed with 100 μl lysis buffer from the Stop and Glow Kit (Promega).

-Each cell lysate was processed according to the Stop and Glow Kit instructions.

-Individual cell lysates were used for triplicate luciferase measurements in a 96-well plate.

-Firefly luciferase activity for each sample was standardized to the corresponding Renilla luciferase activity for that sample.

-Dual luciferase signals were measured with an LMax lumonitor (Molecular Devices).

-Triplicate luciferase measurements for each time point were averaged. The luciferase values for each experiment were analyzed for statistical significance using Prism Graphpad software to identify any changes between the different cell lines.

3.3.46- RNAi Knockdown of Endogenous S100A7

-Using software from Oligoengine, a specific region of S100A7 was targeted for RNAi mediated knock down.

-The oligonucleotides used were RNAi-S100A7-U (5'-GAT CCC CAG CCA AGC CTG CTG ACG ATT TCA AGA GAA TCG TCA GCA GGC TTG GCT TTT TTG GAA A) and RNAi-S100A7-L (5'-AGC TTT TCC AAA AAA GCC AAG CCT GCT GAC GAT TCT CTT GAA ATC GTC AGC AGG CTT GGC TGG G). Both oligos were phosphorylated at the 5' end by the manufacturer (InVitrogen).

-Oligonucleotides were annealed together resulting in the generation of BglII and HindIII sticky ends.

-The expression plasmid pSUPER.retro.puro (Oligoengine) was linearized with BglII and HindIII restriction digests.

- Ligation of the annealed oligonucleotides into pSUPER.retro.puro was performed as described in the Standardized Procedures section.

-The resulting plasmid, pPsorRNAi, was transiently transfected into the human breast cancer cell line MDA-MB-468 using the Effectene transfection reagent (Qiagen).

-Protein was harvested 48 hours post transfection and Western blot performed.

3.3.47- *In-vivo* Studies of Human Breast Cancer Cells

-All experimentation involving animals had a protocol approved by the University of Manitoba Animal Care Committee.

-Breast cancer cells (five experimental groups comprising MDA-MB-231 parental cells, 231-HP1, 231-HP2, 231-PTM.2 and 231-PTM.14) were grown in culture and then $5x10^5$ cells were suspended in 0.2 ml of PBS before injection into mammary fat pads of female nude mice.

-Each experimental group included 5 animals, and two injections were sited bilaterally in each animal to achieve a total of 10 possible tumor sites per group.

-Tumor diameters were measured by calipers at weekly intervals, and the tumor volume was calculated from the formula: volume = $4/3\ \pi(0.5 \text{ X smaller diameter}^2 \text{ X } 0.5 \text{ X larger diameter})$.

-The experiment was continued for up to 8 weeks or when tumor diameter reached 1.5 cm, as required by the protocol.

-8 weeks post injection, all of the animals were euthanized, and all of the injection sites, tumors, and multiple organ tissues (abdominal lymph nodes, lungs, liver, and spleen) were examined grossly for the presence of tumor.

-Representative tissue blocks from all of the primary injection sites and all of the organ sites suspicious for metastatic tumor were subsequently processed by 10% formalin fixation, paraffin embedding, and preparation of H&E-stained sections for light microscopic examination.

3.3.48- Tumor Cohort Studies and Immunohistochemistry

-All breast tumor cases used for this study were selected from the Manitoba Breast Tumor Bank (Winnipeg, Manitoba, Canada) (258), which operates with the approval from the Faculty of Medicine, University of Manitoba, Research Ethics Board.

Antibody Target	Source	Dilution
S100A7	Custom made for P.H.W.	1:3000
Phospho-Akt (Ser 473)	Cell Signaling	1:150
$p27^{Kip1}$	Becton Dickenson	1:1000
Estrogen Receptor-α	Novocastra Laboratories	1:50
Jab1	Santa Cruz	1:200

To determine a relation between S100A7 and Survival

-A study set of 122 consecutive invasive breast carcinomas was selected on the basis of (a) ER-negative status (defined as <10 fmol/mg protein), (b) minimum follow-up duration of 6 months, and (c) predominantly invasive ductal tumor type, either alone or mixed with lobular type, and blocks containing predominantly invasive carcinoma were used for the study.

-5 μm thick tumor sections were cut from a representative formalin-fixed, paraffin-embedded archival tissue block from each tumor.

-Sections were placed on Superfrost (Fisher) microscope slides.

-Immunohistochemical staining for S100A7 was performed using an automated tissue immunostainer (Ventana Medical Systems) and 3,3'-diaminobenzidine immunohistochemistry kit and bulk reagents supplied by manufacturer.

-The staining protocol was set to "Extended Cell Conditioning" procedure, followed by 12-h incubation with primary antibody (concentration 1: 3000) and 32 minute incubation with secondary antibody.

-Positive staining was assessed by light microscopy (P.H.W), and levels of expression were determined by estimation of the proportion of positive epithelial cells within each cross section as described previously. S100A7 cytoplasmic and nuclear expression were assessed separately, and the S100A7 nuclear/cytoplasmic intensity ratio was calculated from the separate intensity scores.

-Associations with clinicopathological variables were determined by Fisher's exact test, and correlations were assessed by the Spearman test.

-Time to progression was defined as the time from initial surgery to the date of any clinically documented local or distant disease recurrence or death attributed to breast cancer.

-Survival was defined as the time from initial surgery to the date of death attributed to breast cancer. All other deaths were censored.

-Overall survival was also assessed and was defined as the time from initial surgery to deaths from any cause, whether known to be breast cancer specific or not. The association with progression and survival was assessed by both univariate (Logrank test and Kaplan-Meier method) and multivariate (Cox regression model) analysis. All tests were performed using SAS statistical analysis software.

S100A7 Expression in Ductal Carcinoma In-Situ

-Cases of pure DCIS of the breast were selected by review of breast surgical resections that were done from 1981 to 1999 at the Health Sciences Centre and St. Boniface Hospitals, Winnipeg, Manitoba.

-Cases of DCIS associated with invasive carcinoma were selected from the Manitoba Breast Tumor Bank (258).

-A total of 90 patients with pure DCIS and 46 patients with DCIS associated with invasive carcinoma were identified. The histologic nuclear grade was determined according to the criteria for the Van Nuys grading system (24).

-The presence of intraductal necrosis, defined as nuclear and eosinophilic debris, was evaluated in hematoxylin–eosin stained sections by light microscopy, and the percentage of ducts exhibiting necrosis was estimated semiquantitatively.

-Periductal inflammation was assessed semiquantitatively as low (absent or very sparse inflammatory cells), high (marked inflammation surrounding over 50% of the ducts), or intermediate.

-Staining for S100A7, ER, Jab1, and $p27^{kip1}$ was performed using an automated tissue immunostainer (Ventana Medical Systems) and DAB immunohistochemistry kit (ABC method; Ventana Medical Systems).

-Staining protocol was set to the 'extended cell conditioning' procedure, followed by 12 hours of incubation with primary antibody before incubation with secondary antibody and detection.

-Immunohistochemistry results for all genes were assessed by light microscopy performed by a pathologist (P.H.W.) independently of the pathologic assessment.

- Levels of expression of S100A7, $p27^{kip1}$, and Jab1 proteins (both nuclear and cytoplasmic staining was assessed separately for each) and ER protein (nuclear staining only was assessed) were all determined by scoring the intensity (0 = no staining, 1 = weak staining, 2 = moderate staining, and 3 = strong staining) and the percentage of neoplastic epithelial cells exhibiting staining within the tissue section.

-The product of the intensity and the percentage was determined to provide a final, semiquantitative immunostaining score (immunohistochemistry scores, ranging from 0 to 300).

-For S100A7 an immunohistochemistry score greater than 0 was regarded as positive (we have found this cut-point can divide invasive carcinomas into good and poor outcome subgroups).

-Among S100A7-positive cases, the lower 25th percentile of expression corresponded to an immunohistochemistry score of 1–9 and the upper 75th percentile corresponded to an immunohistochemistry score of 100 or greater. On this basis, immunohistochemistry scores of 1–9, 10–99, and 100 or greater were regarded as low, intermediate, and high expression.

-For ER an immunohistochemistry score greater than 10 was regarded as positive (equivalent to the clinically validated cut-point in similar immunohistochemistry scoring systems).

-Statistical analysis was performed with Prism Graphpad software (Graphpad Prism v4.00, Graphpad software) and using Spearman correlation, χ^2 test, t-test and Wilcoxon rank sum tests as appropriate. $p< 0.05$ was considered statistically significant.

Tissue Micro Array

-A Tissue Micro Array was constructed based on a cohort of 142 ER negative invasive carcinomas with ductal or lobular histology selected from the Manitoba Breast Tumor Bank (258).

-Duplicate 0.6 mm tissue cores were removed from the central portion of a representative paraffin block from each tumor, using a Beecher Instruments Tissue Arrayer and embedded into a paraffin block the size of a standard microscope slide.

-Immunohistochemical staining for S100A7 and phospho-Akt was performed essentially as described previously using an automated tissue immunostainer (Ventana Medical Systems), and bulk reagents supplied by manufacturer.

-Primary S100A7 antibody (1:3000) or phospho-Akt (Ser 473) antibody (1:150) were incubated for 32 minutes.

-Staining was assessed by light microscopy performed by a pathologist (P.H.W.) and was scored by the intensity and the percentage of positive neoplastic epithelial cells as described to generate a semi-quantitative immunostaining score (immunohistochemistry score = % positive neoplastic epithelial cells x intensity) that ranged from 0-300.

-For categorical statistical analysis, S100A7 immunohistochemistry score >0 was regarded as positive for S100A7. For phospho-Akt, immunohistochemistry scores of >0, ≥20 (median score), and ≥60 (upper quartile score) were used to define positive status in separate analyses since a wide range of cutpoints has been used in the literature (259, 260).

-Statistical analysis was performed with Prism Graphpad software and using Spearman correlation and Fisher's exact tests as appropriate.

3.3.49- Molecular Modeling of Mutant S100A7

-Three residues (Asp58, Leu80 and Gln90) of human S100A7 were substituted with Gly58, Met80 and Lys90 respectively.

-The 3D models were built based on the X-ray structures (Protein Data Bank codes, 3PSR and 2PSR), and compared with the experimental findings (185).

-CAChe WorkSystem Pro 6.1.1 software (Fujitsu Limited) was used to substitute the residues and to build the 3D models.

-The energy of the resulting molecules was optimized using molecular mechanics (MM2) and optimization was continued until the energy change was less than 0.001 kcal/mol.

4.1.0- Identification of Proteins That Physically Interact with S100A7 and Structural Basis for Interaction

Prior to the beginning of this project, S100A7 was regarded as an important gene in non-neopalstic inflammatory skin disease and there was only one report in the literature describing a potential biological function for S100A7 (188), where it was suggested that S100A7 was a potent chemokine for CD4 + lymphocytes in an *in-vitro* system. At this same time, the seminal reports that identified very high levels of S100A7 expression in cancer, when compared to normal cells, had just been published for bladder (193) and breast (105, 107). These reports raised the possibility of a new role in cancer but were purely observational and the questions relating to S100A7's role in breast cancer progression, growth and survival had never been addressed. Our strategy at the time (due

to a lack of functional knowledge about most S100 proteins) was to identify proteins that formed a physical interaction with S100A7 in human breast cancer cells. While identification of such a protein would not in itself answer our question, the gamble was that a functional property of the S100A7-interacting protein might be already known in the literature and so provide a signpost to the cellular pathways that S100A7 affects that could be tested by functional and biological assays.

4.1.1- Yeast 2-Hybrid Assay to Screen for Potential Interactions with S100A7

The Yeast Bait vector pGBT9-psor was used to screen a normal human mammary gland cDNA expression library to identify potential proteins with which S100A7 forms a physical interaction. Prior to initiating the 2-hybrid experiment, Yeast transformed with the pGTBT9-psor expression plasmid were assessed by Western blot. A protein band can be detected at the expected size for the S100A7-Gal4 DNA-Binding Domain fusion protein (S100A7-Gal4BD) using an S100A7 specific antibody (FIG 6). Untransformed Yeast (*Saccharomyces cerevisiae*, strain KGY37) do not manifest this protein band. The total number of colonies that were then screened for an interaction with S100A7-Gal4BD in the 120X screen was 17.27×10^6, which resulted in each independent clone being screened for an interaction with S100A7-Gal4BD approximately 4 times (the number of independent clones within the library was 3.5×10^6). Of these 17.27×10^6 potential interactions, 343 colonies that grew on SC -trp-leu-his +5 mM 3-AT media were picked over an 18-day period for further analysis.

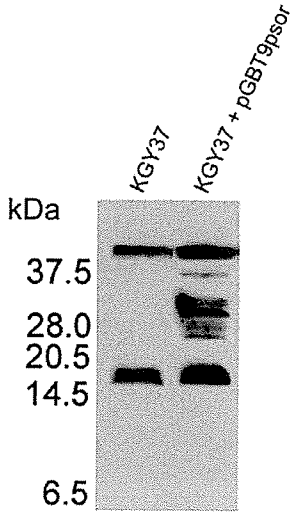

FIG 6 - S100A7 Expression in Yeast.
Western blot showing detection of the 30.5 kDa S100A7-Gal4BD fusion protein in *Saccharomyces cerevisiae* (strain KGY37) that have been transformed with the plasmid pGBT9-psor.

Yeast colonies that grew on selection media were isolated and examined for the strength and specificity of their interaction with S100A7. 242 clones were isolated from the screen that were able to continually grow on selective media. During the initial characterization for the specificity of the interaction with S100A7-Gal4BD, 14 clones were found to strongly activate the LacZ reporter gene. 13 clones weakly activated LacZ while 7 clones were intermediate activators. The 14 clones that were 'strong' LacZ activators were selected for further analysis.

These 14 yeast clones had their cDNA library plasmid isolated by first collecting total plasmid DNA from Yeast followed by electroporation into *E. coli* KC8 that were then grown on M9 –leu selective media. Plasmid preps were performed on these bacteria, and isolated plasmids were electroporated into *E. coli* DH5α, followed by plating onto LB +carbenicillin agar plates. A total of 4 colonies were picked from each LB +carbenicillin plate for each 2-hybrid colony and expanded prior to analysis of the resident plasmids. Following plasmid isolation, plasmids were subjected to restriction enzyme cutting using EcoRI and XhoI. All 4 plasmid preps for each individual 2-hybrid colony/clone gave an

identical restriction digest pattern which suggested that there was only one cDNA-library plasmid taken up by the Yeast during the cDNA-library transformation step.

Individual cDNA-library clones were transformed into *S. cerevisiae* strain KGY37 containing pGBT9-psor plasmid, to determine if the interaction with S100A7 could be recreated. All 14 clones were able to grow on SC -trp -leu -his +5 mM 3-AT selective media when reconstructed.

4.1.2- Analysis of Yeast 2-Hybrid Clones for Specificity of the Interaction With S100A7

The specificity of the interaction between S100A7 and the protein encoded by the cDNA-library plasmid was measured in two ways. First, S100A7-Gal4BD was analyzed for its ability to activate reporter genes on its own, or with an empty Gal4AD plasmid and finally with a Prey fusion protein that was not isolated from the screen. Second, the protein encoded by the cDNA-library plasmid was analyzed for its ability to activate reporter genes on its own, and with a Gal4BD-fusion protein other than S100A7-Gal4BD, or with an empty Gal4BD plasmid.

Yeast transformed with only the Bait plasmid pGBT9-psor were not able to activate the His reporter gene, as they were unable to grow on SC-his +5 mM 3-AT agar plates. Similarly, Yeast with both pGBT9-psor and empty Gal4AD plasmid were unable to activate reporter genes. The same result was observed for Yeast with pGBT9-psor and the

unrelated Prey plasmid, which produced the fusion protein MAD2-AD. These results suggest that S100A7's ability to activate reporter genes in the Yeast 2-hybrid assay was dependent on it having a specific interaction with a Prey fusion protein.

On the basis of these additional tests for specificity, only 4 clones (numbered 6-3, 6-4, 11-10 and 13-18) out of the 14 clones that had an initial strong activation of the LacZ reporter gene, were confirmed to specifically interact with S100A7-Gal4BD. Yeast transformed separately with these 4 clones did not show activation of the His reporter gene on their own, as assayed by growth on the selective medium SC-his +5 mM 3-AT. Reporter gene activation was also absent for these 4 clones when transformed with the unrelated Bait protein RAD18-BD (from R.D. Gietz, University of Manitoba) or the empty Bait plasmid pGBT9. Representative plates for clone 6-3 showing no His gene activation are shown (FIG 7), identical results were obtained for clones 6-4, 11-10 and 13-18. The other 10 clones showed activation of the His reporter gene either by themselves, in the presence of the unrelated Bait fusion protein or both.

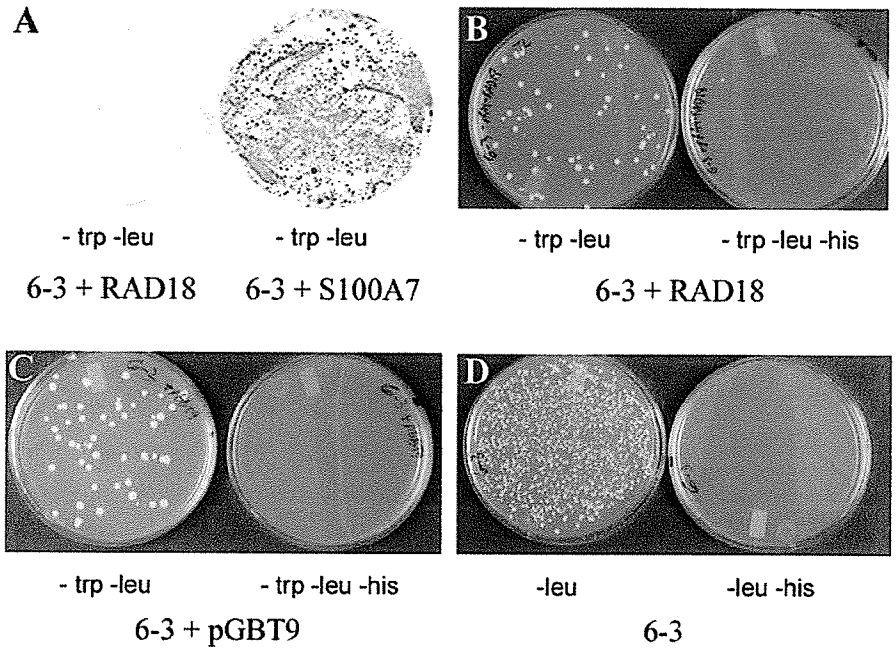

FIG 7 - Confirmation of Specificity of Interactions Observed in Yeast 2-Hybrid Assay. Panels show Yeast transformed with A) 6-3 and RAD18 expression plasmids (left), and 6-3 with S100A7 (right). Activation of LacZ reporter gene (blue color) is specific for S100A7. Yeast transformed with B) 6-3 and RAD18, C) 6-3 and empty prey vector, and D) 6-3 alone. In panels B-D, plates on left are Histidine+ (control) and plates on the right are Histidine- (test). Panels B) and C) show that there is a specific interaction necessary for activation of the reporter gene. Panel D) shows that 6-3 alone cannot activate the Histidine reporter gene as demonstrated by absence of growth on Histidine – plate.

When the four potential positives were transformed with S100A7-Gal4BD and re-assayed for activation of LacZ reporter gene, clone 6-4 did not show LacZ activation but its growth was equal to that of the other 3 clones in the presence of selective medium. DNA sequencing revealed the identity of the cDNA present in the library plasmids. Clone 6-3 was identified as RanBPM (GenBank accession NM 005493) but is missing the first N-terminal 1/3, 6-4 was the C-terminal half of GCP3 (GenBank accession

AF042378), 11-10 was found to be Jab1 (GenBank accession NM 006837) and encoded amino acids 42 to 335, clone 13-18 was identified to contain all the amino acids of a gene called CXX1 (GenBank accession NM 003928). All clones were found to be in the same reading frame as the N-terminal Gal4-AD.

At the time of writing, further analysis of the basis and significance of interactions with three of these candidates (Jab1, RanBPM, hGCP3) has been initiated within our laboratory. Briefly, an *in-vitro* interaction could be confirmed between S100A7 and RanBPM by biochemical interaction assay (261), but not between S100A7 and hGCP3. However, for both these two potential interactions, it has been impossible to confirm an *in-vivo* interaction in mammalian cells or identify a functional significance that might be relevant to an interaction between S100A7 with either RanBPM or hGCP3. The work described below is focused on the interaction with Jab1 that I have primarily pursued.

4.1.3- Deletion Mapping of S100A7 to Identify Jab1-Interacting Region

The interaction between S100A7 and Jab1 in Yeast was further analyzed by creating deletion constructs in an attempt to identify the Jab1-binding domain in S100A7. Two constructs were tested separately for the ability to interact with Jab1: an N-terminal portion of S100A7 containing amino acids 1-52, and a C-terminal portion spanning amino acids 43-101. In the Yeast 2-hybrid assay, the N-terminal construct was not sufficient to stimulate reporter gene production as these Yeast were not able to grow on SC-trp –leu –his +5 mM 3-AT selective medium after one week of incubation (FIG 8).

However, the C-terminal construct was able to interact with Jab1 and stimulate reporter gene production when grown on selective medium (FIG 8). This result might indicate that the Jab1-binding site is contained within the C-terminal portion of S100A7.

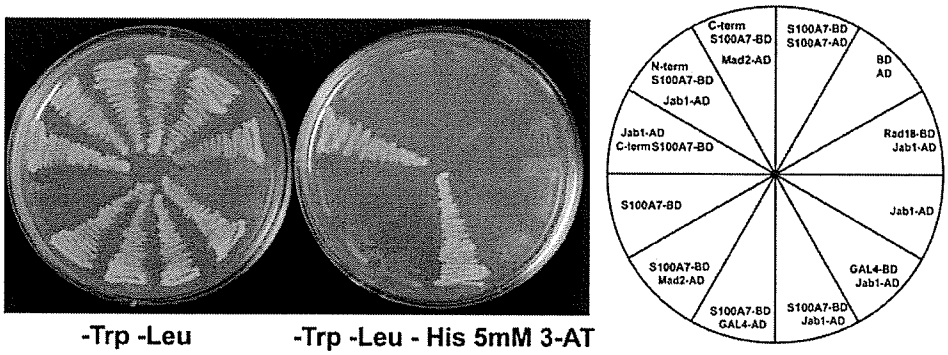

FIG 8 - Deletion Analysis of S100A7 and Specificity of Interaction with Jab1 in Yeast. The S100A7-Jab1 interaction was confirmed in Yeast, by testing S100A7 fused to the GAL4-BD (binding domain) with selected proteins fused to the GAL4-AD (activating domain). Yeast plates (- and + Histidine) are shown on the left, and the plating schema for each sector is shown on the right. Activation of reporter genes on test plate (-His) and colony growth is only present when the full-length S100A7 or the COOH-terminal half of S100A7 is combined with Jab1.

4.1.4- Mutation of the Jab1-binding domain of S100A7 alters the Predicted Physical Conformation of S100A7

To determine if there is a structural basis for the S100A7-Jab1 interaction, sequence analysis of S100A7 was performed which revealed a domain within the C-terminal portion of this protein that is present in other proteins that physically interact with Jab1 (217, 239). To test the role of this putative Jab1-binding domain in mediating the interaction with S100A7, we performed 3D protein modeling of the potential effect of

mutation of the three key amino acids within this domain (217) using the structure for the S100A7 protein which had previously been solved (185, 262). These studies were performed in collaboration with Dr. Sanat Mandal, Memorial University, Newfoundland. The details of the structure of S100A7 have been deposited into the Protein Data Bank (accession 3PSR and 2PSR). Comparison of the 3D models for unmodified S100A7 and S100A7 with specific amino acid substitutions in its putative Jab1-binding domain ($S100A7^{mut}$) shows their structures are different. The thread representation of X-ray structure (FIG 9 A) for S100A7 (gray), and $S100A7^{mut}$ (red) shows the greatest change in conformation around the metal binding sites for Ca^{2+} and Zn^{2+}, as indicated by arrows. A minimal structural error of 0.1767 as determined by RMS (root mean square) is calculated when the three residues Asp58/Gly58, Leu80/Met80 and Gln90/Lys90 are superimposed with each other. Similarly, structural error (RMS value is 0.3981) on metal sites (Ca=blue for S100A7, Ca=red for $S100A7^{mut}$, Zn=magenta for both) is also observed when the three metal cations are superimposed. Numerous differences are also observed when S100A7 and $S100A7^{mut}$ are compared within 3Å around the metal sites. For S100A7, both the Ca^{2+} ions in chain A and in chain B (refers to S100A7 homodimer that resulted from the crystallization procedure) have five residues (Asp62, Asn64, Asp66, Lys68 and Glu73) within 3Å. However, the Ca^{2+} sites (FIG 9 A, Ca red) in $S100A7^{mut}$ have the same residues in each site, but have more hydrogen bonds (blue labeling) resulting in the Ca^{2+} ion being very tightly bound (FIG 9 A, Ca (b)). Therefore, the Ca^{2+} sites (red) are crowded due to the presence of more hydrogen bonds which suggests the structural arrangement of Ca^{2+} sites are unavailable for further binding with their substrates and consequently making them less active compared to S100A7.

Similarly, significant structural changes around the Zn site (FIG 9 A) are also noticed. The Zn site, in both $S100A7^{mut}$ (magenta) and S100A7 (magenta) is coordinated by four residues (His17 and Asp24 from chain A, His86 and His90 from Chain B). Even though the Zn site for both forms of S100A7 has an identical number of residues, in the mutant, the imidazole ring for His100 is twisted horizontally compared with a more vertical inclined in S100A7. The dihedral angle (the angle of two ring C atoms and the two side chain carbon atoms of His100) is slightly different and this difference is due to the conformational change upon substitution. Similarly, conformational change is also observed in His88 and Asp26. However, the change in His15 is insignificant. Differences are also observed in bond angles around His90 and His68. Therefore, the Zn^{2+} ion in the mutant cannot retain the original functionality because of the conformational change in His90 and His86 around it, which in turn can change the geometry around Zn^{2+}.

The differences in position of the metals in the two proteins are further verified by measuring the distances between the metals (FIG 9 A, red triangle). Indeed, the distances between the metals in each protein are quite different (FIG 9 B). The differences around metal sites between the two proteins are further investigated by running theoretical spectra (UV-VIS) around 3Å of each metal site. Spectra (FIG 9 C) clearly show that the metal sites of the two proteins in fact are significantly different.

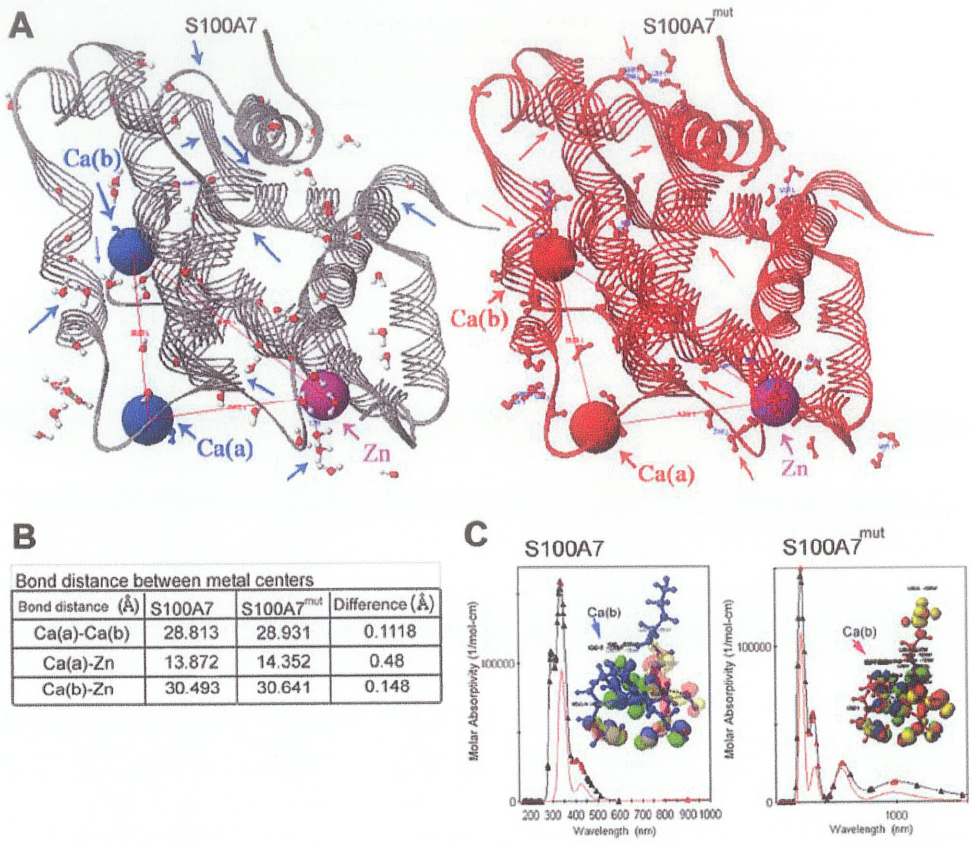

Bond distance between metal centers

Bond distance (Å)	S100A7	S100A7^{mut}	Difference (Å)
Ca(a)-Ca(b)	28.813	28.931	0.1118
Ca(a)-Zn	13.872	14.352	0.48
Ca(b)-Zn	30.493	30.641	0.148

FIG 9 - The Predicted Molecular Structure of S100A7^{mut} is Significantly Different from S100A7. A) Thread representation of S100A7 (3PSR, left) and S100A7^{mut} (right). Ca^{2+} ion (blue) and Zn^{2+} (magenta) are bound to S100A7. Predicted Ca^{2+} (red) and Zn^{2+} (magenta) binding positions are shown for S100A7^{mut}. The arrows indicate the largest differences in the conformation of the chains, the position of the metal ions and changes around them. B) Table showing predicted bond distances between metal sites in part A), and their calculated difference between S100A7 and S100A7^{mut}. C) The differences around metal sites between the two proteins were further investigated by running theoretical spectra (UV-VIS) around 3Å of each metal site. Spectra show the metal sites of the two proteins are significantly different.

Based on the above analysis, we conclude that mutation of the potential Jab1-binding domain of S100A7 could have a significant impact on a potentially important region within the S100A7 protein, but would not dramatically affect overall protein structure or

be expected to significantly affect the ability to homodimerize. On this basis, we proceeded to test the effect of the mutant S100A7 on its interaction with Jab1 and then determine effects after expression in breast cancer cells in culture.

4.1.5- Mutation of the Jab1-Binding Domain of S100A7 Abrogates Its Interaction with Jab1

Within the Yeast 2-hybrid assay, we had already found that the C-terminal half of S100A7 was sufficient for the interaction with Jab1, whereas the N-terminal half could not interact with Jab1 and activate appropriate reporter genes (FIG 8). To assess the effect of mutation of the putative Jab1-binding domain of S100A7 on the interaction with Jab1, we mutated the putative Jab1-binding domain (resulting in the changes Asp58/Gly58, Leu80/Met80 and Gln90/Lys90, as these resulting mutations were found to cause a loss of association with Jab1 (217)) in both the full length S100A7 cDNA as well as a cDNA representing the C-terminal portion alone, and co-expressed these proteins separately with Jab1 in the yeast 2-hybrid assay. We found that in both contexts, these mutations abolished the interaction between S100A7 and Jab1 (FIG 8) as reporter gene activation was not present or reporter gene activation was at a level too low to allow growth.

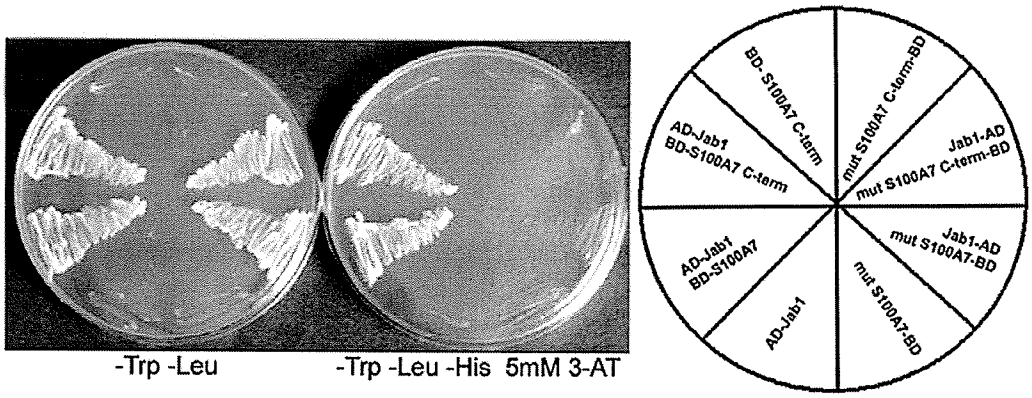

FIG 10 - Mutation of the Jab1-Binding Domain of S100A7 Abolishes an Interaction with Jab1 in Yeast. Yeast 2-hybrid control plate (left plate) shows the presence of both a Bait and Prey plasmid are required for growth in the absence of Tryptophan and Leucine. Both the full length and the C-terminal half of S100A7 can interact with Jab1 on the test plate (right plate), but mutating the Jab1-binding domain prevents an association between these proteins as determined by inactivation of the His gene resulting in the absence of growth. The plating schema for each sector is shown on the right.

To further test the role of this same domain within human breast cancer cells and to enable subsequent functional analysis, we then developed MDA-MB-231 cells with stable expression of the full-length mutated S100A7 cDNA ($S100A7^{mut}$) by substituting Asp58/Gly58, Leu80/Met80 and Gln90/Lys90. Two independent stably transfected clones (231-PTM.2 and 231-PTM.14) were then assayed for an interaction between $S100A7^{mut}$ protein and Jab1 by co-immunoprecipitation (FIG 11). Under the same conditions whereby endogenous and transgene derived S100A7 protein could be co-immunoprecipitated with Jab1 from MDA-MB-468 and 231-HP2 (MDA-MB-231 cells stably expressing high amounts of S100A7), mutation of the Jab1-binding domain within S100A7 abolished or significantly reduced the association between $S100A7^{mut}$ and Jab1 in the 231-PTM.2 and 231-PTM.14 clones respectively. Both of these two clones express

comparable levels of S100A7^{mut} to the previously established S100A7 expressing MDA-MB-231 clones (231-HP1 and 231-HP2) (239) (FIG 14 B). However the higher levels of mutant protein observed in 231-PTM.14 cells revealed a limited residual interaction between S100A7 and Jab1. No S100A7-containing complex was detected in control lanes in the absence of Jab1 antibody or protein G beads (FIG 11). The S100A7-specific antibody immunoprecipitated S100A7 from MDA-MB-468, 231-HP2 and 231-PTM.14 cell lysates, but was unable to co-immunoprecipitate Jab1 (data not shown), presumably because of the proximity and partial overlap of the epitope recognized by the antibody (amino acids 88–101 of S100A7) and the proposed Jab1-binding domain (amino acids 57–89 of S100A7).

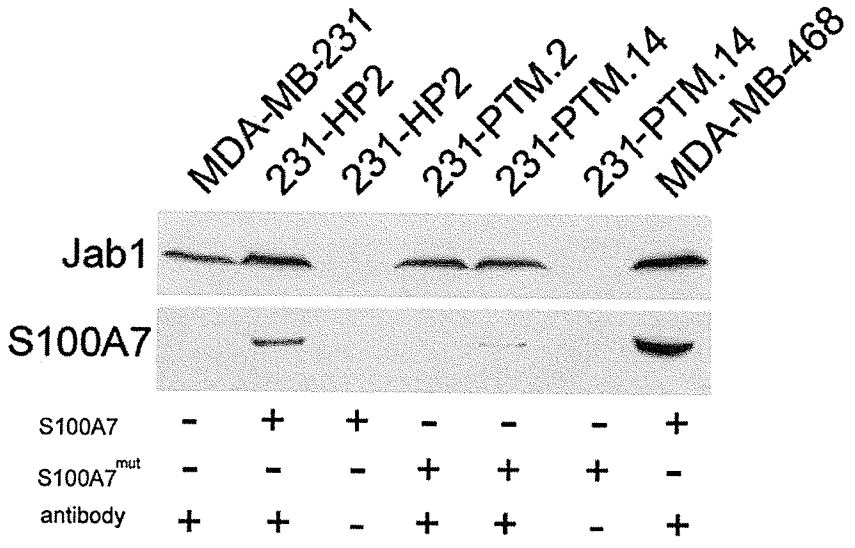

FIG 11- S100A7 Interacts with Jab1 in Human Breast Cancer Cells but not S100A7^{mut}. Western blot of co-immunoprecipitation experiment reveals S100A7 and Jab1 interact in human breast cell lines (MDA-MB-231 transfected with S100A7, and MDA-MB-468), but mutation of the Jab1-binding domain in S100A7 causes a loss or significant decrease in the association between these proteins (231-PTM.2 and 231-PTM.14 lanes respectively). The Jab1 immunoprecipitating antibody was also used for Western blot (Santa Cruz).

4.2.0- Studies of S100A7 in Breast Cancer Cell Line Models to Determine Functional and Biological Effects on Jab1 and Known Jab1 Downstream Pathways

The results from the Yeast 2-hybrid screen suggested that the Jab1 protein was a strong candidate to be a legitimate S100A7-binding protein. Through deletion mapping, bioinformatic identification of a putative Jab1-binding domain and predicted structure of S100A7 with mutation of this putative domain (see above sections 4.1.3 and 4.1.4), all provided further circumstantial support for this idea. Our next challenge was to seek evidence that an interaction between S100A7 and Jab1 may occur in human breast cancer tissues and demonstrate a functional consequence on the activity and function of Jab1 in established experimental cell line models of breast cancer. Once we had established an effect of S100A7 on Jab1 activity in cell lines, we could more easily rationalize the design of correlative experiments with human breast tumors to seek evidence of functional consequences *in-vivo*.

In pursuing the significance of the S100A7-Jab1 interaction we were guided by a rapidly expanding literature on Jab1 and its function. Briefly, Jab1 has become intensively studied in the past few years with several reports in the literature describing a range of functions for Jab1 in human cells (for a more detailed description of Jab1 see sections 2.3.0 and 2.3.1). Jab1 has emerged as a central regulating factor that can influence several pathways known to be important for progression and survival of breast cancer (FIG 12). The next sections describe our experiments to address several questions and themes that emerge from the following two hypotheses: 1) S100A7 is able to alter biological

activities/properties of breast cancer cells and 2) the cause of these alterations is due to the interaction of S100A7 with Jab1.

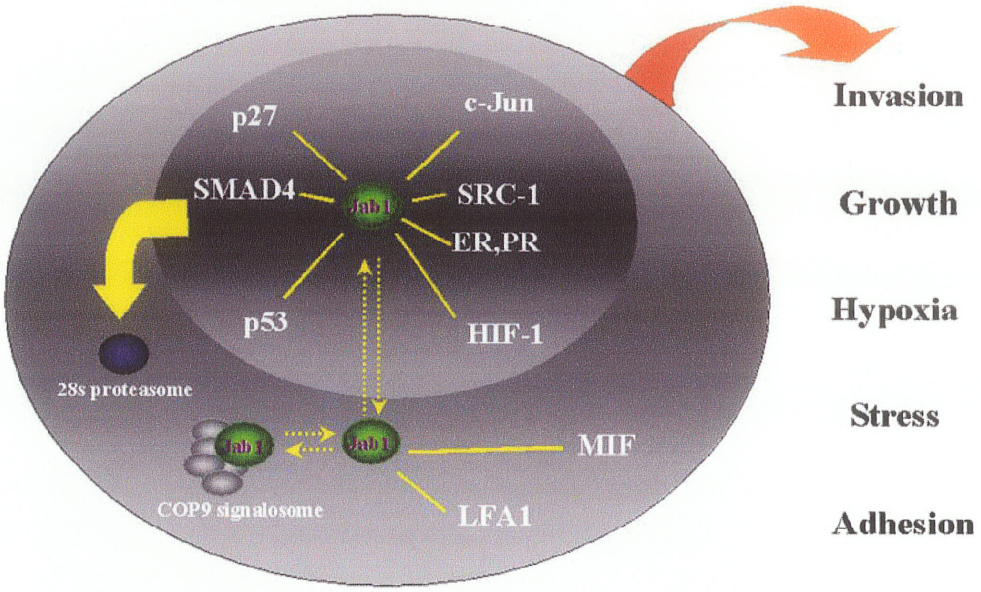

FIG 12- Jab1 Can Interact with Several Factors Known to be Important in Cancer. Jab1 has been reported to interact with several factors that are able to regulate gene transcription (inset right). Some of these interactions lead to proteins being targeted to the proteasome for degradation (inset left). Jab1 can also interact with proteins in the cytoplasm and associate with the large COP9 signalosome multiprotein complex. The result of Jab1's interaction with the factors shown here is to modulate biological pathways known to be important for breast cancer progression and survival.

4.2.1- Cellular Expression and Localization of S100A7 and Jab1 in MDA-MB-231 Breast Cancer Cells

To explore the effect of S100A7 on Jab1 it was first important to develop and characterize an S100A7 specific antibody. We therefore generated a rabbit polyclonal

antibody against the peptide sequence KQSHGAAPCSGGSQ, which corresponds to amino acids 88-101 of S100A7. This region was chosen, as it is unique to S100A7 and thus would not cross-react with other S100 proteins. The specificity of this antibody was confirmed by Western blot (see FIG 32 for example). Blockade of the signal was performed by pre-incubation of the antibody with the peptide and by comparison with other anti-S100A7 antibodies, including a chicken IgY anti-S100A7 antibody that had previously been generated against the same peptide, as described previously (106) (data not shown). The human breast cancer cell line MDA-MB-231 does not express S100A7 endogenously (127), but does express other S100's (263). We could not detect S100A7 expression in our MDA-MB-231 cells as expected, but were able to detect a band at the correct molecular size in MDA-MB-231 clones stably transfected with the S100A7 expression construct pcDNA3.1psor-neo (FIG 14 B). S100A7 expression could also be easily detected in the human breast cancer cell line MDA-MB-468, which has been shown by others to express high levels of endogenous S100A7 (127) (see FIG 31 for example).

We then used this rabbit anti-S100A7 antibody and a commercially available Jab1 antibody to localize S100A7 and Jab1 in the MDA-MB-231 clones by immunohistochemistry. Jab1 protein, like S100A7, has been found previously to be present in both nuclear and cytoplasmic locations in cell types other than breast. We observed both nuclear and cytoplasmic expression in the wild type MDA-MB-231 cells. In the three S100A7-expressing clones, 231-LP1, 231-HP1, and 231-HP2 (FIG 13), we observed a relative increase in Jab1 within the nucleus. However, the total amount of

Jab1 protein as detected by Western blot was similar in all of the cell clones and does not changed in the presence of S100A7 (FIG 14 B). S100A7 in 231-LP1, 231-HP1, and 231-HP2 clones is seen in both the cytoplasmic and nuclear compartments. S100A7 can also be detected by immunoprecipitation of medium conditioned by 231-HP2 and MDA-MB-468 cells (data not shown), suggesting that S100A7 is also secreted by breast cancer cells in culture.

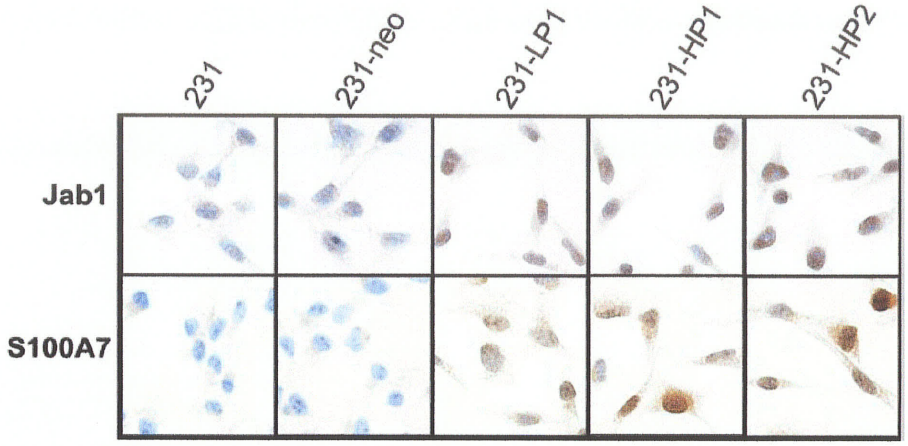

FIG 13- Expression of S100A7 in MDA-MB-231 Cells is Associated with Jab1 Translocating to the Nucleus. S100A7 and Jab1 were detected in cells by immunohistochemistry, and representative fields of each cell line are shown. *Left panels* show lack of S100A7 expression in control MDA-MB-231 cells and 231-neo cells, and the expression in the S100A7 transfected clones (231-LP1, 231-HP1, and 231-HP2). *Top panels* show comparable cytoplasmic Jab1 expression in each of the corresponding cell lines, but with enhanced nuclear Jab1 in all three S100A7 overexpressing clones.

4.2.2- S100A7 Expression Raises AP-1 Activity in MDA-MB-231 Breast Cancer Cells

To determine whether S100A7 influences known Jab1 functions in breast cancer cells, we examined AP-1-dependent transcription in the MDA-MB-231 clones using an AP-1 driven luciferase reporter (FIG 14 A). AP-1 activity was increased in the S100A7-expressing clones (231-HP1 and 231-HP2) where there was a 6.4 $\pm$ 0.2 fold increase (mean $\pm$ SD, n=6) in luciferase activity ($p>0.0001$) when compared to non-expressing control cell lines (MDA-MB-231 and 231-neo). These S100A7-expressing cells showed no difference in total Jab1 levels assessed by Western blot, compared with non-S100A7 expressing controls (FIG 14 B). However, the effect on AP-1 activity was consistent with a redistribution and relative increase in nuclear Jab1 protein, as detected by immunohistochemistry (FIG 13) and the findings of others (205). In clones expressing $S100A7^{mut}$, there was a 3.7 $\pm$ 0.3 (mean $\pm$ SD, n=6) fold increase ($p>0.0001$) in AP-1 reporter activity when compared to non-expressing control cell lines (FIG 14 A). The finding of a weak interaction between $S100A7^{mut}$ and Jab1 (FIG 11), was consistent with the additional finding that Jab1 activation of AP-1 may still occur in cells overexpressing $S100A7^{mut}$, but at a reduced level to that of un-mutated S100A7 where the interaction with Jab1 is much stronger.

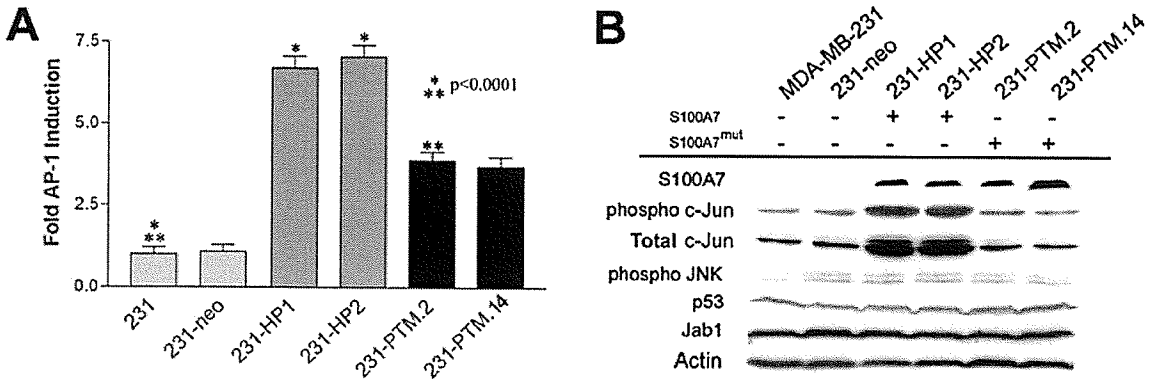

FIG 14- S100A7 Expression in MDA-MB-231 Stimulated AP-1 Activity. A) S100A7 expression can activate AP-1 activity in MDA-MB-231 cells as measured by reporter assay. While S100A7^{mut} can also stimulate AP-1 activity, it is to a lesser degree and is through a phospho c-Jun independent mechanism. B) Western Blot shows that expression of unmutated S100A7 but not S100A7^{mut}, is associated with an increase in the amount of phosphorylated c-Jun and total c-Jun. S100A7 does not alter the amounts of phospho JNK, p53 or Jab1. Actin is used as a loading control.

Expression of endogenous AP-1-dependent genes was next examined by RT-PCR (FIG 15). S100A7 expression was associated with an increase in mRNA levels for the endogenous AP-1-regulated genes VEGF (264) and MMP13 (265) and this increase was proportional to the levels of S100A7 in the MDA-MB-231 control and transfected cells. Clones expressing S100A7^{mut} appeared to be very similar to the non-expressing parental and control cells as both groups did not show a noticeable increase in the expression of VEGF and MMP13 genes as assessed by RT-PCR. Expression of GAPDH was also determined for all samples and was used as a loading control to show equal amounts of total cDNA at the start of the PCR reaction.

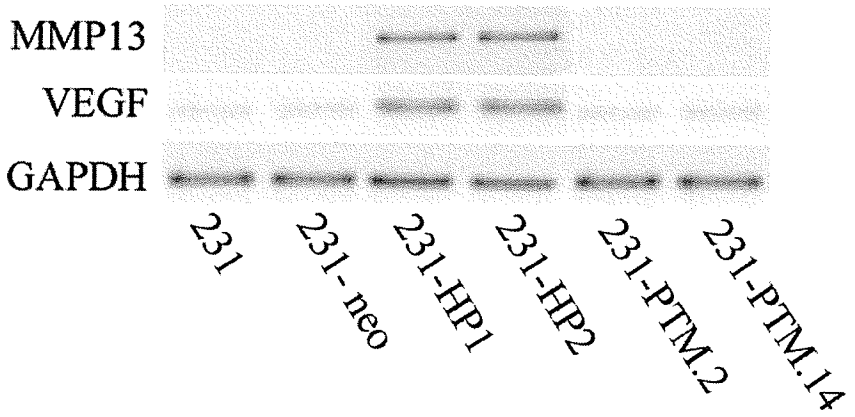

FIG 15- S100A7 Expression in MDA-MB-231 Cells Causes an Increase in Transcription of AP-1 Regulated Genes. Ethidium bromide stained agarose gel for RT-PCR assay to show S100A7 is associated with an increase in mRNA levels of the endogenous AP-1-regulated genes VEGF and MMP13. $S100A7^{mut}$ is not able to stimulate the transcription of AP-1 regulated genes. GAPDH is used as a loading control as its transcription is not AP-1 regulated.

To establish if this increase in AP-1 is directly attributable to altered activity of Jab1, we have examined the phosphoryation status of c-Jun and the requirement for the Jab1-binding site within S100A7. When S100A7 was expressed in MDA-MB-231 cells, there was a dramatic increase in the levels of phosphorylated c-Jun protein levels when compared to non-expressing controls as well as $S100A7^{mut}$ expressing clones (FIG 14 B). This increase in phospho c-Jun is paralleled by a similar increase in total c-Jun levels for S100A7-expressing clones relative to control and mutant clones (FIG 14 B). Our results suggest that an increase in the phosphorylation status of c-Jun is required for an increase in transcription of AP-1 regulated genes. This was demonstrated by the $S100A7^{mut}$ clones which had phospho c-Jun levels comparable to control cells and an elevated activity of

AP-1 in reporter assay, but no increase in endogenous gene transcription compared to control cells.

The increase in phosphorylated c-Jun in S100A7 clones was not due to an increase in the phosphorylation status of c-Jun N-terminal kinase (JNK), as it was not altered by S100A7 or $S100A7^{mut}$ expression (FIG 14 B). However, JNK phosphorylation could be increased in these same cells by transfection of MEKK1 (data not shown). Jab1 is the CSN5 component of the COP9 signalosome (206) which was reported to stabilize c-Jun via direct phosphorylation by a JNK independent mechanism (214). The COP9 signalosome can also directly phosphorylate p53 (220), resulting in increased p53 degradation. However, this phenomenon could be negated by elevating the amounts of c-Jun in-vitro (231). Our findings are consistent with these reports, as there was no noticeable decrease in p53 protein in the presence of S100A7 (FIG 14 B).

4.2.3- S100A7 Expression Stimulates the Hypoxic Response Pathway in MDA-MB-231 Breast Cancer Cells

Jab1 also interacts with the hypoxic stress transcription factor HIF-1 (215) and enhances its activity. HIF-1 targets the transcription of over 60 genes involved in many aspects of cancer biology including cell survival, glucose metabolism, cell invasion and angiogenesis. For review of HIF-1 in cancer, see (266). Expression of HIF-1 and the HIF-1-regulated gene CA9 (carbonic anhydrase 9) (248, 267-269) was examined by Western blot. Under hypoxic conditions (0.7% O_2 for 24 hours), S100A7-expressing MDA-MB-

231 clones showed a marked and higher induction of HIF-1 compared with control cells (FIG 16) and a parallel increase in CA9 protein (FIG 16). However, it was noted that CA9 expression was also increased in S100A7 expressing 231-HP1 and 231-HP2 cells under normoxic conditions. The latter observation is consistent with the finding that CA9 can also be regulated by AP-1 (270) and indicates that a component of the CA9 induction seen under hypoxic conditions might be attributable to AP-1, given the involvement of AP-1 as well as HIF-1 in the cellular hypoxic response (271-273). Clones expressing $S100A7^{mut}$ did not make a detectable amount of CA9 under normoxic conditions. This suggests the interaction of S100A7 with Jab1 is involved in the transcription of CA9 either through a mechanism involving HIF-1, AP-1 or both transcription factors.

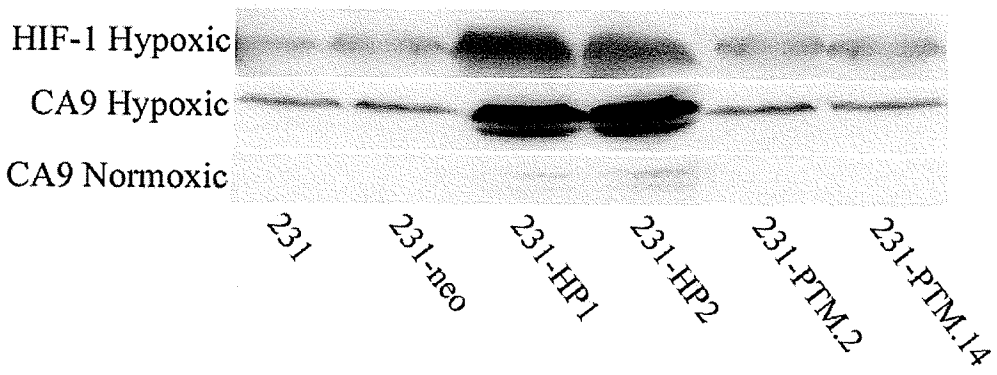

FIG 16- S100A7 Expression Alters the Hypoxic Response of MDA-MB-231 Cells. Western blot to shown that S100A7 expression is associated with up-regulation of HIF-1 and induction of the HIF-1-regulated gene, CA9 (carbonic anhydrase 9). Under normoxic conditions there is an increase in CA9 protein expression in S100A7 expressing clones. Under hypoxic conditions there is a marked increase in induction of both HIF-1 and CA9 protein in the S100A7 expressing clones. $S100A7^{mut}$ expression had no influence in HIF-1 or CA9 expression under both normoxic and hypoxic conditions when compared to non-expressing MDA-MB-231 and 231-neo clones.

4.2.4- S100A7 Expression Stimulates Akt Phosphorylation and NF-κB Activity in MDA-MB-231 Breast Cancer Cells

The activation of the Akt kinase is thought to be a major factor in promoting survival under anchorage independent conditions for epithelial cells (274). A 4.3 ± 0.4 fold increase (mean ± SD, n=3) in the relative amount of phosphorylated Akt (Ser 473) in clones expressing S100A7 when compared to non-expressing control and $S100A7^{mut}$ cells was observed by Western blot analysis (FIG 17 A). The elevation in Akt phosphorylation status could be abolished in S100A7 cells by treatment with the specific PI3K inhibitor LY294002 (FIG 20), suggesting that Akt phosphorylation is occurring in these cells through the activation of the classical pathways. The observed activation of Akt is not due to changes in the amount of its negative regulator PTEN (FIG 17 A), suggesting a mechanism of activation that is not dependant on changes in PI3K levels (discussed later). The elevated amount of phospho-Akt in clones expressing S100A7 has a functional consequence as several targets of Akt action are altered. Akt can phosphorylate the negative cell-cycle regulator $p27^{Kip1}$ in breast cancer cells (275) resulting in p27 being targeted to the proteasome for degradation. In cells expressing un-mutated S100A7, there is a reduction in the amounts of p27, which overlaps with an increase in Akt phosphorylation (FIG 17 A). Akt can also actively phosphorylate the NF-κB repressor IκBα, which activates a suite of genes involved in promoting cell survival (276). As is the case for p27, a reduction in protein levels is also observed for IκBα in the presence of S100A7. This modest reduction in IκBα correlates with an approximate 3.4 ± 0.7 (mean ± SD, n=4) fold induction of NF-κB activity in these same cells (p=0.0324), as measured by reporter assay (FIG 17 B). No such increase is observed in cells expressing

S100A7^{mut}, which is consistent with no observed change in phospho-Akt and p27 levels (FIG 17 A).

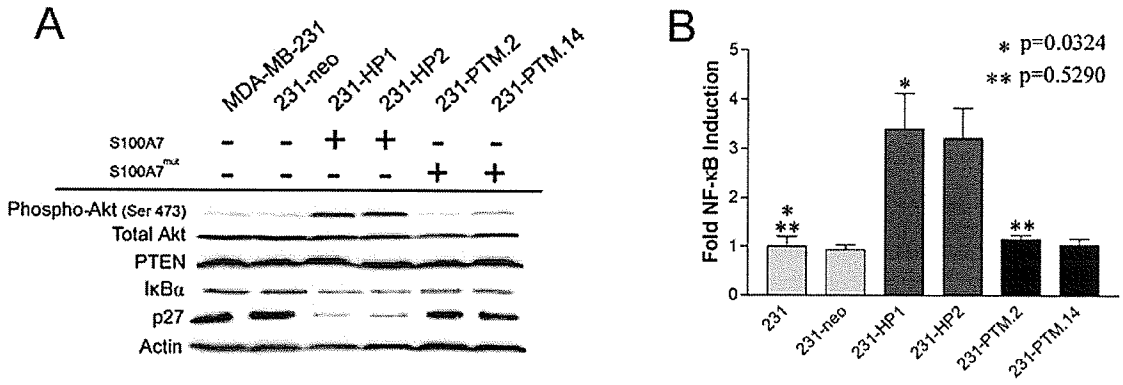

FIG 17- Akt Phosphorylation and NF-κB Activity are Elevated in MDA-MB-231 Cells Expressing S100A7. A) An increase in the phosphorylation status of Akt is observed in cells expressing S100A7 which results in modification of downstream Akt target proteins like p27 and IκBα. S100A7^{mut} is not able to stimulate Akt phosphorylation, or facilitate the increased degradation of p27. Actin is used as a loading control. B) The increased phospho-Akt levels in S100A7 expressing cells correspond to a stimulation of NF-κB reporter gene transcriptional activity. S100A7^{mut} has no effect on NF-κB transcriptional activity as these cells behaved comparably to non-expressing control cells.

4.2.5- S100A7 Increases EGF Production Which Enhances Akt Phosphorylation

Akt activation is classically accomplished via signal transduction cascades emanating from activation of a transmembrane receptor kinase by an extracellular ligand. AP-1 has been shown to be essential for the transcriptional regulation of the epidermal growth factor receptor (EGFR) ligand, EGF in skin (277) and we observe an increase in the transcription of EGF in breast cells stably expressing S100A7 (FIG 18 A). This

corresponds to an increase in AP-1 activity brought about by the S100A7-Jab1 interaction (FIG 14 A). Although the level of EGFR protein shows no change (FIG 18 B), the downstream marker of EGFR activity, p21, is induced in proportion to the increase in EGF production in S100A7 cells (FIG 18 B).

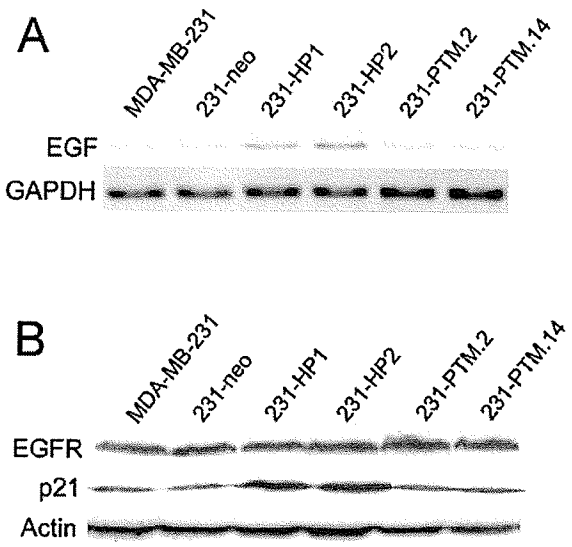

FIG 18- EGF Transcription and EGFR Signalling are Elevated in MDA-MB-231 Cells Expressing S100A7. A) RT-PCR analysis shows increased levels of EGF mRNA in clones expressing S100A7 but not S100A7^{mut}. GAPDH is used as a loading control. B) Western blot analysis shows increased levels of p21 in clones expressing S100A7 but not S100A7^{mut}. Actin is used as a loading control.

To show that activation of EGFR signaling is responsible for the increase in PI3K activity and Akt phosphorylation in S100A7 cells, the EGFR specific inhibitor BPIQ was used. Treatment resulted in the knockdown and equalization of phospho-Akt regardless of whether S100A7 was present or was mutated (FIG 19).

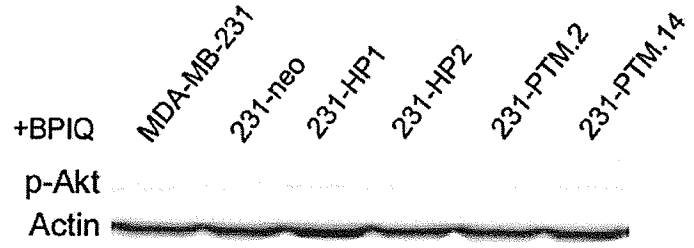

FIG 19- Inhibition of EGFR Signalling in MDA-MB-231 Cells Expressing S100A7 Causes a Decrease in Akt Phosphorylation. phospho-Akt can be equalized and decreased in all clones regardless of S100A7 expression by pre-treatment with the EGFR inhibitor BPIQ. Actin is used as a loading control.

Inhibition of PI3-kinase with the specific inhibitor LY294002 also resulted in the knockdown and equalization of phospho-Akt regardless of whether S100A7 was present or was mutated (FIG 20). These results demonstrate that in MDA-MB-231 cells, S100A7 can increase EGF production which results in an increase in EGFR signaling to Akt, and an increase in its phosphorylation state. A strong interaction with Jab1 is required for these events to occur, as mutation of the Jab1-binding domain in S100A7 did not result in an increase of both EGF transcription and Akt phosphorylation.

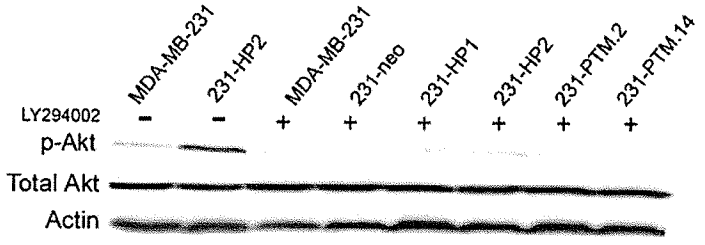

FIG 20- PI3 Kinase Inhibition Decreases Akt Phosphorylation in MDA-MB-231 Cells Expressing S100A7. Western blot analysis shows that both enhanced expression of phospho-Akt in cells expressing S100A7 and baseline phospho-Akt expression in parental cells and cell expressing $S100A7^{mut}$ can be significantly reduced or eliminated by treatment with a specific PI3K inhibitor, LY294002. Actin is used as a loading control.

When untransfected wild type MDA-MB-231 cells were grown in media derived from and conditioned by cultures of MDA-MB-231, 231-HP2 and MDA-MB-468 cells for 48 hours, there was an increase in the amount of phosphorylated Akt attributable to factors within 231-HP2 and MDA-MB-468 conditioned media compared to cells grown in MDA-MB-231 conditioned media (FIG 21). This implies that an increase in the production of secreted factors (of which EGF is likely one) brought about by the S100A7-Jab1 interaction may occur and that these are able to stimulate the signaling of cell surface receptors that signal through PI3K leading to Akt phosphorylation.

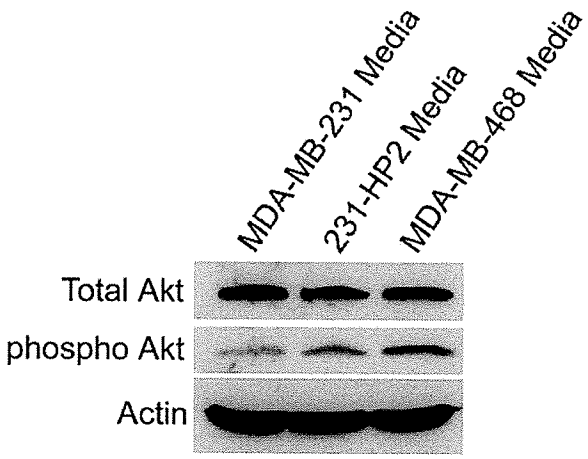

FIG 21- Cultured Cells Expressing S100A7 Secrete a Factor That Can Stimulate Akt Phosphorylation. Western blot showing amount of phosphorylated Akt in MDA-MB-231 cells that were grown for 48 hours in conditioned media from MDA-MB-231, 231-HP2 and MDA-MB-468 cells.

4.2.6- Knockdown of Endogenous S100A7 in the Breast Cancer Cell Line MDA-MB-468 Causes Changes in Jab1 and Potential Downstream Jab1 Pathways

Utilizing RNAi technology (278-281), S100A7 protein was transiently knocked down in the endogenously expressing breast cancer cell line MDA-MB-468 (127). Knockdown of S100A7 was confirmed 48-hours post transfection via Western Blot (FIG 22) and revealed a 70% depletion (n=3) in S100A7 protein levels when compared to MDA-MB-468 cells harvested 48-hours after being transfected with empty RNAi expression vector. Total amounts of Jab1 protein do not change in the presence of S100A7 RNAi, but other proteins previously shown to be altered by induction of S100A7 expression into an S100A7-null background (see above text) were found to be altered. Knockdown of S100A7 also resulted in a modest but consistent reduction in the amounts of phosphorylated c-Jun and phosphorylated Akt (FIG 22). Knockdown of S100A7 on the other hand resulted in the accumulation of p27 in this cell line. While expressing S100A7 in a non-expressing background activates Jab1 activity, removal of S100A7 from an endogenously expressing cell line appeared to decrease Jab1 associated activities. Numerous attempts were made to generate stable S100A7 knockdown clones in the MDA-MB-468 line, but were never successful. For all stable transfection attempts, no clonal outgrowths were ever detected 3 weeks after addition of selective agent, using various concentrations, but in all cases we were unable to obtain or select antibiotic resistant colonies that might yield stable transfectants.

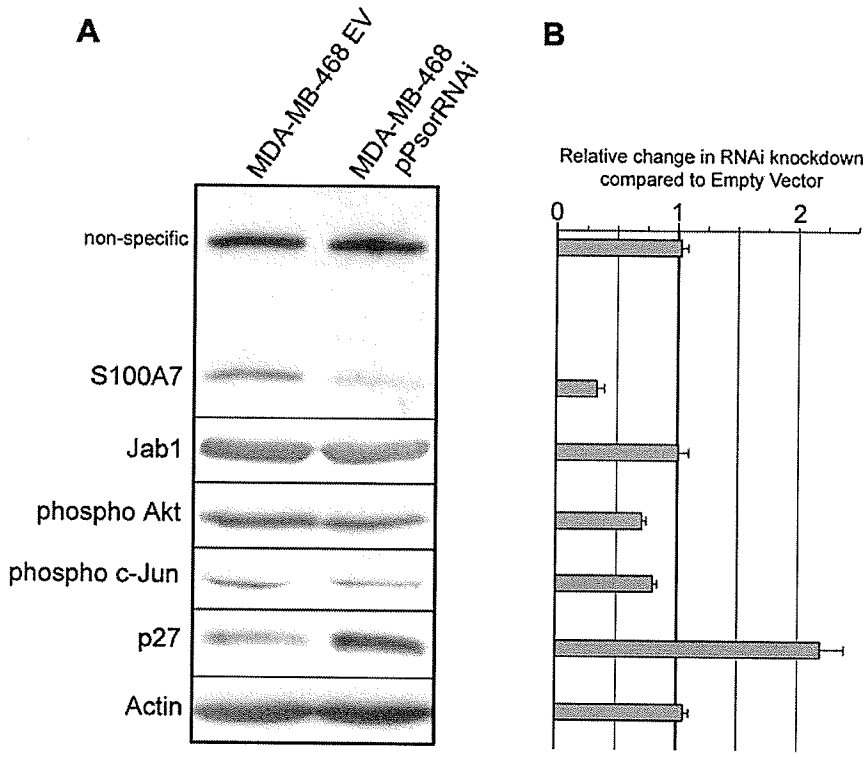

FIG 22- Knockdown of S100A7 Expression in MDA-MB-468 Cells.
A) Representative Western Blot showing that S100A7 RNAi is specific for S100A7 and is capable of depleting S100A7 levels. S100A7 RNAi has no effect on amounts of Jab1, but does cause a decrease in the relative amount of phosphorylated c-Jun and Akt while allowing for accumulation of p27. Actin levels do not significantly change +/- S100A7 RNAi and were used as a loading control. B) Densitometry intensity plot showing relative changes in protein band signals from S100A7 RNAi treated samples compared to empty vector treated control samples. Densitometry values of band intensities were measured for 3 separate experiments from protein lysates obtained from independent transfection experiments. The respective average densitometry for each empty vector control band were averaged and assigned a value of 1. Changes in band signal intensity in the presence of S100A7 RNAi are plotted in relation to their respective control. Error bars represent standard deviation.

4.2.7- S100A7 Expression in MDA-MB-231 Breast Cancer Cells Influences Breast Tumor Progression *In-vitro*

A relationship between S100A7 expression and biological end points relevant to tumor progression in breast cancer cells was explored in the context of the same MDA-MB-231 cell models. The effect of S100A7 on growth of MDA-MB-231 cells was examined under standard culture conditions and found to be associated with a modest but significant increase in growth rate (FIG 23) of up to 1.3 fold ($p>0.0009$). The growth rate of these cells were not examined under more stringent conditions e.g. low serum.

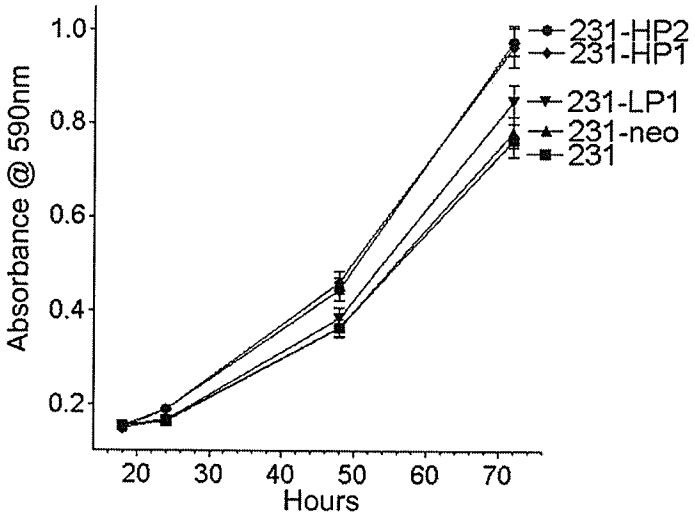

FIG 23- S100A7 Increases Growth Rate of MDA-MB-231 Cells. Graph to show the growth rate of control cells (MDA-MB-231 and 231-neo) and relative increased growth of S100A7-expressing clones (231-LP1, 231-HP1, and 231-HP2). Lines and data points represent the means of three independent experiments, with 12 data points at each time point within each experiment.

The influence of S100A7 on cellular adhesion, an important parameter of invasion (282-284) was measured in an *in-vitro* assay. We observed a consistent reduction in cell-substrate adhesion (Table 2) in S100A7 expressing clones plated on plastic (0.42-fold reduction; p>0.0001), collagen I (0.20-fold reduction; p>0.0001), and fibronectin (0.18-fold reduction; p>0.0001).

Table 2- The Influence of S100A7 on Cellular Adhesion to Selected Physical Surfaces

	Plastic	p-value	Collagen I	p-value	Fibronectin	p-value
231	1.000	-	1.000	-	1.000	-
231-neo	1.015 +/- 0.101	ns	1.008 +/- 0.065	ns	1.005 +/- 0.058	ns
231-LP1	0.752 +/- 0.089	p<0.0001	0.935 +/- 0.077	p=0.0027	0.941 +/- 0.067	p=0.0017
231-HP1	0.574 +/- 0.074	p<0.0001	0.802 +/- 0.076	p<0.0001	0.826 +/- 0.066	p<0.0001
231-HP2	0.591 +/- 0.080	p<0.0001	0.792 +/- 0.076	p<0.0001	0.819 +/- 0.065	p<0.0001

The influence of S100A7 on invasion was then assessed in a modified transwell Boyden chamber assay (285-287). There was a 1.4-fold increase in invasiveness in the high S100A7-expressing clones (p>0.0001) after 12 hours (FIG 24), at which time there was no significant difference in growth (data not shown).

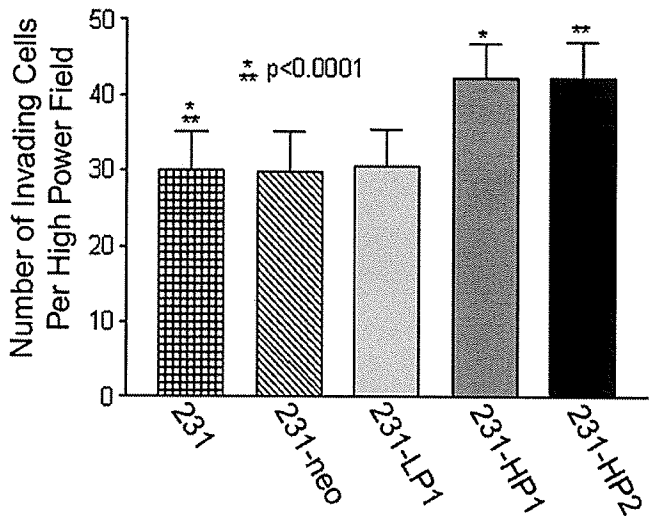

FIG 24- S100A7 Enhances Invasive Properties of MDA-MB-231 Cells. Graph to show increased invasiveness in S100A7-overexpressing cells in the *in-vitro* Boyden chamber assay. Columns and bars represent means and Standard Deviations of three independent experiments where each cell line was assayed in triplicate. Statistical significance between cell lines was determined by t-test as shown by single and double asterix marks.

4.2.8- S100A7 Expression in MDA-MB-231 Breast Cancer Cells Influences Breast Tumor Progression *In-vivo*

To determine whether S100A7 expression can also influence invasion and metastasis *in-vivo*, S100A7-overexpressing cells (231-LP1 and 231-HP1) and control cells (parental MDA-MB-231 and empty vector transfected 231-neo) were injected into the mammary fat pad of nude mice, and the generation of tumors and metastasis was assessed (FIG 25).

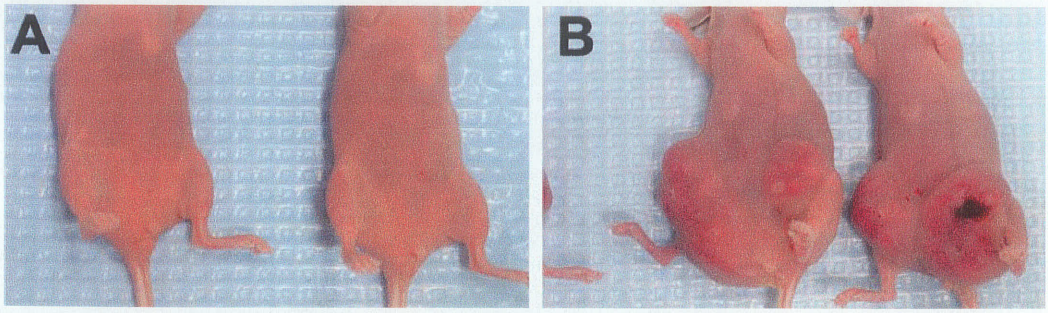

FIG 25- Formation of Tumors in Nude Mice. Groups of 5 mice for each cell line received an injection of $5x10^5$ cells into the mammary fat pads. Selected images show representative mice at 8 weeks from treatment group that received MDA-MB-231 cells (A), or 231-HP2 cells (B).

Control cell lines not expressing S100A7 (231 and 231-neo) generated tumors in 2 of 10 and 3 of 10 sites, respectively, after 8 weeks. These tumors were first noted between 2 and 3 weeks after injection, and increased slowly in size (FIG 26). Both S100A7-expressing cell lines (231-LP1 and 231-HP1) generated grossly detectable tumors in 7 of 10 and 6 of 10 sites. These tumors were also first noted between 2 and 4 weeks after injection but increased rapidly in size (FIG 26). By week 8 there was no difference in incidence or mean tumor size between parental 231 cells and 231-neo controls, or between the two S100A7-expressing clones (FIG 26). However, both S100A7-expressing clones were significantly different from both parental and neo-transfected control cells ($p< 0.017$ and $p< 0.024$, Mann Whitney; FIG 26).

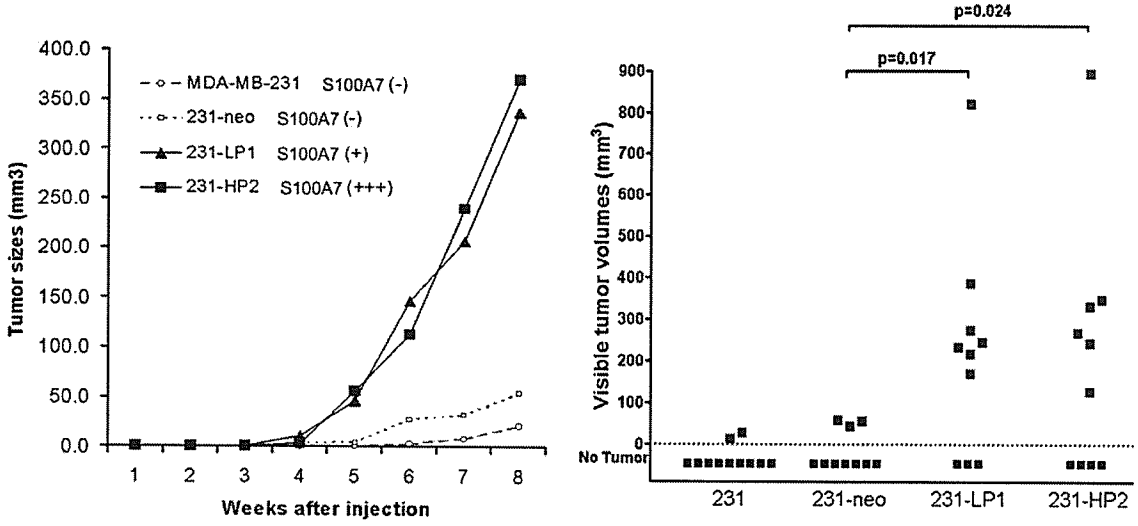

FIG 26- Effect of S100A7 on Tumor Growth in Nude Mice. A) Relative growth curves for mice in each group. Lines and data points indicate the mean tumor volumes at each time point. B) Distribution of tumor volumes at 8 weeks. Statistical significance between groups was determined by Mann-Whitney test.

Overall mean ^{SD} tumor sizes (mm^3) for each experimental group were; MDA-MB-231 = 21^{11}, 231-neo = 54^{8}, 231-LP1 = 336^{223}, and 231-HP1 = 370^{270}. When control groups and S100A7 transfectant groups were combined, the mean ^{SD} tumor sizes (mm3) were also significantly different: MDA-213 + 231-neo = 40^{20} and 231-LP1 + 231-HP1 = 352^{236} combined ($p< 0.0016$, Mann Whitney test). Microscopic examination of primary injection sites identified one additional microscopic tumor in the 231-LP1 cell line group. The primary tumors derived from both control and S100A7-expressing cells showed similar histological appearances (data not shown). Expression of S100A7 was confirmed in representative tumors derived from S100A7-transfected cell clones by immunohistochemistry (data not shown) and by Western blot (FIG 27). S100A7 expression was only detected in tumors from S100A7-transfected cells (although only a

very weak signal was detected in the 231-LP1 cell line). p27 expression was reduced in both S100A7-transfected cell clone tumors (FIG 27).

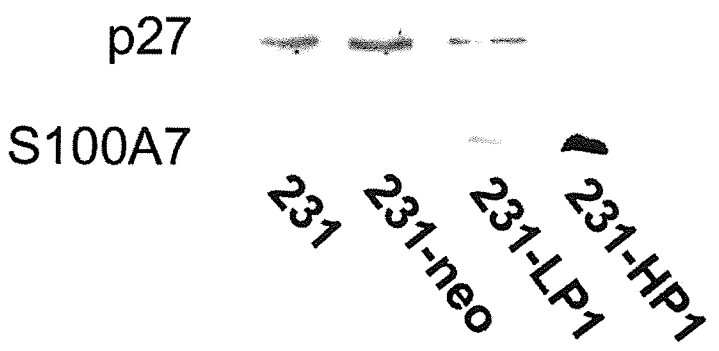

FIG 27- Protein Analysis of Mouse Tumors. Expression of S100A7 and p27 protein determined by Western blot on extracts from representative cell xenograft tumors in mice. 200 μg total protein was loaded per lane.

Grossly evident metastases were identified and confirmed by microscopy in abdominal lymph nodes distant from the primary injection sites in 2 of 10 mice injected with S100A7 overexpressing cells (both in the 231-HP1 cell line group) compared with 0 of 10 mice in the control experimental groups. Differences in lymphocytic infiltration that might occur if S100A7 is a chemotactic factor could not be assessed in the immunocompromised mouse model.

4.2.9- S100A7^{mut} Does Not Alter Tumorigenicity *In-vivo* Compared to S100A7 When Expressed in MDA-MB-231 Breast Cancer Cells

To determine if abrogation of the S100A7-Jab1 interaction affects the promotion of tumorigenesis *in-vivo*, the S100A7^{mut} expressing MDA-MB-231 cell lines were injected into the mammary fat pad of nude mice and the generation of tumors was assessed in comparison with S100A7-expressing lines and control parental cells. All cell lines generated tumors that were detectable in most animals by 3 weeks. However, S100A7 cells developed larger tumors significantly more rapidly than the S100A7^{mut} cells, which in turn developed tumors similarly to and showed no significant difference from parental controls (FIG 28).

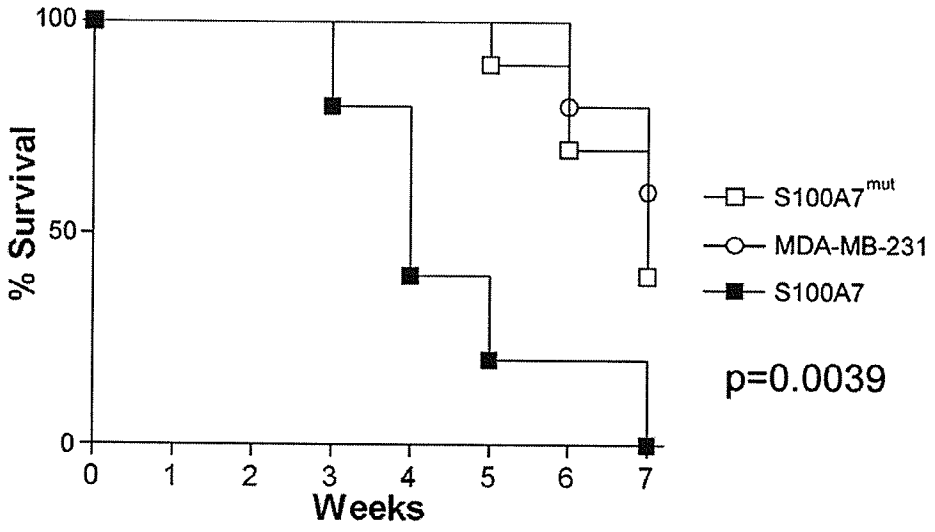

FIG 28- S100A7 but not S100A7^{mut} Promotes Growth *In-vitro*. Survival plot showing that cells expressing S100A7^{mut} demonstrate no significant difference from parental control cells (MDA-MB-231) with respect to tumor growth and survival, as compared to cells expressing S100A7. MDA-MB-231 cell clones were injected into the mammary fat pads of nude mice. Three animal groups represent mice injected with MDA-MB-231 parental cells (n=5), S100A7^{mut} cells (n=10), S100A7 cells (n=10). Statistical significance was tested by log-rank test.

At 6 weeks post injection, tumors greater than 1.5 cm had developed in 5/5 and 3/5 231-HP1 and 231-HP2 cell injected mice, but in 0/5, 1/5 and 0/5 for 231-PTM.2 and 231-PTM.14 and parental control MDA-MB-231 cell injected mice. This same difference was reflected in a significantly ($p=0.0039$) worse overall survival time for animals injected with S100A7 cells, as compared to parental control cells as previously shown (FIG 26 and FIG 28, 231 vs. HP2). However tumors derived from both $S100A7^{mut}$ cells showed no significant difference from the parental control (FIG 28). Together, these data suggest that an intact Jab1-binding domain in S100A7 is required for enhanced tumorigenesis *in-vivo*, which is mediated through an interaction with Jab1.

4.2.10- S100A7 Expression in MDA-MB-231 Breast Cancer Cells is Associated with Increased Resistance to Apoptosis

Having observed relatively modest changes *in-vitro* for growth and invasion in cells expressing S100A7 (see above section 4.2.7), but significant changes in tumorigenicity *in-vivo* (section 4.2.8), we sought to identify another parameter that was altered by S100A7 that could contribute to the discrepancy between *in-vitro* and *in-vivo* effects.

We observed S100A7 expression in some lung and breast tumors can be prominent in apparently detached but morphologically viable tumor cells adjacent to and within regions of necrosis and/or increased apoptosis (FIG 29).

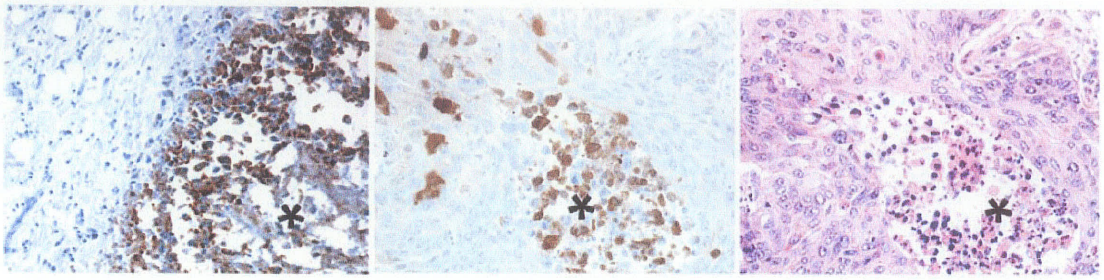

FIG 29- S100A7 Expression is Found in Regions of Detached Cells *In-vivo*. S100A7 expression detected by immunohistochemistry is prominent in regions of tumors where there is cell detachment and apoptosis (highlighted by *) in tumors from breast (left) and lung (middle). The right panel is an H&E stained serial section of the middle panel for reference. Image generated by the Manitoba Breast Tumor Bank.

To explain this observation in conjunction with the associated changes in adhesion and Akt phosphorylation/NF-κB activation that we have also observed *in-vitro*, we speculated that S100A7 confers resistance to detachment induced cell death (anoikis) in MDA-MB-231 cells. In order to determine if S100A7 protected cells from entering into early stages of apoptosis, the nuclear architecture of cells expressing S100A7, S100A7^{mut} and non-expressing controls were assessed after 72 hours of growth under anchorage independent conditions (FIG 30 A). Cells expressing S100A7 had an 83.1% $\pm$ 0.006 (mean $\pm$ SD, n=3) reduction in their relative apoptotic rate compared to non-expressing parental cells and controls (FIG 30 B). The expression of S100A7^{mut} was sufficient to confer an enhancement in survival, but not to the extent of unmutated S100A7. When both 231-PTM.2 and 231-PTM.14 cell lines were assessed in the context of anoikis they demonstrated similar but only partial resistance to apoptosis (231-PTM.2 mean relative apoptotic rate 50.7% $\pm$ 0.156 (mean $\pm$ SD), 231-PTM.14, mean relative apoptotic rate

54.6% ± 0.103) in comparison with cells expressing unmutated S100A7 protein (FIG 30 B). This is presumably due to incomplete abrogation of the interaction with Jab1 (FIG 11), which seemingly activates pro-survival pathways when stimulated. These data suggest that S100A7 functions to activate pro-survival pathways at least in part via its interaction with Jab1.

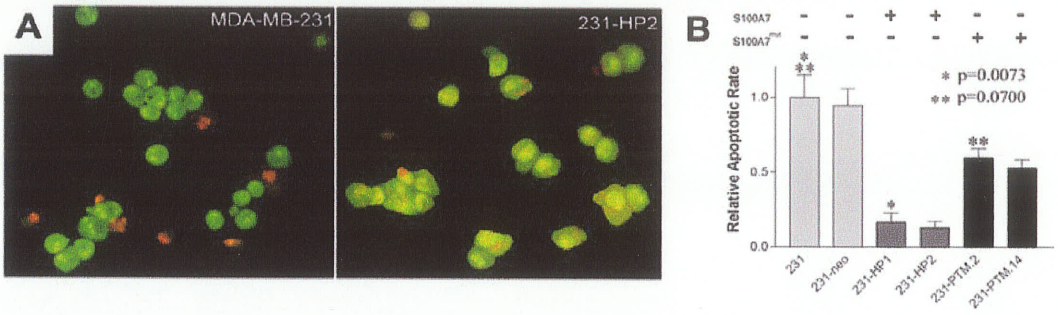

FIG 30- S100A7 Expression in MDA-MB-231 Cells is Associated with Enhanced Survival in Anchorage Independent Conditions. A) Representative images showing nuclear architecture of parental MDA-MB-231 cells and 231-HP2 cells expressing S100A7 after 72h of anchorage independent growth. B) Bar graph to show the relative apoptotic rate in MDA-MB-231 cells expressing S100A7 (231-HP1 and 231-HP2) compared to parental (231) and control transfected (231-neo) cells. Columns and bars represent the means and standard deviations of triplicate independent experiments. Statistical significance between groups was determined by t-test.

In our experimental cell model, expression of S100A7 was found to confer increased resistance to a specific form of apoptosis (anoikis, FIG 30 B) after growth in anchorage independent conditions for 72 hours when compared to non-expressing control cells. The S100A7-expressing cells showed increased resistance to anoikis that is reflected by the coordinate increase in Akt phosphorylation and NF-κB activity. This suggests these pro-survival pathways are active and have a measurable biological consequence that results in

an enhancement in survival when grown in anchorage independent conditions. Even though cells expressing S100A7^{mut} did show a modest increase in their ability to survive in anchorage independent conditions, this increase did not result in statistical significance (FIG 30 B). Presumably, this very small change in resistance to anoikis is due to a persistent but much diminished affinity in the interaction between S100A7^{mut} and Jab1 (FIG 11) that might activate pro-survival mechanism(s).

4.2.11- S100A7 expression in MCF-7 Breast Cancer Cells

MCF7 cells that had been previously engineered to stably express the bacterial reverse tetracycline transcription activator protein (MCF7 clone 89 cells (288)) were stably transfected with an S100A7 expression construct that is tetracycline regulated (pTRE2-hygro-psor). Four independent hygromycin resistant cell clones were isolated that were derived from the same transfection experiment: Mag01 and Mag02 do not make S100A7 when treated with doxycycline (dox), where as clones Mag06 and Mag07 induce S100A7 expression when treated with doxycycline (FIG 31). S100A7 protein expression can be detected 2 hours after dox treatment and expression persists beyond 72 hours (data not shown), with maximum expression observed after 24 hours dox treatment.

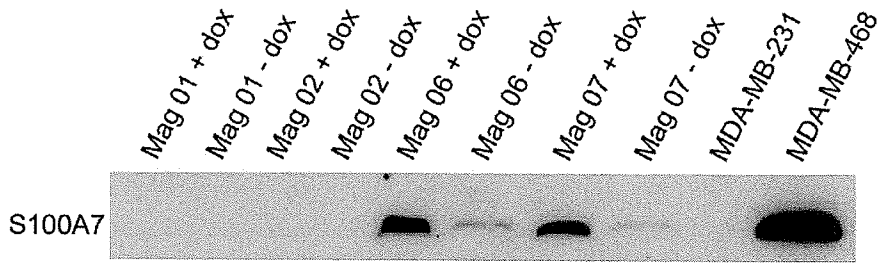

FIG 31- Doxycycline Inducible Expression of S100A7 in MCF7 Cells. Western blot showing S100A7 protein expression after 24 hour doxycycline treatment. Mag01 and Mag02 clones do not express S100A7 while Mag06 and Mag07 are inducible. S100A7 expression is detected in expressing clones in the absence of dox suggesting modest activation from stably incorporated expression construct. MDA-MB-231 and MDA-MB-468 extracts were used for negative and positive controls, respectively.

S100A7 expression was examined in Mag clones for conferring an enhancement in the ability to invade as assayed by the transwell modified Boyden chamber, but invasion was never observed for any of the clones (data not shown). The observation that MCF7 cells are not invasive in this assay has been previously reported by others (289). S100A7 did not have an effect on growth of these cells, as after 96 hours there was no difference between the non-expressing clones (Mag01 and Mag02) with expressing (Mag06 and Mag07), as determined by both cell-counting and crystal violet assay (data not shown).

S100A7 expression in the MDA-MB-231 cell line was able alter HIF-1 and CA9 expression under normoxic and hypoxic conditions (FIG 16) which we believe is due to the S100A7-Jab1 interaction. We wondered if a similar effect was occurring in MCF7 cells. Under normoxic conditions, Mag07 have a very strong induction of the CA9 gene compared to Mag01 clones where CA9 is undetectable (FIG 32). CA9 production under

normoxic conditions in the presence of S100A7 is much higher in MCF7 cells than MDA-MB-231 cells (FIG 32). For all MCF7 clones, HIF-1 is not detected under normoxic conditions. When these same clones are subjected to hypoxic conditions (0.7% O_2 for 24 hours) there is a greater induction of both HIF-1 and CA9 in S100A7 expressing cells (FIG 32). If the S100A7-Jab1 interaction exists in MCF7 cells (has not been examined yet), it might have stronger effects on HIF-1 activity in MCF7 cells than in MDA-MB-231 cells, which seem to favor activation of AP-1.

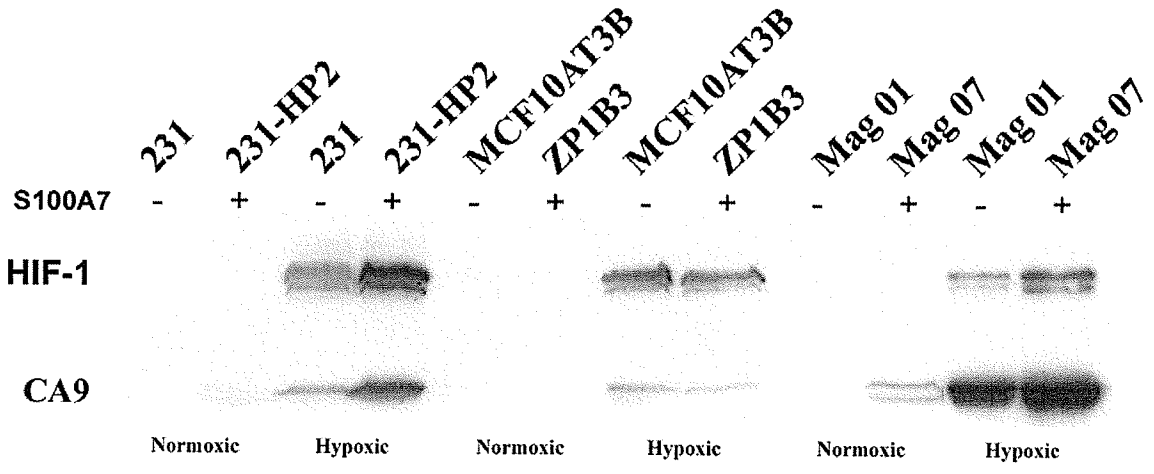

FIG 32- Effect of S100A7 Expression on Genes Regulated by Hypoxia In Breast Cell Lines. Western blot showing representative cell lines from MDA-MB-231, MCF10AT3B and MCF7 that were subjected to normoxic and hypoxic treatment. HIF-1 is only detected in all cell lines after hypoxic treatment. MDA-MB-231 and MCF7 cells expressing S100A7 have higher amount of HIF-1 than cells not expressing S100A7. The hypoxically regulated CA9 gene can be detected under normoxic conditions in both MDA-MB-231 and MCF7 cells expressing S100A7. There is also greater production of CA9 in these same cells after hypoxic treatment. HIF-1 and CA9 levels in MCF10AT3B cells are not altered by S100A7 under both normoxic and hypoxic conditions. 100 μg total protein loaded per sample.

To examine a possible effect of S100A7 on Jab1 function, the AP-1 activity of Mag01 and Mag06 clones were analyzed by reporter assay. Mag06 clones induced to express S100A7 by treatment with dox for 24 hours, had a modest 1.2 fold increase in their AP-1 activity compared to Mag01 cells also treated with dox (1.22 ± 0.17, mean $\pm$ SD, n=5, p=0.0509, data not shown). These data are consistent with a modest change in the level of c-Jun phosphorylation between MCF7 clones expressing S100A7 and non-expressing controls (FIG 33).

MCF7 cells that were treated for 24 hours with dox to induce expression of S100A7 had no change in the amount of p27 protein and phospho Akt when compared to non-S100A7 expressing controls (FIG 33).

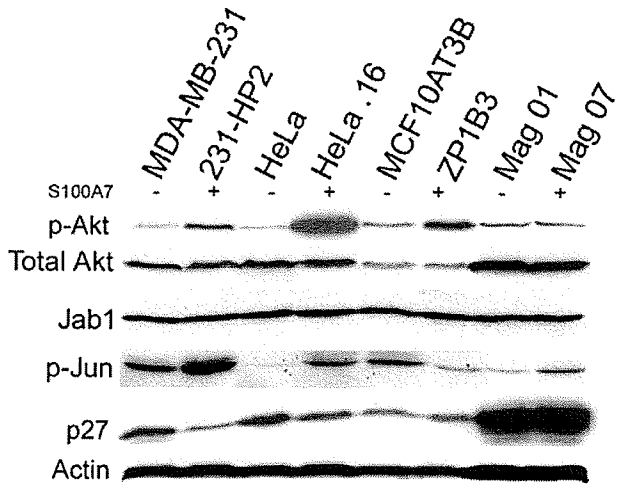

FIG 33– Effect of S100A7 Expression on Jab1 Downstream Genes in HeLa, MCF10 and MCF7. MDA-MB-231 and 231-HP2 are used for reference only as these data are discussed earlier. Western blot showing an increase in the amount of phosphorylated Akt in cells expressing S100A7 for HeLa (HeLa .16) and MCF10AT3B (ZP1B3). S100A7 has no effect on phospho Akt in the MCF7 line. Jab1 levels do not change in the presence of S100A7 and the same is true for Actin which is used as a loading control. A change in phosphorylated c-Jun is seen in clones expressing S100A7 for HeLa and MCF7, but a decrease in phosphorylated c-Jun is seen in ZP1B3. p27 levels are lower in HeLa cells expressing S100A7 but do not change in MCF10AT3B or MCF7. 100 μg total protein loaded per sample.

4.2.12- S100A7 Expression in MCF10AT3B Breast Cancer Cells

S100A7 was stably transfected into the S100A7-null background of MCF10AT3B cells and after many attempts, only one clone was isolated that expressed the transgene (clone ZP1B3). This one clone was found not to have a change in its growth rate after 96 hours compared to its parental cell line, nor did it acquire the ability to become invasive in the transwell Boyden chamber assay (data not shown). There was no detectable CA9 production under normoxic conditions, as well the HIF-1 and CA9 induction under hypoxic conditions were equal to that of non-expressing control cells (FIG 32). Our data suggest that S100A7 cannot alter hypoxic response pathways in this cell line. One explanation may be the presence of a dominantly active Ras pathway (290).

MCF10AT3B cells stably transfected with S100A7 (clone ZP1B3, FIG 33) did not show a change in the amount of p27 protein. But there was a consistent increase in the amount of phosphorylated Akt in these same cells. Interestingly, the levels of phospho c-Jun decreased in S100A7 expressing clones when compared to non-S100A7 expressing controls (FIG 33).

4.3.0- Studies of S100A7 in Human Breast Tumors to Determine if S100A7 is Associated with Clinically Significant Parameters and Changes Attributable to an Alteration in Jab1 Function

Having made the observations that S100A7 expression in a human breast cancer cell line could alter biochemical pathways which in turn could alter biological properties that are

associated with a more aggressive phenotype (see above sections), we examined if breast tumors expressing S100A7 were different from those not expressing S100A7. The highest levels of S100A7 expression in breast cancer were previously found to occur in DCIS (105). To investigate a possible role for S100A7 in the transition of DCIS to invasive disease, we examined S100A7 expression in a cohort of DCIS cases, some of which were purely DCIS and others had both DCIS and invasive components.
Our efforts focused on two main questions: 1) can S100A7 expression be correlated with clinically relative parameters such as hormone receptor status and patient survival? and 2) in tumors expressing S100A7, is there evidence of enhanced Jab1 activity or downstream factors compared to tumors not expressing S100A7?

The specificity of the rabbit S100A7 antibody we had generated (see section 3.3.43) was confirmed by blockade of the signal by preincubation with a S100A7 peptide and by comparison with other anti-S100A7 antibodies, including a chicken IgY anti-S100A7 antibody that had previously been generated against the same peptide, as described (106). Experiments were also performed to compare immunoblotting signals with immunohistochemical profiles in cell lines and invasive breast ductal carcinomas (FIG 34). Expression of a 11.7 kDa S100A7 band was present by Western blot only in the MDA-MB-468 cell line (known to express S100A7) but not in MDA-MB-231 or MCF-7 cells that are known not to usually express S100A7 (127), but express several other S100 proteins (154, 196, 263). In tumors, S100A7 was also seen by Western blot assay in cases that exhibited strong S100A7 immunohistochemistry staining but was absent in tumors that were negative by immunohistochemistry.

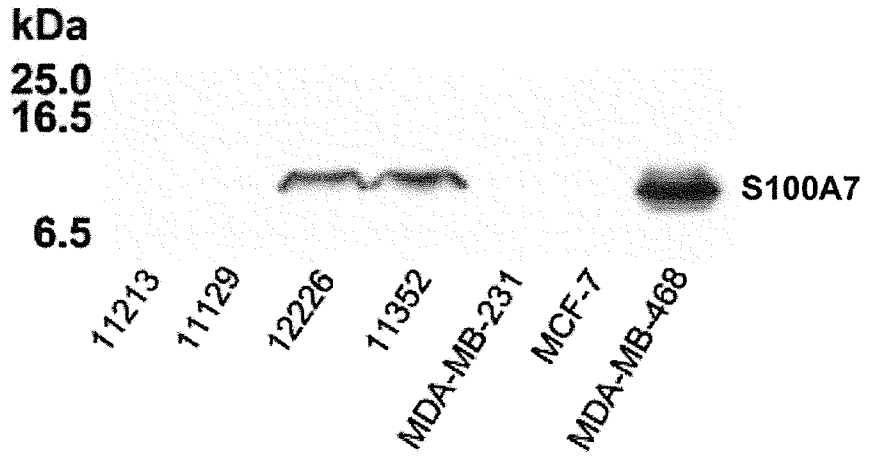

FIG 34- Detection of S100A7 Protein in Selected Breast Tumors and Cell Lines. S100A7 expression is detected as a single specific band (*Mr* 11.7 kDa) by Western blot in tumors 12226 and 11352 that were shown to express S100A7 by immunohistochemistry. MDA-MB-468 cell line is a positive control. MDA-MB-231 and MCF7 cells are negative controls. 100 μg total protein loaded per sample.

4.3.1- Association of S100A7 Expression in DCIS with Clinically Important Parameters

In a series of 136 cases of ductal carcinoma in-situ (DCIS) studied by immunohistochemistry, 63 out of 136 (46%) DCIS lesions expressed detectable S100A7. The S100A7 immunohistochemistry scores ranged from 0 to 270 (mean ± standard deviation: 28 ± 62; median 0). In cases with detectable S100A7 expression, it was high in 16 cases, intermediate in 34 cases, and low in 13 cases. In all positive cases, the predominant cellular localization for expression was cytoplasmic. S100A7 nuclear expression was infrequent, being present only in 13 out of 63 (21%) of S100A7-positive cases, and was not significantly associated with any specific clinical/pathologic factors. Expression was restricted to epithelial tumor cells and was not observed in adjacent

normal ducts or lobules, as described previously (106). Representative examples of S100A7 staining in DCIS are illustrated in FIG 35.

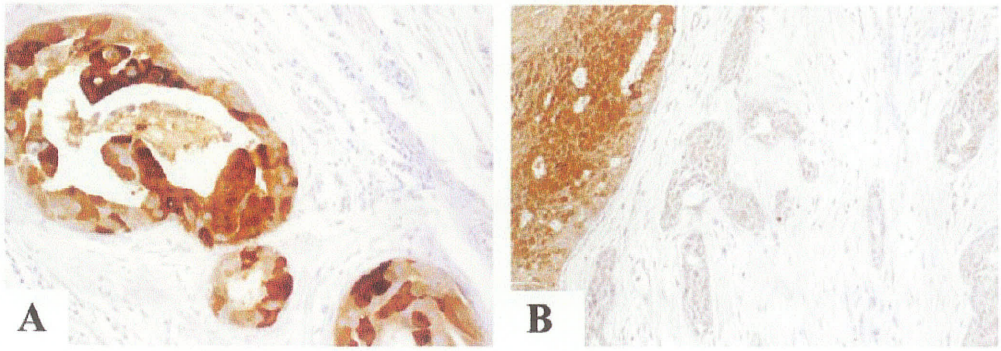

FIG 35- S100A7 Expression in DCIS by Immunohistochemistry. S100A7 expression detected by immunohistochemistry in A) pure ductal carcinoma in-situ (DCIS) and in B) DCIS associated with invasive carcinoma. Note the reduced expression in the invasive component (panel B), right) relative to the in-situ component (panel B), left. Figure generated by the Manitoba Breast Tumor Bank.

S100A7 expression in the entire series correlated with high nuclear grade ($r = 0.57$; $p<0.0001$, Spearman test), low ER levels ($r = -0.38$; $p<0.0001$), extent of necrosis ($r = 0.48$; $p<0.0001$), and the presence of inflammation ($r = 0.39$; $p<0.0001$). Similarly, when S100A7 and prognostic factors were considered as categorical variables (positive or negative), S100A7 expression was also significantly associated with ER-negative status ($p=0.0005$), high grade, and presence of necrosis and inflammation ($p<0.0001$, X^2 test; Table 3). ER-negative status was determined by Immunohistochemical scoring (nuclear staining only) of tissue sections and was defined as having an IHC score <10. IHC score is the product of the intensity of staining (value of 0-3) and the percentage within the

tissue section. The product of the intensity of staining (value of 0-3) and the percentage of neoplastic epithelial cells exhibiting staining, was determined to provide a semiquantitative immunostaining score (IHC scores, ranging from 0 to 300).

Table 3 **Clinical/pathological features and frequency of S100A7 expression in ductal carcinoma in situ**

Clinical/pathological features		DCIS⁻			DCIS⁺			All DCIS		
		n	S100A7⁺	*P*	*n*	S100A7⁺	*P*	*n*	S100A7⁺	*P*
ER	Negative	23	83%	<0.0001	29	52%	0.76 (NS)	52	65%	0.0005
	Positive	67	30%		17	53%		84	35%	
Grade	Low	34	15%	<0.0001	9	11%	0.0041	43	14%	<0.0001
	Moderate	32	47%		19	47%		51	47%	
	High	24	79%		18	78%		42	79%	
Necrosis	Negative	47	23%	<0.0001	15	20%	0.0024	q	23%	<0.0001
	Positive	43	65%		31	68%		74	66%	
Inflammation	Low	47	26%	0.0017	15	27%	0.054 (NS)	62	26%	<0.0001
	Moderate	26	62%		16	63%		42	62%	
	High	17	65%		15	67%		32	66%	

P values were calculated using χ^2 tests. DCIS⁻, pure ductal carcinoma *in situ*; DCIS⁺, DCIS associated with invasive carcinoma; ER, estrogen receptor; NS, not significant; S100A7⁺, proportion of S100A7 positive cases.

In subgroup analysis, S100A7 was expressed in 25 out of 31 (81%) high grade/ER-negative/necrosis-positive DCIS cases, as compared with six out of 40 (15%) low-grade/ ER-positive/necrosis-negative DCIS cases ($p<0.0001$, X^2 test). The finding of S100A7 in ER-positive DCIS cases surprised us because of our earlier findings (106). But in these previous experiments, ER status was not determined by immunohistochemistry, but rather by the ligand binding assay. S100A7 expression in ER-positive tumors has also been recently shown by others (291) where immunohistochemistry was also used to determine ER status.

4.3.2- Correlation of S100A7 Expression in DCIS to $p27^{Kip1}$ and Jab1

Expression of Jab1 and $p27^{kip1}$ was also assessed in DCIS in a subgroup of 47 cases in which there was sufficient material available (FIG 36). These included 26 cases of pure DCIS and 21 cases of DCIS associated with invasive carcinoma.

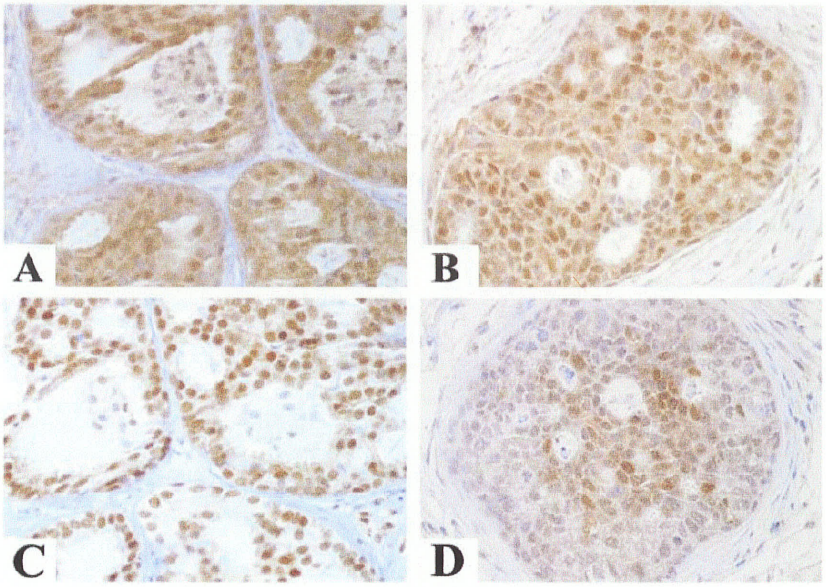

FIG 36- Jab1 and $p27^{kip1}$ Expression in DCIS by Immunohistochemistry. Top panels show Jab1 expression in A) S100A7-negative and B) S100A7-positive DCIS cases. The lower panels show C) high and D) low $p27^{kip1}$ expression in the same two DCIS cases shown above for A) and B). Figure generated by the Manitoba Breast Tumor Bank.

Reduced expression of $p27^{kip1}$ was associated with high grade (p=0.0002, t-test), ER-negative status (p=0.0008), and presence of necrosis (p=0.025). Nuclear Jab1 expression was higher in lesions with necrosis (p=0.026) and exhibited a trend toward higher levels

in ER negative and high-grade lesions, whereas cytoplasmic Jab1 was lower in high-grade lesions. These differences were not significant and overall Jab1 levels were similar in all subgroups. S100A7 expression levels in DCIS correlated positively with nuclear Jab1 ($r = 0.44$; $p=0.029$, Spearman test) and inversely with cytoplasmic $p27^{kip1}$ ($r = -0.32$; $p= 0.028$). When nuclear, cytoplasmic, and total combined expression of Jab1 was considered relative to S100A7 status, S100A7-positive DCIS was associated with higher relative localization of nuclear Jab1 ($p=0.0019$, t-test), but there was no difference in cytoplasmic or overall Jab1 expression between S100A7-positive and S100A7-negative DCIS (FIG 37). Conversely, S100A7-positive DCIS was associated with significantly lower overall expression of $p27^{kip1}$ ($p=0.0168$, t-test), and similar but nonsignificant trends toward lower nuclear and cytoplasmic localization (FIG 37).

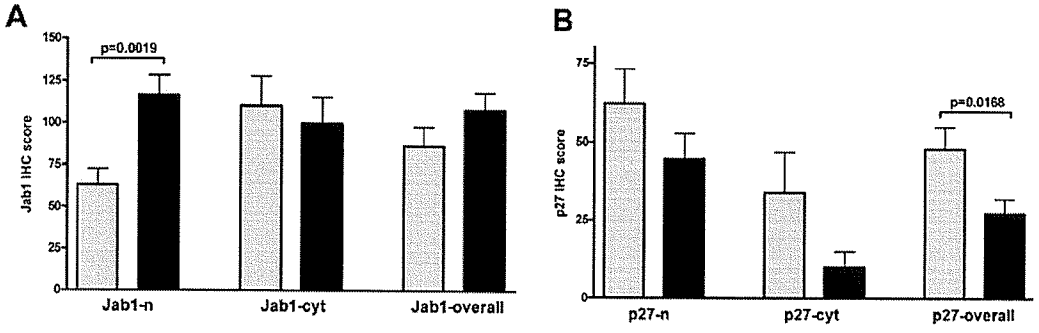

FIG 37- Jab1 and $p27^{kip1}$ Expression Relative to S100A7 Status. A) The graph illustrates higher Jab1 nuclear expression (Jab-n) in S100A7-positive (black columns) than in S100A7-negative (grey columns) cases, but similar cytoplasmic (Jab-cyt) and overall expression. B) The graph illustrates lower overall $p27^{kip1}$ expression in S100A7-positive cases. The columns represent mean immunohistochemistry (IHC) scores and bars indicate standard deviations. Significant *P* values, as determined by t-test, are shown.

4.3.3- S100A7 Expression in DCIS and Association with Presence of Invasive Disease

The entire DCIS series included two categories of DCIS: those cases with and those without associated invasive carcinoma. When pure DCIS cases were compared to DCIS cases with associated invasive carcinoma, there was an increased proportion that were ER negative, necrosis positive, and high grade DCIS; this was statistically significant for the former two factors ($p<0.0001$ and $p=0.039$, respectively, X^2 test) but not for grade ($p=0.08$). S100A7-positive cases were also more frequent in DCIS associated with invasive carcinoma (24/46, 52%) than in pure DCIS (39/90, 43%), but this was not statistically significant. However, when only high levels of S100A7 were considered as positive (IHC score >100), there was a significantly higher proportion of S100A7-positivity among cases of DCIS with associated invasive carcinoma (10/46, 22%) than among pure DCIS cases (5/90, 6%; $p=0.0037$, X^2 test). Furthermore, the overall S100A7 immunohistochemistry scores were also higher in the subgroup of DCIS associated with invasive components (mean ± standard deviation: 51 ± 84) than in the pure DCIS subgroup (17 ± 45; $p=0.0026$, t-test).

In the 46 DCIS cases associated with concurrent invasive carcinoma, differential S100A7 expression was observed between in-situ and invasive components. S100A7 was expressed in 25 out of 46 cases. Although it was present in both the DCIS and invasive components in 14 out of 46 cases, it was limited to the DCIS component in 10 out of

46 cases and to the invasive component in one case. However, even when expressed in both components, S100A7 expression levels were consistently lower in the invasive component than in the matching in-situ component ($p < 0.0001$, Wilcoxon test; FIG 38).

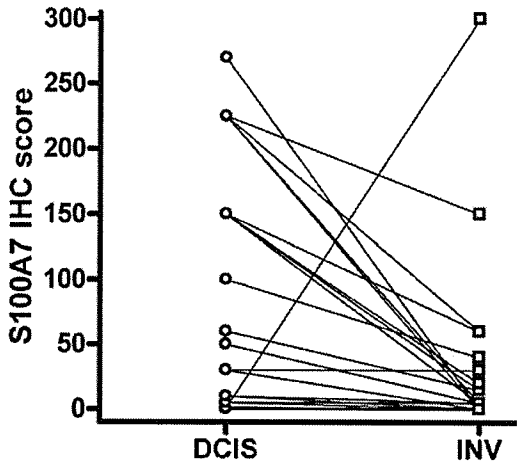

FIG 38- Levels of S100A7 in Matched DCIS and Invasive Components. Graph shows levels of S100A7 in matched ductal carcinoma in-situ (DCIS) and invasive (INV) components within the 24 out of 46 cases of DCIS associated with invasive carcinoma that showed expression in either component.

In those cases with high levels of S100A7 expression in DCIS, 10 out of 11 cases exhibited a 50% or greater reduction in immunohistochemistry score in the invasive component. There was no significant change in Jab1 expression but there was a decrease in $p27^{kip1}$ cytoplasmic expression ($p=0.047$) between DCIS and invasive components.

4.3.4- Recurrence in Patients that had Pure DCIS and Associated S100A7 Expression

Among the 90 patients with pure DCIS, 45 had been treated by local excision. In this subset, 36 (80%) patients did not develop a recurrence whereas nine (20%) patients did develop a recurrence (DCIS in eight, and DCIS with an invasive component in one). There was no significant difference in patient age, excision margin status, or frequency of additional radiation or hormonal treatment between the subgroups with or without recurrence. Similarly, there was no significant difference between the clinical/pathologic characteristics of these DCIS cases associated with different outcomes, although lesion size could not be accurately determined and was not included in the analysis. The subset with recurrence exhibited more frequent necrosis (66% versus 51%) and ER-negative status (44% versus 20%), and a lower proportion of cases that were treated by radiotherapy (13% versus 27%); however, none of these differences was statistically significant. There was also no significant difference in the frequency of S100A7 expression between the cases with (4/9, 44%) and those without (21/36, 58%) recurrence. In seven DCIS cases with recurrence, the tissue blocks from the recurrence were also available for assessment for S100A7 expression. Although both nuclear grade and the presence of necrosis were concordant in only four out of seven (57%) cases, ER status was concordant in five out of six (83%) and S100A7 status was concordant in seven out of seven (100%) cases.

4.3.5- S100A7 Expression is More Commonly Found in Estrogen Receptor-Alpha Negative Breast Tumors

Our initial observation for S100A7 expression in breast tumors was that it was restricted to those that were ER negative, as determined by ligand binding assay (106). This is an interesting finding as tumors that are ER negative are not candidates for hormonal therapy such as tamoxifen (292-294) and have a worse clinical outcome than tumors that express ER (295, 296). This is the reason why we initially restricted our studies to ER negative cell lines and human tumor cases. Subsequently, the relationship between S100A7 and ER status has been assessed in several large tumor cohorts and by using both whole tumor tissue cross sections and more recently by tumor core sections in the context of tissue microarrays. The results with both tumor tissue formats has been similar, but some differences have emerged in the frequency of expression in cohorts where ER status is determined by different assays (ligand binding assay versus immunohistochemical assessment). We and others (196) have shown that some ER positive tumors that were assessed by immunohistochemistry can be S100A7 positive (the latter status confirmed with several different S100A7 antibodies raised in chicken, mouse and rabbit). We have pursued this observation, but have not resolved it.

S100A7 was expressed in 52% and 53% of ER negative invasive tumors in two independent tumor cohorts (cohort #1 n=122, cohort #2 n=246) where ER negative status was determined solely by ligand binding ER assay in both cohorts. Conversely S100A7 was expressed in 18% and 18% of two other ER positive invasive tumor cohorts (n=129, n=151) where ER status was determined by ligand binding assay and

immunohistochemistry respectively, but often at lower expression levels. Similar results were also obtained from studies of smaller cohorts of ER positive (defined by the ligand binding assay as binding >10 fmol of radiolabeled ligand per mg protein) and ER negative DCIS where 65% of ER negative (n=52) and 35% of ER positive (n=84) in-situ lesions were also S100A7 positive.

4.3.6- S100A7 Expression in Breast Tumors is Associated with an Increase in Phosphorylated Akt

To examine if the relationship between S100A7 and phospho-Akt that was identified *in-vitro* could be detected *in-vivo* within human breast tumors, we next examined the association between their expression *in-vivo*. S100A7 protein expression was detected using our rabbit polyclonal antibody described earlier. In a cohort of 142 invasive carcinomas in the context of a tissue microarray, S100A7 expression was seen in 78/142 invasive carcinomas and phospho-Akt protein expression was expressed in 108/142 tumors. These are comparable to the frequencies previously observed within breast tumors by ourselves for S100A7 (198) and others for phospho-Akt (259). Overall, there was a significant correlation between the levels of expression for S100A7 and phospho-Akt within this cohort ($p<0.0001$, $r=0.34$, Spearman correlation). The association between S100A7 and phospho-Akt status was also evident in categorical analysis and remained significant ($p < 0.0001$, Fisher's exact test) even if using different cutpoints to distinguish positive from negative phospho-Akt status (FIG 39).

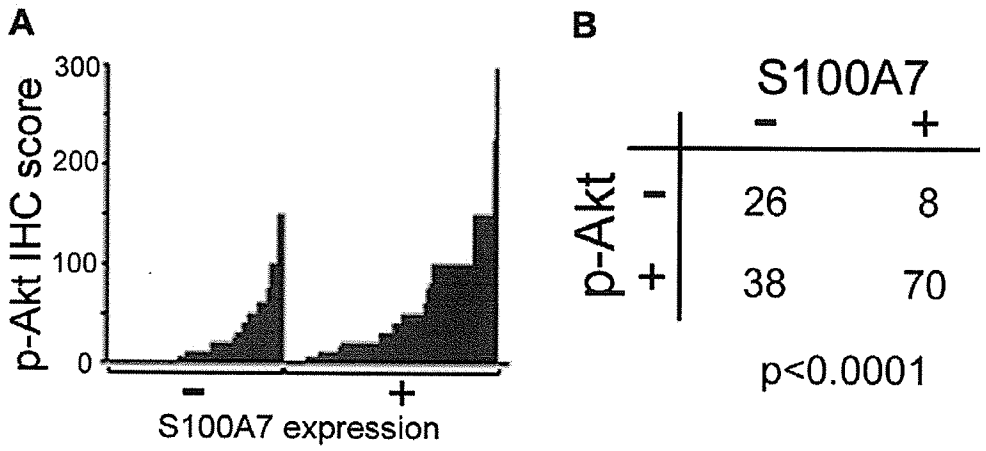

FIG 39- S100A7 Expression is Correlated with Increased phospho-Akt in Breast Tumors. A) Histogram representation of the relative levels of phospho-Akt expression (p-Akt IHC score) amongst S100A7 negative (n=64) and S100A7 positive (n=78) tumor subgroups as determined by immunohistochemistry in a tumor tissue microarray.
B) Contingency table analysis of S100A7 and phospho-Akt status. S100A7 and phospho-Akt IHC scores >0 were used to define a tumor as positive and statistical significance was tested by Fisher's exact test.

4.3.7- S100A7 Expression is Associated with Poor Patient Clinical Outcome in Estrogen Receptor Negative Ductal Invasive Breast Cancer

The clinicopathological features of the cohort of 122 women with invasive ductal breast carcinoma are described in detail in Table 4. Among these patients, the median age was 52 years, the median tumor size was 2.7 cm, and the median ER and PR levels were 2 and 7.5 fmol/mg, respectively. The median duration of follow-up for the entire cohort was 45 months (range, 6–106 months). At the time of analysis, 58 women were alive and well (48%), 47 women (38%) had died of breast cancer, and 8 women were alive with recurrent disease. Nine (9) women had died of unknown or other causes. Expression of S100A7 was detected in 64 of 122 cases (52%). S100A7 expression was focal (≤10% of

tumor cells) in 23 of 64 cases, heterogeneous (>10 to <75% of tumor cells) in 29 of 64 cases, and marked (>75% of tumor cells) in 12 of 64 cases. All positive tumors showed cytoplasmic expression, and among these, nuclear expression of S100A7 was also observed in 37 (30%) tumors (Table 4 and FIG 40).

Table 4 Clinical/Pathological Features and Frequency of S100A7 Expression in Invasive Breast Cancer

				S100A7 expression			
		Tumors		Cytoplasmic		Nuclear	
Parameter		#	%	#	%	#	%
ER[a]	−ve	122	(100)	64	(52)	37	(30)
	+ve	0	(0)				
PR[b]	−ve	100	(82)	59	(59)	34	(34)
	+ve	22	(18)	5	(23)	3	(14)
Nodal status	−ve	56	(46)	29	(52)	13	(23)
	+ve	65	(53)	34	(52)	23	(35)
	Unknown	1	(1)	1	(100)	1	(100)
Grade[c]	Low	10	(8)	2	(20)	1	(10)
	Intermediate	52	(43)	30	(58)	18	(35)
	High	60	(49)	32	(53)	18	(30)
Size	≤2 cm	30	(25)	15	(50)	6	(20)
	>2 cm	88	(72)	47	(53)	29	(33)
	Unknown	4	(3)	2	(50)	2	(50)
INFL[d]	Low	77	(63)	41	(53)	23	(30)
	High	45	(37)	23	(51)	14	(31)
Type	Ductal	117	(96)	62	(53)	36	(31)
	Lobular mixed	5	(4)	2	(40)	1	(20)
Age	≤50	54	(44)	26	(48)	16	(30)
	>50	68	(56)	38	(56)	21	(31)

[a] ER −ve, <10 fmol/mg protein.
[b] PR −ve, <15 fmol/mg protein.
[c] Nottingham system.
[d] Tumor inflammation/immune response was assessed in the H&E-stained tumor tissue section as either low (absent or sparse lymphocytic infiltrates) or high (lymphoid aggregates and/or prominent diffuse lymphocytic infiltrates).

Positive staining was also frequently observed within stromal inflammatory and fibroblast-like cells in the stroma immediately adjacent to regions of positivity within the tumor cell compartment but not in stroma in distant regions or normal tissues. Occasional weak staining was observed in normal ducts, benign and hyperplastic epithelial elements, and expression was observed within associated DCIS components. For the purpose of subsequent statistical analysis, all cases with positive cells were considered as positive

cases, and this fraction corresponded to the proportion of ER-negative tumors found to be S100A7 positive by Western blot in a previous study (106).

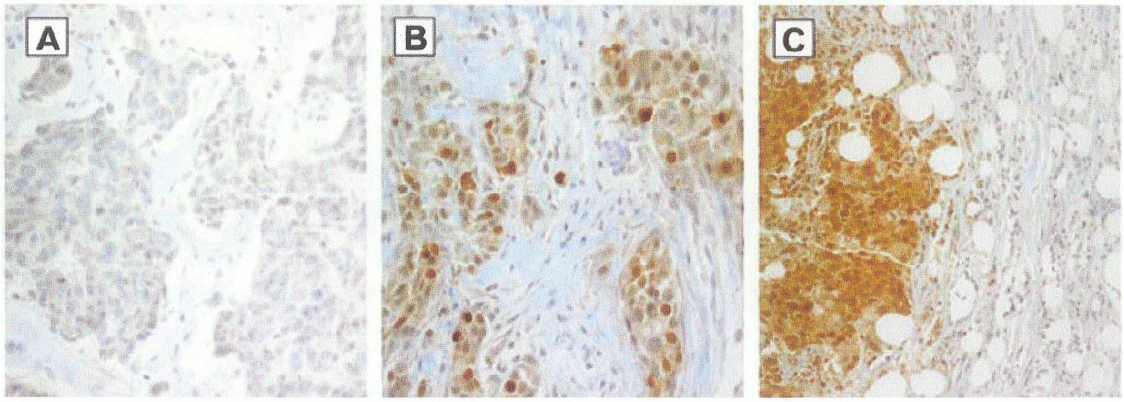

FIG 40- S100A7 Expression Determined by Immunohistochemistry for Invasive Breast Cancer. Tumors demonstrate negative A), positive (predominantly nuclear) B), and positive (predominantly cytoplasmic) C) S100A7 expression.

In univariate analysis (stastical analysis performed by Dr. Catherine Njue, Cancer Care Manitoba, and Dr. Erich V. Kliewer, Department of Community Health Sciences, University of Manitoba), S100A7 expression measured as cytoplasmic or nuclear expression was not correlated with other prognostic factors (including PR, size, grade, stage, and nodal status). In addition, no association was seen with inflammatory cell infiltration in this cohort. However, both cytoplasmic and nuclear S100A7 expression were associated with a shorter time to progression ($p<0.0374$ and $p<0.0166$ respectively) and breast cancer-specific survival ($p=0.0235$ and $p= 0.0273$; FIG 41). Among other prognostic factors, a significant association was also found between stage and outcome

(time to progression, p<0.0001; survival, p<0.0001), nodal status and outcome (time to progression, p= 0.0074; survival, p=0.0055), but not with grade, size, or PR. A high nuclear/cytoplasmic S100A7 ratio was also associated with both early recurrence and survival (p= 0.0009 and p=0.02). Additional analysis of S100A7 relative to overall survival (rather than breast cancer-specific survival) showed similar and significant associations with poor overall survival for cytoplasmic and nuclear S100A7 expression (p= 0.0082 and p= 0.0077) and also higher S100A7 nuclear/cytoplasmic ratio (p= 0.0026).

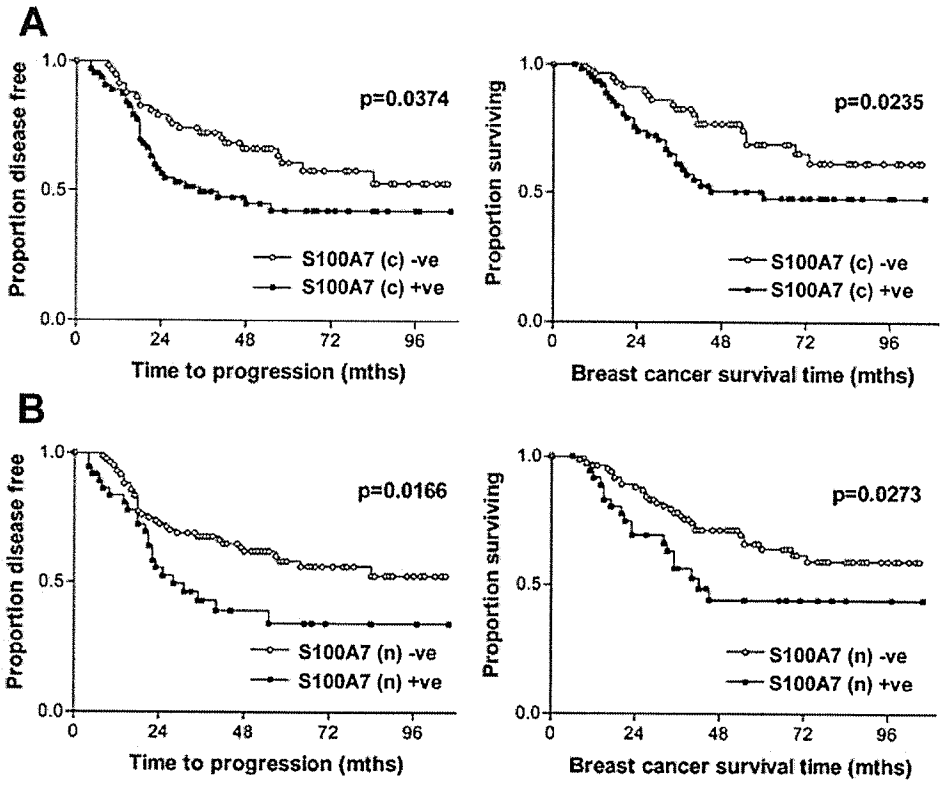

FIG 41 - Correlation of S100A7 Expression with Clinical Outcome in Invasive Breast Cancer. Kaplan Meier curves to demonstrate a relationship between cytoplasmic A) and nuclear B) S100A7 expression and time to progression, and breast cancer survival within the entire cohort. S100A7-negative cases (○), and positive cases (■). P values were determined by Log-rank test.

Multivariate analysis was performed using the Cox proportional hazard model and included stage, nodal status, tumor size, PR status, age, and grade together with the nuclear S100A7 and cytoplasmic S100A7 status. Only tumor stage and cytoplasmic S100A7 expression emerged as significant independent poor prognostic predictors of time to progression (stage, hazard ratio, 2.92, 95% CI, 1.83–4.67, p> 0.0001; cytoplasmic S100A7 hazard ratio, 1.86, 95% CI, 1.02–3.39, p= 0.044) and survival (stage, hazard ratio, 2.91, 95% CI, 1.69–5.02, p>0.0001; cytoplasmic S100A7 hazard ratio, 2.12, 95% CI, 1.06–4.23, p= 0.033).

4.4.0- Expression of S100A7 in the Mouse Mammary Gland

Having determined S100A7 expression in a breast cell line model and breast tumors is sufficient to confer the acquisition of a more aggressive behavior, and accepting the limitations of one cell line model and correlative tissue studies, we found the need to develop an *in-vivo* animal model to further assay the biological function(s) of S100A7. By targeting S100A7 expression to the epithelial cells of the mouse mammary gland, we could examine if S100A7 has a role at different stages of mammary development by assessing histological structure in normal, pregnant and involuting tissue. The transgenic mice could also be mated with established tumorigenic mice to examine an ability to promote the development of neoplasia.

4.4.1- Targeting S100A7 Expression to the Epithelial Cells of the Mouse Mammary Gland

The cDNA sequence of human S100A7 that encodes the full protein sequence was cloned into the pJ5 vector (ATCC) (257) such that it became fused to the long terminal repeat (LTR) regulatory element of the mouse mammary tumor virus (MMTV) promoter. This promoter is active in several tissues of the mouse such as the salivary gland and skin (297), but its highest level of activity is seen in the epithelial cells of the mouse mammary gland. Therefore, S100A7 expression should be maximally and specifically targeted to the mouse mammary epithelium.

The MMTV-S100A7 expression construct was injected into the pro-nuclei of fertilized CD-1 mouse eggs by the staff of the Genetic Models Centre at the University of Manitoba followed by implantation into the womb of a pseudo-pregnant mouse. When a litter of potential founder mice was weaned, a piece of their tail was removed for genetic analysis. Genomic DNA was extracted and used for PCR with S100A7 specific primers to detect the presence of the transgene. 6 potential founders were identified by PCR analysis from a total of 12 mice from 2 litters, and these mice were bred with CD-1 wildtype mice to ensure stable incorporation of the transgene. The progeny mice of the founder/CD-1 cross (F1 generation) had a piece of tail removed at time of weaning to confirm the presence of the transgene by Southern analysis. 2 founder lines were identified that contained the transgene (FIG 42 A). These lines were then inter-bred with their respective littermates to produce the F2 generation that had their genotype checked as this population is a mix of homozygotes, heterozygotes and wild-type. Analysis was

performed by Southern Blot using equal amounts of digested genomic DNA for each mouse. Heterozygotes (transgene on one allele) have a signal from the transgene that is half the intensity of the homozygote (transgene on both alleles) (FIG 42 B), while wild-type mice have no transgene signal.

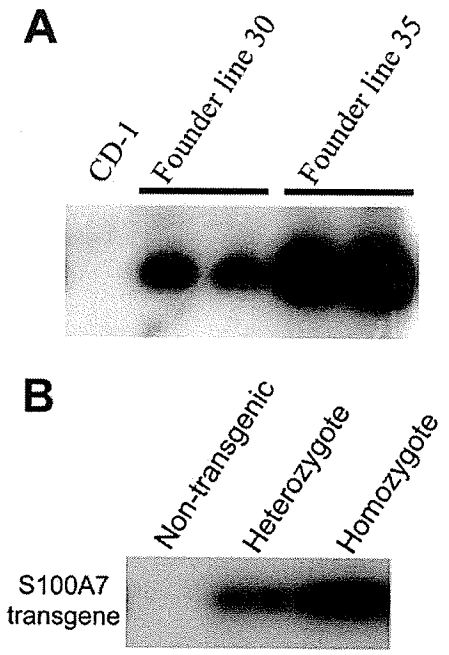

FIG 42- Identification of Mice with Stable Incorporation of S100A7 Transgene. Southern blot showing A) identification of two founder lines that have stable incorporation of S100A7 transgene. Note the absence of signal in the CD1 background control mouse and the difference in intensity of signal in the two founder lines. This is due to different numbers of transgene incorporation into the genome for the two lines. B) Litters of the two founder lines were interbred and produced non-transgenic (no detectable transgene), heterozygotes (transgene on one allele) and homozygotes (transgene on both alleles).

Female virgin animals that were 10 weeks old for both transgenic lines and CD-1 control, were randomly selected for sacrifice. Lumbar mammary glands were isolated and total protein was extracted. Protein expression of human S100A7 in the mammary glands was confirmed by Western blot for both transgenic lines, whereas S100A7 protein was not detected in non-transgenic mice (FIG 43). Immunohistochemical analysis of formalin fixed-paraffin embedded tissue sections suggested that protein expression was present and confined exclusively to the ductal epithelial cells, but a uniform background signal was detected in all control samples (data not shown). Nevertheless, subjective scoring showed that relative overall signal intensity was higher in the transgenic lines compared to the CD-1 control.

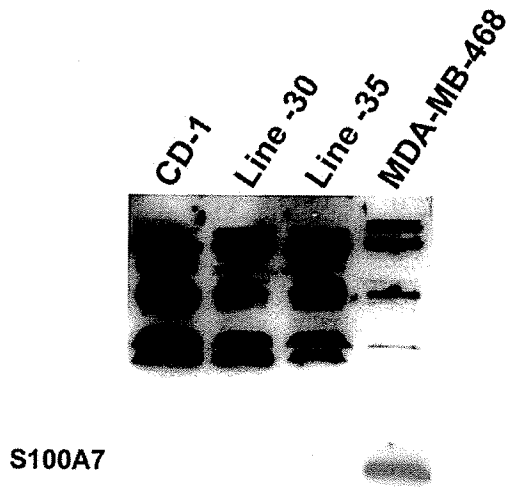

FIG 43- S100A7 Protein Expression in the Mammary Gland of Transgenic Mice. Western blot showing human S100A7 transgene expression from mammary glands isolated from virgin 10 week old mice. S100A7 can be detected from the two independent founder lines 30 and 35, but not from the non-transgenic background strain CD-1. MDA-MB-468 is used as a positive control. 200 μg total mouse mammary protein was loaded per lane.

5.1.0- Discussion: Altered S100 Protein Expression During Neoplasia

The S100 gene family comprises over 20 genes that share chromosomal localization and gene structure (141). They are believed to act as signaling modulators through specific interactions with target proteins, and through specificities determined by the variable C-terminal domains (298). These interactions and the conformation of the S100 proteins are also influenced by binding to calcium (and other ions) through conserved N-terminal EF hand motifs (135). Tissue and pathology specific regulation and expression is also consistent with different functional roles, as S100's are thought to influence many important facets of cell biology including differentiation, growth and metastasis (299). Molecular analysis of a range of tumor types has identified a role for several S100's in tumorigenesis and/or progression, including S100A2, S100A4 and more recently S100A7 (141, 298, 300, 301). We have focused our efforts exclusively on S100A7 as we had previously found it to be a gene that was highly expressed in pre-invasive ductal carcinoma, with reduced amounts in adjacent invasive disease (105). This expression profile suggested to us that S100A7 might be involved in promoting the transition of DCIS to invasive carcinoma. Ascribing a biological function to S100A7 in breast cancer and the elucidation of its mechanism of action would aid in the understanding of the molecular alterations that occur in DCIS to promote the transition to invasive carcinoma.

5.1.1- The Expression Profile of S100A7 in Different Tumor Types is Similar and May Relate to a Common Function

In neoplasia, S100A7 has now been reported by several groups to be expressed in several tumor types. In addition, S100A7 is induced and sometimes highly expressed within cells of the skin undergoing abnormal differentiation in the context of inflammatory dermatoses (298). S100A7 expression has been found to be responsive to a collection of diverse stress stimuli within both *in-vitro* and *in-vivo* conditions. These conditions include serum depletion, cellular compaction/confluency, loss of substrate attachment (196) and ultra-violet-B radiation (302) and have been tested in both breast and skin systems. Stress stimuli are also likely to be prominent factors within the disordered neoplastic epithelium, and particularly in pre-invasive lesions where there is cellular crowding, loss of attachment, and necrosis in a restricted but expanding cell population. These crowded conditions contribute to the cancer cells becoming disconnected from the nutrients and mechanical support of the stroma by an intact basement membrane. We and others (196) have speculated that upregulation of S100A7 in pre-invasive carcinoma is indicative of this stress and that downregulation in invasive carcinoma, in both skin (194) and breast (105, 202), may reflect a change in the intensity of this environmental stress. As invasive carcinoma cells distance themselves from the stressful environment of the primary site by moving to a new location that has a closer proximity to vasculature and lymphatics within the stroma, the protective effects of S100A7 are no longer needed, resulting in down-regulation of the gene.

Promoting cell survival is a role previously suspected for several other members of the S100 family of proteins. We now propose that S100A7 is also one of the many similar factors that influence the balance between survival and apoptosis in breast cancer. However, a key observation that has identified S100A7 as being potentially distinctive in this key balance is that several groups have confirmed, using distinct technical approaches, that S100A7 is frequently differentially expressed during the development of and transition from pre-invasive to invasive carcinoma in skin and breast. Furthermore, S100A7 is amongst the most highly expressed mRNA's and proteins in DCIS (105, 127, 196, 303, 304). It is our belief that the S100A7-Jab1 pro-survival pathway has the potential to have a significant impact in promoting breast cancer at this, the most critical stage in tumor progression.

5.1.2- The Intracellular Action of S100A7 in Breast Cancer Cells is Via Interaction with and Stimulation of Jab1

The ER alpha-negative MDA-MB-231 breast cell line was selected as the basis of our initial model, to reflect the context of S100A7 expression that has been observed previously in breast tumors *in-vivo* (106, 196). We have since engineered S100A7 expression in the ER negative MCF10AT3B cell line, and the ER alpha-positive cell line MCF7 to extend our understanding of the function of this gene. The rationale for these models includes more recent observation by ourselves and others that suggests S100A7 can be expressed at lower levels in normal breast cells and in receptor-positive tumors (196, 305). While these cells did not acquire enhanced biological activity as a result of

S100A7 expression, such as changes in growth rate or invasiveness, there were changes in the amounts of some intracellular proteins relevant to the Jab1 pathways. Phospho-Akt was observed to change in the MCF10AT3B cell in a manner similar to that which was observed in the MDA-MB-231 cell line but exceptions were observed in the ER positive cell line MCF7. Interestingly, S100A7 expression in an ER positive background was found to have very minimal changes in downstream Jab1 effects with only phosphorylation of c-Jun being slightly increased in the presence of S100A7. While there are clearly many differences between the genetic backgrounds of these cells, one interpretation of these observations is that they may suggest that S100A7 can only be biologically active in tumors and cell lines where ER-alpha is absent as seen in the MDA-MB-231 cell line and in ER negative invasive breast tumors.

In the context of the MDA-MB-231 cell model, S100A7 expression results in many changes that appear to be attributable to an action on Jab1 and its downstream pathways. To explain the observed increase in c-Jun phosphorylation in these transfected cells, in the absence of increased JNK phosphorylation, we speculate that the mechanism of COP9 associated phosphorylation of c-Jun (214) is functioning in our cells expressing S100A7, but not in those expressing $S100A7^{mut}$ due to a loss of interaction with Jab1. In our experiments with ER negative MDA-MB-468 breast cancer cells where endogenous S100A7 expression has been forcibly decreased, there is a modest but consistent decrease in the phosphorylation levels of c-Jun, which we believe is caused by a slight decrease in Jab1 activity due S100A7 being less available to bind to Jab1.

We have found a recently described Jab1-binding site to be present within the C-terminal region of S100A7. This binding site was originally identified through site directed mutagenesis as present in both p27 and c-Jun and also necessary for their interaction with Jab1. In the case of p27, triple mutations at the key amino acids within this site (Asp-108, Leu-130, Asn-140) were shown not to substantially alter the gross protein conformation but reduced the binding ability with Jab1 to 15% of the wild type (217). Our data here also show that mutation of the three key amino acids that define this same motif in S100A7 leaves the overall predicted 3D protein structure unchanged but causes subtle regional changes in particular around the metal binding sites.

The observation of increased AP-1 activity in clones expressing $S100A7^{mut}$, albeit reduced compared to unmutated S100A7, without a detectable increase in phosphorylated c-Jun levels was surprising. This could be consistent with an effect derived from a weak and persistent $S100A7^{mut}$-Jab1 interaction that could be detected in some clones, and may indicate the existence of other mechanisms by which Jab1 or S100A7 promote AP-1 activity that does not bear down on the transcription of VEGF and MMP13 genes. Also supporting our data that increased production of AP-1 regulated genes in the presence of S100A7 originates from within the cell and is not due to a secreted factor stimulating an autocrine loop, is the observation that MDA-MB-231 cells do not increase their production of certain MMP's when treated with cytokines or TPA, substances known to dramatically stimulate AP-1 activity in these cells (306).

In parallel with the level of the molecular alteration, S100A7 transfected breast cells demonstrate changes in growth, adhesion and invasiveness in *in-vitro* assays, and also display increased growth and tumorigenicity *in-vivo* (239). The more prominent manifestation of these properties *in-vivo* may reflect a predominant effect on extracellular parameters or on survival under complex stress. The modest although significant increase in proliferation and invasiveness seen in our *in-vitro* assays may reflect the fact that this cell line is already a highly proliferative and invasive cell in *in-vitro* assay. More striking increases in growth and invasiveness were observed *in-vivo* in the nude mice experiments, where metastasis was also associated with S100A7-expressing tumors. Interestingly, tumors expressing $S100A7^{mut}$ had no change in their ability to grow as they behaved identically to control tumors that did not express S100A7. We believe this to reflect a much decreased affinity in the interaction between $S100A7^{mut}$ with Jab1, which does not result in a significant perturbation of the Jab1 pathways. This lack of effect results in no detectable stimulation of growth or invasion pathways, as is seen in tumors expressing unmutated S100A7, where a strong interaction between Jab1 and S100A7 can take place. The difference in growth and ability to form metastases in tumors expressing S100A7 is consistent with the anticipated effects of enhanced metalloproteinase and VEGF expression on extracellular matrix and angiogenesis. These influences on angiogenesis and alteration of the extracellular matrix are not adequately replicated in *in-vitro* assays, and have been observed by others studying the effects of overexpression of VEGF in breast cell lines (307). Nevertheless, additional detailed studies will be necessary to confirm the direct relationship and functional role of these specific factors in the enhanced growth and invasiveness seen in this model *in-vivo*.

The change in growth rate of cells expressing S100A7 could be due to many factors working either separately or cooperatively. Cells expressing S100A7 have a decreased amount of the negative cell cycle regulating protein p27 when grown *in-vitro* and *in-vivo* (239). A possible explanation for tumors expressing $S100A7^{mut}$ not having an increase in growth rate is that their p27 levels are unchanged when compared to control tumors not expressing S100A7. Again, we attribute this to a loss of interaction between $S100A7^{mut}$ and Jab1, where stimulation of Jab1 activity does not occur but is needed for p27 degradation (217). This is supported by our experiments to inhibit S100A7 expression. When endogenous expression of S100A7 is partly eliminated in MDA-MB-468 cells, p27 protein accumulates, presumably due to a loss in Jab1 activity caused by a decrease in the interaction with S100A7. While high levels of p27 protein are expressed in normal human mammary epithelium, loss of p27 is frequent and is of independent prognostic significance in breast cancers (308-310). Low p27 is also a poor prognostic factor in breast cancer, and enhanced proteasomal degradation (217) may be the cause of loss of p27 in tumor cells. Loss of p27 has not been significantly correlated with breast tumor proliferation in all studies where it has been examined (308), which is presumed to be a result of its complex regulation *in-vivo*.

5.1.3- S100A7 Enhances Jab1's Intersection With Key Factors Known to be Important in Breast Cancer

S100A7 may play a role as a secreted chemotactic factor in mediating the inflammatory response in psoriasis (188) or the protection of skin from infection (311). However other

data point to an intracellular action. S100A7 has been associated with several proteins *in-vitro*. These include S100A7 interactions with Jab1 (c-Jun activation domain binding protein 1), E-FABP (epidermal fatty acid binding protein), RanBPM (Ran binding protein Microtubule), and Transglutaminase (199, 239, 261, 312, 313). However, only the S100A7-Jab1 interaction has as yet been associated with any functional effect (239). Jab1 was originally identified as a factor influencing c-Jun transcription of AP-1 regulated genes (205). It is now known that Jab1 is a component of a multimeric protein complex (the CSN/COP9 signalosome) and it is also the only known mammalian deneddylating protein, which plays a critical role in the active control of the SCF-cullin ubiquitin ligases (314). In addition, Jab1 interacts with many components of cell signalling pathways in the context of both phosphorylation and proteasomal activities. The interaction of S100A7 with Jab1 is associated with a cellular redistribution of Jab1 (also a feature of other Jab1 interactions) resulting in an accumulation in the nucleus (202, 239), and a stimulation of Jab1 related activities not involving the SCF-cullin ubiquitin ligase complex (239). The interaction of S100A7 with Jab1 has been further defined by the observation noted above that S100A7 contains a recently described Jab1-binding domain that, as our work here demonstrates, is necessary for its interaction with Jab1 and a number of biological effects that may be relevant to tumor progression. The putative Jab1-binding domain within the C-terminal portion of S100A7 is not common to all S100 proteins. Of the S100 gene family, other than S100A7, only S100A1, A12 and A13 are predicted to have this domain based on protein sequence alignment (data not shown). However, the expression of these S100's in breast cancer has not been described as of yet

and whether an interaction with Jab1 can occur and is biologically analogous to that of S100A7 remains untested.

In common with other S100's, S100A7 has been described to be a nuclear, cytoplasmic and secreted protein, both in breast tumors and in breast cell lines. While its extracellular function is not clearly known, an intracellular mechanism of action has now begun to be defined. The interaction of S100A7 with Jab1 has no effect on overall Jab1 expression but can cause a cellular redistribution of Jab1 to become predominately nuclear (239). This redistribution parallels an enhancement in activity of nuclear Jab1 that may be due to an increase in its nuclear concentration, resulting in an enhancement in transcriptional activities. Jab1 itself plays a central role in multiple signaling pathways and modulation of Jab1 activity could therefore be responsible for many of the observed effects attributed to S100A7. While Jab1 influences many transcription factors, in breast cells these include AP-1 (205), HIF-1 (215), NF-κB (315) and p53 (220), all of which share a common role in modifying the expression of pro-survival genes. A net effect on the survival response is also consistent with the observation that S100A7 expression is highly induced by UV-B stimulation in skin (302) and several stress factors in breast (196). A key part of the UV-B response is the induction of the AP-1 pathway and production of pro-survival factors (316). S100A7's interaction with Jab1 could be a central player in this normal pathway that is 'hijacked' by the abnormal cancer cell to enable it to evade apoptosis in the stressful microenvironment of an overcrowded breast duct.

5.1.4- An Important Outcome of the S100A7-Jab1 Interaction is the Stimulation of Pro-Survival Pathways

Another possible explanation for the observation that S100A7-expressing cell populations manifest a growth rate that is only slightly higher than similar control cells *in-vitro* but significantly higher *in-vivo*, is that the difference relates to cell survival under stress. Under the controlled and sheltered environment of an *in-vitro* culture system, cell stress is minimized, but within the *in-vivo* environment, stress factors will be exerted within the context of the 3-dimensional tumor mass that place a premium on and select for cells better adapted to cope and survive under marginal conditions. We therefore wondered if there could be a common explanation for the observations of increased tumor growth of S100A7 expressing cells when grown in mice, as well as the ability to survive in conditions of anchorage independence and form metastases. One test for this was to examine the relation between S100A7 expression and anoikis (apoptosis induced by detachment of cells from a surface) in the MDA-MB-231 breast cell line model. When grown under anchorage independent conditions, S100A7-expressing cells had developed an increase in their resistance to a specific form of apoptosis, termed anoikis (cell death as a result of anchorage detachment from a surface or other cells) (317). There was a significant relationship between S100A7 and cell survival that was paralleled by increased activity of both the NF-κB pathway, previously known to lie downstream of Jab1, but also phospho-Akt. To determine if both these effects are mediated through the interaction with Jab1, we generated MDA-MB-231 cells expressing S100A7 mutated in the region of the putative Jab1-binding domain. The mutated S100A7 protein did not interact with Jab1 in a Yeast 2-hybrid assay or when expressed within the context of the

MDA-MB-231 cell. Further analysis of MDA-MB-231 cells expressing mutated S100A7 confirmed that the Jab1-binding site is necessary for S100A7's functional effect on NF-κB and Akt activation. It is therefore our belief that the S100A7-Jab1 pathway acts primarily to enhance survival under conditions of cellular stress such as anoikis, which may promote progression of breast cancer.

This survival function, like the perhaps less prominent but direct growth and invasion functions, is coupled to upregulation of Jab1 downstream pathways including AP-1 (as previously described (202)) and NF-κB, and induction of phospho-Akt via a PI3-Kinase dependent mechanism. We have also now established that the above effects are largely dependent on an intact Jab1-binding site (217). Our data here also shows that mutation of the three key amino acids that define this same motif in S100A7 leaves the overall predicted 3D protein structure unchanged but causes subtle regional changes in particular around the metal binding sites. Nevertheless this is sufficient to significantly reduce the *in-vitro* and *in-vivo* interaction with Jab1 and significantly diminishes signaling (e.g. induction of phospho c-Jun, Akt and NF-κB activity) and biological (e.g. anoikis resistance and tumorigenesis in mice) effects of S100A7.

A link between Jab1 and Akt has not been previously identified. We can speculate that in breast cells, S100A7 mediated induction of phospho-Akt is attributable to increased production of AP-1 and possibly also NF-κB regulated growth factors and cytokines that can act in an autocrine fashion to stimulate PI3K through their cognate receptors. One such pathway, based on our current data, may be the EGF-EGFR-PI3K signaling

pathway. A similar autocrine effect has recently been recognized in relation to overexpression of another EGFR ligand in breast cells (318). We have also shown here that the relation between S100A7 and increased phospho-Akt observed in a cell line model can also be identified in-vivo, in ER alpha-negative tumors. While Akt activation is associated with localization of p27 to the cytoplasm, S100A7 is associated with reduced p27 in DCIS and invasive breast cancer. This is consistent with the association of reduced p27 with ER alpha-negative status previously observed by others (319).

The effect of S100A7 on NF-κB is consistent with the known role of NF-κB in promoting cell survival in breast cancer (320). In breast tumors, S100A7 expression is strongly correlated with the ER alpha-negative phenotype in both DCIS and invasive disease (106). In ER alpha negative breast cell lines, a critical role for EGFR- NF-κB signaling has been defined in mediating cell cycle progression (321) and resistance to chemotherapeutic agent induced apoptosis (322). HER2 signaling can also alter NF-κB activity which correlates with reduced apoptosis. More recently, it has also been shown that an ER negative subset of invasive tumors demonstrates increased activation of NF-κB. In this small series (320), 56% of ER negative invasive tumors manifested higher levels of NF-κB activation, which is similar to the frequency of S100A7 expression in the same tumor phenotype.

To understand the possible connections between S100A7 expression and survival in breast cancer cells, it may be relevant to consider similar pathways in keratinocytes in the skin under circumstances where S100A7 is also highly expressed. As already noted, these

include inflammatory dermatoses (323) and the response to UV-B related stress (302), resistance to anoikis, and response to wound healing, where altered signaling pathways have been relatively well defined (277, 324-326). In these circumstances, induction of Akt, NF-κB, and AP-1 are often critical components. In breast cells, Akt and NF-κB have also been implicated in cell survival under anoikis conditions (327, 328), however phosphorylation of Akt may not necessarily be critical for enhanced survival (329) .

5.1.5- S100A7 and its Cumulative Influence on Breast Cancer Progression

The transition of normal breast epithelium through a spectrum of lesions to DCIS (53, 54) and eventually leading to the formation of invasive breast cancer, is presumed to involve many complex processes that are influenced by active changes in gene expression (291). Arguably, the most critical of these processes is the acquisition of the invasive phenotype (229) that occurs with the transition from DCIS to invasive disease. This critical event transforms an otherwise local disease into one that is capable of spreading to distant sites and so able to threaten the life of the patient. It is likely that some of the genes that show alterations in expression between pre-invasive and invasive components of breast tissues may be relevant to the process of invasion and offer markers of risk of early tumor progression (291). In several studies by ourselves and others (105, 106, 108, 196), the expression profile for S100A7 in human breast lesions has been characterized and confirmed to be preferentially associated with DCIS lesions, as well as being associated with poor prognostic factors when expression persists in invasive disease. In our

experimental model of human breast cancer, S100A7 has been shown to also have a direct biological function on the epithelial tumor cells, as S100A7 is able to influence biological processes such as enhancing growth, adhesion and cell survival, and invasiveness of a breast cancer cell line in *in-vitro* assays and tumorigenicity in nude mice *in-vivo*. So even if secreted, S100A7 can exert a chemotactic effect on host immune cells, it is clear that an internal function within the epithelial cell is also an important aspect to this S100, as has been suggested for other S100 proteins. Furthermore, a previously unsuspected mechanism for these pleiotropic effects has been defined by our experiments that requires a direct interaction between S100A7 and the multifunctional intracellular protein Jab1 (205). Because S100A7 can be expressed at very high levels in some pathologies, and in particular in carcinoma in-situ, it is possible that the S100A7-Jab1 interaction has a critical role in modulating signaling pathways at a critical stage in tumor progression.

Challenges to normal cellular homeostasis invoke cellular stress. In early breast tumor progression this is determined by changes in cellular relationships such as altered adhesion, microenvironment factors such as distance from vascular supply, and physical factors such as constraint of expanding numbers of cells within the confined space of the duct. DCIS is very likely to be a highly stressful environment. We believe that S100A7 expression in this context promotes cellular survival by stimulating pro-survival pathways. Once the tumor cell has left the duct and invaded into the surrounding tissue, it is now in a different microenvironment where nutrients and space are not as limited. In

this instance where cellular stress has become reduced, high levels of S100A7 expression may not be warranted, therefore S100A7 becomes downregulated.

5.1.6- Can Jab1 Have a Role in Tumorigenesis?

Jab1 was originally identified in mammalian cells as a factor influencing c-Jun transcription of AP-1-regulated genes (205). It soon became clear that Jab1 was also a component (CSN5) of the multimeric CSN protein complex (208, 330). The CSN/COP9 signalosome had been studied previously in other systems and shown to be involved in protein degradation via the ubiquitin proteasome (Ub-26S) (207, 210). Jab1 has since been shown to be involved in a diversity of interactions with components of cell signaling pathways *in-vitro* using yeast, and human cell line model systems. These interactions appear to result in either translocation of Jab1 from the cytoplasm to the nucleus, as is the case for integrin LFA-1 (211) and HER2 signaling (216). Interaction with Jab1 results in enhanced activity of the transcription factors c-Jun/AP-1 (205), HIF-1 (215, 331), steroid receptors and cofactors (214, 219) or regulating the degradation of the interacting protein, as is the case for SMAD4 (219), p53 (220), HIF-1 (215), MIF (238), and $p27^{Kip1}$ (217, 218), often but not always associated with translocation from nucleus to cytoplasm. However, the physiological relevance of some of these interactions, and specifically in the context of breast epithelial cells, is mostly unknown.

In ovarian tumors, increased nuclear Jab1 is associated with progression and poor outcome (240), and altered Jab1 has also been implicated in renal cancer (241). A direct

role for Jab1 in breast cancer has not been identified previously. However, several proteins including p53 and HER2, which are known to interact with or to influence Jab1, are altered at an early stage within high-risk DCIS (245, 246, 332, 333) and may exert some of their effects through Jab1. The interaction between S100A7 and Jab1 also has the potential to directly facilitate several aspects of early tumor progression. We have shown here that overexpression of S100A7 is associated with translocation of Jab1 to the nucleus, alterations in expression of several Jab1 "downstream" genes, and increased proliferation, altered response to hypoxia, and promotion of invasion. Increased proliferation may be specifically attributable to increased AP-1 activity and down-regulation of the cell cycle inhibitor $p27^{Kip1}$ in this model. Alteration of Jab1 might also lead to increased activation of ER and progesterone receptor, and up-regulation of cyclin D1 and alteration of transforming growth factor-β signaling in other cell models (216, 222, 334), but these aspects of Jab1 function remain to be examined in the context of breast cancer. Increased capacity to survive hypoxic stress may occur through augmented HIF-1 activity and hypoxic response (331). Increased invasiveness may result from activation of AP-1 and HIF-1-dependent genes (223, 225), such as matrix metalloproteinases and VEGF, which are already implicated as critical factors in breast tumor progression (229, 335). It remains to be seen if secreted S100A7 exerts its possible effects on host immune cells through a similar interaction with Jab1 in these non-epithelial cells.

Alteration of Jab1 activity in tumors could be attributable in part to alterations in either the cytoplasmic-nuclear distribution (206, 211, 241) as appears to be the case for the

effect of S100A7. But other scenarios exist for Jab1 localization, such as the ratio of free Jab1:COP9-associated Jab1(206), competition between different interacting proteins (220), or direct elevation of Jab1 expression. The relevance of these potential mechanisms of action to breast cancer remains to be resolved, both for S100A7 and several other Jab1-interacting proteins. Nevertheless, it has been demonstrated that the many important activities of Jab1 can be influenced by competition between different interacting proteins (220). For example, p53 can compete with and down-regulate Jab1 activation of c-Jun (231), and inhibition of Jab1 causes reciprocal up-regulation of p53 (220) and down-regulation of c-Jun in HeLa cells (231). It is also interesting to note that the chemokine MIF can exert the opposite effect on Jab1 to S100A7 (238) with respect to modulation of AP-1 activity and $p27^{Kip1}$ expression. This raises the question of whether these different chemokine molecules might compete to modulate Jab1 activity.

Whereas our data support the involvement of Jab1 in mediating many of the biological actions of S100A7, additional experiments will be needed to further confirm that a direct interaction occurs between the putative Jab1-binding motif (217) on S100A7 and the Jab1 protein, and that direct alterations of Jab1 indeed exert effects on these specific target genes and pathways. It is also possible that some of the functions of S100A7 are mediated through other pathways (136). For example, it has been shown that other secreted S100 proteins (S100B and S100A12) can bind to and stimulate the receptor for advanced glycation of end products (RAGE), leading to activation of intracellular signaling pathways including up-regulation of ras, mitogen-activating protein kinase and NF-κB in immune cells (189, 336). Expression of receptor for advanced glycation of end

products is also associated with invasion in gastric carcinoma (337) and is functionally involved in metastasis (190). Unlike some other S100's with chemokine activities such as S100A9 and S100A12, which are expressed by both epithelial and stromal inflammatory cells (338), expression of S100A7 is restricted to epithelium, at least in skin and breast. However, S100A7 is also secreted and could potentially interact with cell surface receptors on immune or epithelial cells.

An interesting observation that has emerged from studying S100A7 in tumor samples is the location of S100A7 expression at different stages of progression. While S100A7 is found to be both nuclear and cytoplasmic in MDA-MB-231 cells (FIG 13) and in MDA-MB-468 cells (data not shown), trends have emerged from breast cancer tissue. In DCIS, S100A7 expression is predominately localized to the cytoplasm (section 4.3.1), while in invasive disease S100A7 expression is mostly found in the nucleus (Table 4). This observation suggests a dual role for the S100A7-Jab1 interaction, depending on where it is most likely to occur. In DCIS, where S100A7 is predominately cytoplasmic, the effect of the Jab1-S100A7 interaction may be preferentially acting through the COP9 signalosome (FIG 12) to target proteins to the proteasome for degradation. We see such an example in DCIS cases expressing S100A7 where there is an associated decrease between S100A7 and the relative amount of the negative cell cycle regulator $p27^{kip1}$ (FIG 37 B). In invasive disease, perhaps the S100A7-Jab1 interaction is involved in upregulation of AP-1 dependant genes such as EGF and cytokines that are eventually secreted, but feed back to activate cell surface receptors in an autocrine loop. S100A7 expression in invasive disease (nuclear localization) is found to be associated with an

increase in the phosphorylation status of the Akt kinase (FIG 37). Akt phosphorylation is achieved by first stimulating a cell surface receptor, which in turn fire off a set of events that result in Akt phosphorylation. By defining separate cytoplasmic and nuclear consequences for the S100A7-Jab1 interaction, we would have a better understanding of the function of the interaction in general as well as knowing which Jab1 downstream effects are stimulated and which are unchanged.

5.1.7- Other S100-Protein Interactions and Pathways

While the S100A7-Jab1 interaction and its downstream effects in breast cancer are unique, there are other interactions involving S100 proteins that can exert a similar effect in other cell types. Several S100's are emerging as having a role in cell motility. In phagocyte cells, removal of MRP14 (S100A9) prevented transendothelial migration of phagocytes (339). A mechanism is beginning to emerge where MRP14 is specifically phosphorylated by p38 mitogen-activated protein kinase (MAPK). This phosphorylation inhibits MRP8/MRP14-induced tubulin polymerization. MAPK p38 fails to stimulate migration of MRP14(-/-) granulocytes *in-vitro* and MRP14(-/-) mice show a diminished recruitment of granulocytes into the granulation tissue during wound healing *in-vivo* (339). Knockdown of S100A10 in colorectal cells was found to cause a complete loss in plasminogen-dependent cellular invasiveness (340). The mechanism of S100A10 promoting invasion is thought to involve remodeling of the plasma membrane and cytoarchitecture, which are crucial for the regulation of epithelial cell adhesion and permeability. At the plasma membrane, the AHNAK protein associates as a multimeric

complex with actin and the annexin A2/S100A10 complex. Down regulation of either S100A10 or annexin A2 prevents cortical actin cytoskeleton reorganization required to support cell height (341) which is believed to be due to a loss of function for AHNAK which can regulate cortical actin cytoskeleton organization and cell membrane cytoarchitecture. S100A10 is also thought to influence cell-cell adhesion through E-cadherin. If the localization of the annexin 2-S100A10 complex at the plasma membrane is abolished, the result is an inhibition in the re-connection of E-cadherin molecules between cells (342). S100P has emerged as a protein having many characteristics in common with S100A7. S100P is expressed in pre-invasive lesions (of the pancreas) and has been found to interact with a protein in the nucleus (343). Thus, there are an ever increasing number reports describing S100 proteins as having altered expression levels at different stages of cancer progression and acting through direct interactions with genes, pathways, and biological properties that may influence invasion and metastasis..

5.2.0- Summary

We have shown that S100A7 is an important gene in DCIS and may provide a clue to critical cellular pathways in the process of early breast tumor progression. S100A7 is frequently altered in early stages of breast cancer, its expression is related to established prognostic factors in DCIS and invasive cancer, and outcome in specific groups of cancer patients. The mechanism of action of S100A7 (at least in part) involves a specific intracellular interaction with a multi-functional protein called Jab1. The outcome of this interaction may be modulated by the breast cancer cell phenotype, but can lead to

changes in multiple cell signaling pathways and biological properties that can contribute to breast tumor progression. Foremost amongst these properties may be the ability to confer increased survival under conditions of cellular stress that cause anoikis. Although other important cellular proteins also influence and may compete for Jab1, S100A7 is one of the most abundant proteins in high-risk DCIS and is therefore likely to exert an important and dominant effect on Jab1 activity in breast tumor cells and specifically at a critical early stage of tumor progression. Thus, therapies aimed at modulating the effect of S100A7 may have significant potential in the treatment of early breast cancer.

6.0.0- Future Directions

Our studies on S100A7 have revealed this protein to have an intracellular biological function in breast epithelial cancer cells, which appears to be primarily mediated through its interaction with Jab1. But S100A7 most likely can interact with other proteins *in-vivo*, as has been shown for other S100 proteins, but these have yet to be identified. We had utilized the Yeast 2-hybrid screen to identify protein-protein interactions with S100A7, but there now exist more advanced techniques that were not available at the onset of this study. A proteomic screen utilizing recent advances in mass spectrometry may identify further interactions not detectable in the Yeast system. Alternatively, using the transfected cell lines described in this study, it might now be possible to purify S100A7 from cell lysates under native conditions using an affinity column technique. Proteins that bound to S100A7 could then be collected, purified and sequenced using high throughput protein identification and sequencing technologies. The $S100A7^{mut}$ expressing clones could be useful in these types of studies to verify any potential new interactions as

S100A7^{mut} is altered in its physical conformation in the unique C-terminal region and this might influence its interaction with other proteins besides Jab1. Once new S100A7-interaction proteins are identified, the interaction needs to be first confirmed by other methods such as co-immunoprecipitation and then secondly the biological importance of the interaction would need to be tested using many of the assays described in this study. There are several aspects to the rationale for seeking to identify new S100A7-interacting proteins. To begin with, many S100s have been shown to functionally interact with more than one target protein and this may be an inherent property of these signaling molecules. In the case of S100A7, it has now been associated with different functions in two cell types that may involve quite different mechanisms. In addition, not all of the enhanced biological features we observe in the presence of S100A7 can be explained exclusively by changes in Jab1 activity and not all activities were completely abolished by inhibition of the Jab1 interaction. For example, AP-1 activity and resistance to anoikis were only partially inhibited by effective inhibition of a significant S100A7-Jab1 interaction (see Figs 14 and 30). Moreover, it is possible that other interactions and functional outcomes exist specifically in the ER alpha positive phenotype. NF-κB activation can also be accomplished by several factors bearing down on this protein complex. Identification of alternative pathways and players involved would open new branches of study regarding the biological function of S100A7 that may be relevant to the acquisition of the invasive phenotype.

The studies described in this report focused exclusively on an intracellular action for S100A7 in breast epithelial cells. We have observed evidence to support the original contention that S100A7 is also a secreted protein and we have observed this for both breast tumors as well as under culture conditions for breast cell lines. This raises the question of an additional extracellular function of S100A7, as was originally proposed in the context of psoriasis. The possibility exists that S100A7 has a cell surface receptor that it can bind to and in turn activate signal transduction pathways. A good candidate receptor is RAGE (receptor for advanced glycation of end-products) as a few S100 proteins have recently been described to "en-RAGE", i.e. engage RAGE and activate signal transduction pathways. The expression of RAGE in breast tumors or breast cell lines has yet to be well described, but commercially available antibodies are now available. The experiments to be performed would be to generate and add recombinant S100A7 to a panel of breast cells and then analyze them for changes in key players of known signal transduction pathways. After a biochemical change had been identified and attributed to a change in RAGE activity, a change in biological activity would need to be measured. This would involve performing cell growth or invasion assays in both the presence and absence of recombinant S100A7. If changes in signal transduction pathways were detected, namely alteration in the phosphorylation level of signaling proteins, it would be discriminating to add small molecule inhibitors that inhibit the phosphorylation of individual kinases and proteins in experiments involving recombinant S100A7. Several of these compounds already exist for the MAPK and Akt pathways. These studies would help to tease out the exact pathways that extracellular S100A7 might activate to give the cells an enhanced biological activity. If a receptor is identified for extracellular

S100A7, the production of a molecule to block this interaction to prevent activation of signal transduction pathways would have utility in understanding the biological function of S100A7 in breast cancer. As well this compound could be tested for any clinical benefit in preventing or delaying breast cancer growth in patients expressing S100A7.

The identification of a small molecule inhibitor that prevents the interaction between S100A7 and Jab1 would be useful to further define the importance of their interaction. By preventing their interaction in the presence of unmodified S100A7, a better understanding regarding the importance of the interaction in promoting growth and invasion could be determined. If S100A7 and Jab1 are not allowed to interact but these cells have an enhancement in their invasive and growth properties, we would know that S100A7 is able to influence another pathway that is not Jab1 dependant which results in stimulation of the same biological endpoint. To identify such a compound, libraries of molecules could be screened using the interaction between S100A7 and Jab1 in Yeast as the assay. The effect of individual molecules on the reporter gene LacZ or an inhibition of growth in the absence of Histidine could be used to show a loss of interaction. This process could be automated to screen several thousand compounds.

To expand on the *in-vitro* and xenograft transplantation studies described in this report, it will be necessary to evaluate the effect of S100A7 expression within an intact and fully functional *in-vivo* setting. Having an *in-vivo* model will provide a more complete

environment to study S100A7 in breast cells because an animal model will provide two key features that are not present in our previous studies: an active immune system and an intact stromal environment, which have both been shown to be capable of influencing cancer formation and progression. Our most recent studies have begun to look at the effect of S100A7 expression on breast cancer tumorigenesis using the transgenic mouse we have generated. These studies involve crossing our transgenic mouse with another mouse line that develops mammary tumors due to the fact that these mice have been engineered to over express the HER2 gene in the mouse mammary gland. Another experiment using our S100A7 transgenic mouse to examine breast tumorigenesis would involve treating the mice and a control group with the carcinogen DMBA. The advantage of this experiment is that all the S100A7 transgenic mice would be homozygotes for the transgene, which would theoretically allow for maximal S100A7 expression and a better chance to detect any effect due to S100A7. The disadvantage of this experiment is that DMBA is a carcinogen that is not specific to the breast or necessarily relevant to human breast carcinogenesis and would generate several tumors at sites other than the mammary gland resulting in some issues in distinguishing primary tumors and metastatic tumors and a larger number of mice being required to enable specific study of mammary tumors to determine any change in tumor formation or growth in this organ. The formation of mammary tumors in mice resulting from DMBA treatment is certainly through a different mechanism than that involving HER2 overexpression, but this has not been well characterized. However, S100A7's effect may not be detectable in the HER2 background as this pathway that may also influence Jab1 and could be exerting a dominant and maximal effect on Jab1 already. Therefore the DMBA experiment may be more

appropriate to detect an effect due to S100A7 expression. The transgenic mouse model will also allow for the assessment of S100A7 expression during normal mammary development. Groups of transgenic and control mice will need to be assembled to look at the normal mammary epithelial network during the developmental stages of virgin, pregnancy and involution. In this way, a possible functional role for S100A7 in normal mammary tissue may be uncovered, such as a role in the involution phase of mammary physiology, where inflammation is an important component. Preliminary results have found that S100A7 transgenic mice do not form mammary tumors spontaneously during a 15 months time period. As well, these mice do not present with an abnormal phenotype and are of normal size and fertile and give birth to normal pups.

Some intriguing factors and proteins that influence S100A7 have been identified in cell lines by ourselves and others, However the dominant components involved in regulation of S100A7 transcription during breast tumorigenesis are not currently known. Why some tumors express large amounts of S100A7 while similar tumors do not is a mystery. We have uncovered a strong association of S100A7 expression with the absence of ER alpha negative expression in breast tumors. While S100A7 can be expressed in some tumors classified as ER positive, this weak association may be dependant on the method of ER assessment. A small proportion of tumors expressing S100A7 that have been categorized by ligand binding assay as being ER negative can be re-classified as being ER positive when assayed by immunohistochemistry. Is the ER not active (in terms of ligand binding) in this cohort even though its expression can be detected? Can this observation give a clue as to the *in-vivo* regulation of S100A7? The association of S100A7 with ER is an interesting area of investigation as it could explain why MDA-MB-231 cells (ER -ve)

expressing S100A7 have a measurable change in biological activities while S100A7 expression in MCF7 cells (ER +ve) do not appear to be altered.

The mouse homologue to the human S100A7 gene has been identified by the mouse genome sequencing project. Using its putative mRNA sequence, we have determined that it is located within the S100 gene family and have designed molecular tool to allow us to study its expression (data not shown). In mouse skin, we found S100A7/psoriasin mRNA to be significantly upregulated in relation to inflammation (192). In murine mammary gland, expression is also upregulated in mammary tumors where it is localized to areas of squamous differentiation. This mirrors the context of expression in human tumor types where both squamous and glandular differentiation occur, including cervical and lung carcinomas. Additionally, mouse S100A7/psoriasin possesses a putative Jab1 binding motif that mediates many downstream functions of the human S100A7 gene. We speculate that because of the mirrored expression profiles of the mouse and human S100A7 gene during cancer progression, this gene is performing a similar function in neoplasia in both mouse and human. Because of a putative Jab1-binding site in mouse S100A7/psoriasin, it is attractive to think that an interaction with Jab1 is possible (human and mouse Jab1 are 99% homologous) resulting in the activation of pathways seen in human breast cells and tissue. To explore the function of mouse S100A7/psoriasin in the process of mouse mammary tumor formation, the S100A7/psoriasin knockout mouse will need to be generated. If the S100A7/psoriasin knockout mouse is viable, it will need to be mated with a mammary tumorigenic mouse strain and then offspring analyzed for an

effect on mammary tumor formation. Another approach would be to treat the knockout mouse with the carcinogen DMBA as described above for the S100A7-transgenic mouse. Analysis would also need to be performed to assess if Jab1 activity was altered in tumors from the knockout mouse. We would expect the absence of S100A7/psoriasin would result in a delay in tumor formation and a decrease in Jab1 associated activities.

Notwithstanding the discussion points above, we currently believe that the S100A7-Jab1 pathway is the major pathway through which S100A7 exerts its effects in breast cells. Experiments involving the S100A7 transgenic mouse will be useful to validate *in-vitro* and xenograft models used so far. The next priority will be to develop small molecule inhibitors that block the S100A7-Jab1 interaction and test the overall function of the interaction *in-vivo*. This molecule could then be tested as a preventive or therapeutic agent.

7.0.0- Publications Resulting From This Study

Emberley ED, Niu Y, Curtis L, Troup S, Mandal S, Myers JN, Gibson SB, Murphy LC, Watson PH
The S100A7-Jab1 pathway enhances pro-survival pathways in breast cancer
Submitted

Webb M, Emberley ED, Lizardo M, Alowami S, Qing G, Alfia'ar A, Snell-Curtis LJ, Niu Y, Civetta A, Myal Y, Shiu R, Murphy LC, Watson PH
Expression analysis of the mouse S100A7/psoriasin gene in skin inflammation and mammary tumorigenesis
BMC Cancer. 2005 Feb 17;5(1):17

Emberley ED, Murphy LC, Watson PH
S100 proteins and their influence on pro-survival pathways in cancer
Biochemistry and Cell Biology 2004 Aug;82(4):508-15 (review)

Emberley ED, Murphy LC, Watson PH
S100A7 and the progression of breast cancer
Breast Cancer Res 2004, 6:153-159 (review)

Emberley ED, Alowami S, Snell L, Murphy LC, Watson PH.
S100A7 (psoriasin) expression is associated with aggressive features and alteration of Jab1 in ductal carcinoma in situ of the breast.
Breast Cancer Res 2004, 6:R308-R315

Emberley ED, Niu Y, Njue C, Kliewer EV, Murphy LC, Watson PH
Psoriasin (S100A7) expression is associated with poor outcome in estrogen receptor-negative invasive breast cancer.
Clin Cancer Res. 2003 Jul;9(7):2627-31.

Emberley ED, Niu Y, Leygue E, Tomes L, Gietz RD, Murphy LC, Watson PH
Psoriasin interacts with Jab1 and influences breast cancer progression.
Cancer Res. 2003 Apr 15;63(8):1954-61.

References

1. Ernster VL, Barclay J. Increases in ductal carcinoma in situ (DCIS) of the breast in relation to mammography: a dilemma. J Natl Cancer Inst Monogr 1997;151-156.

2. Leonard GD, Swain SM. Ductal carcinoma in situ, complexities and challenges. J Natl Cancer Inst 2004;96:906-920.

3. Lu YJ, Osin P, Lakhani SR, Di Palma S, Gusterson BA, Shipley JM. Comparative genomic hybridization analysis of lobular carcinoma in situ and atypical lobular hyperplasia and potential roles for gains and losses of genetic material in breast neoplasia. Cancer Res 1998;58:4721-4727.

4. Buerger H, Simon R, Schafer KL, Diallo R, Littmann R, Poremba C, van Diest PJ, Dockhorn-Dworniczak B, Bocker W. Genetic relation of lobular carcinoma in situ, ductal carcinoma in situ, and associated invasive carcinoma of the breast. Mol Pathol 2000;53:118-121.

5. Holland R, Peterse JL, Millis RR, Eusebi V, Faverly D, van de Vijver MJ, Zafrani B. Ductal carcinoma in situ: a proposal for a new classification. Semin Diagn Pathol 1994;11:167-180.

6. Shackney SE, Shankey TV. Common patterns of genetic evolution in human solid tumors. Cytometry 1997;29:1-27.

7. Sasson AR, Fowble B, Hanlon AL, Torosian MH, Freedman G, Boraas M, Sigurdson ER, Hoffman JP, Eisenberg BL, Patchefsky A. Lobular carcinoma in situ increases the risk of local recurrence in selected patients with stages I and II breast carcinoma treated with conservative surgery and radiation. Cancer 2001;91:1862-1869.

8. Abner AL, Connolly JL, Recht A, Bornstein B, Nixon A, Hetelekidis S, Silver B, Harris JR, Schnitt SJ. The relation between the presence and extent of lobular carcinoma in situ and the risk of local recurrence for patients with infiltrating carcinoma of the breast treated with conservative surgery and radiation therapy. Cancer 2000;88:1072-1077.

9. Ernster VL, Barclay J, Kerlikowske K, Grady D, Henderson C. Incidence of and treatment for ductal carcinoma in situ of the breast. JAMA 1996;275:913-918.

10. Ernster VL, Ballard-Barbash R, Barlow WE, Zheng Y, Weaver DL, Cutter G, Yankaskas BC, Rosenberg R, Carney PA, Kerlikowske K, Taplin SH, Urban N, Geller BM. Detection of ductal carcinoma in situ in women undergoing screening mammography. J Natl Cancer Inst 2002;94:1546-1554.

11. Stomper PC, Connolly JL, Meyer JE, Harris JR. Clinically occult ductal carcinoma in situ detected with mammography: analysis of 100 cases with radiologic-pathologic correlation. Radiology 1989;172:235-241.

12. Olivotto I, Levine M. Clinical practice guidelines for the care and treatment of breast cancer: the management of ductal carcinoma in situ (summary of the 2001 update). CMAJ 2001;165:912-913.

13. Litherland J. The role of needle biopsy in the diagnosis of breast lesions. Breast 2001;10:383-387.

14. Dershaw DD. Stereotaxic breast biopsy. Semin Ultrasound CT MR 1996;17:444-459.

15. de Paredes ES, Langer TG, Cousins J. Interventional breast procedures. Curr Probl Diagn Radiol 1998;27:133-184.

16. Darling ML, Smith DN, Lester SC, Kaelin C, Selland DL, Denison CM, DiPiro PJ, Rose DI, Rhei E, Meyer JE. Atypical ductal hyperplasia and ductal carcinoma in situ as revealed by large-core needle breast biopsy: results of surgical excision. AJR Am J Roentgenol 2000;175:1341-1346.

17. Bonnett M, Wallis T, Rossmann M, Pernick NL, Carolin KA, Segel M, Bouwman D, Visscher D. Histologic and radiographic analysis of ductal carcinoma in situ diagnosed using stereotactic incisional core breast biopsy. Mod Pathol 2002;15:95-101.

18. Schnitt SJ, Connolly JL, Tavassoli FA, Fechner RE, Kempson RL, Gelman R, Page DL. Interobserver reproducibility in the diagnosis of ductal proliferative breast lesions using standardized criteria. Am J Surg Pathol 1992;16:1133-1143.

19. Shoker BS, Sloane JP. DCIS grading schemes and clinical implications. Histopathology 1999;35:393-400.

20. Schnitt SJ, Harris JR, Smith BL. Developing a prognostic index for ductal carcinoma in situ of the breast. Are we there yet? Cancer 1996;77:2189-2192.

21. Walker RA, Jones JL, Chappell S, Walsh T, Shaw JA. Molecular pathology of breast cancer and its application to clinical management. Cancer Metastasis Rev 1997;16:5-27.

22. Badve S, A'Hern RP, Ward AM, Millis RR, Pinder SE, Ellis IO, Gusterson BA, Sloane JP. Prediction of local recurrence of ductal carcinoma in situ of the breast using five histological classifications: a comparative study with long follow-up. Hum Pathol 1998;29:915-923.

23. Gupta SK, Douglas-Jones AG, Fenn N, Morgan JM, Mansel RE. The clinical behavior of breast carcinoma is probably determined at the preinvasive stage (ductal carcinoma in situ). Cancer 1997;80:1740-1745.

24. Silverstein MJ, Poller DN, Waisman JR, Colburn WJ, Barth A, Gierson ED, Lewinsky B, Gamagami P, Slamon DJ. Prognostic classification of breast ductal carcinoma-in-situ. Lancet 1995;345:1154-1157.

25. Fisher ER, Dignam J, Tan-Chiu E, Costantino J, Fisher B, Paik S, Wolmark N. Pathologic findings from the National Surgical Adjuvant Breast Project (NSABP) eight-year update of Protocol B-17: intraductal carcinoma. Cancer 1999;86:429-438.

26. Jordan VC. Is tamoxifen the Rosetta stone for breast cancer? J Natl Cancer Inst 2003;95:338-340.

27. Jordan VC. Tamoxifen: a most unlikely pioneering medicine. Nat Rev Drug Discov 2003;2:205-213.

28. Jordan VC, Dowse LJ. Tamoxifen as an anti-tumour agent: effect on oestrogen binding. J Endocrinol 1976;68:297-303.

29. Fonseca R, Hartmann LC, Petersen IA, Donohue JH, Crotty TB, Gisvold JJ. Ductal carcinoma in situ of the breast. Ann Intern Med 1997;127:1013-1022.

30. Lagios MD, Westdahl PR, Margolin FR, Rose MR. Duct carcinoma in situ. Relationship of extent of noninvasive disease to the frequency of occult invasion, multicentricity, lymph node metastases, and short-term treatment failures. Cancer 1982;50:1309-1314.

31. Veronesi U, Cascinelli N, Mariani L, Greco M, Saccozzi R, Luini A, Aguilar M, Marubini E. Twenty-year follow-up of a randomized study comparing breast-conserving surgery with radical mastectomy for early breast cancer. N Engl J Med 2002;347:1227-1232.

32. Mansfield CM, Komarnicky LT, Schwartz GF, Rosenberg AL, Krishnan L, Jewell WR, Rosato FE, Moses ML, Haghbin M, Taylor J. Ten-year results in 1070 patients with stages I and II breast cancer treated by conservative surgery and radiation therapy. Cancer 1995;75:2328-2336.

33. Fisher B, Dignam J, Wolmark N, Mamounas E, Costantino J, Poller W, Fisher ER, Wickerham DL, Deutsch M, Margolese R, Dimitrov N, Kavanah M. Lumpectomy and radiation therapy for the treatment of intraductal breast cancer: findings from National Surgical Adjuvant Breast and Bowel Project B-17. J Clin Oncol 1998;16:441-452.

34. Julien JP, Bijker N, Fentiman IS, Peterse JL, Delledonne V, Rouanet P, Avril A, Sylvester R, Mignolet F, Bartelink H, Van Dongen JA. Radiotherapy in breast-conserving treatment for ductal carcinoma in situ: first results of the EORTC randomised phase III trial 10853. EORTC Breast Cancer Cooperative Group and EORTC Radiotherapy Group. Lancet 2000;355:528-533.

35. Boyages J, Delaney G, Taylor R. Predictors of local recurrence after treatment of ductal carcinoma in situ: a meta-analysis. Cancer 1999;85:616-628.

36. Fisher B, Dignam J, Wolmark N, Wickerham DL, Fisher ER, Mamounas E, Smith R, Begovic M, Dimitrov NV, Margolese RG, Kardinal CG, Kavanah MT, Fehrenbacher L, Oishi RH. Tamoxifen in treatment of intraductal breast cancer: National Surgical Adjuvant Breast and Bowel Project B-24 randomised controlled trial. Lancet 1999;353:1993-2000.

37. Smith IE. Aromatase inhibitors-extending the benefits of adjuvant therapy beyond tamoxifen. Breast 2004;13 Suppl 1:3-9.

38. Morandi P, Rouzier R, Altundag K, Buzdar AU, Theriault RL, Hortobagyi G. The role of aromatase inhibitors in the adjuvant treatment of breast carcinoma: the M. D. Anderson Cancer Center evidence-based approach. Cancer 2004;101:1482-1489.

39. Lonning PE. Aromatase inhibitors in breast cancer. Endocr Relat Cancer 2004;11:179-189.

40. Johnston SR, Dowsett M. Aromatase inhibitors for breast cancer: lessons from the laboratory. Nat Rev Cancer 2003;3:821-831.

41. Mokbel K. Focus on anastrozole and breast cancer. Curr Med Res Opin 2003;19:683-688.

42. Lundgren S. Progestins in breast cancer treatment. A review. Acta Oncol 1992;31:709-722.

43. Baum M, Budzar AU, Cuzick J, Forbes J, Houghton JH, Klijn JG, Sahmoud T. Anastrozole alone or in combination with tamoxifen versus tamoxifen alone for adjuvant treatment of postmenopausal women with early breast cancer: first results of the ATAC randomised trial. Lancet 2002;359:2131-2139.

44. Buzdar AU. The ATAC (Arimidex, Tamoxifen, Alone or in Combination) trial: an update. Clin Breast Cancer 2004;5 Suppl 1:S6-S12.

45. Wellings SR, Jensen HM, Marcum RG. An atlas of subgross pathology of the human breast with special reference to possible precancerous lesions. J Natl Cancer Inst 1975;55:231-273.

46. Wellings SR, Jensen HM. On the origin and progression of ductal carcinoma in the human breast. J Natl Cancer Inst 1973;50:1111-1118.

47. Alpers CE, Wellings SR. The prevalence of carcinoma in situ in normal and cancer-associated breasts. Hum Pathol 1985;16:796-807.

48. Page DL, Dupont WD, Rogers LW, Jensen RA, Schuyler PA. Continued local recurrence of carcinoma 15-25 years after a diagnosis of low grade ductal carcinoma in situ of the breast treated only by biopsy. Cancer 1995;76:1197-1200.

49. Page DL, Dupont WD, Rogers LW, Landenberger M. Intraductal carcinoma of the breast: follow-up after biopsy only. Cancer 1982;49:751-758.

50. Palli D, Rosselli dT, Simoncini R, Bianchi S. Benign breast disease and breast cancer: a case-control study in a cohort in Italy. Int J Cancer 1991;47:703-706.

51. London SJ, Connolly JL, Schnitt SJ, Colditz GA. A prospective study of benign breast disease and the risk of breast cancer. JAMA 1992;267:941-944.

52. Dupont WD, Parl FF, Hartmann WH, Brinton LA, Winfield AC, Worrell JA, Schuyler PA, Plummer WD. Breast cancer risk associated with proliferative breast disease and atypical hyperplasia. Cancer 1993;71:1258-1265.

53. Beckmann MW, Niederacher D, Schnurch HG, Gusterson BA, Bender HG. Multistep carcinogenesis of breast cancer and tumour heterogeneity. J Mol Med 1997;75:429-439.

54. Allred DC, Mohsin SK, Fuqua SA. Histological and biological evolution of human premalignant breast disease. Endocr Relat Cancer 2001;8:47-61.

55. Schnitt SJ. Microinvasive carcinoma of the breast: a diagnosis in search of a definition. Adv Anat Pathol 1998;5:367-372.

56. James LA, Mitchell EL, Menasce L, Varley JM. Comparative genomic hybridisation of ductal carcinoma in situ of the breast: identification of regions of DNA amplification and deletion in common with invasive breast carcinoma. Oncogene 1997;14:1059-1065.

57. Aubele M, Mattis A, Zitzelsberger H, Walch A, Kremer M, Welzl G, Hofler H, Werner M. Extensive ductal carcinoma In situ with small foci of invasive ductal carcinoma: evidence of genetic resemblance by CGH. Int J Cancer 2000;85:82-86.

58. Vogelstein B, Fearon ER, Hamilton SR, Kern SE, Preisinger AC, Leppert M, Nakamura Y, White R, Smits AM, Bos JL. Genetic alterations during colorectal-tumor development. N Engl J Med 1988;319:525-532.

59. Simpson PT, Reis-Filho JS, Gale T, Lakhani SR. Molecular evolution of breast cancer. J Pathol 2005;205:248-254.

60. Reis-Filho JS, Lakhani SR. The diagnosis and management of pre-invasive breast disease: genetic alterations in pre-invasive lesions. Breast Cancer Res 2003;5:313-319.

61. Farabegoli F, Champeme MH, Bieche I, Santini D, Ceccarelli C, Derenzini M, Lidereau R. Genetic pathways in the evolution of breast ductal carcinoma in situ. J Pathol 2002;196:280-286.

62. Lakhani SR. The transition from hyperplasia to invasive carcinoma of the breast. J Pathol 1999;187:272-278.

63. Schnitt SJ, Vincent-Salomon A. Columnar cell lesions of the breast. Adv Anat Pathol 2003;10:113-124.

64. Burstein HJ, Polyak K, Wong JS, Lester SC, Kaelin CM. Ductal carcinoma in situ of the breast. N Engl J Med 2004;350:1430-1441.

65. Silverstein MJ. Ductal carcinoma in situ of the breast. Br J Surg 1997;84:145-146.

66. Silverstein MJ. Ductal carcinoma in situ of the breast. BMJ 1998;317:734-739.

67. Singletary SE, Allred C, Ashley P, Bassett LW, Berry D, Bland KI, Borgen PI, Clark G, Edge SB, Hayes DF, Hughes LL, Hutter RV, Morrow M, Page DL, Recht A, Theriault RL, Thor A, Weaver DL, Wieand HS, Greene FL. Revision of the American Joint Committee on Cancer staging system for breast cancer. J Clin Oncol 2002;20:3628-3636.

68. Ernster VL, Barclay J, Kerlikowske K, Wilkie H, Ballard-Barbash R. Mortality among women with ductal carcinoma in situ of the breast in the population-based surveillance, epidemiology and end results program. Arch Intern Med 2000;160:953-958.

69. Miller AB, To T, Baines CJ, Wall C. Canadian National Breast Screening Study-2: 13-year results of a randomized trial in women aged 50-59 years. J Natl Cancer Inst 2000;92:1490-1499.

70. Bissell MJ, Radisky D. Putting tumours in context. Nat Rev Cancer 2001;1:46-54.

71. Stampfer MR, Yaswen P. Culture models of human mammary epithelial cell transformation. J Mammary Gland Biol Neoplasia 2000;5:365-378.

72. Ozzello L, Sordat B, Merenda C, Carrel S, Hurlimann J, Mach JP. Transplantation of a human mammary carcinoma cell line (BT 20) into nude mice. J Natl Cancer Inst 1974;52:1669-1672.

73. Ozzello L, Sordat M. Behavior of tumors produced by transplantation of human mammary cell lines in athymic nude mice. Eur J Cancer 1980;16:553-559.

74. Miller FR. Models of progression spanning preneoplasia and metastasis: the human MCF10AneoT.TGn series and a panel of mouse mammary tumor subpopulations. Cancer Treat Res 1996;83:243-263.

75. Miller FR. Xenograft models of premalignant breast disease. J Mammary Gland Biol Neoplasia 2000;5:379-391.

76. Soule HD, Maloney TM, Wolman SR, Peterson WD, Jr., Brenz R, McGrath CM, Russo J, Pauley RJ, Jones RF, Brooks SC. Isolation and characterization of a spontaneously immortalized human breast epithelial cell line, MCF-10. Cancer Res 1990;50:6075-6086.

77. Wolman SR, Mohamed AN, Heppner GH, Soule HD. Chromosomal markers of immortalization in human breast epithelium. Genes Chromosomes Cancer 1994;10:59-65.

78. Miller FR, Soule HD, Tait L, Pauley RJ, Wolman SR, Dawson PJ, Heppner GH. Xenograft model of progressive human proliferative breast disease. J Natl Cancer Inst 1993;85:1725-1732.

79. Basolo F, Elliott J, Tait L, Chen XQ, Maloney T, Russo IH, Pauley R, Momiki S, Caamano J, Klein-Szanto AJ, . Transformation of human breast epithelial cells by c-Ha-ras oncogene. Mol Carcinog 1991;4:25-35.

80. Dawson PJ, Wolman SR, Tait L, Heppner GH, Miller FR. MCF10AT: a model for the evolution of cancer from proliferative breast disease. Am J Pathol 1996;148:313-319.

81. Holland PA, Knox WF, Potten CS, Howell A, Anderson E, Baildam AD, Bundred NJ. Assessment of hormone dependence of comedo ductal carcinoma in situ of the breast. J Natl Cancer Inst 1997;89:1059-1065.

82. Gandhi A, Holland PA, Knox WF, Potten CS, Bundred NJ. Effects of a pure antiestrogen on apoptosis and proliferation within human breast ductal carcinoma in situ. Cancer Res 2000;60:4284-4288.

83. Chan KC, Knox WF, Gee JM, Morris J, Nicholson RI, Potten CS, Bundred NJ. Effect of epidermal growth factor receptor tyrosine kinase inhibition on epithelial proliferation in normal and premalignant breast. Cancer Res 2002;62:122-128.

84. Kuperwasser C, Chavarria T, Wu M, Magrane G, Gray JW, Carey L, Richardson A, Weinberg RA. Reconstruction of functionally normal and malignant human breast tissues in mice. Proc Natl Acad Sci U S A 2004;101:4966-4971.

85. Bhathal PS, Brown RW, Lesueur GC, Russell IS. Frequency of benign and malignant breast lesions in 207 consecutive autopsies in Australian women. Br J Cancer 1985;51:271-278.

86. Nielsen M, Thomsen JL, Primdahl S, Dyreborg U, Andersen JA. Breast cancer and atypia among young and middle-aged women: a study of 110 medicolegal autopsies. Br J Cancer 1987;56:814-819.

87. Holst CR, Nuovo GJ, Esteller M, Chew K, Baylin SB, Herman JG, Tlsty TD. Methylation of p16(INK4a) promoters occurs in vivo in histologically normal human mammary epithelia. Cancer Res 2003;63:1596-1601.

88. Nandi S, Guzman RC, Yang J. Hormones and mammary carcinogenesis in mice, rats, and humans: a unifying hypothesis. Proc Natl Acad Sci U S A 1995;92:3650-3657.

89. Hooper ML. Tumour suppressor gene mutations in humans and mice: parallels and contrasts. EMBO J 1998;17:6783-6789.

90. Cardiff RD, Moghanaki D, Jensen RA. Genetically engineered mouse models of mammary intraepithelial neoplasia. J Mammary Gland Biol Neoplasia 2000;5:421-437.

91. Schulze-Garg C, Lohler J, Gocht A, Deppert W. A transgenic mouse model for the ductal carcinoma in situ (DCIS) of the mammary gland. Oncogene 2000;19:1028-1037.

92. Cardiff RD, Anver MR, Gusterson BA, Hennighausen L, Jensen RA, Merino MJ, Rehm S, Russo J, Tavassoli FA, Wakefield LM, Ward JM, Green JE. The mammary pathology of genetically engineered mice: the consensus report and recommendations from the Annapolis meeting. Oncogene 2000;19:968-988.

93. Pittius CW, Sankaran L, Topper YJ, Hennighausen L. Comparison of the regulation of the whey acidic protein gene with that of a hybrid gene containing the whey acidic protein gene promoter in transgenic mice. Mol Endocrinol 1988;2:1027-1032.

94. Cato AC, Weinmann J, Mink S, Ponta H, Henderson D, Sonnenberg A. The regulation of expression of mouse mammary tumor virus DNA by steroid hormones and growth factors. J Steroid Biochem 1989;34:139-143.

95. Stamp G, Fantl V, Poulsom R, Jamieson S, Smith R, Peters G, Dickson C. Nonuniform expression of a mouse mammary tumor virus-driven int-2/Fgf-3 transgene in pregnancy-responsive breast tumors. Cell Growth Differ 1992;3:929-938.

96. Leder A, Pattengale PK, Kuo A, Stewart TA, Leder P. Consequences of widespread deregulation of the c-myc gene in transgenic mice: multiple neoplasms and normal development. Cell 1986;45:485-495.

97. Sinn E, Muller W, Pattengale P, Tepler I, Wallace R, Leder P. Coexpression of MMTV/v-Ha-ras and MMTV/c-myc genes in transgenic mice: synergistic action of oncogenes in vivo. Cell 1987;49:465-475.

98. Muller WJ, Sinn E, Pattengale PK, Wallace R, Leder P. Single-step induction of mammary adenocarcinoma in transgenic mice bearing the activated c-neu oncogene. Cell 1988;54:105-115.

99. Guy CT, Cardiff RD, Muller WJ. Induction of mammary tumors by expression of polyomavirus middle T oncogene: a transgenic mouse model for metastatic disease. Mol Cell Biol 1992;12:954-961.

100. Li Y, Hively WP, Varmus HE. Use of MMTV-Wnt-1 transgenic mice for studying the genetic basis of breast cancer. Oncogene 2000;19:1002-1009.

101. Crist KA, Chaudhuri B, Shivaram S, Chaudhuri PK. Ductal carcinoma in situ in rat mammary gland. J Surg Res 1992;52:205-208.

102. Thompson HJ, McGinley JN, Wolfe P, Singh M, Steele VE, Kelloff GJ. Temporal sequence of mammary intraductal proliferations, ductal carcinomas in situ and adenocarcinomas induced by 1-methyl-1-nitrosourea in rats. Carcinogenesis 1998;19:2181-2185.

103. Korkola JE, Archer MC. Resistance to mammary tumorigenesis in Copenhagen rats is associated with the loss of preneoplastic lesions. Carcinogenesis 1999;20:221-227.

104. Harris, R. J. and Henderson, I. C. Staging and prognostic factors. Breast Diseases, 2nd Eddition , 327-346. 1987. Philadelphia, Lippincott.

105. Leygue E, Snell L, Hiller T, Dotzlaw H, Hole K, Murphy LC, Watson PH. Differential expression of psoriasin messenger RNA between in situ and invasive human breast carcinoma. Cancer Res 1996;56:4606-4609.

106. Al Haddad S, Zhang Z, Leygue E, Snell L, Huang A, Niu Y, Hiller-Hitchcock T, Hole K, Murphy LC, Watson PH. Psoriasin (S100A7) expression and invasive breast cancer. Am J Pathol 1999;155:2057-2066.

107. Moog-Lutz C, Bouillet P, Regnier CH, Tomasetto C, Mattei MG, Chenard MP, Anglard P, Rio MC, Basset P. Comparative expression of the psoriasin (S100A7) and S100C genes in breast carcinoma and co-localization to human chromosome 1q21-q22. Int J Cancer 1995;63:297-303.

108. Wulfkuhle JD, Sgroi DC, Krutzsch H, McLean K, McGarvey K, Knowlton M, Chen S, Shu H, Sahin A, Kurek R, Wallwiener D, Merino MJ, Petricoin EF, III, Zhao Y, Steeg PS. Proteomics of human breast ductal carcinoma in situ. Cancer Res 2002;62:6740-6749.

109. Shoker BS, Jarvis C, Clarke RB, Anderson E, Hewlett J, Davies MP, Sibson DR, Sloane JP. Estrogen receptor-positive proliferating cells in the normal and precancerous breast. Am J Pathol 1999;155:1811-1815.

110. Shoker BS, Jarvis C, Sibson DR, Walker C, Sloane JP. Oestrogen receptor expression in the normal and pre-cancerous breast. J Pathol 1999;188:237-244.

111. Allred DC, Clark GM, Molina R, Tandon AK, Schnitt SJ, Gilchrist KW, Osborne CK, Tormey DC, McGuire WL. Overexpression of HER-2/neu and its relationship with other prognostic factors change during the progression of in situ to invasive breast cancer. Hum Pathol 1992;23:974-979.

112. Rudas M, Neumayer R, Gnant MF, Mittelbock M, Jakesz R, Reiner A. p53 protein expression, cell proliferation and steroid hormone receptors in ductal and lobular in situ carcinomas of the breast. Eur J Cancer 1997;33:39-44.

113. Smith HS, Lu Y, Deng G, Martinez O, Krams S, Ljung BM, Thor A, Lagios M. Molecular aspects of early stages of breast cancer progression. J Cell Biochem Suppl 1993;17G:144-152.

114. Zhang D, Salto-Tellez M, Putti TC, Do E, Koay ES. Reliability of tissue microarrays in detecting protein expression and gene amplification in breast cancer. Mod Pathol 2003;16:79-84.

115. Zhang DH, Salto-Tellez M, Chiu LL, Shen L, Koay ES. Tissue microarray study for classification of breast tumors. Life Sci 2003;73:3189-3199.

116. Jeffrey SS, Pollack JR. The diagnosis and management of pre-invasive breast disease: promise of new technologies in understanding pre-invasive breast lesions. Breast Cancer Res 2003;5:320-328.

117. Lampejo OT, Barnes DM, Smith P, Millis RR. Evaluation of infiltrating ductal carcinomas with a DCIS component: correlation of the histologic type of the in situ component with grade of the infiltrating component. Semin Diagn Pathol 1994;11:215-222.

118. Warnberg F, Nordgren H, Bergkvist L, Holmberg L. Tumour markers in breast carcinoma correlate with grade rather than with invasiveness. Br J Cancer 2001;85:869-874.

119. Buerger H, Otterbach F, Simon R, Schafer KL, Poremba C, Diallo R, Brinkschmidt C, Dockhorn-Dworniczak B, Boecker W. Different genetic pathways in the evolution of invasive breast cancer are associated with distinct morphological subtypes. J Pathol 1999;189:521-526.

120. Radford DM, Phillips NJ, Fair KL, Ritter JH, Holt M, Donis-Keller H. Allelic loss and the progression of breast cancer. Cancer Res 1995;55:5180-5183.

121. Stratton MR, Collins N, Lakhani SR, Sloane JP. Loss of heterozygosity in ductal carcinoma in situ of the breast. J Pathol 1995;175:195-201.

122. O'Connell P, Pekkel V, Fuqua SA, Osborne CK, Clark GM, Allred DC. Analysis of loss of heterozygosity in 399 premalignant breast lesions at 15 genetic loci. J Natl Cancer Inst 1998;90:697-703.

123. Aubele MM, Cummings MC, Mattis AE, Zitzelsberger HF, Walch AK, Kremer M, Hofler H, Werner M. Accumulation of chromosomal imbalances from intraductal proliferative lesions to adjacent in situ and invasive ductal breast cancer. Diagn Mol Pathol 2000;9:14-19.

124. Tsuda H, Fukutomi T, Hirohashi S. Pattern of gene alterations in intraductal breast neoplasms associated with histological type and grade. Clin Cancer Res 1995;1:261-267.

125. Buerger H, Otterbach F, Simon R, Poremba C, Diallo R, Decker T, Riethdorf L, Brinkschmidt C, Dockhorn-Dworniczak B, Boecker W. Comparative genomic hybridization of ductal carcinoma in situ of the breast-evidence of multiple genetic pathways. J Pathol 1999;187:396-402.

126. Murphy DS, Hoare SF, Going JJ, Mallon EE, George WD, Kaye SB, Brown R, Black DM, Keith WN. Characterization of extensive genetic alterations in ductal carcinoma in situ by fluorescence in situ hybridization and molecular analysis. J Natl Cancer Inst 1995;87:1694-1704.

127. Porter DA, Krop IE, Nasser S, Sgroi D, Kaelin CM, Marks JR, Riggins G, Polyak K. A SAGE (serial analysis of gene expression) view of breast tumor progression. Cancer Res 2001;61:5697-5702.

128. Porter D, Lahti-Domenici J, Keshaviah A, Bae YK, Argani P, Marks J, Richardson A, Cooper A, Strausberg R, Riggins GJ, Schnitt S, Gabrielson E, Gelman R, Polyak K. Molecular markers in ductal carcinoma in situ of the breast. Mol Cancer Res 2003;1:362-375.

129. Ma XJ, Salunga R, Tuggle JT, Gaudet J, Enright E, McQuary P, Payette T, Pistone M, Stecker K, Zhang BM, Zhou YX, Varnholt H, Smith B, Gadd M, Chatfield E, Kessler J, Baer TM, Erlander MG, Sgroi DC. Gene expression profiles of human breast cancer progression. Proc Natl Acad Sci U S A 2003;100:5974-5979.

130. Adeyinka A, Emberley E, Niu Y, Snell L, Murphy LC, Sowter H, Wykoff CC, Harris AL, Watson PH. Analysis of gene expression in ductal carcinoma in situ of the breast. Clin Cancer Res 2002;8:3788-3795.

131. Seth A, Kitching R, Landberg G, Xu J, Zubovits J, Burger AM. Gene expression profiling of ductal carcinomas in situ and invasive breast tumors. Anticancer Res 2003;23:2043-2051.

132. Menard S, Casalini P, Tomasic G, Pilotti S, Cascinelli N, Bufalino R, Perrone F, Longhi C, Rilke F, Colnaghi MI. Pathobiologic identification of two distinct breast carcinoma subsets with diverging clinical behaviors. Breast Cancer Res Treat 1999;55:169-177.

133. Perin T, Canzonieri V, Massarut S, Bidoli E, Rossi C, Roncadin M, Carbone A. Immunohistochemical evaluation of multiple biological markers in ductal carcinoma in situ of the breast. Eur J Cancer 1996;32A:1148-1155.

134. Zafrani B, Leroyer A, Fourquet A, Laurent M, Trophilme D, Validire P, Sastre-Garau X. Mammographically-detected ductal in situ carcinoma of the breast analyzed with a new classification. A study of 127 cases: correlation with estrogen and progesterone receptors, p53 and c-erbB-2 proteins, and proliferative activity. Semin Diagn Pathol 1994;11:208-214.

135. Donato R. Functional roles of S100 proteins, calcium-binding proteins of the EF-hand type. Biochim Biophys Acta 1999;1450:191-231.

136. Donato R. S100: a multigenic family of calcium-modulated proteins of the EF-hand type with intracellular and extracellular functional roles. Int J Biochem Cell Biol 2001;33:637-668.

137. Schafer BW, Heizmann CW. The S100 family of EF-hand calcium-binding proteins: functions and pathology. Trends Biochem Sci 1996;21:134-140.

138. Zimmer DB, Cornwall EH, Landar A, Song W. The S100 protein family: history, function, and expression. Brain Res Bull 1995;37:417-429.

139. Heizmann CW, Fritz G, Schafer BW. S100 proteins: structure, functions and pathology. Front Biosci 2002;7:d1356-d1368.

140. Most P, Boerries M, Eicher C, Schweda C, Ehlermann P, Pleger ST, Loeffler E, Koch WJ, Katus HA, Schoenenberger CA, Remppis A. Extracellular S100A1 protein inhibits apoptosis in ventricular cardiomyocytes via activation of the extracellular signal-regulated protein kinase 1/2 (ERK1/2). J Biol Chem 2003;278:48404-48412.

141. Marenholz I, Heizmann CW, Fritz G. S100 proteins in mouse and man: from evolution to function and pathology (including an update of the nomenclature). Biochem Biophys Res Commun 2004;322:1111-1122.

142. Donato R. Intracellular and extracellular roles of S100 proteins. Microsc Res Tech 2003;60:540-551.

143. Boni R, Burg G, Doguoglu A, Ilg EC, Schafer BW, Muller B, Heizmann CW. Immunohistochemical localization of the Ca2+ binding S100 proteins in normal human skin and melanocytic lesions. Br J Dermatol 1997;137:39-43.

144. Camby I, Nagy N, Lopes MB, Schafer BW, Maurage CA, Ruchoux MM, Murmann P, Pochet R, Heizmann CW, Brotchi J, Salmon I, Kiss R, Decaestecker C. Supratentorial pilocytic astrocytomas, astrocytomas, anaplastic astrocytomas and glioblastomas are characterized by a differential expression of S100 proteins. Brain Pathol 1999;9:1-19.

145. Davey GE, Murmann P, Heizmann CW. Intracellular Ca2+ and Zn2+ levels regulate the alternative cell density-dependent secretion of S100B in human glioblastoma cells. J Biol Chem 2001;276:30819-30826.

146. Hamberg AP, Korse CM, Bonfrer JM, de Gast GC. Serum S100B is suitable for prediction and monitoring of response to chemoimmunotherapy in metastatic malignant melanoma. Melanoma Res 2003;13:45-49.

147. Bianchi R, Pula G, Ceccarelli P, Giambanco I, Donato R. S-100 protein binds to annexin II and p11, the heavy and light chains of calpactin I. Biochim Biophys Acta 1992;1160:67-75.

148. Baudier J, Delphin C, Grunwald D, Khochbin S, Lawrence JJ. Characterization of the tumor suppressor protein p53 as a protein kinase C substrate and a S100b-binding protein. Proc Natl Acad Sci U S A 1992;89:11627-11631.

149. Lin J, Blake M, Tang C, Zimmer D, Rustandi RR, Weber DJ, Carrier F. Inhibition of p53 transcriptional activity by the S100B calcium-binding protein. J Biol Chem 2001;276:35037-35041.

150. Scotto C, Deloulme JC, Rousseau D, Chambaz E, Baudier J. Calcium and S100B regulation of p53-dependent cell growth arrest and apoptosis. Mol Cell Biol 1998;18:4272-4281.

151. Sorci G, Riuzzi F, Agneletti AL, Marchetti C, Donato R. S100B causes apoptosis in a myoblast cell line in a RAGE-independent manner. J Cell Physiol 2004;199:274-283.

152. Millward TA, Heizmann CW, Schafer BW, Hemmings BA. Calcium regulation of Ndr protein kinase mediated by S100 calcium-binding proteins. EMBO J 1998;17:5913-5922.

153. Huttunen HJ, Kuja-Panula J, Sorci G, Agneletti AL, Donato R, Rauvala H. Coregulation of neurite outgrowth and cell survival by amphoterin and S100 proteins through receptor for advanced glycation end products (RAGE) activation. J Biol Chem 2000;275:40096-40105.

154. Ilg EC, Schafer BW, Heizmann CW. Expression pattern of S100 calcium-binding proteins in human tumors. Int J Cancer 1996;68:325-332.

155. Gupta S, Hussain T, MacLennan GT, Fu P, Patel J, Mukhtar H. Differential expression of S100A2 and S100A4 during progression of human prostate adenocarcinoma. J Clin Oncol 2003;21:106-112.

156. Feng G, Xu X, Youssef EM, Lotan R. Diminished expression of S100A2, a putative tumor suppressor, at early stage of human lung carcinogenesis. Cancer Res 2001;61:7999-8004.

157. Wicki R, Franz C, Scholl FA, Heizmann CW, Schafer BW. Repression of the candidate tumor suppressor gene S100A2 in breast cancer is mediated by site-specific hypermethylation. Cell Calcium 1997;22:243-254.

158. Nagy N, Brenner C, Markadieu N, Chaboteaux C, Camby I, Schafer BW, Pochet R, Heizmann CW, Salmon I, Kiss R, Decaestecker C. S100A2, a putative tumor suppressor gene, regulates in vitro squamous cell carcinoma migration. Lab Invest 2001;81:599-612.

159. Barraclough R, Kimbell R, Rudland PS. Increased abundance of a normal cell mRNA sequence accompanies the conversion of rat mammary cuboidal epithelial cells to elongated myoepithelial-like cells in culture. Nucleic Acids Res 1984;12:8097-8114.

160. Davies BR, Davies MP, Gibbs FE, Barraclough R, Rudland PS. Induction of the metastatic phenotype by transfection of a benign rat mammary epithelial cell line with the gene for p9Ka, a rat calcium-binding protein, but not with the oncogene EJ-ras-1. Oncogene 1993;8:999-1008.

161. Grigorian M, Ambartsumian N, Lykkesfeldt AE, Bastholm L, Elling F, Georgiev G, Lukanidin E. Effect of mts1 (S100A4) expression on the progression of human breast cancer cells. Int J Cancer 1996;67:831-841.

162. Nikitenko LL, Lloyd BH, Rudland PS, Fear S, Barraclough R. Localisation by in situ hybridisation of S100A4 (p9Ka) mRNA in primary human breast tumour specimens. Int J Cancer 2000;86:219-228.

163. Takenaga K, Nakanishi H, Wada K, Suzuki M, Matsuzaki O, Matsuura A, Endo H. Increased expression of S100A4, a metastasis-associated gene, in human colorectal adenocarcinomas. Clin Cancer Res 1997;3:2309-2316.

164. Yonemura Y, Endou Y, Kimura K, Fushida S, Bandou E, Taniguchi K, Kinoshita K, Ninomiya I, Sugiyama K, Heizmann CW, Schafer BW, Sasaki T. Inverse expression of S100A4 and E-cadherin is associated with metastatic potential in gastric cancer. Clin Cancer Res 2000;6:4234-4242.

165. Hernan R, Fasheh R, Calabrese C, Frank AJ, Maclean KH, Allard D, Barraclough R, Gilbertson RJ. ERBB2 up-regulates S100A4 and several other prometastatic genes in medulloblastoma. Cancer Res 2003;63:140-148.

166. Davies BR, O'Donnell M, Durkan GC, Rudland PS, Barraclough R, Neal DE, Mellon JK. Expression of S100A4 protein is associated with metastasis and reduced survival in human bladder cancer. J Pathol 2002;196:292-299.

167. Davies MP, Rudland PS, Robertson L, Parry EW, Jolicoeur P, Barraclough R. Expression of the calcium-binding protein S100A4 (p9Ka) in MMTV-neu transgenic mice induces metastasis of mammary tumours. Oncogene 1996;13:1631-1637.

168. Takenaga K, Nakamura Y, Sakiyama S. Expression of antisense RNA to S100A4 gene encoding an S100-related calcium-binding protein suppresses metastatic potential of high-metastatic Lewis lung carcinoma cells. Oncogene 1997;14:331-337.

169. Mandinova A, Atar D, Schafer BW, Spiess M, Aebi U, Heizmann CW. Distinct subcellular localization of calcium binding S100 proteins in human smooth muscle cells and their relocation in response to rises in intracellular calcium. J Cell Sci 1998;111 (Pt 14):2043-2054.

170. Kriajevska M, Tarabykina S, Bronstein I, Maitland N, Lomonosov M, Hansen K, Georgiev G, Lukanidin E. Metastasis-associated Mts1 (S100A4) protein modulates protein kinase C phosphorylation of the heavy chain of nonmuscle myosin. J Biol Chem 1998;273:9852-9856.

171. Takenaga K, Nakamura Y, Sakiyama S, Hasegawa Y, Sato K, Endo H. Binding of pEL98 protein, an S100-related calcium-binding protein, to nonmuscle tropomyosin. J Cell Biol 1994;124:757-768.

172. Lakshmi MS, Parker C, Sherbet GV. Metastasis associated MTS1 and NM23 genes affect tubulin polymerisation in B16 melanomas: a possible mechanism of their regulation of metastatic behaviour of tumours. Anticancer Res 1993;13:299-303.

173. Grigorian M, Andresen S, Tulchinsky E, Kriajevska M, Carlberg C, Kruse C, Cohn M, Ambartsumian N, Christensen A, Selivanova G, Lukanidin E. Tumor suppressor p53 protein is a new target for the metastasis-associated Mts1/S100A4 protein: functional consequences of their interaction. J Biol Chem 2001;276:22699-22708.

174. Chen H, Fernig DG, Rudland PS, Sparks A, Wilkinson MC, Barraclough R. Binding to intracellular targets of the metastasis-inducing protein, S100A4 (p9Ka). Biochem Biophys Res Commun 2001;286:1212-1217.

175. Tonini GP, Casalaro A, Cara A, Di Martino D. Inducible expression of calcyclin, a gene with strong homology to S-100 protein, during neuroblastoma cell differentiation and its prevalent expression in Schwann-like cell lines. Cancer Res 1991;51:1733-1737.

176. Breen EC, Tang K. Calcyclin (S100A6) regulates pulmonary fibroblast proliferation, morphology, and cytoskeletal organization in vitro. J Cell Biochem 2003;88:848-854.

177. Niki I, Okazaki K, Iino S, Kobayashi S, Hidaka H. Calcyclin, a calcium-binding protein, which regulates insulin secretion from the permeabilized pancreatic beta-cell. Adv Exp Med Biol 1997;426:85-89.

178. Komatsu K, Andoh A, Ishiguro S, Suzuki N, Hunai H, Kobune-Fujiwara Y, Kameyama M, Miyoshi J, Akedo H, Nakamura H. Increased expression of S100A6 (Calcyclin), a calcium-binding protein of the S100 family, in human colorectal adenocarcinomas. Clin Cancer Res 2000;6:172-177.

179. Kim J, Kim J, Yoon S, Joo J, Lee Y, Lee K, Chung J, Choe I. S100A6 protein as a marker for differential diagnosis of cholangiocarcinoma from hepatocellular carcinoma. Hepatol Res 2002;23:274.

180. Maelandsmo GM, Florenes VA, Mellingsaeter T, Hovig E, Kerbel RS, Fodstad O. Differential expression patterns of S100A2, S100A4 and S100A6 during progression of human malignant melanoma. Int J Cancer 1997;74:464-469.

181. Golitsina NL, Kordowska J, Wang CL, Lehrer SS. Ca2+-dependent binding of calcyclin to muscle tropomyosin. Biochem Biophys Res Commun 1996;220:360-365.

182. Filipek A, Wojda U, Lesniak W. Interaction of calcyclin and its cyanogen bromide fragments with annexin II and glyceraldehyde 3-phosphate dehydrogenase. Int J Biochem Cell Biol 1995;27:1123-1131.

183. Sudo T, Hidaka H. Regulation of calcyclin (S100A6) binding by alternative splicing in the N-terminal regulatory domain of annexin XI isoforms. J Biol Chem 1998;273:6351-6357.

184. Mani RS, McCubbin WD, Kay CM. Calcium-dependent regulation of caldesmon by an 11-kDa smooth muscle calcium-binding protein, caltropin. Biochemistry 1992;31:11896-11901.

185. Brodersen DE, Etzerodt M, Madsen P, Celis JE, Thogersen HC, Nyborg J, Kjeldgaard M. EF-hands at atomic resolution: the structure of human psoriasin (S100A7) solved by MAD phasing. Structure 1998;6:477-489.

186. Kulski JK, Lim CP, Dunn DS, Bellgard M. Genomic and phylogenetic analysis of the S100A7 (Psoriasin) gene duplications within the region of the S100 gene cluster on human chromosome 1q21. J Mol Evol 2003;56:397-406.

187. Madsen P, Rasmussen HH, Leffers H, Honore B, Dejgaard K, Olsen E, Kiil J, Walbum E, Andersen AH, Basse B, . Molecular cloning, occurrence, and expression of a novel partially secreted protein "psoriasin" that is highly up-regulated in psoriatic skin. J Invest Dermatol 1991;97:701-712.

188. Jinquan T, Vorum H, Larsen CG, Madsen P, Rasmussen HH, Gesser B, Etzerodt M, Honore B, Celis JE, Thestrup-Pedersen K. Psoriasin: a novel chemotactic protein. J Invest Dermatol 1996;107:5-10.

189. Hofmann MA, Drury S, Fu C, Qu W, Taguchi A, Lu Y, Avila C, Kambham N, Bierhaus A, Nawroth P, Neurath MF, Slattery T, Beach D, McClary J, Nagashima M, Morser J, Stern D, Schmidt AM. RAGE mediates a novel proinflammatory axis: a central cell surface receptor for S100/calgranulin polypeptides. Cell 1999;97:889-901.

190. Taguchi A, Blood DC, del Toro G, Canet A, Lee DC, Qu W, Tanji N, Lu Y, Lalla E, Fu C, Hofmann MA, Kislinger T, Ingram M, Lu A, Tanaka H, Hori O, Ogawa S, Stern DM, Schmidt AM. Blockade of RAGE-amphoterin signalling suppresses tumour growth and metastases. Nature 2000;405:354-360.

191. Hsieh HL, Schafer BW, Sasaki N, Heizmann CW. Expression analysis of S100 proteins and RAGE in human tumors using tissue microarrays. Biochem Biophys Res Commun 2003;307:375-381.

192. Webb M, Emberley ED, Lizardo M, Alowami S, Qing G, Alfia'ar A, Snell-Curtis LJ, Niu Y, Civetta A, Myal Y, Shiu R, Murphy LC, Watson PH. Expression analysis of the mouse S100A7/psoriasin gene in skin inflammation and mammary tumorigenesis. BMC Cancer 2005;5:17.

193. Celis JE, Rasmussen HH, Vorum H, Madsen P, Honore B, Wolf H, Orntoft TF. Bladder squamous cell carcinomas express psoriasin and externalize it to the urine. J Urol 1996;155:2105-2112.

194. Alowami S, Qing G, Emberley E, Snell L, Watson PH. Psoriasin (S100A7) expression is altered during skin tumorigenesis. BMC Dermatol 2003;3:1.

195. El Rifai W, Moskaluk CA, Abdrabbo MK, Harper J, Yoshida C, Riggins GJ, Frierson HF, Jr., Powell SM. Gastric cancers overexpress S100A calcium-binding proteins. Cancer Res 2002;62:6823-6826.

196. Enerback C, Porter DA, Seth P, Sgroi D, Gaudet J, Weremowicz S, Morton CC, Schnitt S, Pitts RL, Stampl J, Barnhart K, Polyak K. Psoriasin expression in mammary epithelial cells in vitro and in vivo. Cancer Res 2002;62:43-47.

197. Tavakkol A, Zouboulis CC, Duell EA, Voorhees JJ. A retinoic acid-inducible skin-specific gene (RIS-1/psoriasin): molecular cloning and analysis of gene expression in human skin in vivo and cultured skin cells in vitro. Mol Biol Rep 1994;20:75-83.

198. Emberley ED, Niu Y, Njue C, Kliewer EV, Murphy LC, Watson PH. Psoriasin (S100A7) expression is associated with poor outcome in estrogen receptor-negative invasive breast cancer. Clin Cancer Res 2003;9:2627-2631.

199. Ruse M, Lambert A, Robinson N, Ryan D, Shon KJ, Eckert RL. S100A7, S100A10, and S100A11 are transglutaminase substrates. Biochemistry 2001;40:3167-3173.

200. Hagens G, Masouye I, Augsburger E, Hotz R, Saurat JH, Siegenthaler G. Calcium-binding protein S100A7 and epidermal-type fatty acid-binding protein are associated in the cytosol of human keratinocytes. Biochem J 1999;339 (Pt 2):419-427.

201. Mandal, M., Jasser, S., Yigitbasi, O., Patel, V., Gutkind, S., Wang, J., Coombes, K., Emberley, E., Watson, P. H., El-Naggar, A., Younes, M., Hittleman, W. N., and Myers, J. N. S100A7 (Psoriasin) mediates anoikis resistance and tumor progression in squamous cell carcinoma of the oral cavity. Proceedings of the AACR 45. 2004.

202. Emberley ED, Alowami S, Snell L, Murphy LC, Watson PH. S100A7 (psoriasin) expression is associated with aggressive features and alteration of Jab1 in ductal carcinoma *in situ* of the breast. Breast Cancer Research 2004;6:R308-R315.

203. Gaki V, Tsopanomichalou M, Sourvinos G, Tsiftsis D, Spandidos DA. Allelic loss in chromosomal region 1q21-23 in breast cancer is associated with peritumoral angiolymphatic invasion and extensive intraductal component. Eur J Surg Oncol 2000;26:455-460.

204. Semprini S, Capon F, Bovolenta S, Bruscia E, Pizzuti A, Fabrizi G, Schietroma C, Zambruno G, Dallapiccola B, Novelli G. Genomic structure, promoter characterisation and mutational analysis of the S100A7 gene: exclusion of a candidate for familial psoriasis susceptibility. Hum Genet 1999;104:130-134.

205. Claret FX, Hibi M, Dhut S, Toda T, Karin M. A new group of conserved coactivators that increase the specificity of AP-1 transcription factors. Nature 1996;383:453-457.

206. Chamovitz DA, Segal D. JAB1/CSN5 and the COP9 signalosome. A complex situation. EMBO Rep 2001;2:96-101.

207. Chamovitz DA, Glickman M. The COP9 signalosome. Curr Biol 2002;12:R232.

208. Seeger M, Kraft R, Ferrell K, Bech-Otschir D, Dumdey R, Schade R, Gordon C, Naumann M, Dubiel W. A novel protein complex involved in signal transduction possessing similarities to 26S proteasome subunits. FASEB J 1998;12:469-478.

209. Wei N, Tsuge T, Serino G, Dohmae N, Takio K, Matsui M, Deng XW. The COP9 complex is conserved between plants and mammals and is related to the 26S proteasome regulatory complex. Curr Biol 1998;8:919-922.

210. Schwechheimer C, Deng XW. COP9 signalosome revisited: a novel mediator of protein degradation. Trends Cell Biol 2001;11:420-426.

211. Bianchi E, Denti S, Granata A, Bossi G, Geginat J, Villa A, Rogge L, Pardi R. Integrin LFA-1 interacts with the transcriptional co-activator JAB1 to modulate AP-1 activity. Nature 2000;404:617-621.

212. Yang HY, Zhou BP, Hung MC, Lee MH. Oncogenic signals of HER-2/neu in regulating the stability of the cyclin-dependent kinase inhibitor p27. J Biol Chem 2000;275:24735-24739.

213. Lu C, Li Y, Zhao Y, Xing G, Tang F, Wang Q, Sun Y, Wei H, Yang X, Wu C, Chen J, Guan KL, Zhang C, Chen H, He F. Intracrine hepatopoietin potentiates AP-1 activity through JAB1 independent of MAPK pathway. FASEB J 2002;16:90-92.

214. Naumann M, Bech-Otschir D, Huang X, Ferrell K, Dubiel W. COP9 signalosome-directed c-Jun activation/stabilization is independent of JNK. J Biol Chem 1999;274:35297-35300.

215. Bae MK, Ahn MY, Jeong JW, Bae MH, Lee YM, Bae SK, Park JW, Kim KR, Kim KW. Jab1 interacts directly with HIF-1alpha and regulates its stability. J Biol Chem 2002;277:9-12.

216. Chauchereau A, Georgiakaki M, Perrin-Wolff M, Milgrom E, Loosfelt H. JAB1 interacts with both the progesterone receptor and SRC-1. J Biol Chem 2000;275:8540-8548.

217. Tomoda K, Kubota Y, Arata Y, Mori S, Maeda M, Tanaka T, Yoshida M, Yoneda-Kato N, Kato JY. The cytoplasmic shuttling and subsequent degradation of p27Kip1 mediated by Jab1/CSN5 and the COP9 signalosome complex. J Biol Chem 2002;277:2302-2310.

218. Tomoda K, Kubota Y, Kato J. Degradation of the cyclin-dependent-kinase inhibitor p27Kip1 is instigated by Jab1. Nature 1999;398:160-165.

219. Wan M, Cao X, Wu Y, Bai S, Wu L, Shi X, Wang N, Cao X. Jab1 antagonizes TGF-beta signaling by inducing Smad4 degradation. EMBO Rep 2002;3:171-176.

220. Bech-Otschir D, Kraft R, Huang X, Henklein P, Kapelari B, Pollmann C, Dubiel W. COP9 signalosome-specific phosphorylation targets p53 to degradation by the ubiquitin system. EMBO J 2001;20:1630-1639.

221. Nordgard O, Dahle O, Andersen TO, Gabrielsen OS. JAB1/CSN5 interacts with the GAL4 DNA binding domain: a note of caution about two-hybrid interactions. Biochimie 2001;83:969-971.

222. Shaulian E, Karin M. AP-1 in cell proliferation and survival. Oncogene 2001;20:2390-2400.

223. Ozanne BW, McGarry L, Spence HJ, Johnston I, Winnie J, Meagher L, Stapleton G. Transcriptional regulation of cell invasion: AP-1 regulation of a multigenic invasion programme. Eur J Cancer 2000;36:1640-1648.

224. Simon C, Simon M, Vucelic G, Hicks MJ, Plinkert PK, Koitschev A, Zenner HP. The p38 SAPK pathway regulates the expression of the MMP-9 collagenase via AP-1-dependent promoter activation. Exp Cell Res 2001;271:344-355.

225. Smith LM, Wise SC, Hendricks DT, Sabichi AL, Bos T, Reddy P, Brown PH, Birrer MJ. cJun overexpression in MCF-7 breast cancer cells produces a tumorigenic, invasive and hormone resistant phenotype. Oncogene 1999;18:6063-6070.

226. Dickson RB, Lippman ME. Molecular determinants of growth, angiogenesis, and metastases in breast cancer. Semin Oncol 1992;19:286-298.

227. Wykoff CC, Pugh CW, Maxwell PH, Harris AL, Ratcliffe PJ. Identification of novel hypoxia dependent and independent target genes of the von Hippel-Lindau (VHL) tumour suppressor by mRNA differential expression profiling. Oncogene 2000;19:6297-6305.

228. Blancher C, Moore JW, Talks KL, Houlbrook S, Harris AL. Relationship of hypoxia-inducible factor (HIF)-1alpha and HIF-2alpha expression to vascular endothelial growth factor induction and hypoxia survival in human breast cancer cell lines. Cancer Res 2000;60:7106-7113.

229. Stetler-Stevenson WG, Yu AE. Proteases in invasion: matrix metalloproteinases. Semin Cancer Biol 2001;11:143-152.

230. Kelloff GJ, Crowell JA, Steele VE, Lubet RA, Malone WA, Boone CW, Kopelovich L, Hawk ET, Lieberman R, Lawrence JA, Ali I, Viner JL, Sigman CC. Progress in cancer chemoprevention: development of diet-derived chemopreventive agents. J Nutr 2000;130:467S-471S.

231. Pollmann C, Huang X, Mall J, Bech-Otschir D, Naumann M, Dubiel W. The constitutive photomorphogenesis 9 signalosome directs vascular endothelial growth factor production in tumor cells. Cancer Res 2001;61:8416-8421.

232. Mukhopadhyay A, Bueso-Ramos C, Chatterjee D, Pantazis P, Aggarwal BB. Curcumin downregulates cell survival mechanisms in human prostate cancer cell lines. Oncogene 2001;20:7597-7609.

233. Chen YR, Tan TH. Inhibition of the c-Jun N-terminal kinase (JNK) signaling pathway by curcumin. Oncogene 1998;17:173-178.

234. Hong RL, Spohn WH, Hung MC. Curcumin inhibits tyrosine kinase activity of p185neu and also depletes p185neu. Clin Cancer Res 1999;5:1884-1891.

235. Shao ZM, Shen ZZ, Liu CH, Sartippour MR, Go VL, Heber D, Nguyen M. Curcumin exerts multiple suppressive effects on human breast carcinoma cells. Int J Cancer 2002;98:234-240.

236. Verma SP, Salamone E, Goldin B. Curcumin and genistein, plant natural products, show synergistic inhibitory effects on the growth of human breast cancer MCF-7 cells induced by estrogenic pesticides. Biochem Biophys Res Commun 1997;233:692-696.

237. Kim MS, Kang HJ, Moon A. Inhibition of invasion and induction of apoptosis by curcumin in H-ras-transformed MCF10A human breast epithelial cells. Arch Pharm Res 2001;24:349-354.

238. Kleemann R, Hausser A, Geiger G, Mischke R, Burger-Kentischer A, Flieger O, Johannes FJ, Roger T, Calandra T, Kapurniotu A, Grell M, Finkelmeier D, Brunner H, Bernhagen J. Intracellular action of the cytokine MIF to modulate AP-1 activity and the cell cycle through Jab1. Nature 2000;408:211-216.

239. Emberley ED, Niu Y, Leygue E, Tomes L, Gietz RD, Murphy LC, Watson PH. Psoriasin interacts with Jab1 and influences breast cancer progression. Cancer Res 2003;63:1954-1961.

240. Sui L, Dong Y, Ohno M, Watanabe Y, Sugimoto K, Tai Y, Tokuda M. Jab1 expression is associated with inverse expression of p27(kip1) and poor prognosis in epithelial ovarian tumors. Clin Cancer Res 2001;7:4130-4135.

241. Gemmill RM, Bemis LT, Lee JP, Sozen MA, Baron A, Zeng C, Erickson PF, Hooper JE, Drabkin HA. The TRC8 hereditary kidney cancer gene suppresses growth and functions with VHL in a common pathway. Oncogene 2002;21:3507-3516.

242. Korbonits M, Chahal HS, Kaltsas G, Jordan S, Urmanova Y, Khalimova Z, Harris PE, Farrell WE, Claret FX, Grossman AB. Expression of phosphorylated p27(Kip1) protein and Jun activation domain-binding protein 1 in human pituitary tumors. J Clin Endocrinol Metab 2002;87:2635-2643.

243. Esteva FJ, Sahin AA, Rassidakis GZ, Yuan LX, Smith TL, Yang Y, Gilcrease MZ, Cristofanilli M, Nahta R, Pusztai L, Claret FX. Jun activation domain binding protein 1 expression is associated with low p27(Kip1)levels in node-negative breast cancer. Clin Cancer Res 2003;9:5652-5659.

244. Kouvaraki MA, Rassidakis GZ, Tian L, Kumar R, Kittas C, Claret FX. Jun activation domain-binding protein 1 expression in breast cancer inversely correlates with the cell cycle inhibitor p27(Kip1). Cancer Res 2003;63:2977-2981.

245. Done SJ, Arneson CR, Ozcelik H, Redston M, Andrulis IL. P53 protein accumulation in non-invasive lesions surrounding p53 mutation positive invasive breast cancers. Breast Cancer Res Treat 2001;65:111-118.

246. Kang JH, Kim SJ, Noh DY, Choe KJ, Lee ES, Kang HS. The timing and characterization of p53 mutations in progression from atypical ductal hyperplasia to invasive lesions in the breast cancer. J Mol Med 2001;79:648-655.

247. Guy CT, Cardiff RD, Muller WJ. Activated neu induces rapid tumor progression. J Biol Chem 1996;271:7673-7678.

248. Wykoff CC, Beasley N, Watson PH, Campo L, Chia SK, English R, Pastorek J, Sly WS, Ratcliffe P, Harris AL. Expression of the hypoxia-inducible and tumor-associated carbonic anhydrases in ductal carcinoma in situ of the breast. Am J Pathol 2001;158:1011-1019.

249. Weaver VM, Fischer AH, Peterson OW, Bissell MJ. The importance of the microenvironment in breast cancer progression: recapitulation of mammary tumorigenesis using a unique human mammary epithelial cell model and a three-dimensional culture assay. Biochem Cell Biol 1996;74:833-851.

250. Shaw LM. Integrin function in breast carcinoma progression. J Mammary Gland Biol Neoplasia 1999;4:367-376.

251. Ignatoski KM, Maehama T, Markwart SM, Dixon JE, Livant DL, Ethier SP. ERBB-2 overexpression confers PI 3' kinase-dependent invasion capacity on human mammary epithelial cells. Br J Cancer 2000;82:666-674.

252. Gietz RD, Triggs-Raine B, Robbins A, Graham KC, Woods RA. Identification of proteins that interact with a protein of interest: applications of the yeast two-hybrid system. Mol Cell Biochem 1997;172:67-79.

253. Schagger H, Von Jagow G. Tricine-sodium dodecyl sulfate-polyacrylamide gel electrophoresis for the separation of proteins in the range from 1 to 100 kDa. Anal Biochem 1987;166:368-379.

254. Girvitz SC, Bacchetti S, Rainbow AJ, Graham FL. A rapid and efficient procedure for the purification of DNA from agarose gels. Anal Biochem 1980;106:492-496.

255. Dower WJ, Miller JF, Ragsdale CW. High efficiency transformation of E. coli by high voltage electroporation. Nucleic Acids Res 1988;16:6127-6145.

256. Gietz RD, Woods RA. Transformation of yeast by lithium acetate/single-stranded carrier DNA/polyethylene glycol method. Methods Enzymol 2002;350:87-96.

257. Morgenstern JP, Land H. A series of mammalian expression vectors and characterisation of their expression of a reporter gene in stably and transiently transfected cells. Nucleic Acids Res 1990;18:1068.

258. Watson PH, Snell L, Parisien M. The NCIC-Manitoba Breast Tumor Bank: a resource for applied cancer research. CMAJ 1996;155:281-283.

259. Shin I, Yakes FM, Rojo F, Shin NY, Bakin AV, Baselga J, Arteaga CL. PKB/Akt mediates cell-cycle progression by phosphorylation of p27(Kip1) at threonine 157 and modulation of its cellular localization. Nat Med 2002;8:1145-1152.

260. Shi W, Zhang X, Pintilie M, Ma N, Miller N, Banerjee D, Tsao MS, Mak T, Fyles A, Liu FF. Dysregulated PTEN-PKB and negative receptor status in human breast cancer. Int J Cancer 2003;104:195-203.

261. Emberley ED, Gietz RD, Campbell JD, HayGlass KT, Murphy LC, Watson PH. RanBPM interacts with psoriasin in vitro and their expression correlates with specific clinical features in vivo in breast cancer. BMC Cancer 2002;2:28.

262. Nolsoe S. Crystallization and preliminary X-ray diffraction studies of psoriasin. Acta Crystallogr D Biol Crystallogr 1997;53:119-121.

263. Pedrocchi M, Schafer BW, Mueller H, Eppenberger U, Heizmann CW. Expression of Ca(2+)-binding proteins of the S100 family in malignant human breast-cancer cell lines and biopsy samples. Int J Cancer 1994;57:684-690.

264. Kolch W, Martiny-Baron G, Kieser A, Marme D. Regulation of the expression of the VEGF/VPS and its receptors: role in tumor angiogenesis. Breast Cancer Res Treat 1995;36:139-155.

265. Pendas AM, Balbin M, Llano E, Jimenez MG, Lopez-Otin C. Structural analysis and promoter characterization of the human collagenase-3 gene (MMP13). Genomics 1997;40:222-233.

266. Quintero M, Mackenzie N, Brennan PA. Hypoxia-inducible factor 1 (HIF-1) in cancer. Eur J Surg Oncol 2004;30:465-468.

267. Wykoff CC, Beasley NJ, Watson PH, Turner KJ, Pastorek J, Sibtain A, Wilson GD, Turley H, Talks KL, Maxwell PH, Pugh CW, Ratcliffe PJ, Harris AL. Hypoxia-inducible expression of tumor-associated carbonic anhydrases. Cancer Res 2000;60:7075-7083.

268. Potter C, Harris AL. Hypoxia inducible carbonic anhydrase IX, marker of tumour hypoxia, survival pathway and therapy target. Cell Cycle 2004;3:164-167.

269. Potter CP, Harris AL. Diagnostic, prognostic and therapeutic implications of carbonic anhydrases in cancer. Br J Cancer 2003;89:2-7.

270. Kaluzova M, Pastorekova S, Svastova E, Pastorek J, Stanbridge EJ, Kaluz S. Characterization of the MN/CA 9 promoter proximal region: a role for specificity protein (SP) and activator protein 1 (AP1) factors. Biochem J 2001;359:669-677.

271. Laderoute KR, Calaoagan JM, Gustafson-Brown C, Knapp AM, Li GC, Mendonca HL, Ryan HE, Wang Z, Johnson RS. The response of c-jun/AP-1 to chronic hypoxia is hypoxia-inducible factor 1 alpha dependent. Mol Cell Biol 2002;22:2515-2523.

272. Ausserer WA, Bourrat-Floeck B, Green CJ, Laderoute KR, Sutherland RM. Regulation of c-jun expression during hypoxic and low-glucose stress. Mol Cell Biol 1994;14:5032-5042.

273. Michiels C, Minet E, Michel G, Mottet D, Piret JP, Raes M. HIF-1 and AP-1 cooperate to increase gene expression in hypoxia: role of MAP kinases. IUBMB Life 2001;52:49-53.

274. Khwaja A, Rodriguez-Viciana P, Wennstrom S, Warne PH, Downward J. Matrix adhesion and Ras transformation both activate a phosphoinositide 3-OH kinase and protein kinase B/Akt cellular survival pathway. EMBO J 1997;16:2783-2793.

275. Viglietto G, Motti ML, Bruni P, Melillo RM, D'Alessio A, Califano D, Vinci F, Chiappetta G, Tsichlis P, Bellacosa A, Fusco A, Santoro M. Cytoplasmic relocalization and inhibition of the cyclin-dependent kinase inhibitor p27(Kip1) by PKB/Akt-mediated phosphorylation in breast cancer. Nat Med 2002;8:1136-1144.

276. Karin M, Cao Y, Greten FR, Li ZW. NF-kappaB in cancer: from innocent bystander to major culprit. Nat Rev Cancer 2002;2:301-310.

277. Li G, Gustafson-Brown C, Hanks SK, Nason K, Arbeit JM, Pogliano K, Wisdom RM, Johnson RS. c-Jun is essential for organization of the epidermal leading edge. Dev Cell 2003;4:865-877.

278. Bantounas I, Phylactou LA, Uney JB. RNA interference and the use of small interfering RNA to study gene function in mammalian systems. J Mol Endocrinol 2004;33:545-557.

279. Campbell TN, Choy FY. RNA interference: past, present and future. Curr Issues Mol Biol 2005;7:1-6.

280. Silva J, Chang K, Hannon GJ, Rivas FV. RNA-interference-based functional genomics in mammalian cells: reverse genetics coming of age. Oncogene 2004;23:8401-8409.

281. Brummelkamp TR, Bernards R, Agami R. Stable suppression of tumorigenicity by virus-mediated RNA interference. Cancer Cell 2002;2:243-247.

282. Fata JE, Werb Z, Bissell MJ. Regulation of mammary gland branching morphogenesis by the extracellular matrix and its remodeling enzymes. Breast Cancer Res 2004;6:1-11.

283. Kim JB, Stein R, O'Hare MJ. Three-dimensional in vitro tissue culture models of breast cancer-- a review. Breast Cancer Res Treat 2004;85:281-291.

284. Streuli CH. Cell adhesion in mammary gland biology and neoplasia. J Mammary Gland Biol Neoplasia 2003;8:375-381.

285. Thompson EW, Reich R, Martin GR, Albini A. Factors regulating basement membrane invasion by tumor cells. Cancer Treat Res 1988;40:239-249.

286. Pilkington GJ, Bjerkvig R, De Ridder L, Kaaijk P. In vitro and in vivo models for the study of brain tumour invasion. Anticancer Res 1997;17:4107-4109.

287. Shaw LM. Tumor cell invasion assays. Methods Mol Biol 2004;294:97-106.

288. Venditti M, Iwasiow B, Orr FW, Shiu RP. C-myc gene expression alone is sufficient to confer resistance to antiestrogen in human breast cancer cells. Int J Cancer 2002;99:35-42.

289. Simon N, Noel A, Foidart JM. Evaluation of in vitro reconstituted basement membrane assay to assess the invasiveness of tumor cells. Invasion Metastasis 1992;12:156-167.

290. Malaney S, Daly RJ. The ras signaling pathway in mammary tumorigenesis and metastasis. J Mammary Gland Biol Neoplasia 2001;6:101-113.

291. Polyak K. Molecular alterations in ductal carcinoma in situ of the breast. Curr Opin Oncol 2002;14:92-96.

292. Fabian CJ. Breast cancer chemoprevention: beyond tamoxifen. Breast Cancer Res 2001;3:99-103.

293. Boland GP, Knox WF, Bundred NJ. Molecular markers and therapeutic targets in ductal carcinoma in situ. Microsc Res Tech 2002;59:3-11.

294. Muss HB. Role of adjuvant endocrine therapy in early-stage breast cancer. Semin Oncol 2001;28:313-321.

295. Putti TC, El Rehim DM, Rakha EA, Paish CE, Lee AH, Pinder SE, Ellis IO. Estrogen receptor-negative breast carcinomas: a review of morphology and immunophenotypical analysis. Mod Pathol 2004.

296. Williams MR, Todd JH, Ellis IO, Dowle CS, Haybittle JL, Elston CW, Nicholson RI, Griffiths K, Blamey RW. Oestrogen receptors in primary and advanced breast cancer: an eight year review of 704 cases. Br J Cancer 1987;55:67-73.

297. Hennighausen L, Wall RJ, Tillmann U, Li M, Furth PA. Conditional gene expression in secretory tissues and skin of transgenic mice using the MMTV-LTR and the tetracycline responsive system. J Cell Biochem 1995;59:463-472.

298. Eckert RL, Broome AM, Ruse M, Robinson N, Ryan D, Lee K. S100 proteins in the epidermis. J Invest Dermatol 2004;123:23-33.

299. Emberley, E. D., Curtis, L., Myers, J. N., Murphy, L. C., and Watson, P. H. Psoriasin (S100A7) stimulates pro-survival pathways through activation of Jab1 in breast cancer. Proceedings of the AACR 45. 4-1-2004.

300. Emberley ED, Murphy LC, Watson PH. S100 proteins and their influence on pro-survival pathways in cancer. Biochem Cell Biol 2004;82:508-515.

301. Emberley ED, Murphy LC, Watson PH. S100A7 and the progression of breast cancer. Breast Cancer Res 2004;6:153-159.

302. Di Nuzzo S, Sylva-Steenland RM, Koomen CW, de Rie MA, Das PK, Bos JD, Teunissen MB. Exposure to UVB induces accumulation of LFA-1+ T cells and enhanced expression of the chemokine psoriasin in normal human skin. Photochem Photobiol 2000;72:374-382.

303. Olsen E, Rasmussen HH, Celis JE. Identification of proteins that are abnormally regulated in differentiated cultured human keratinocytes. Electrophoresis 1995;16:2241-2248.

304. van Ruissen F, Jansen BJ, de Jongh GJ, Vlijmen-Willems IM, Schalkwijk J. Differential gene expression in premalignant human epidermis revealed by cluster analysis of serial analysis of gene expression (SAGE) libraries. FASEB J 2002;16:246-248.

305. Jones C, Mackay A, Grigoriadis A, Cossu A, Reis-Filho JS, Fulford L, Dexter T, Davies S, Bulmer K, Ford E, Parry S, Budroni M, Palmieri G, Neville AM, O'Hare MJ, Lakhani SR. Expression profiling of purified normal human luminal and myoepithelial breast cells: identification of novel prognostic markers for breast cancer. Cancer Res 2004;64:3037-3045.

306. Mackay AR, Ballin M, Pelina MD, Farina AR, Nason AM, Hartzler JL, Thorgeirsson UP. Effect of phorbol ester and cytokines on matrix metalloproteinase and tissue inhibitor of metalloproteinase expression in tumor and normal cell lines. Invasion Metastasis 1992;12:168-184.

307. Karpanen T, Egeblad M, Karkkainen MJ, Kubo H, Yla-Herttuala S, Jaattela M, Alitalo K. Vascular endothelial growth factor C promotes tumor lymphangiogenesis and intralymphatic tumor growth. Cancer Res 2001;61:1786-1790.

308. Alkarain A, Jordan R, Slingerland J. p27 deregulation in breast cancer: prognostic significance and implications for therapy. J Mammary Gland Biol Neoplasia 2004;9:67-80.

309. Alkarain A, Slingerland J. Deregulation of p27 by oncogenic signaling and its prognostic significance in breast cancer. Breast Cancer Res 2004;6:13-21.

310. Cariou S, Catzavelos C, Slingerland JM. Prognostic implications of expression of the cell cycle inhibitor protein p27Kip1. Breast Cancer Res Treat 1998;52:29-41.

311. Glaser R, Harder J, Lange H, Bartels J, Christophers E, Schroder JM. Antimicrobial psoriasin (S100A7) protects human skin from Escherichia coli infection. Nat Immunol 2005;6:57-64.

312. Ruse M, Broome AM, Eckert RL. S100A7 (psoriasin) interacts with epidermal fatty acid binding protein and localizes in focal adhesion-like structures in cultured keratinocytes. J Invest Dermatol 2003;121:132-141.

313. Broome AM, Ryan D, Eckert RL. S100 protein subcellular localization during epidermal differentiation and psoriasis. J Histochem Cytochem 2003;51:675-685.

314. Cope GA, Suh GS, Aravind L, Schwarz SE, Zipursky SL, Koonin EV, Deshaies RJ. Role of predicted metalloprotease motif of Jab1/Csn5 in cleavage of Nedd8 from Cul1. Science 2002;298:608-611.

315. Dechend R, Hirano F, Lehmann K, Heissmeyer V, Ansieau S, Wulczyn FG, Scheidereit C, Leutz A. The Bcl-3 oncoprotein acts as a bridging factor between NF-kappaB/Rel and nuclear co-regulators. Oncogene 1999;18:3316-3323.

316. Woodgett JR, Pulverer BJ, Plyte S, Hughes K, Nikolakaki E. Nuclear onco-protein targets of signal transduction pathways. Pigment Cell Res 1994;7:96-100.

317. Grossmann J. Molecular mechanisms of "detachment-induced apoptosis--Anoikis". Apoptosis 2002;7:247-260.

318. Campiglio M, Locatelli A, Olgiati C, Normanno N, Somenzi G, Vigano L, Fumagalli M, Menard S, Gianni L. Inhibition of proliferation and induction of apoptosis in breast cancer cells by the epidermal growth factor receptor (EGFR) tyrosine kinase inhibitor ZD1839 ('Iressa') is independent of EGFR expression level. J Cell Physiol 2004;198:259-268.

319. Barnes A, Pinder SE, Bell JA, Paish EC, Wencyk PM, Robertson JF, Elston CW, Ellis IO. Expression of p27kip1 in breast cancer and its prognostic significance. J Pathol 2003;201:451-459.

320. Biswas DK, Shi Q, Baily S, Strickland I, Ghosh S, Pardee AB, Iglehart JD. NF-kappa B activation in human breast cancer specimens and its role in cell proliferation and apoptosis. Proc Natl Acad Sci U S A 2004;101:10137-10142.

321. Biswas DK, Cruz AP, Gansberger E, Pardee AB. Epidermal growth factor-induced nuclear factor kappa B activation: A major pathway of cell-cycle progression in estrogen-receptor negative breast cancer cells. Proc Natl Acad Sci U S A 2000;97:8542-8547.

322. Biswas DK, Martin KJ, McAlister C, Cruz AP, Graner E, Dai SC, Pardee AB. Apoptosis caused by chemotherapeutic inhibition of nuclear factor-kappaB activation. Cancer Res 2003;63:290-295.

323. Algermissen B, Sitzmann J, LeMotte P, Czarnetzki B. Differential expression of CRABP II, psoriasin and cytokeratin 1 mRNA in human skin diseases. Arch Dermatol Res 1996;288:426-430.

324. Di Poi N, Tan NS, Michalik L, Wahli W, Desvergne B. Antiapoptotic role of PPARbeta in keratinocytes via transcriptional control of the Akt1 signaling pathway. Mol Cell 2002;10:721-733.

325. Iordanov MS, Choi RJ, Ryabinina OP, Dinh TH, Bright RK, Magun BE. The UV (Ribotoxic) stress response of human keratinocytes involves the unexpected uncoupling of the Ras-extracellular signal-regulated kinase signaling cascade from the activated epidermal growth factor receptor. Mol Cell Biol 2002;22:5380-5394.

326. Zenz R, Scheuch H, Martin P, Frank C, Eferl R, Kenner L, Sibilia M, Wagner EF. c-Jun regulates eyelid closure and skin tumor development through EGFR signaling. Dev Cell 2003;4:879-889.

327. Reginato MJ, Mills KR, Paulus JK, Lynch DK, Sgroi DC, Debnath J, Muthuswamy SK, Brugge JS. Integrins and EGFR coordinately regulate the pro-apoptotic protein Bim to prevent anoikis. Nat Cell Biol 2003;5:733-740.

328. Wang F, Weaver VM, Petersen OW, Larabell CA, Dedhar S, Briand P, Lupu R, Bissell MJ. Reciprocal interactions between beta1-integrin and epidermal growth factor receptor in three-dimensional basement membrane breast cultures: a different perspective in epithelial biology. Proc Natl Acad Sci U S A 1998;95:14821-14826.

329. Eckert LB, Repasky GA, Ulku AS, McFall A, Zhou H, Sartor CI, Der CJ. Involvement of Ras activation in human breast cancer cell signaling, invasion, and anoikis. Cancer Res 2004;64:4585-4592.

330. Kwok SF, Solano R, Tsuge T, Chamovitz DA, Ecker JR, Matsui M, Deng XW. Arabidopsis homologs of a c-Jun coactivator are present both in monomeric form and in the COP9 complex, and their abundance is differentially affected by the pleiotropic cop/det/fus mutations. Plant Cell 1998;10:1779-1790.

331. Bemis L, Chan DA, Finkielstein CV, Qi L, Sutphin PD, Chen X, Stenmark K, Giaccia AJ, Zundel W. Distinct aerobic and hypoxic mechanisms of HIF-alpha regulation by CSN5. Genes Dev 2004;18:739-744.

332. Lagios MD. Classification of duct carcinoma in situ (DCIS) with a characterization of high grade lesions: defining cohorts for chemoprevention trials. J Cell Biochem Suppl 1996;25:108-111.

333. Ringberg A, Anagnostaki L, Anderson H, Idvall I, Ferno M. Cell biological factors in ductal carcinoma in situ (DCIS) of the breast-relationship to ipsilateral local recurrence and histopathological characteristics. Eur J Cancer 2001;37:1514-1522.

334. Pouliot F, Labrie C. Expression profile of agonistic Smads in human breast cancer cells: absence of regulation by estrogens. Int J Cancer 1999;81:98-103.

335. Hanahan D, Folkman J. Patterns and emerging mechanisms of the angiogenic switch during tumorigenesis. Cell 1996;86:353-364.

336. Schmidt AM, Yan SD, Yan SF, Stern DM. The biology of the receptor for advanced glycation end products and its ligands. Biochim Biophys Acta 2000;1498:99-111.

337. Kuniyasu H, Oue N, Wakikawa A, Shigeishi H, Matsutani N, Kuraoka K, Ito R, Yokozaki H, Yasui W. Expression of receptors for advanced glycation end-products (RAGE) is closely associated with the invasive and metastatic activity of gastric cancer. J Pathol 2002;196:163-170.

338. Robinson MJ, Hogg N. A comparison of human S100A12 with MRP-14 (S100A9). Biochem Biophys Res Commun 2000;275:865-870.

339. Vogl T, Ludwig S, Goebeler M, Strey A, Thorey IS, Reichelt R, Foell D, Gerke V, Manitz MP, Nacken W, Werner S, Sorg C, Roth J. MRP8 and MRP14 control microtubule reorganization during transendothelial migration of phagocytes. Blood 2004;104:4260-4268.

340. Zhang L, Fogg DK, Waisman DM. RNA interference-mediated silencing of the S100A10 gene attenuates plasmin generation and invasiveness of Colo 222 colorectal cancer cells. J Biol Chem 2004;279:2053-2062.

341. Benaud C, Gentil BJ, Assard N, Court M, Garin J, Delphin C, Baudier J. AHNAK interaction with the annexin 2/S100A10 complex regulates cell membrane cytoarchitecture. J Cell Biol 2004;164:133-144.

342. Yamada A, Irie K, Hirota T, Ooshio T, Fukuhara A, Takai Y. Involvement of the annexin II-S100A10 complex in the formation of E-cadherin-based adherens junctions in MDCK cells. J Biol Chem 2004.

343. Dowen SE, Crnogorac-Jurcevic T, Gangeswaran R, Hansen M, Eloranta JJ, Bhakta V, Brentnall TA, Luttges J, Kloppel G, Lemoine NR. Expression of S100P and its novel binding partner S100PBPR in early pancreatic cancer. Am J Pathol 2005;166:81-92.